epaResearch

Updated High-resolution Climate Projections for Ireland

Authors: Paul Nolan

Annual Ensemble Mean Temperature Change w.r.t 1981-2010

Rialtas na hÉireann
Government of Ireland
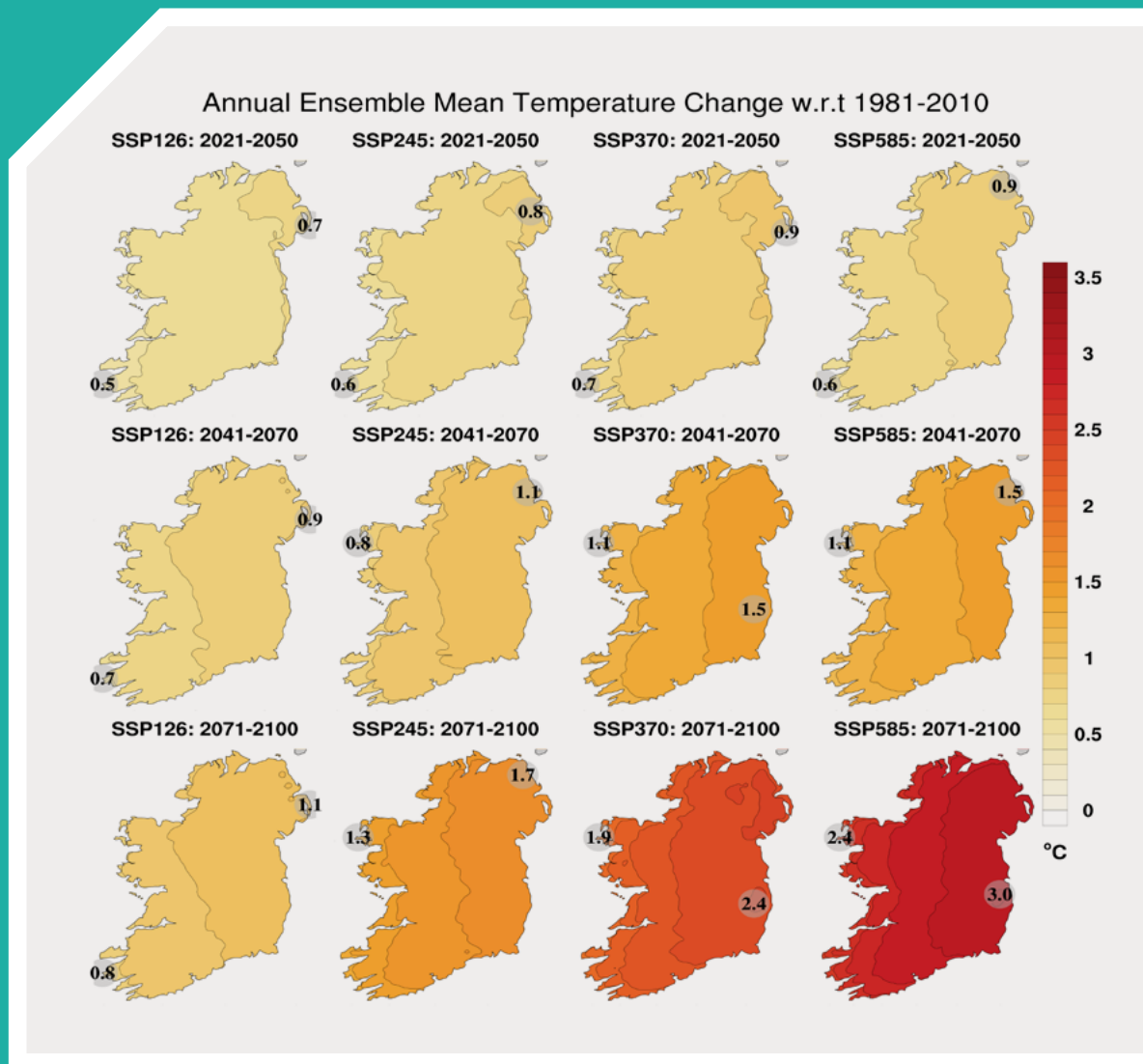
Environmental Protection Agency

The EPA is responsible for protecting and improving the environment as a valuable asset for the people of Ireland. We are committed to protecting people and the environment from the harmful effects of radiation and pollution.

The work of the EPA can be divided into three main areas:

Regulation: Implementing regulation and environmental compliance systems to deliver good environmental outcomes and target those who don't comply.

Knowledge: Providing high quality, targeted and timely environmental data, information and assessment to inform decision making.

Advocacy: Working with others to advocate for a clean, productive and well protected environment and for sustainable environmental practices.

Our Responsibilities Include:

Licensing
- Large-scale industrial, waste and petrol storage activities;
- Urban waste water discharges;
- The contained use and controlled release of Genetically Modified Organisms;
- Sources of ionising radiation;
- Greenhouse gas emissions from industry and aviation through the EU Emissions Trading Scheme.

National Environmental Enforcement
- Audit and inspection of EPA licensed facilities;
- Drive the implementation of best practice in regulated activities and facilities;
- Oversee local authority responsibilities for environmental protection;
- Regulate the quality of public drinking water and enforce urban waste water discharge authorisations;
- Assess and report on public and private drinking water quality;
- Coordinate a network of public service organisations to support action against environmental crime;
- Prosecute those who flout environmental law and damage the environment.

Waste Management and Chemicals in the Environment
- Implement and enforce waste regulations including national enforcement issues;
- Prepare and publish national waste statistics and the National Hazardous Waste Management Plan;
- Develop and implement the National Waste Prevention Programme;
- Implement and report on legislation on the control of chemicals in the environment.

Water Management
- Engage with national and regional governance and operational structures to implement the Water Framework Directive;
- Monitor, assess and report on the quality of rivers, lakes, transitional and coastal waters, bathing waters and groundwaters, and measurement of water levels and river flows.

Climate Science & Climate Change
- Publish Ireland's greenhouse gas emission inventories and projections;
- Provide the Secretariat to the Climate Change Advisory Council and support to the National Dialogue on Climate Action;
- Support National, EU and UN Climate Science and Policy development activities.

Environmental Monitoring & Assessment
- Design and implement national environmental monitoring systems: technology, data management, analysis and forecasting;
- Produce the State of Ireland's Environment and Indicator Reports;
- Monitor air quality and implement the EU Clean Air for Europe Directive, the Convention on Long Range Transboundary Air Pollution, and the National Emissions Ceiling Directive;
- Oversee the implementation of the Environmental Noise Directive;
- Assess the impact of proposed plans and programmes on the Irish environment.

Environmental Research and Development
- Coordinate and fund national environmental research activity to identify pressures, inform policy and provide solutions;
- Collaborate with national and EU environmental research activity.

Radiological Protection
- Monitoring radiation levels and assess public exposure to ionising radiation and electromagnetic fields;
- Assist in developing national plans for emergencies arising from nuclear accidents;
- Monitor developments abroad relating to nuclear installations and radiological safety;
- Provide, or oversee the provision of, specialist radiation protection services.

Guidance, Awareness Raising, and Accessible Information
- Provide independent evidence-based reporting, advice and guidance to Government, industry and the public on environmental and radiological protection topics;
- Promote the link between health and wellbeing, the economy and a clean environment;
- Promote environmental awareness including supporting behaviours for resource efficiency and climate transition;
- Promote radon testing in homes and workplaces and encourage remediation where necessary.

Partnership and Networking
- Work with international and national agencies, regional and local authorities, non-governmental organisations, representative bodies and government departments to deliver environmental and radiological protection, research coordination and science-based decision making.

Management and Structure of the EPA

The EPA is managed by a full time Board, consisting of a Director General and five Directors. The work is carried out across five Offices:

1. Office of Environmental Sustainability
2. Office of Environmental Enforcement
3. Office of Evidence and Assessment
4. Office of Radiation Protection and Environmental Monitoring
5. Office of Communications and Corporate Services

The EPA is assisted by advisory committees who meet regularly to discuss issues of concern and provide advice to the Board.

Updated High-resolution Climate Projections for Ireland

Author: Paul Nolan

Lead organisations: Irish Centre for High-End Computing (ICHEC) and Met Éireann

Identifying pressures

Climate change poses a significant risk to Ireland's economy, society and environment, and therefore it is imperative that planners and policymakers are adequately informed about future climate change so that appropriate mitigation and adaptation measures can be implemented. The main objective of this project was to evaluate the effects of climate change on the future climate of Ireland using high-resolution regional climate modelling. Previous regional climate projection research for Ireland shows large uncertainty for certain climate projections such as precipitation. Since extreme events such as flooding and droughts are likely to be a critical issue for Ireland, it is important to address this research gap. The project simulated the future climate (up to the year 2100) at high resolution (4 km grid spacing) using the most up-to-date regional climate models, Coupled Model Intercomparison Project Phase 6 (CMIP6) Earth system models and new shared socioeconomic pathway and representative concentration pathway (SSP-RCP) (SSP1-2.6, SSP2-4.5, SSP3-7.0 and SSP5-8.5) emission scenarios. The scenario-based projections are supplemented with global warming threshold scenario projections for temperature and precipitation.

Informing policy

This research will inform national policy and further the understanding of the impacts of climate change in Ireland at a local scale. Below are examples of climate projections that are of particular interest to policymakers:

- Near-surface temperature is projected to increase by 0.5–0.7°C for SSP1-2.6 (2021–2050) and 2.4–3.0°C for SSP5-8.5 (2071–2100), with the largest increases in the east.
- Warming is enhanced for the extremes, resulting in substantial projected increases in heatwaves and decreases in frost and ice days.
- The future autumn and winter months are projected to be wetter (increases of up to 10% for SSP5-8.5, 2071–2100), while summer is projected to be drier (decreases of 8% for SSP5-8.5, 2071–2100).
- The precipitation climate is projected to become more variable, with substantial projected increases in both dry periods and heavy rainfall events.

- Snowfall is projected to decrease by between 31% (SSP1-2.6, 2021–2050) and 84% (SSP5-8.5, 2071–2100).
- The projections indicate an average increase in the length of the growing and grazing seasons, soil temperature, crop heat units and growing degree days for a range of crops.
- The energy content of the 120 m wind is projected to decrease for all seasons, with the largest decreases noted for the summer months (reductions of 23% for SSP5-8.5, 2071–2100).
- Photovoltaic power is projected to decrease for all seasons, with decreases enhanced for the winter and summer months.
- The projections show that over the coming decades there will be a substantial reduction in the requirement for heating in Ireland.

Developing solutions

This research provides Ireland with a data resource to explore its future climate and enables the assessment of the scale of impacts across sectors, at regional and local levels. This report provides an outline of the regional climate modelling undertaken to assess the impacts of climate change in Ireland, based on a number of future scenarios, and highlights the key findings. The project has also provided a large database that can be interrogated for various meteorological parameters, which is essential for detailed analysis across a diverse range of sectoral concerns.

The national climate projections of the current report are in broad agreement with previous research, which adds a measure of confidence to the projections. The research improves on previous research by simulating the future climate at a higher spatial resolution (4 km) using the most up-to-date regional climate models to downscale an ensemble of CMIP6 global datasets under the new SSP-RCP emission scenarios. The increased ensemble size of projections allows for a more accurate quantification of climate change uncertainty. Furthermore, the current report provides projections for additional climate variables and derived metrics that are critically important to biodiversity and to key Irish sectors, including agriculture, health, energy and transport.

Updated High-resolution Climate Projections for Ireland

(2018-CCRP-MS.56)

EPA Research Report

A high-resolution version of this report is available on request from research@epa.ie

Prepared for the Environmental Protection Agency

by

Irish Centre for High-End Computing (ICHEC) and Met Éireann

Author:

Paul Nolan

ACKNOWLEDGEMENTS

DISCLAIMER

Project Partners

Dr Paul Nolan
Irish Centre for High-End Computing (ICHEC)
University of Galway
Grand Canal Quay
Dublin 2
Ireland
Tel.: +353 1 529 1032
Email: paul.nolan@ichec.ie

Contents

List of Figures

List of Tables

List of Boxes

Executive Summary

Climate changes pose significant risks to Ireland's economy, society and environment, and it is therefore imperative for policymakers and planners to have access to robust climate projections. The main objective of this study was to evaluate the effects of climate change on the future climate of Ireland using the method of high-resolution regional climate modelling. Previous regional climate projection research for Ireland has found great uncertainty for certain climate projections such as precipitation. Since extreme events such as flooding and droughts are likely to be a critical issue for Ireland as a result of climate change, it is important to address this research gap. The project addressed this issue by simulating the future climate of Ireland (up to the year 2100) at high resolution (~4 km grid spacing) using the most up-to-date regional climate models, Coupled Model Intercomparison Project (CMIP) Phase 6 Earth system models (ESMs) and the new scenarios, which comprise shared socioeconomic pathway (SSP) and representative concentration pathway (RCP) emission scenarios. The ensemble approach of the current project analyses the output of two regional climate models, driven by several ESMs, to simulate climate change. The increased ensemble size is essential for a more accurate quantification of climate change uncertainty and provides more reliable projections of climate change. To account for the uncertainty in future global emissions, the future climate is simulated under all four tier 1 SSP–RCP (SSP1-2.6, SSP2-4.5, SSP3-7.0 and SSP5-8.5) emission scenarios. Differences between the 30-year reference period (1981–2010) and three future 30-year periods (2021–2050, 2041–2070 and 2071–2100) were analysed to assess projected changes in the Irish climate.

A second component of the project involved simulating global climate change using the EC-Earth ESM. These EC-Earth simulations constituted Ireland's contribution to CMIP6, and their results informed the Intergovernmental Panel on Climate Change Assessment Report 6 Working Group 1 report.

The national climate projections of the current report are in broad agreement with previous research, which adds a measure of confidence to the projections.

Moreover, the current report presents projections of additional climate fields and derived variables that are of vital importance to Irish sectors such as agriculture, health, energy and transport and to biodiversity. It is envisaged that the research will inform national policy and further the understanding of the potential environmental impacts of climate change in Ireland at a local scale.

Summary of Climate Projections for Ireland

Temperature, frost and ice days, and heatwave projections. The mean annual 2 m temperature over Ireland is projected to increase by 0.5–3°C depending on time period and SSP–RCP scenario: 0.5–0.7°C for SSP1-2.6 (2021–2050) and 2.4–3.0°C for SSP5-8.5 (2071–2100). Temperature projections show a clear west to east gradient, with the largest increases in the east. The largest projected increases in temperature are for summer and autumn, with increases of up to 3.6°C in the south-east for SSP5-8.5 (2071–2100). Warming is enhanced for the extremes (i.e. hot days and cold nights), which results in projected increases in heatwaves and a decrease in frost and ice days. The projected increase in the number of heatwave periods (as measured by two metrics) over the 30-year period of interest ranges from 0.5 to 5.9 for metric-1 (from 1.8 to 6 for metric-2) for SSP1-2.6 (2021–2050) and from 12 to 57 for metric-1 (from 23 to 45 for metric-2) for SSP5-8.5 (2071–2100), with the largest increases in the south-east. Averaged over the whole country (the island of Ireland), the mean projected decrease in the number of frost days (days when the minimum near-surface temperature is less than 0°C) ranges from 29% (2021–2050 under SSP1-2.6) to 82% (2071–2100 under SSP5-8.5). Similarly, the projected decrease in the number of ice days (days when the maximum temperature is less than 0°C) ranges from 57% (2021–2050 under SSP1-2.6) to 94% (2071–2100 under SSP5-8.5). It is worth noting that periods of frost and ice are important environmental drivers that trigger phenological phases in many plant and animal species. Changes in the occurrence of these weather types may disrupt the life cycles of these species. The projected increase in extreme temperatures and heatwaves will have a direct impact

on public health and mortality, but this may be offset by the projected decrease in frost and ice days.

Precipitation, evapotranspiration, snow, surface humidity and 10 m wind speed projections.
The projected precipitation changes exhibit higher uncertainty than the temperature-related projections. The projections of precipitation show small changes (~0%) over the full year and for spring. The future autumn and winter months are projected to be wetter with enhanced, and more *robust*,[1] increases for the higher SSP–RCPs and later time periods (increases of up to ~10% for SSP5-8.5 2071–2100). Summer is projected to be drier, with robust projected decreases ranging from 0.7% for SSP1-2.6 (2071–2100) to ~8% for SSP5-8.5 (2071–2100). The precipitation climate is projected to become more variable, with substantial projected increases in both dry periods and heavy precipitation events.

The frequencies of heavy precipitation events (days with precipitation > 30 mm) show notable increases for all seasons, with *likely* projected increases of 56% (annual), 66% (winter), 26% (spring), 30% (summer) and 71% (autumn) for SSP5-8.5 by the end of the century. The projected increase in evapotranspiration, noted for all seasons for higher SSP–RCPs and later time periods, may offset flooding events caused by the expected increases in heavy rainfall. The number of extended dry periods (defined as at least 5 consecutive days for which the daily precipitation is < 1 mm) is also projected to increase substantially for the higher SSP–RCPs and/or later time periods. The largest projected increases in dry periods are noted for summer, with robust increases ranging from 6.3% for SSP3-7.0 (2021–2050) to 20% for SSP5-8.5 (2071–2100).

Snowfall is projected to decrease substantially over Ireland, with decreases, averaged over the whole country, ranging from 31% (2021–2050 under SSP1-2.6) to 84% (2071–2100 under SSP5-8.5).

Near-surface (2 m) specific humidity is projected to increase for all seasons, with increases enhanced for the higher SSP–RCPs and later time periods. The largest increases are noted for the summer

and autumn months, ranging from ~6% for 2021–2050 under SSP1-2.6 to ~27% for 2071–2100 under SSP5-8.5. Projections of the mean annual near-surface relative humidity show small changes (~0%) or small projected increases (< 2%), which are enhanced for the higher SSP–RCPs and later time periods. The largest projected increases in relative humidity are noted for summer.

The mean annual 10 m wind speed is projected to decrease for all seasons and SSP–RCP scenarios. Averaged over the country, the mean projected decrease in annual 10 m wind speed ranges from 1.2% (2021–2050 under SSP1-2.6) to 3.2% (2071–2100 under SSP5-8.5). The largest projected decreases are noted for summer, with reductions ranging from ~2% (2021–2050 under SSP1-2.6) to ~8% (2071–2100 under SSP5-8.5).

Agricultural impacts. The projections, outlined above, of increases in extreme temperatures, heatwaves, humidity, heavy precipitation and dry periods/droughts along with decreases in frost and ice days will have direct and substantial effects on agriculture in Ireland. In addition, the projections indicate an average increase in the length of the growing season ranging from 6.6% (2021–2050 under SSP1-2.6) to 17.7% (2071–2100 under SSP5-8.5). Similarly, 10 cm soil temperature, the grazing season, crop heat units and growing degree days for a range of crops are projected to increase substantially. These results suggest that a warming climate may present some positive opportunities for agriculture in Ireland. However, it should be borne in mind that a warming climate will also result in an increase in pests because of an increase in pest-growing degree days and a decrease in frost and ice days, which will increase pest survival over winter. Furthermore, the projected increase in the frequency of both droughts and heavy rainfall events, and projected decreases in surface radiation, could be detrimental to the potential gains of a warming climate to the agricultural sector.

Energy impacts. The energy content of the 120 m (turbine height) wind is projected to decrease for all seasons, SSP–RCPs and future time periods.

---

1 A climate projection is defined as robust if more than 66% of the ensemble members agree on the sign of the projected change. See section 1.4.2 for a full description.

Averaged over the whole country, the mean projected decrease in annual wind power[2] ranges from 4.6% (2021–2050 under SSP1-2.6) to 8.6% (2071–2100 under SSP5-8.5). The largest decreases are noted for the summer months, with reductions ranging from ~7% (SSP1-2.6, 2021–2050) to 23% (SSP5-8.5, 2071–2100). To assess the impact of climate change on solar power in Ireland, projections of solar photovoltaic power were analysed. Photovoltaic power is projected to decrease for all seasons, with decreases enhanced for the higher SSP–RCPs and later time periods. There exists a clear south-east to north-west gradient in the projections, with the largest decreases in the north-west. The annual projected photovoltaic power decreases range from 2.3% (2021–2050 under SSP1-2.6) to 7.5% (2071–2100 under SSP5-8.5). The largest decreases are noted for the winter and summer months, with reductions, for both seasons, ranging from ~3% (2021–2050 under SSP1-2.6) to ~9% (2071–2100 under SSP5-8.5).

The projections of heating degree days show that over the coming decades there will be a greatly reduced requirement for heating in Ireland. The annual heating requirement is projected to decrease by ~8% for SSP1-2.6 (2021–2050) and 33% for SSP5-8.5 (2071–2100). The projections show that cooling degree days are projected to increase slightly, suggesting a very small increase in air conditioning requirements in the coming decades. However, the amounts are small compared with heating degree days and therefore have a negligible effect on the projected changes in the total energy demand (heating degree days + cooling degree days).

---

2   Here, we consider the constrained wind power for cut-in and cut-out wind speeds of 3 and $25\,\mathrm{m\,s^{-1}}$, respectively, for a typical large wind turbine. See section 3.21 for further details.

1   Introduction

Increasing greenhouse gas emissions and changing land use are having significant effects on the Earth's climate. The Intergovernmental Panel on Climate Change (IPCC) has concluded that "it is unequivocal that human influence has warmed the atmosphere, ocean and land" and "widespread and rapid changes in the atmosphere, ocean, cryosphere and biosphere have occurred" (IPCC, 2023). Furthermore, observed increases in extremes such as heatwaves, heavy precipitation and droughts, and intensification of tropical cyclones have been attributed to human influence (IPCC, 2023). The climate of Ireland has mirrored these global trends. The EPA report *Ireland's Climate Change Assessment. Volume 1: Climate Science – Ireland in a Changing World* states that "recent changes in heat extremes and heavy precipitation events in Ireland can be linked, albeit indirectly, to human-induced climate change" (Noone *et al*., 2023). The authors include examples of recent extreme weather events, probably human induced, such as the July heatwave of 2022 in which temperatures reached 33°C (at Phoenix Park, Dublin) "for the first time nationally in over a century and may constitute the hottest temperature reliably recorded, given the uncertainties recently documented about the long-standing national heat record", "intense short-lived rainfall events such as those at New Ross in August 2022 or in County Donegal in August 2017", and increases in the probability and intensity of "multi-day rainfall events, such as those culminating in Storm Desmond in December 2015" (Noone *et al*., 2023).

These changes pose significant risks to Ireland's economy, society and environment, and therefore it is imperative that planners and policymakers are adequately informed about future climate change so that appropriate mitigation and adaptation measures can be implemented. In this context, the main objective of this study was to evaluate the effects of climate change on the future climate of Ireland using the method of high-resolution regional climate modelling. Previous regional climate projection research for Ireland shows large uncertainty for certain climate projections such as precipitation (e.g. Nolan, 2015; Nolan *et al*., 2017; Nolan and Flanagan, 2020). Since extreme events such as flooding and

droughts are likely to be a critical issue for Ireland under climate change, it is important to address this research gap. The project addressed this issue by simulating the future climate (up to the year 2100) at high resolution (~4 km grid spacing) using the most up-to-date regional climate models (RCMs), Coupled Model Intercomparison Project (CMIP) Phase 6 Earth system models (ESMs) and new scenarios, which comprise shared socioeconomic pathway (SSP) and representative concentration pathway (RCP) emission scenarios. Moreover, an increased ensemble size of regional climate projections was achieved, which is essential for a more accurate quantification of climate change uncertainty and more reliable projections of climate change. A second component of the project involved simulating global climate change using the EC-Earth ESM. These EC-Earth simulations constituted Ireland's contribution to CMIP6, and their results informed the IPCC Assessment Report (AR) 6 Working Group 1 report (IPCC, 2021).

1.1   Observed and Projected Climate Change

The global observational record shows that "each of the last four decades has been successively warmer than any decade that preceded it since 1850", with global surface temperatures during the last two decades (2001–2020) increasing by 0.99°C [0.84–1.10°C] relative to 1850–1900 (IPCC, 2021). The authors note an increase in observed global extreme events due to human-induced climate change. For example, it is "virtually certain that hot extremes have become more frequent and more intense across most land regions since the 1950s", the frequency and intensity of heavy precipitation events have increased since the 1950s over most land areas (high confidence level), and "it is likely that the global proportion of major (Category 3–5) tropical cyclone occurrence has increased over the last four decades" (IPCC, 2021). Future projections of the CMIP6 multi-model ensemble show that the global surface temperature averaged over the period 2081–2100 (relative to 1850–1900) is very likely to increase by 1.0–1.8°C (for SSP1-1.9), by 2.1–3.5°C (for SSP2-4.5) and by 3.3–5.7°C

(for SSP5-8.5) (IPCC, 2021). Continued global warming is projected to further intensify the global water cycle, including its variability, and the severity of wet and dry events, and to accelerate the decline in Arctic sea ice (IPCC, 2021).

The historical climate of Ireland has mirrored the global trends. The *Climate Status Report for Ireland 2020* (Cámaro García and Dwyer, 2021) found that "the annual average surface air temperature in Ireland has increased by approximately 0.9°C over the last 120 years,[3] with a rise in temperatures being observed in all seasons". Furthermore, the Irish observational record shows an increase in the number of both warm and wet spell days over the preceding decades (Cámaro García and Dwyer, 2021). A more recent study has shown that the average temperature and average rainfall over Ireland increased by approximately 0.7°C and 7%, respectively, between the periods 1961–1990 and 1991–2020 (Met Éireann, 2023). Regional variations are also evident, with the west and north of Ireland showing the greatest increases in annual rainfall (Met Éireann, 2023).

Temperature projections for Ireland are in line with global projections, with an expected increase in annual 2 m temperatures over Ireland of approximately 1–1.2°C (RCP4.5 scenario) and 1.3–1.6°C (RCP8.5 scenario) by mid-century, with the strongest signals noted in the east (Nolan, 2015; O'Sullivan *et al*., 2016; Nolan and Flanagan, 2020). Temperature increases are enhanced at the extremes: mid-century summer day-time and winter night-time temperatures are projected to increase by 1.0–2.2°C and 1.0–2.4°C, respectively (Nolan, 2015; Nolan and Flanagan, 2020). The number of frost and ice days is expected to decrease by approximately 50% by mid-century (Nolan, 2015; Nolan and Flanagan, 2020). Rainfall is projected to become more variable with an increase in extended dry periods during summer and an increase in the number of heavy rainfall events during autumn and winter (Nolan, 2015; Nolan *et al*., 2017; Nolan and Flanagan, 2020). More recently, O'Brien and Nolan (2023) (through the Met Éireann TRANSLATE project) described how a set of future climate projections for Ireland were produced by detrending, bias-correcting and further statistically downscaling the output from high-resolution RCM ensembles. The results show

that the temperature in Ireland is projected to increase broadly in line with global changes, at least up to global warming levels of 2.5°C. For global warming levels higher than that, Irish temperatures equilibrate at levels progressively lower than global temperatures. Meanwhile, precipitation is projected to increase slightly on an annual basis, with the wet periods becoming more concentrated in the autumn and winter, while conditions become slightly drier during spring and summer (O'Brien and Nolan, 2023).

Regional climate projections for Ireland are consistent with projected changes in the UK climate. The United Kingdom Climate Projections (UKCP) 18 project analysed an ensemble of global projections (CMIP5-RCP8.5 60 km grid spacing) and dynamically downscaled CMIP5 projections with 25 km (range of RCPs), and 12 km and 2.2 km (RCP8.5) grid spacing, and found that "general climate change trends projected over UK land for the 21st century in UKCP18 are broadly consistent with earlier projections (UKCP09) showing an increased chance of warmer, wetter winters and hotter, drier summers along with an increase in the frequency and intensity of extremes" (Met Office, 2022). It was found that the high-resolution 2.2 km RCM data provide the most physically realistic projections of local extremes such as large convective storms in the summer. However, the 2.2 km projections span a narrower range of uncertainty than the larger ensemble of lower resolution simulations (Met Office, 2022).

Regional climate projection research for Ireland shows large uncertainty for certain climate projections such as annual precipitation and annual wind speeds (e.g. Nolan, 2015; Nolan *et al*., 2017; Nolan and Flanagan, 2020). Since extreme events such as flooding, droughts and storms will probably be critical issues for Ireland under climate change, it is important to address this research gap. The current project attempted to address this issue by simulating the future climate at high resolution (~4 km) using the most up-to-date RCMs, CMIP6 global climate models and new SSP–RCP emission scenarios. Moreover, an increased ensemble size of regional climate projections is essential for a more accurate quantification of climate change uncertainty and will provide more robust projections of climate change in the decades ahead.

---

3   More recent data from Met Éireann show that, as of 2023, this figure has risen to 1°C.

A second component of the project involved using the EC-Earth ESM to simulate climate change on a global scale and contribute to the CMIP6 project.

1.2 The EC-Earth Earth System Model and CMIP6 Contributions

The impacts of increasing greenhouse gas emissions and changing land use on climate change can be simulated using ESMs. Since 1995, the CMIP has coordinated climate model experiments involving multiple international modelling teams. The CMIP has led to a better understanding of the past, present and future climate, and CMIP model experiments have routinely been the basis of future climate change assessments made by the IPCC. Ireland's participation in CMIP6 comes through the EC-Earth climate modelling consortium (Döscher *et al*., 2022). EC-Earth is an IPCC-class ESM developed by a European consortium of which Met Éireann and the Irish Centre for High-End Computing (ICHEC) are members. The CMIP6 version of EC-Earth (v3.3) comprises the European Centre for Medium-Range Weather Forecasts (ECMWF) Integrated Forecasting System (IFS) atmospheric model, the Nucleus for European Modelling of the Ocean (NEMO) model, the Louvain-la-Neuve sea ice model (LIM), the Tracer Model version 5 (TM5) atmospheric composition model, the Lund–Potsdam–Jena General Ecosystem Simulator (LPJ-GUESS) vegetation model and the Pelagic Interactions Scheme for Carbon and Ecosystem Studies (PISCES) ocean biogeochemistry model. Coupling is provided by OASIS3-MCT (the Ocean Atmosphere Sea Ice Soil (OASIS) coupler interfaced with the Model Coupling Toolkit (MCT)). EC-Earth (CMIP6 configuration, v3.3) is optimised for a standard horizontal resolution of T255 (~80 km) with 91 vertical layers for the atmosphere, and for 1 degree with 75 layers for the ocean. In addition, high-resolution configurations are available: 0.25 degrees and 75 layers in the ocean, and T511 (~39 km) and T799 (~25 km) in the atmosphere.

The CMIP6 version of EC-Earth (v3.3) was a substantial improvement on the CMIP5 version (v2.2). For example, all ESM components were updated with improved physical and dynamic features, new ESM components were included (e.g. PISCES biogeochemistry model in the ocean) and the atmosphere and ocean were simulated with enhanced spatial resolution. In addition, the EC-Earth CMIP6 ensemble size was substantially larger than that of CMIP5. Validations show that the CMIP6 EC-Earth model accurately simulates the global climate and outperforms the CMIP5 version for the majority of variables analysed. See Döscher *et al*. (2022) for a more comprehensive overview of the EC-Earth model, improvements compared with the CMIP5 version, validations and CMIP6 experiments.

As part of the current and a previous project (Nolan and McKinstry, 2020),[4] the following EC-Earth CMIP6 contributions were completed (approximately 3600 years of simulated data in total):

- 7 × EC-Earth atmospheric–ocean general circulation model (AOGCM)/Veg Historical simulations 1850–2014;
- 28 × EC-Earth AOGCM/Veg Scenario Model Intercomparison Project (ScenarioMIP) 2015–2100 SSP–RCP simulations; 7 × SSP1-2.6, 7 × SSP2-4.5, 7 × SSP3-7.0 and 7 × SSP5-8.5.

Please refer to Chapter 4 for a brief overview of the EC-Earth CMIP6 contributions.

1.2.1 The SSP–RCP scenario matrix[5]

The CMIP6 ScenarioMIP utilises a parallel process of combining future socioeconomic pathways with forcing pathways to assess climate change (Moss *et al*., 2010; Riahi *et al*., 2017). This process includes the RCPs, which cover the climate forcing dimension of different possible futures (van Vuuren *et al*., 2011), and served as the basis for the development of climate change projections assessed in the IPCC AR5 (Taylor *et al*.,

---

4   Note that approximately 50% of these simulations were completed as part of the EPA report *EC-Earth Global Climate Simulations: Ireland's Contributions to CMIP6* (Nolan and McKinstry, 2020).

5   Text and figures in section 1.2.1 are taken from Riahi *et al.* (2017) and from the Carbon Brief website (https://www.carbonbrief. org/explainer-how-shared-socioeconomic-pathways-explore-future-climate-change; accessed 5 December 2023). The article by Riahi *et al*. (2017) is an open access article distributed under the terms of the Creative Commons CC BY 4.0 licence (https:// creativecommons.org/licenses/by/4.0), which permits unrestricted use, distribution and reproduction in any medium, provided the original work is properly cited. Material from the Carbon Brief web page can be reproduced unadapted under the terms of the Creative Commons CC BY-NC-ND 4.0 licence (https://creativecommons.org/licenses/by-nc-nd/4.0/deed.en).

2012; IPCC, 2013). The RCPs describe different levels of greenhouse gases and likely radiative forcings. Four pathways were developed, spanning a broad range of forcing in 2100 (2.6, 4.5, 6.0 and 8.5 W m^{-2}), but purposefully did not include any socioeconomic "narratives" to go alongside them. Other groups have focused on modelling how socioeconomic factors may change over the next century (Ebi *et al*., 2014; Kriegler *et al*., 2014; O'Neill *et al*., 2014; van Vuuren *et al*., 2014). These SSPs look at five different ways in which the world might evolve in the absence of climate policy and how different levels of climate change mitigation could be achieved. The SSPs are based on five narratives describing alternative socioeconomic

Table 1.1. Summary of SSP narratives

SSP	Summary
SSP1	**Sustainability – Taking the Green Road (low-level challenges to mitigation and adaptation)**
	The world shifts gradually, but pervasively, towards a more sustainable path, emphasising the need for more inclusive development that respects perceived environmental boundaries. Management of the global commons slowly improves, educational and health investments accelerate the demographic transition, and the emphasis on economic growth shifts towards a broader emphasis on human well-being. Driven by an increasing commitment to achieving development goals, inequality is reduced both across and within countries. Consumption is oriented towards low material growth and lower resource and energy intensity.
SSP2	**Middle of the Road (medium-level challenges to mitigation and adaptation)**
	The world follows a path in which social, economic and technological trends do not shift markedly from historical patterns. Development and income growth proceeds unevenly, with some countries making relatively good progress while others fall short of expectations. Global and national institutions work towards but make slow progress in achieving the Sustainable Development Goals. Environmental systems experience degradation, although there are some improvements and the overall intensity of resource and energy use declines. Global population growth is moderate and levels off in the second half of the century. Income inequality persists or improves only slowly, and challenges to reducing vulnerability to societal and environmental changes remain.
SSP3	**Regional Rivalry – A Rocky Road (high-level challenges to mitigation and adaptation)**
	A resurgent nationalism, concerns about competitiveness and security, and regional conflicts push countries to increasingly focus on domestic or, at most, regional issues. Policies shift over time to become increasingly oriented towards national and regional security issues. Countries focus on achieving energy and food security goals within their own regions at the expense of broader based development. Investments in education and technological development decline. Economic development is slow, consumption is material intensive and inequalities persist or worsen over time. Population growth is low in industrialised nations and high in developing countries. Addressing environmental concerns is a low international priority, leading to strong environmental degradation in some regions.
SSP4	**Inequality – A Road Divided (low-level challenges to mitigation, high-level challenges to adaptation)**
	Highly unequal investments in human capital, combined with increasing disparities in economic opportunity and political power, lead to increasing inequalities and stratification both across and within countries. Over time, a gap widens between an internationally connected society that contributes to the knowledge- and capital-intensive sectors of the global economy, and a fragmented collection of lower-income, poorly educated societies that work in a labour-intensive, low-tech economy. Social cohesion degrades, and conflict and unrest become increasingly common. Technological development is high in the high-tech economy and sectors. The globally connected energy sector diversifies, with investments in both carbon-intensive fuels, such as coal and unconventional oil, and low-carbon energy sources. Environmental policies focus on local issues in middle- and high-income areas.
SSP5	**Fossil-fuelled Development – Taking the Highway (high-level challenges to mitigation, low-level challenges to adaptation)**
	This world places increasing faith in competitive markets, innovation and participatory societies to produce rapid technological progress and develop human capital as the path to sustainable development. Global markets are increasingly integrated. There are also strong investments in health, education and institutions to enhance human and social capital. At the same time, the push for economic and social development is coupled with the exploitation of abundant fossil fuel resources and the adoption of resource- and energy-intensive lifestyles around the world. All these factors lead to rapid growth of the global economy, while global population peaks and declines in the 21st century. Local environmental problems such as air pollution are successfully managed. There is faith in the ability to effectively manage social and ecological systems, including by geoengineering if necessary.

Source: Riahi *et al*., 2017; reproduced under the terms of the Creative Commons CC BY 4.0 licence (https://creativecommons.org/licenses/by/4.0).

developments, including sustainable development, regional rivalry, inequality, fossil-fuelled development and middle-of-the-road development (Table 1.1). The RCPs and SSPs were designed to be complementary. The RCPs set pathways for greenhouse gas concentrations and, effectively, the amount of warming that could occur by the end of the century, whereas the SSPs set the stage on which reductions in emissions will (or will not) be achieved. The new framework employed by the CMIP6 ScenarioMIP combines the SSPs and the RCPs in a scenario matrix architecture (Figure 1.1).

1.3   Regional Climate Modelling

Owing to computational constraints, long climate simulations using ensembles of ESMs are currently feasible only with horizontal resolutions of ≈50 km or coarser. Because climate fields such as precipitation, wind speed and temperature are closely correlated to the local topography, this resolution is inadequate to simulate the detail and pattern of climate change and its effects on the future climate at a regional scale. Furthermore, and of particular relevance to Ireland and western Europe, numerous studies have shown that, even at 50 km grid spacing, global models severely under-resolve both the number and the intensity of cyclones (e.g. Zhao *et al*., 2009; Camargo, 2013; Zappa *et al*., 2013).

To overcome these limitations, the RCM method dynamically downscales the coarse information provided by the global models and provides high-resolution information on a subdomain covering Ireland. The computational cost of running the RCM, for a given resolution, is considerably less than that of a global model. The approach has its flaws: all models have errors, which are cascaded in this technique, and new errors are introduced via the flow of data through the boundaries of the regional model. Nevertheless, numerous studies have demonstrated that high-resolution RCMs improve the simulation of fields such as precipitation (Lucas-Picher *et al*., 2012; Kendon *et al*., 2012, 2014; Nolan, 2015; Bieniek *et al*., 2016; Nolan *et al*., 2017, 2020) and topography-influenced phenomena and extremes with relatively small spatial or short temporal character (Feser *et al*., 2011; Feser and Barcikowska, 2012; Shkol'nik *et al*., 2012; IPCC, 2013). An additional advantage
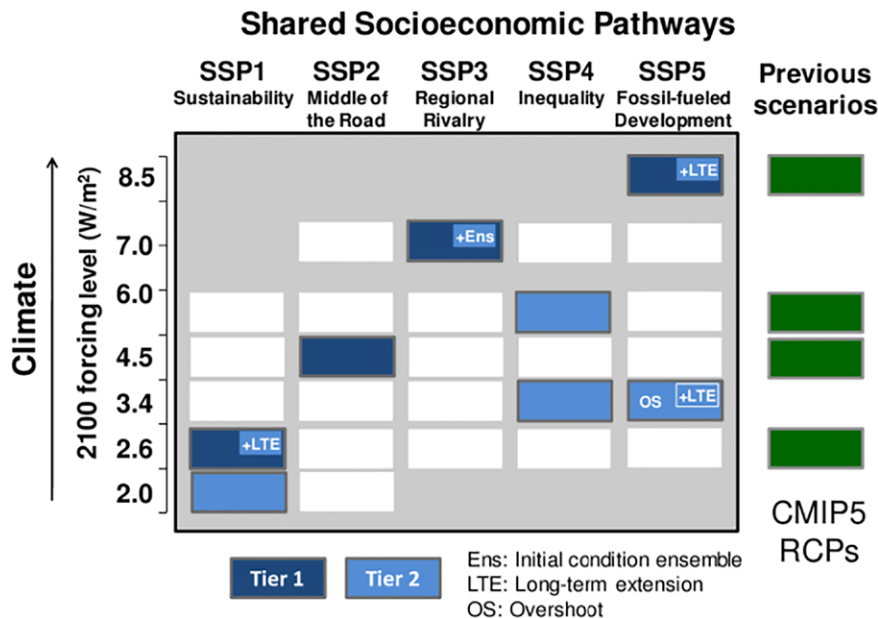
Figure 1.1. SSP–RCP scenario matrix illustrating ScenarioMIP scenarios. Each cell in the matrix indicates a combination of a socioeconomic development pathway (i.e. an SSP) and a climate outcome based on a particular forcing pathway that current integrated assessment model runs have shown to be feasible (Riahi *et al*., 2017). Dark blue cells indicate scenarios that serve as the basis for climate model projections in tier 1 of ScenarioMIP; light blue cells indicate scenarios in tier 2. Source: O'Neill *et al*. (2016); reproduced under the terms of the Creative Commons Attribution 3.0 licence (https:// creativecommons.org/licenses/by/3.0/).

is that the physics-based RCMs explicitly resolve more small-scale atmospheric features and provide a better representation of convective precipitation (Rauscher *et al*., 2010) and extreme precipitation (Kanada *et al*., 2008; Nolan *et al.,* 2017). Other examples of the added value of RCMs are improved simulations of near-surface temperature (Feser, 2006; Di Luca *et al*., 2016; Nolan and Flanagan, 2020), European storm damage (Donat *et al*., 2010), strong mesoscale cyclones (Cavicchia and Storch, 2012), North Atlantic tropical cyclone tracks (Daloz *et al*., 2015) and near-surface wind speeds (e.g. Kanamaru and Kanamitsu, 2007; Nolan *et al*., 2014; Nolan, 2015; Nolan and Flanagan, 2020), particularly in coastal areas with complex topography (Feser *et al*., 2011; Winterfeldt *et al*., 2011). The added value of RCMs in the simulation of cyclones is particularly important for the current study, as low-pressure systems are the main delivery mechanism for precipitation and wind in Ireland and western Europe.

Furthermore, numerous studies have demonstrated that increased RCM spatial resolution results in a more accurate representation of the climate system. Low-resolution RCMs use parameterised convection schemes, meaning that the heaviest precipitation events (e.g. convective systems on hot summer days) may not be adequately represented in the simulations (Prein *et al*., 2013; Kendon *et al*., 2014). Zängl *et al*. (2015) investigated heavy rainfall events over the North-Alpine region and found that increased resolution (9, 3 and 1 km) resulted in a stepwise improvement in model skill. Similarly, Nolan *et al*. (2017) found that RCM accuracy increased with higher spatial resolution; however, reducing the horizontal grid spacing below 4 km provided relatively little added value. The IPCC has concluded that there is "high confidence that downscaling adds value to the simulation of spatial climate detail in regions with highly variable topography (e.g. distinct orography, coastlines) and for mesoscale phenomena and extremes" (IPCC, 2013).

1.4 Regional Climate Model Experiments of the Current Study

The climate of Ireland was simulated at high spatial resolution (4 km) using the Consortium for Small-scale Modeling-Climate Limited-area Modelling

(COSMO-CLM; v5.0.17)[6] (Rockel *et al*., 2008) and the Weather Research and Forecasting (WRF; v4.2.1) (Skamarock *et al*., 2008; Powers *et al*., 2017) RCMs. The choice of model physics and parameterisation schemes was informed by long-term validation experiments (e.g. Nolan, 2015; Nolan *et al*., 2014, 2017; Werner *et al*., 2019; Flanagan and Nolan, 2020; Nolan and Flanagan, 2020) and the recommendations of the respective RCM development team. For example, the WRF simulations did not include a convection parameterisation scheme (convection resolving), while the COSMO-CLM5 simulations utilised the Mass Flux Tiedtke parameterisation scheme (Tiedtke, 1989). A more comprehensive overview of the RCM configurations is provided by Nolan *et al*. (2017) and Nolan and Flanagan (2020).

To account for the uncertainty arising from the estimation of future global emissions of greenhouse gases, the future climate was simulated under all four "tier 1" CMIP6 SSP–RCP (SSP1-2.6, SSP2-4.5, SSP3-7.0 and SSP5-8.5) scenarios. The outer domain (used to drive the inner 4 km domain) was run at 12 km (COSMO-CLM5) and 20 km (WRF), and roughly corresponded to the EURO-CORDEX (Coordinated Regional Climate Downscaling Experiment) domain. The advantage of high-resolution RCM simulations is highlighted in Figure 1.2, which shows how the surface topography is better resolved by the higher resolution data. For the current study, only 4 km grid spacing RCM data were considered. The higher resolution data allowed improved estimates of the regional variations of climate projections. The climate fields of the RCM simulations were archived at 3-hourly intervals. An overview of the COSMO-CLM5 archived fields is provided in Table 1.2. The WRF archived fields are similar.

The choice of CMIP6 data for downscaling was informed by CMIP6 validation studies (e.g. Bock *et al*., 2020; Eyring *et al*., 2021) and a careful review conducted by EURO-CORDEX partners (COSMO-CLM team, personal communication). This study identified an initial set of CMIP6 datasets based on many factors, e.g. model-level data availability, SSP–RCP coverage (SSP1-2.6, SSP2-4.5, SSP3-7.0 and SSP5-8.5), model resolution, equilibrium climate sensitivity (low, medium and high), model skill, e.g. June–August/December–February extratropical storm tracks, transient climate response, circulation and

---

6 www.clm-community.eu (accessed 5 December 2023).
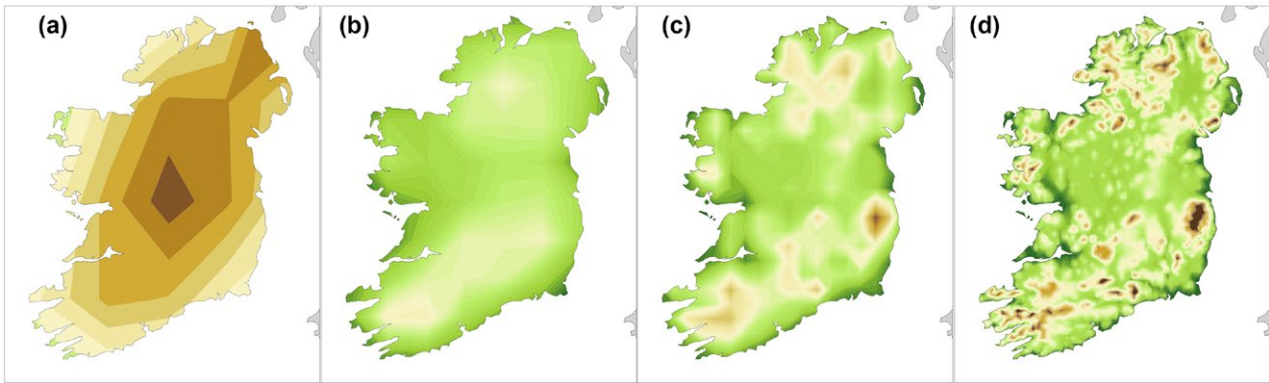
Figure 1.2. The topography of Ireland as resolved by an ESM and the the COSMO-CLM RCM for different spatial resolutions for (a) ESM 125 km grid spacing, (b) COSMO-CLM 50 km grid spacing, (c) COSMO-CLM 18 km grid spacing and (d) COSMO-CLM 4 km grid spacing.

sea surface temperature validations. Informed by this study, and with particular weight given to ensuring a plausible spread of equilibrium climate sensitivity, the CMIP6 datasets presented in Table 1.3 (blue shading) were chosen for initial downscaling over the Irish domain. ESM realisations result from running the same ESM with slightly different initial conditions, i.e. the starting date of historical simulations. The choice of CMIP6 data is corroborated by a separate 2021 study conducted by the Finnish Meteorological Institute (Ruosteenoja, 2021). This filtering of CMIP6 models resulted in a high-quality, representative and manageable ensemble for downscaling over Ireland.

More recently, Palmer *et al*. (2023) completed a performance-based assessment of CMIP6 based on the ability of the models to represent 26 key physical processes that are important for representing the European climate (1995–2014). The performance metrics analysed were seasonal; they were blocking frequency, large-scale circulation assessed by 850 hPa wind speed and direction, North Atlantic sea surface temperature bias, 2 m air temperature bias, storm track and the Atlantic Meridional Overturning Circulation (AMOC). In addition, seasonal performance metrics for three European regions (northern Europe, central Europe and the Mediterranean) were calculated for 2 m air temperature bias, annual precipitation cycle and storm track assessed as cyclones per season within the respective European region. Models that were found to show poor skill in terms of their ability to represent key physical processes were denoted "inadequate". With respect to the CMIP6 datasets

downscaled as part of the current study (Table 1.3, blue shading), MPI-ESM1-2-HR, EC-Earth3 and EC-Earth3-Veg were found to adequately represent all 26 key physical processes. While MIROC6 was found to be "inadequate" for summer (June–August) 2 m temperature over Europe, central Europe and the Mediterranean, it adequately represented the majority of the key processes (Palmer *et al*., 2023).

An overview of the ensemble of RCM simulations is presented in Table 1.4. Data from a 30-year reference period (1981–2010) and three future 30-year periods (2021–2050, 2041–2070 and 2071–2100) were used for the analysis of projected changes in the Irish climate. The historical period was compared with the corresponding future period for all simulations within the same RCM–ESM realisation. This resulted in 10 future anomalies for each future 30-year time period and SSP–RCP, i.e. the difference between future and past. In this study, the ensemble members of the downscaled ESM simulations are treated as independent estimates of the climate system and are given equal weight. Only the differences between the simulations of the past and future climate for each model are used in the analysis (e.g. WRF– EC-Earth-Veg-r12i1p1f1 SSP1-2.6 is compared only with WRF–EC-Earth-Veg-r12i1p1f1 historical and WRF–EC-Earth-Veg-r14i1p1f1 SSP1-2.6 is compared only with WRF–EC-Earth-Veg-r14i1p1f1 historical). While model biases may not be invariant under future scenarios of greenhouse gas emissions, this approach may reduce the impact of model bias.[7]

---

7 The assumption is that the biases in the "past" and "future" model data cancel each other out in the "future–past" climate change metric.

Table 1.2. Archived data of the COSMO-CLM5 RCM simulations (WRF archived data are similar)

Variable	Unit	Variable	Unit
Surface pressure	Pa	Showalter index	K
Mean sea level pressure	Pa	Surface net downward SW radiation	W m^{-2}
Surface temperature	K	Average surface net downward SW radiation	W m^{-2}
2 m temperature	K	Direct surface downward SW radiation	W m^{-2}
2 m dew point temperature	K	Averaged direct surface downward SW radiation	W m^{-2}
U-component of 10 m wind	m s^{-1}	Averaged surface diffuse downward SW radiation	W m^{-2}
V-component of 10 m wind	m s^{-1}	Averaged surface diffuse upward SW radiation	W m^{-2}
Surface roughness length	m	Averaged downward LW radiation at the surface	W m^{-2}
Maximum 10 m wind speed	m s^{-1}	Averaged upward LW radiation at the surface	W m^{-2}
Surface-specific humidity	kg kg^{-1}	Averaged surface net downward LW radiation	W m^{-2}
2 m specific humidity	kg kg^{-1}	Surface albedo	0–1 (fraction)
2 m relative humidity	%	Surface latent heat flux	W m^{-2}
Snow surface temperature	K	Surface sensible heat flux	W m^{-2}
Thickness of snow	m	Surface evaporation	kg m^{-2}
Height of freezing level	m	Surface albedo	0–1 (fraction)
Total precipitation amount	kg m^{-2}		
Precipitation rate	kg m^{-2}s^{-1}	Soil temperature (eight levels)	K
Large-scale rainfall	kg m^{-2}	Soil water content (eight levels)	m
Convective rainfall	kg m^{-2}		
Large-scale snowfall	kg m^{-2}	Daily average 2 m temperature	K
Convective snowfall	kg m^{-2}	Daily maximum 2 m temperature	K
Large-scale graupel	kg m^{-2}	Daily minimum 2 m temperature	K
Surface run-off	kg m^{-2}	Daily duration of sunshine	s
Subsurface run-off	kg m^{-2}	Daily relative duration of sunshine	s
Vertical integrated water vapour	kg m^{-2}	Daily evapotranspiration	mm
Vertical integrated cloud ice	kg m^{-2}	**Below variables archived at 60, 80, 100, 120, 160 and 200 m**	
Vertical integrated cloud water	kg m^{-2}		
Total cloud cover	0–1 (fraction)	U-component of wind	m s^{-1}
Low cloud cover	0–1 (fraction)	V-component of wind	m s^{-1}
Medium cloud cover	0–1 (fraction)	Air density	kg m^{-3}
High cloud cover	0–1 (fraction)	Wind speed	m s^{-1}
CAPE 3 km	J kg^{-1}	Cube wind speed	m^{3}s^{-3}
Surface lifted index	K	Wind direction	degree

CAPE, convective available potential energy; LW, long wave; SW, short wave.

The RCM simulations presented in Table 1.4 comprise ~3800 years of simulated high-resolution (4 m) downscaled data (~200 TB). The RCM simulations were run on the ICHEC and ECMWF supercomputers. Running such a large ensemble of high-resolution RCMs was a substantial computational task and required extensive use of the supercomputer systems over a period of 3–4 years. This archive of data will be made available to the wider research community and general public through Climate Ireland[8] (maps and visualisations) and ICHEC and Met Éireann (data hosting and sharing) platforms.

---

8   www.climateireland.ie (accessed 6 November 2023).

Table 1.3. Initial CMIP6 data selected for downscaling over Ireland and analysed as part of the current study (blue shading). The datasets shaded in orange are CMIP6 datasets currently being downscaled or highlighted for future downscaling[a]

CMIP6 model	Ensemble realisation	Equilibrium climate sensitivity	Atmospheric resolution
MIROC6	r1i1p1f1	2.61	200 km
MPI-ESM1-2-HR (× 2)	r1i1p1f1	2.98	100 km
	r2i1p1f1		
EC-Earth3	r11i1p1f1	4.2	79 km
EC-Earth3-Veg (× 2)	r12i1p1f1	4.31	79 km
	r14i1p1f1		
NorESM2-MM	r1i1p1f1	2.5	100 km
CMCC-CM2-SR5	r1i1p1f1	3.52	100 km
CMCC-ESM2	r1i1p1f1	3.57	100 km
ACCESS-ESM1-5	r1i1p1f1	3.87	250 km
EC-Earth3-Veg	r1i1p1f1	4.31	79 km
CNRM-ESM2-1	r1i1p1f2	4.76	110 km

[a]This planned large ensemble of high-resolution RCMs will allow a more accurate quantification of climate change uncertainty, which is of particular importance when assigning confidence levels to projections of extreme events.

Table 1.4. Details of the completed ensemble of RCM–CMIP6 simulations analysed as part of the current study. The columns present information on the RCM, CMIP6 ESM (number in brackets indicates the number of separate ESM realisations downscaled), ESM realisation ensemble identifiers, nesting strategy and historical (1980–2014) and future SSP–RCP (2015–2100) simulations

RCM	CMIP6 ESM	ESM ensemble members	RCM nesting strategy	Historical (no. RCM runs)	SSP1-2.6 (no. RCM runs)	SSP2-4.5 (no. RCM runs)	SSP3-7.0 (no. RCM runs)	SSP5-8.5 (no. RCM runs)
WRF	EC-Earth AOGCM (× 1)	r11i1p1f1	20 km → 4 km	1980–2014 (1)	2015–2100 (1)	2015–2100 (1)	2015–2100 (1)	2015–2100 (1)
WRF	EC-Earth-Veg (× 2)	r12i1p1f and r14i1p1f1	20 km → 4 km	1980–2014 (2)	2015–2100 (2)	2015–2100 (2)	2015–2100 (2)	2015–2100 (2)
WRF	MPI-ESM1-2-HR (× 2)	r1i1p1f1 and r2i1p1f1	20 km → 4 km	1980–2014 (2)	2015–2100 (2)	2015–2100 (2)	2015–2100 (2)	2015–2100 (2)
COSMO-CLM5	EC-Earth-Veg (× 2)	r12i1p1f and r14i1p1f1	12 km → 4 km	1980–2014 (2)	2015–2100 (2)	2015–2100 (2)	2015–2100 (2)	2015–2100 (2)
COSMO-CLM5	MPI-ESM1-2-HR (× 2)	r1i1p1f1 and r2i1p1f1	12 km → 4 km	1980–2014 (2)	2015–2100 (2)	2015–2100 (2)	2015–2100 (2)	2015–2100 (2)
COSMO-CLM5	MIROC6 (× 1)	r1i1p1f1	12 km → 4 km	1980–2014 (1)	2015–2100 (1)	2015–2100 (1)	2015–2100 (1)	2015–2100 (1)

1.4.1 Changes in the distribution of climate fields

To provide a more comprehensive examination of climate change, projected changes in the standard deviation are considered in the context of changes in the mean. Analyses of changes in the standard deviation provide information on projected changes in the shape (or variability) of the distribution of a climate field. In particular, analyses of changes in the mean and standard deviation provide a more comprehensive understanding of projections of extreme events. To illustrate this concept, Figure 1.3 presents a schematic of past and future probability distributions
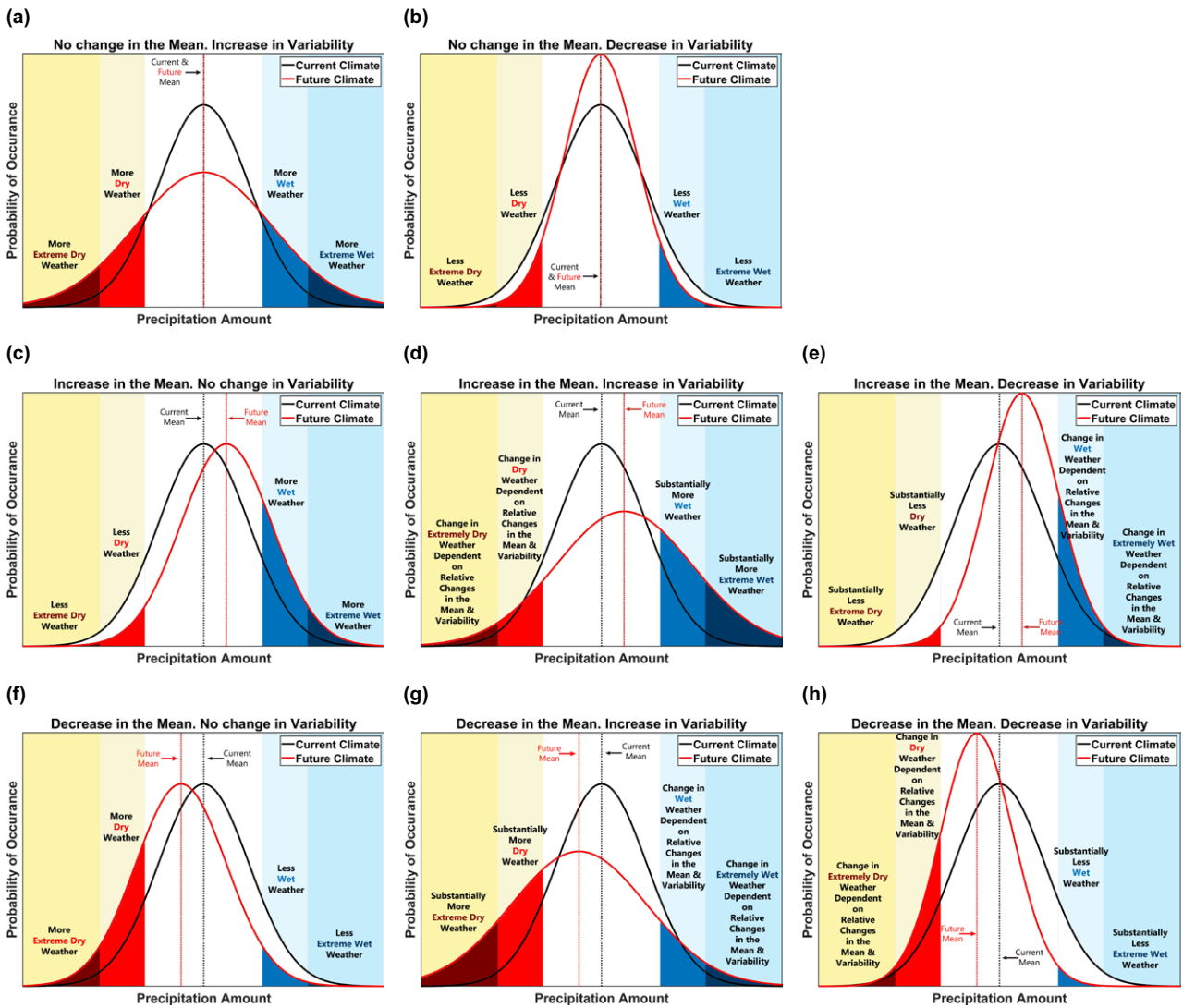
Figure 1.3. Schematic illustrating the effects of changes in the mean and standard deviation (SD) on the probability of low and high precipitation for (a) increase in SD with no change in the mean; (b) decrease in SD with no change in the mean; (c) increase in the mean with no change in SD; (d) increase in the mean and SD; (e) increase in the mean and decrease in SD; (f) a decrease in the mean with no change in SD; (g) decrease in the mean and increase in SD; and (h) decrease in the mean and SD.

of precipitation.[9] For example, Figure 1.3a presents a future with no change in mean precipitation and an increase in the standard deviation. In this future world, the total amount of precipitation remains constant, with an increase in both dry and wet events (i.e. increased variability). Conversely, Figure 1.3b shows that a decrease in variability, coupled with no change in mean precipitation, results in a decrease in both dry and wet events. Other combinations of changes in the mean and standard deviation, and their effects on the

tails of the distribution, are presented in Figure 1.3c–h. These figures will be referred to when discussing the projected changes in future distributions of temperature, precipitation and wind speed (Chapter 3).

1.4.2 Overview of climate projection uncertainty

Climate change projections are subject to uncertainty, which limits their utility. Fronzek *et al*. (2012) suggest

---

9 The figures are schematic representations of the distribution of standardised precipitation data. The distribution of raw precipitation data does not generally follow a normal distribution. The purpose of Figure 1.3 is simply to illustrate the concepts of how projected changes in the mean and variance can lead to substantial changes in the extremes.

that there are four main sources of uncertainty: (1) the natural variability of the climate system; (2) uncertainties on account of the formulation of the models themselves; (3) uncertainties in the future regional climate because of the coarse resolution of ESMs; and (4) uncertainties in the future atmospheric composition, which affects the radiative balance of the Earth. The uncertainties arising from (1) and (2) can be addressed, in part, by employing a multi-model ensemble approach (Déqué *et al*., 2007; van der Linden and Mitchell, 2009; Jacob *et al*., 2014) using the most up-to-date climate models. The ensemble approach of the current project analysed the output of two RCMs, driven by several ESMs, to simulate climate change (see Table 1.4). Through the ensemble approach, the uncertainty in the projections can be partly quantified, providing a measure of confidence in the predictions. The uncertainty arising from (3) is addressed in the current work by running the RCM simulations at the high spatial resolution of ≈4 km grid spacings. To account for the uncertainty arising from (4), the future climate is simulated under all four tier-1 SSP–RCPs (SSP1-2.6, SSP2-4.5, SSP3-7.0 and SSP5-8.5).

A disagreement between RCM ensemble projections can result in large individual outliers, skewing the mean[10] ensemble projection. For this reason, it can be informative to also consider percentiles when analysing an ensemble of future projections. In this study, a projection is defined as "not robust" (or "uncertain") if the 33rd and 66th percentiles of the ensemble of projections differ in sign. This is equivalent to ≤66% of the ensemble members agreeing on the sign of the projected change. Conversely, a projection is defined as "robust"

(or more certain) if the 33rd and 66th percentiles of the ensemble of projections agree on the sign of projected change. This is equivalent to >66% of the ensemble members agreeing on the sign of the projected change.

The method of quantifying robustness/uncertainty in this report is consistent with "Approach B" of the IPCC AR6 reports, based on ≥80% of the models agreeing on the sign of change (see Gutiérrez *et al*., 2021, their Cross-Chapter Box Atlas.1). It is noted that (as is the case with the current report) "model agreement is computed using "model democracy" (i.e. without discarding/weighting models)". The IPCC AR6 uses a second, more advanced ("Approach C"), quantification of robustness based on both *model agreement* (≥80% threshold) and *significance* (relating the multi-model mean climate change signal to internal variability). Different thresholds (along with tests of significance) have been used in previous IPCC reports and in the literature. In CORDEX studies, 80% has been widely used (Dosio and Fischer, 2018; Rana *et al*., 2020). The IPCC special reports IPCC SR1.5 (Hoegh-Guldberg *et al*., 2018) and the *Special Report on the Ocean and Cryosphere in a Changing Climate* (IPCC, 2019) used the ≥66% model agreement threshold to characterise robustness. Once the ensemble size of regional climate projections for Ireland is expanded, the quantification of robustness/uncertainty will be extended to include both *model agreement* (≥80% threshold) and *significance*, similar to the IPCC AR6 "Approach C" (Gutiérrez *et al*., 2021, their Cross-Chapter Box Atlas.1). See Chapter 5 for preliminary climate projections for Ireland with robustness/uncertainty characterised by both *model agreement* (≥80% threshold) and *significance.*

---

10 The mean, as opposed to the median, of the ensemble of projections is presented in the climate projection figures of this report (e.g. Figure 1.4). The main disadvantage of the median is that the variability of the ensemble members may not be captured (in particular, outliers are not represented). Conversely, the mean may be skewed by large outliers. While both metrics have merit, the ensemble mean is analysed for all such projection figures in this report, as it is the most commonly used metric in climate projections analysis and the results can be compared with similar national (e.g. Nolan and Flanagan, 2020; O'Brien and Nolan, 2023) and international climate projection studies (e.g. Jacob *et al*., 2014; Gutiérrez *et al*., 2021). For each figure, the median of the ensemble of projections (averaged over Ireland) is presented in the accompanying table (e.g. Table 1.5).

Box 1.1. How to interpret climate change figures and tables in this report

To explain how the projection figures and tables of the current report should be interpreted, consider Figure 1.4, the spatial distribution of mean winter change in precipitation (%) for three future 30-year time periods (2021–2050, 2041–2070 and 2071–2100) relative to 1981–2010. The figure presents the ensemble mean of projected changes (colour shading) and areas where ≤66% of the ensemble members agree on the sign of the projected change (hatching). The abundance of hatching in Figure 1.4 for the earlier time periods and lower SSP–RCPs demonstrates disagreement between ensemble members and higher uncertainty in the winter precipitation projections (for these time periods and SSP–RCPs). Conversely, the scarcity of hatching for SSP3-7.0 and SSP5-8.5 during 2041–2070 and 2071–2100 demonstrates agreement (>66% agree on the sign of projection) between ensemble members and higher certainty in winter precipitation projections for these time periods and SSP–RCPs.

The uncertainty in the precipitation projections is further quantified in Table 1.5, which presents the mean and 33rd, 50th (median) and 66th percentiles of the ensemble of winter precipitation projections averaged over all land points. It is noted that, for SSP2-4.5 (2071–2100) and for SSP3-7.0 and SSP5-8.5 (2041–2070 and 2071–2100), the 33rd and 66th percentile statistics have the same sign (highlighted within the red outline border), indicating that over 66% of the ensemble members agree on the sign of the projected change. Furthermore, the small spread between the statistics[11] adds confidence to the projections. In conclusion, the projected increases in precipitation during winter have higher certainty for the higher SSP–RCPs and later time periods, with *robust* (i.e. 33rd percentile (P33) and 66th percentile (P66) statistics have the same sign) increases (averaged over country) ranging from 2.9% for SSP2-4.5 (2041–2070) to 9.8% for SSP5-8.5 (2071–2100).

A similar figure, table and analysis is provided for every climate projection discussed in this report.

This method of analysing percentiles allows a better understanding of climate change uncertainty and allows quantification of conservative and robust ("likely") projections. Conversely, the likelihood method allows policymakers to consider more "unlikely" (and possibly high-impact) climate projections. In this report, *likelihood* definitions that are consistent with the IPCC AR5 and AR6 reports are used. For example, Table 1.5 shows that the robust (highlighted within red outline border) winter projections for SSP5-8.5 (2071–2100) show that over 67% (P33) of the ensemble members project an increase of 6.5% in winter precipitation. That is to say, it is "likely" that increases in winter precipitation will be greater than or equal to this value[12] (for this scenario and time period). Similarly, the 50th percentile statistic (P50) provides information on the "as likely as not" projection. The P66 statistic provides information on the "unlikely" projection and can be useful for the analysis of high-impact, low-probability projections. For example, the *unlikely* winter projection for SSP5-8.5 (2071–2100) (Table 1.5) is an increase of 13% in precipitation. These definitions, based on an ensemble of 10 members for each SSP–RCP and 30-year time period, provide a statistically based descriptive measure of the climate change projection uncertainty. Other likelihood definitions (see Chapter 5) include "very likely" (≥90% agreement) and "very unlikely" (<10% agreement).

---

11 The spread is defined as "small" if the signal to noise ratio, $SNR = \frac{|\mu|}{\sigma} > 1$, where μ and σ are the mean and standard deviation, respectively.

12 The ensembles members project general increases in winter precipitation (the magnitude of projections increase with increasing percentiles), so the 33rd percentile is denoted the "likely" projection in this case. Conversely, if projections are generally negative (magnitude of projections decrease with increasing percentiles), the 66th percentile is denoted the "likely" projection. An example of this is the projected decrease in summer precipitation (Table 3.12, fourth panel).

Box 1.1. Continued

Winter Ensemble Mean Precipitation Change w.r.t 1981-2010
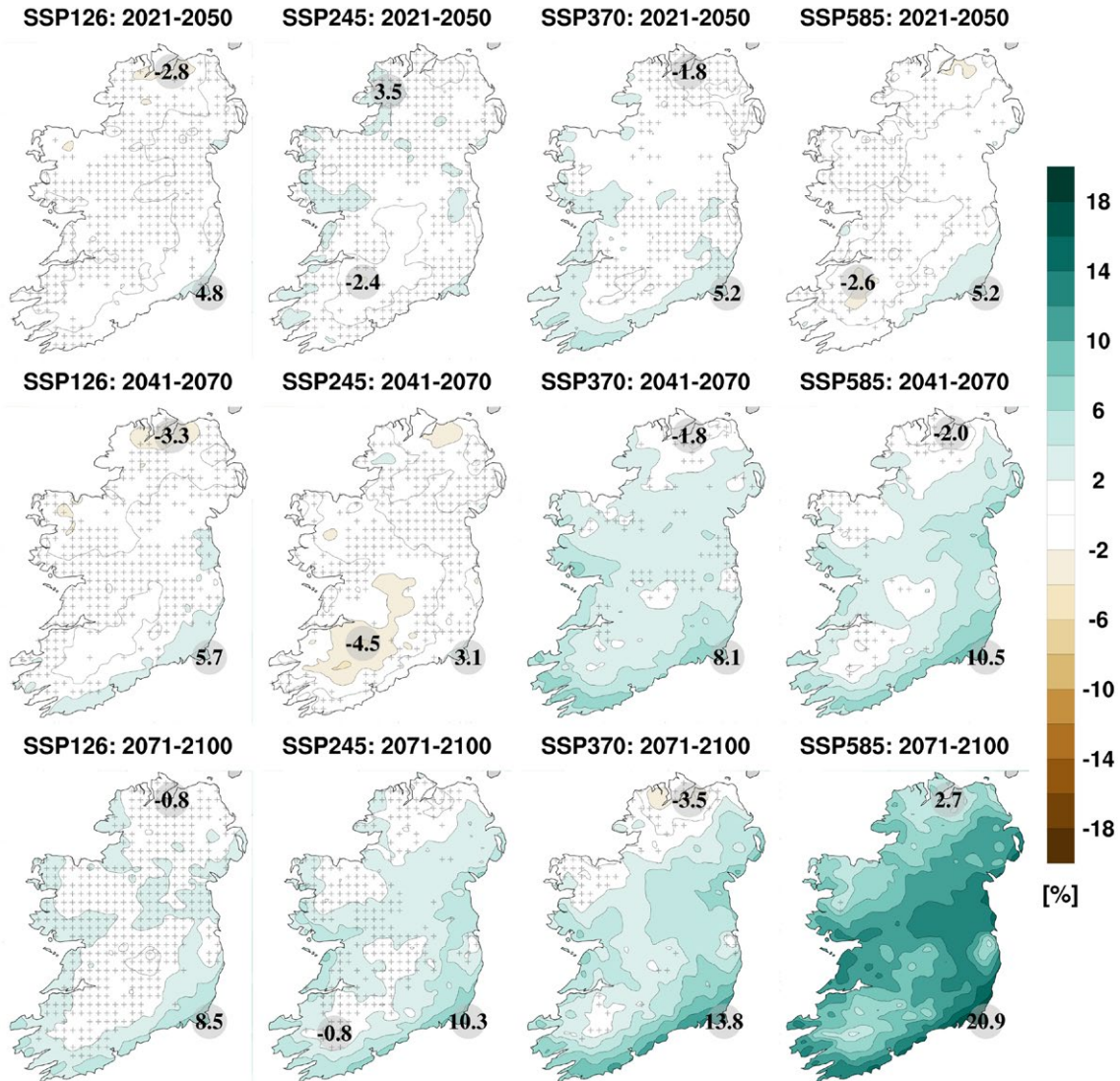
Figure 1.4. RCM–CMIP6 ensemble projections of mean winter precipitation (%). All RCM ensemble members were run with 4 km grid spacing. In each case, the future 30-year period is compared with the past period, 1981–2010. The results were obtained from analysing 10 SSP1-2.6, 10 SSP2-4.5, 10 SSP3-7.0 and 10 SSP5-8.5 RCM simulations. The colour shading represents the ensemble mean of projected changes, and the numbers included on each plot are the minimum and maximum projected changes, displayed at their locations. Hatchings (+) indicate areas where the 33rd and 66th percentiles of projections disagree on the sign of change and highlight areas of uncertainty.

Box 1.1. Continued

Table 1.5. Winter precipitation projections (%). This table corresponds to Figure 1.4 and shows the 33rd (*likely* within red border) percentile, 50th (*as likely as not*) percentile, mean and 66th (*unlikely* within red border) percentile averaged over the island of Ireland. A small spread, and same sign of projection, between statistics corresponds to higher certainty in the projections. Conversely, large spread (and disagreement in sign) corresponds to higher uncertainty

	Winter precipitation (%)															
	SSP1-2.6				SSP2-4.5				SSP3-7.0				SSP5-8.5			
Time period	P33	P50	Mean	P66	P33	P50	Mean	P66	P33	P50	Mean	P66	P33	P50	Mean	P66
2021–2050	−2.1	−0.7	−0.2	2.3	−2.3	−1.2	1.0	2.6	−0.3	1.0	1.4	3.2	−0.9	0.1	0.2	1.7
2041–2070	−2.6	−1.5	0.3	1.4	−2.4	−1.4	−0.5	0.9	1.0	2.2	3.2	5.1	1.5	2.4	3.1	4.7
2071–2100	−1.4	−0.3	2.0	4.6	0.2	1.9	2.9	5.3	2.2	3.4	4.0	5.8	6.5	9.3	9.8	13

Note that the accuracy of these statistical descriptions is based on the assumption that the ensemble members represent an unbiased sampling of the (unknown) future climate. It is also important to stress that the likelihood values presented in the current study (and similarly in studies such as Murphy *et al*., 2009; IPCC, 2013, 2021; Lowe *et al*., 2018; Nolan and Flanagan, 2020) are derived from the most up-to-date evidence available. Therefore, the "likelihood" values apply only to the specific sets of high-resolution models and experimental design of the current study. Future improvements in modelling will alter the projections, as uncertainty is expected to be further reduced. Future work will focus on reducing this uncertainty by greatly increasing the ensemble size and employing more up-to-date RCMs (including fully coupled atmosphere–ocean–wave models) to downscale additional CMIP6 ESMs (see Table 1.3). Furthermore, the RCM data will be provided to the Met Éireann TRANSLATE project (O'Brien and Nolan, 2023; O'Brien *et al*., 2024) to be statistically downscaled and bias-corrected with the aim of providing standardised future climate projections for Ireland.

2   Regional Climate Model Validations

The RCM configurations were validated by running simulations of the past Irish climate for the period 1981–2010, driven by both fifth-generation ECMWF atmospheric reanalysis of the global climate (ERA5) (Hersbach *et al*., 2020) and the CMIP6 ESM datasets, and comparing the output against observational data. Uncertainty estimates of bias and mean absolute error (MAE) were calculated for precipitation and 2 m temperature, utilising gridded datasets of observations made available by Met Éireann (Walsh 2016, 2017).

Figure 2.1 compares observed mean annual precipitation for 1981–2010 (top left panel) with precipitation resolved by the COSMO-CLM5– ERA5 and the downscaled CMIP6 simulations. It is noted that the COSMO-CLM5–ERA5 and downscaled CMIP6 data accurately capture the magnitude and spatial characteristics of the historical precipitation climate, e.g. higher rainfall amounts in the west and over mountains. WRF was found to generally overestimate precipitation, whereas COSMO-CLM5 underestimates it.

Figure 2.2 shows that the percentage errors range from approximately –35% to approximately +30% for the WRF and COSMO-CLM5 RCMs. The percentage error at each grid point (i, j) is given by:

$$per\_bias_{(i,j)} = 100 \times \left(\frac{bias_{(i,j)}}{OBS_{(i,j)}} \right) \qquad (2.1)$$

where

$$bias_{(i,j)} = \overline{RCM}_{(i,j)} - \overline{OBS}_{(i,j)} \qquad (2.2)$$

and the $\overline{RCM}_{(i,j)}$ and $\overline{OBS}_{(i,j)}$ terms represent the RCM and observed values, respectively, at grid point (i, j), averaged over the period 1981–2010.

Figure 2.2 highlights a clear underestimation of precipitation over the mountainous regions for the COSMO-CLM5 model. This is probably because the COSMO-CLM5 RCM underestimates heavy precipitation; previous validation studies (e.g. Nolan *et al*., 2017) have demonstrated a decrease in RCM skill with increasing magnitude of heavy precipitation events. Note that the high-resolution RCM data were found to consistently outperform both the underlying low-resolution RCM and global model data. To quantify the overall bias evident in Figure 2.2, the mean was calculated over all grid points covering Ireland (Table 2.1, second column).

The bias metric allows the evaluation of the systematic errors of the RCMs, but this can hide large errors, as positive and negative values can cancel each other out. For this reason, the percentage MAE metric was also used to evaluate the RCM precipitation errors:

$$per\_MAE_{(i,j)} = 100 \times \left(\frac{MAE_{(i,j)}}{OBS_{(i,j)}} \right) \qquad (2.3)$$

where

$$MAE_{(i,j)} = \left| \overline{RCM}_{(i,j)} - \overline{OBS}_{(i,j)} \right| \qquad (2.4)$$

Again, the mean was calculated over all grid points covering Ireland (Table 2.1, third column). The percentage bias values range from 1.55% (COSMO-CLM5–MPI-ESM1-2-HR-r2i1p1f1) to 34.21% (WRF–MPI-ESM1-2-HR-r1i1p1f1) and the percentage MAE values range from 9.59% (COSMO-CLM5–EC-Earth3-Veg-r12i1p1f1) to 34.23% (WRF–MPI-ESM1-2-HR-r1i1p1f1). While the WRF biases are generally larger, it is noted that the bias and MAE are similar (i.e. the sign of the bias is consistent over the country). This is desirable for the bias-correcting that will be carried out as part of the Met Éireann TRANSLATE project. It should be noted that the observed precipitation dataset has a margin of error of approximately ±10%, so the RCM validations should be considered within this context.

Figure 2.3 compares observed mean annual 2 m temperature for 1981–2010 (top left panel) with temperature resolved by the COSMO-CLM5– ERA5 and the downscaled CMIP6 simulations. It is noted that the COSMO-CLM5–ERA5 and downscaled CMIP6 data accurately capture the spatial characteristics of the historical temperature climate. The bias is presented in Figure 2.4; all RCMs exhibit a cold bias, except for COSMO-CLM5–ECEarth3-Veg-r14i1p1f1 (slight warm bias), with the bias pronounced for WRF. The largest cold bias is noted for WRF–ECEarth3-r11i1p1f1. This is attributed to the slight cold bias of the WRF model and the fact that the
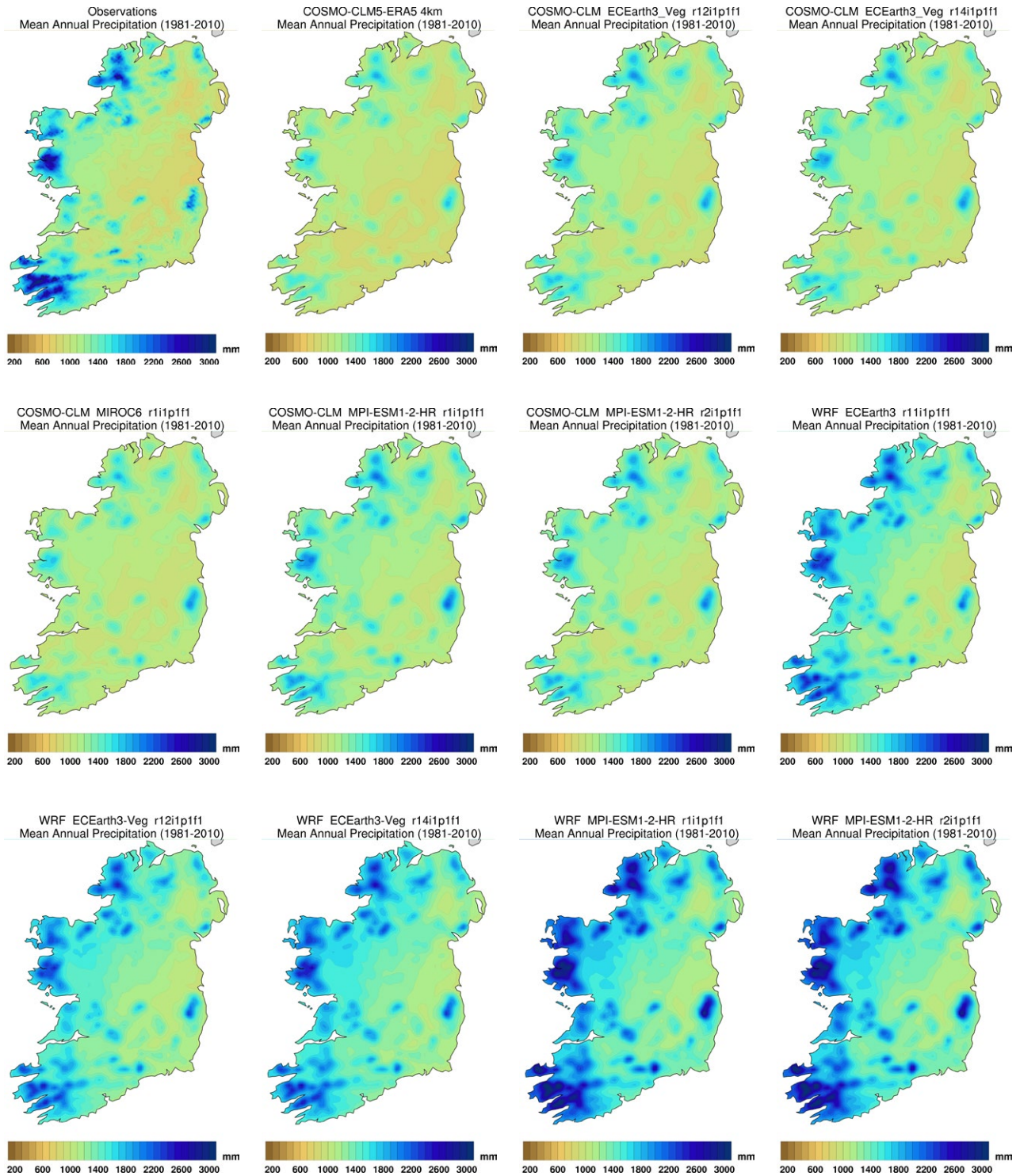
Figure 2.1. Mean annual precipitation (mm) (1981–2010) for observations, COSMO-CLM5–ERA5 and the RCM–CMIP6 ensemble members.

driving ESM (EC-Earth3-r11i1p1f1) has a large cold bias (Nolan and McKinstry, 2020).

The bias and MAE values for 2 m temperature are presented in Table 2.2; bias values range from –0.14°C (COSMO-CLM5–ERA5) to –2.23°C (WRF–EC-Earth-r11i1p1f1), and MAE values range from 0.21°C (COSMO-CLM5–ERA5) to 2.23°C (WRF–EC-Earth-r11i1p1f1). While the WRF biases are generally larger, it is noted that the bias and MAE are similar (i.e. the sign of the bias is consistent). This is desirable for the bias-correcting that will be carried out as part of the Met Éireann TRANSLATE project.
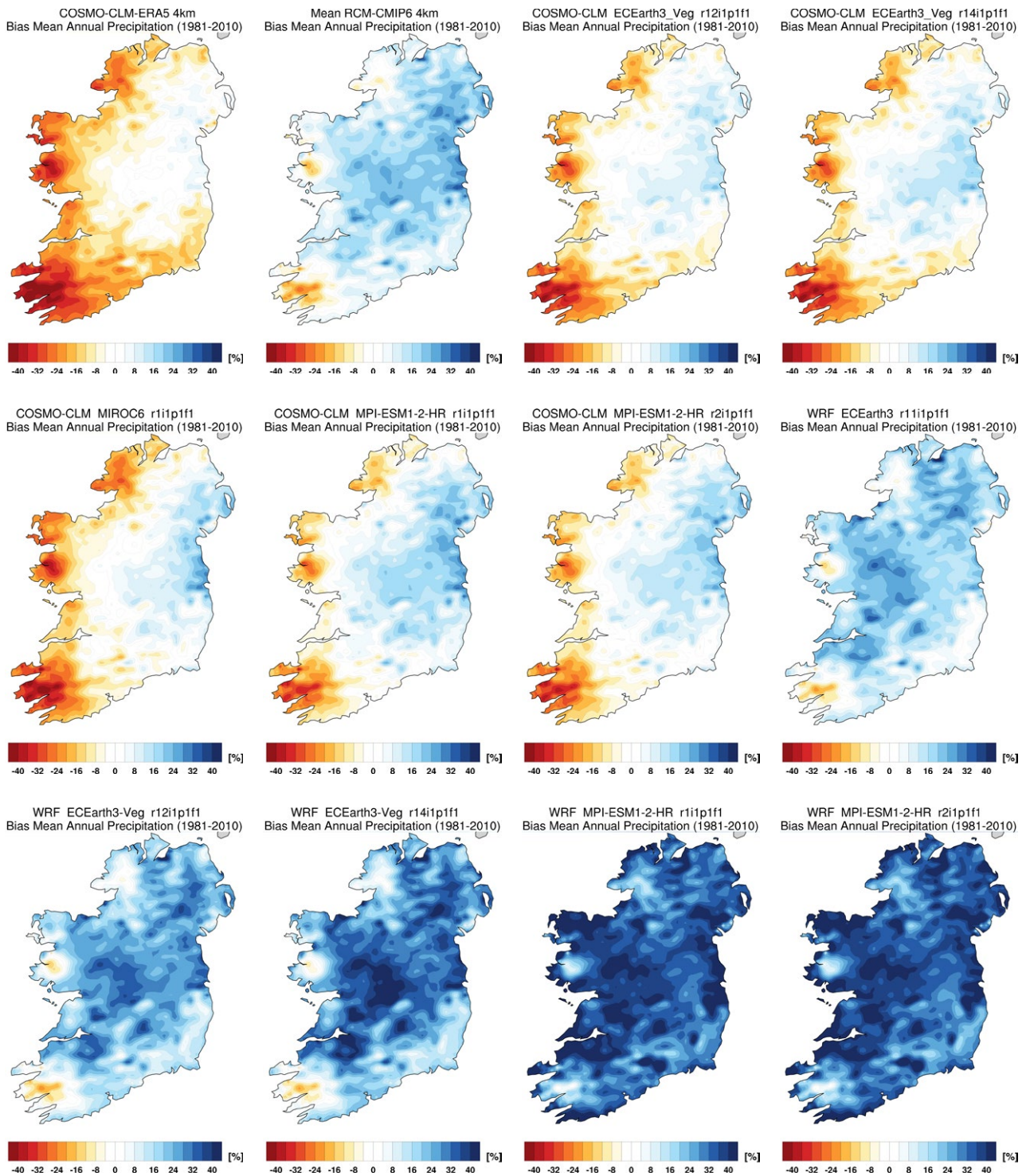
Figure 2.2. Annual precipitation bias (%) (1981–2010) for COSMO-CLM5–ERA5 and RCM–CMIP6 ensemble members and mean of RCM–CMIP6 ensemble.

The observed gridded 2 m temperature dataset has an estimated MAE of 0.19°C and a root mean square error of 0.41°C, so the RCM validations should be considered within this context.

For an in-depth validation of additional climate fields (e.g. wind speed, humidity, radiation, derived climate

indices) please refer to Nolan *et al*. (2014, 2017), Nolan (2015), Flanagan *et al*. (2019), Werner *et al.* (2019), Flanagan and Nolan (2020) and Nolan and Flanagan (2020). Additional experiments were carried out to assess the added value of high-resolution RCM models, the results of which demonstrated

Table 2.1. Precipitation uncertainty estimates (%) found for COSMO-CLM5–ERA5, each RCM–CMIP6 ensemble member and mean of the RCM–CMIP6 ensemble, through comparison with Met Éireann gridded observations (1981–2010). For each metric, the best- and worst-performing scores are highlighted in blue and red text, respectively

RCM simulation	Bias (%)	MAE (%)
COSMO-CLM5–ERA5 4 km	−11.42	12.80
Mean RCM–CMIP6 4 km	12.56	14.27
COSMO-CLM5–EC-Earth3-Veg-r12i1p1f1	−3.25	9.59
COSMO-CLM5–EC-Earth3-Veg-r14i1p1f1	−2.30	10.08
COSMO-CLM5–MIROC6-r1i1p1f1	−3.53	11.23
COSMO-CLM5–MPI-ESM1-2-HR-r1i1p1f1	4.16	11.31
COSMO-CLM5–MPI-ESM1-2-HR-r2i1p1f1	1.55	10.22
WRF–EC-Earth3-r11i1p1f1	15.38	16.25
WRF–EC-Earth3-Veg-r12i1p1f1	20.03	20.83
WRF–EC-Earth3-Veg-r14i1p1f1	25.39	25.93
WRF–MPI-ESM1-2-HR-r1i1p1f1	34.21	34.23
WRF–MPI-ESM1-2-HR-r2i1p1f1	34.09	34.11

the improved skill of RCMs over the global models. Moreover, an increase in the spatial resolution of the RCMs was found to result in a general increase in skill (e.g. Nolan *et al*., 2017). Furthermore, it was shown that heavy precipitation events are more accurately resolved by the higher spatial resolution RCM data. However, it was found that, although the RCM accuracy increased with higher spatial resolution, reducing the horizontal grid spacing below 4 km provided relatively little added value (Nolan *et al*., 2017). Werner *et al*. (2019) completed a validation of agri-climate fields derived from downscaled ECMWF global atmospheric reanalysis (ERA-Interim) COSMO-CLM5 and WRF datasets. The authors compared derived fields, such as evapotranspiration and soil moisture deficits, with observations and found that both RCMs exhibit high skill, with WRF slightly outperforming COSMO-CLM5.
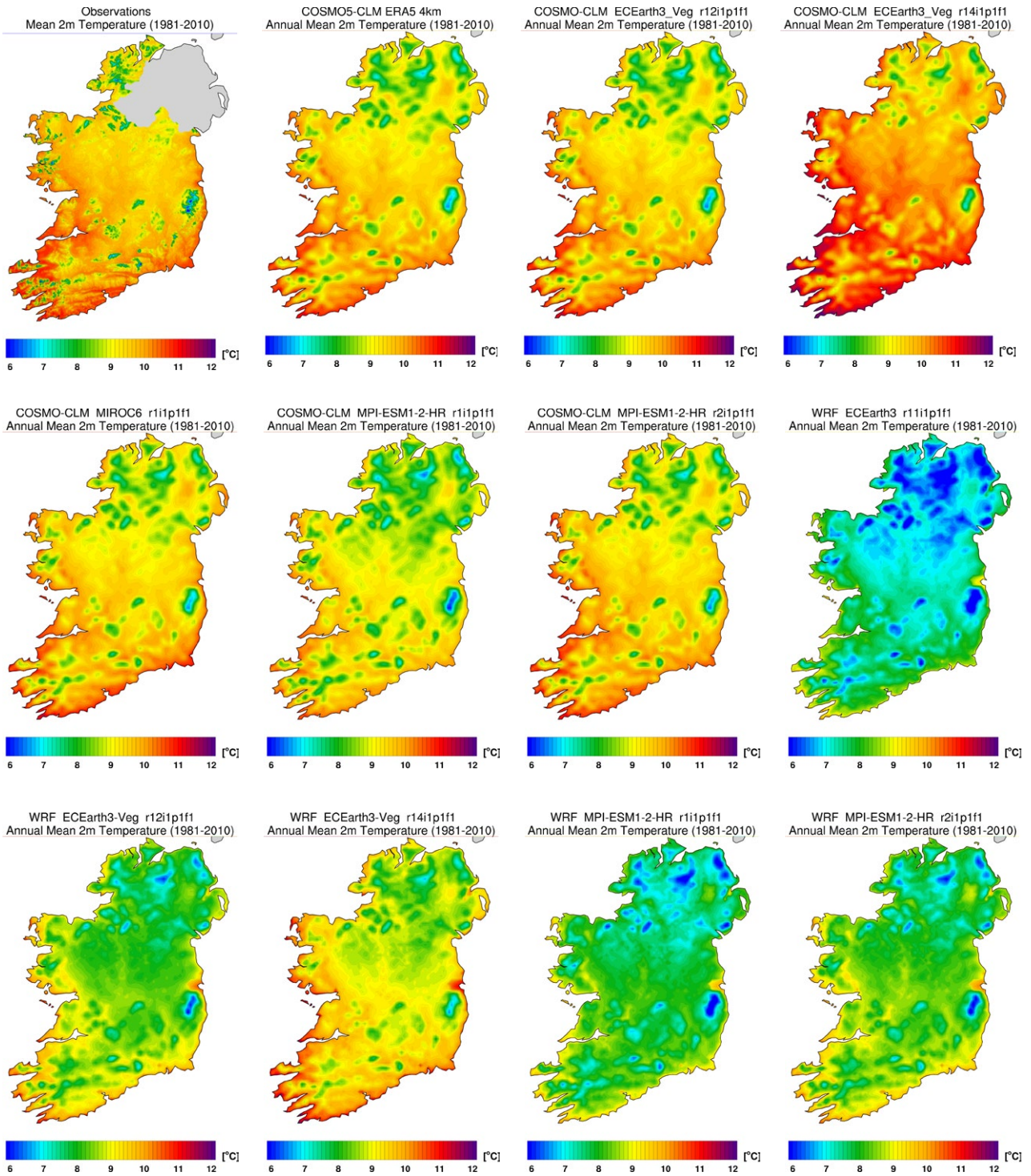
Figure 2.3. Mean annual 2 m temperature (°C) (1981–2010) for observations, COSMO-CLM5–ERA5 and RCM–CMIP6 ensemble members.
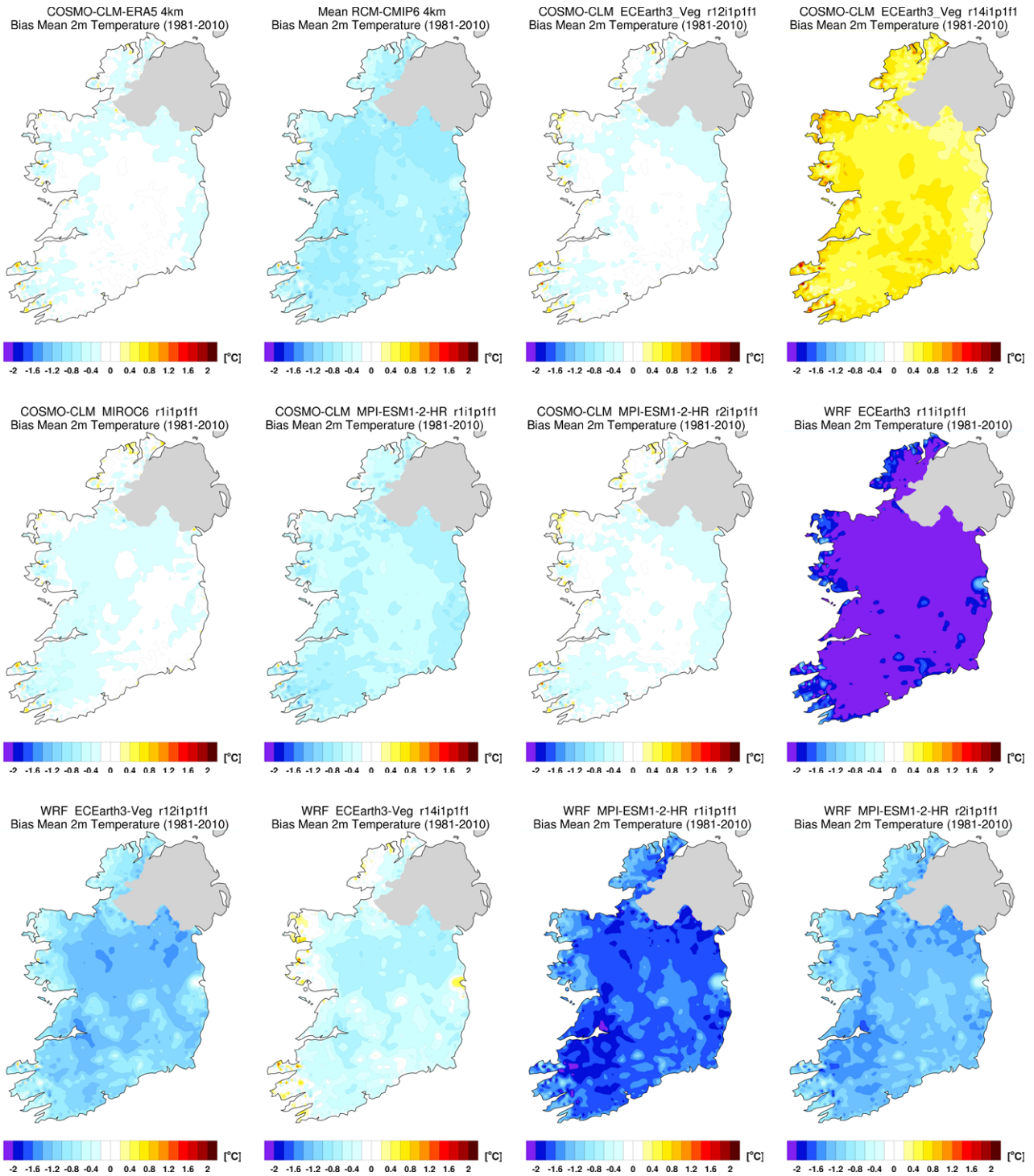
Figure 2.4. Annual mean 2 m temperature bias (1981–2010) for COSMO-CLM5–ERA5 and RCM–CMIP6 ensemble members, and mean of the RCM–CMIP6 ensemble. Data in this figure apply only to Ireland.

Table 2.2. Mean 2 m temperature uncertainty estimates (°C) found for COSMO-CLM5–ERA5 and each RCM–CMIP6 ensemble member, and mean of the RCM–CMIP6 ensemble, through comparison with Met Éireann gridded observations (1981–2010). For each metric, the best- and worst-performing scores are highlighted in blue and red, respectively

RCM simulation	Bias (°C)	MAE (°C)
COSMO-CLM5–ERA5 4 km	−0.14	0.21
Mean RCM–CMIP6 4 km	−0.72	0.73
COSMO-CLM5 EC-Earth3-Veg-r12i1p1f1	−0.15	0.23
COSMO-CLM5–EC-Earth3-Veg-r14i1p1f1	0.54	0.54
COSMO-CLM5–MIROC6-r1i1p1f1	−0.21	0.27
COSMO-CLM5–MPI-ESM1-2-HR-r1i1p1f1	−0.57	0.59
COSMO-CLM5– MPI-ESM1-2-HR-r2i1p1f1	−0.18	0.24
WRF–EC-Earth3-r11i1p1f1	−2.23	2.23
WRF–EC-Earth3-Veg-r12i1p1f1	−1.09	1.10
WRF–EC-Earth3-Veg-r14i1p1f1	−0.43	0.50
WRF–MPI-ESM1-2-HR-r1i1p1f1	−1.64	1.64
WRF–MPI-ESM1-2-HR-r2i1p1f1	−1.26	1.26

Data in this table apply only to Ireland.

3 Regional Climate Projections for Ireland

3.1 Temperature Projections

Figure 3.1 presents the spatial distribution of annual temperature changes for three future 30-year time periods (2021–2050, 2041–2070 and 2071–2100) relative to 1981–2010. The 30-year baseline period 1981–2010 is used in this report, as it had been the "climate normal" period recommended by the World Meteorological Organization (WMO, 2017). In 2021, the WMO updated the climate normal period to 1991–2020. However, it was not feasible to use this period for the climate change analysis in the current report, as the "future" CMIP6 SSP–RCP simulations start in 2015. The 1981–2010 period is also used as a baseline period (one of five) in the IPCC AR6 Interactive Atlas (Gutiérrez *et al*., 2021).
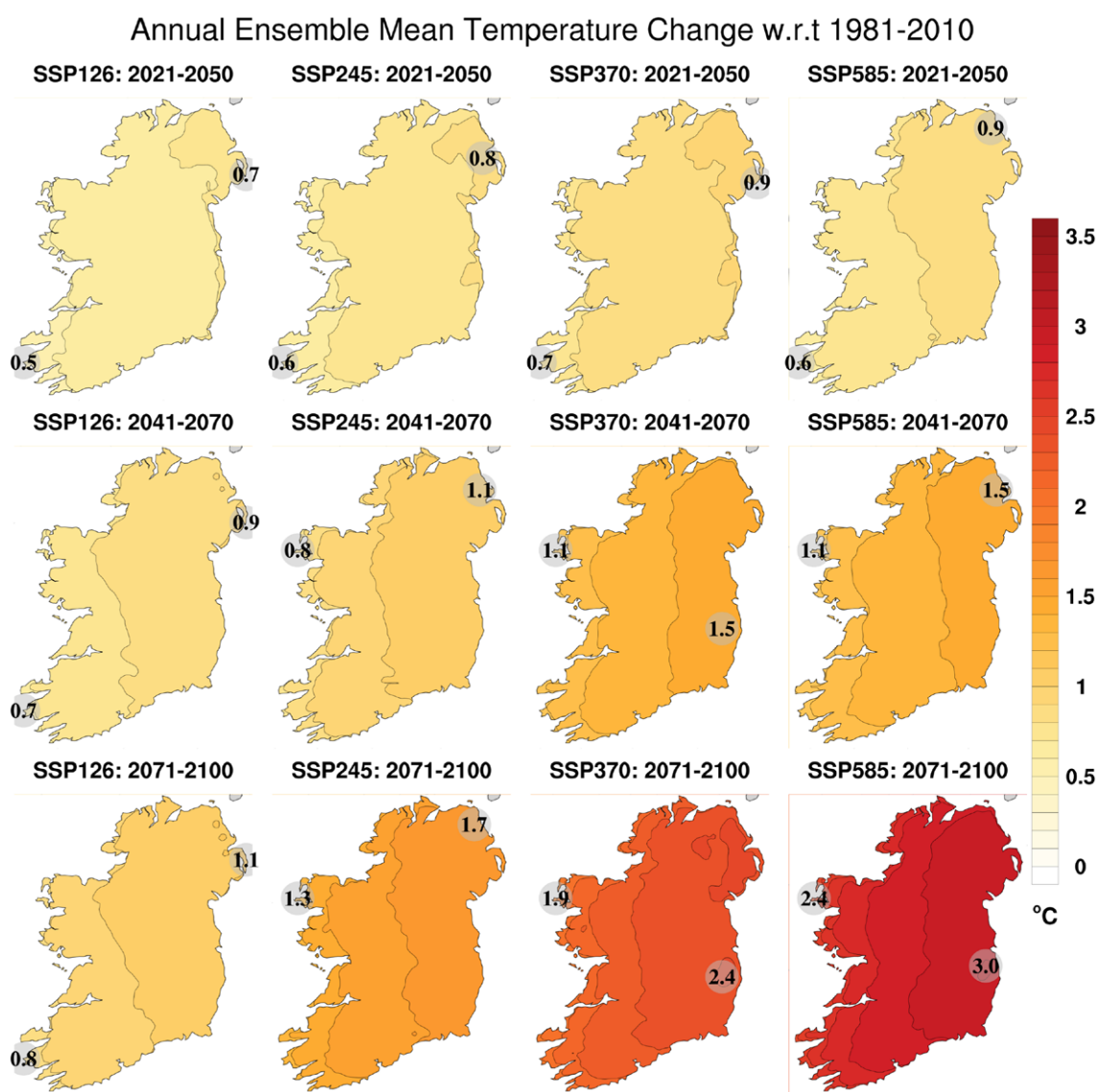
Figure 3.1. RCM–CMIP6 ensemble projections of mean annual 2 m temperature (°C). All RCM ensemble members were run with 4 km grid spacing. In each case, the future 30-year period is compared with the past period, 1981–2010. The results were obtained from analysing 10 SSP126, 10 SSP245, 10 SSP370 and 10 SSP585 RCM simulations. The numbers included on each plot are the minimum and maximum projected changes, displayed at their locations.

The mean annual temperature (Figure 3.1) is projected to increase by 0.5–3°C depending on the time period and SSP–RCP[13] scenario: 0.5–0.7°C for SSP126 (2021–2050) and 2.4–3.0°C for SSP585 (2071–2100). Temperature projections show a clear west-to-east gradient, with the largest increases in the east.

The seasonal temperature projections are presented in Figure 3.2; winter temperatures show increases ranging from 0.4°C in the south-west to 0.7°C in the north-east for SSP126, 2021–2050 (2.0°C in the west and 2.7°C in the north-east for SSP585, 2071–2100). The patterns for spring are similar to winter, with a
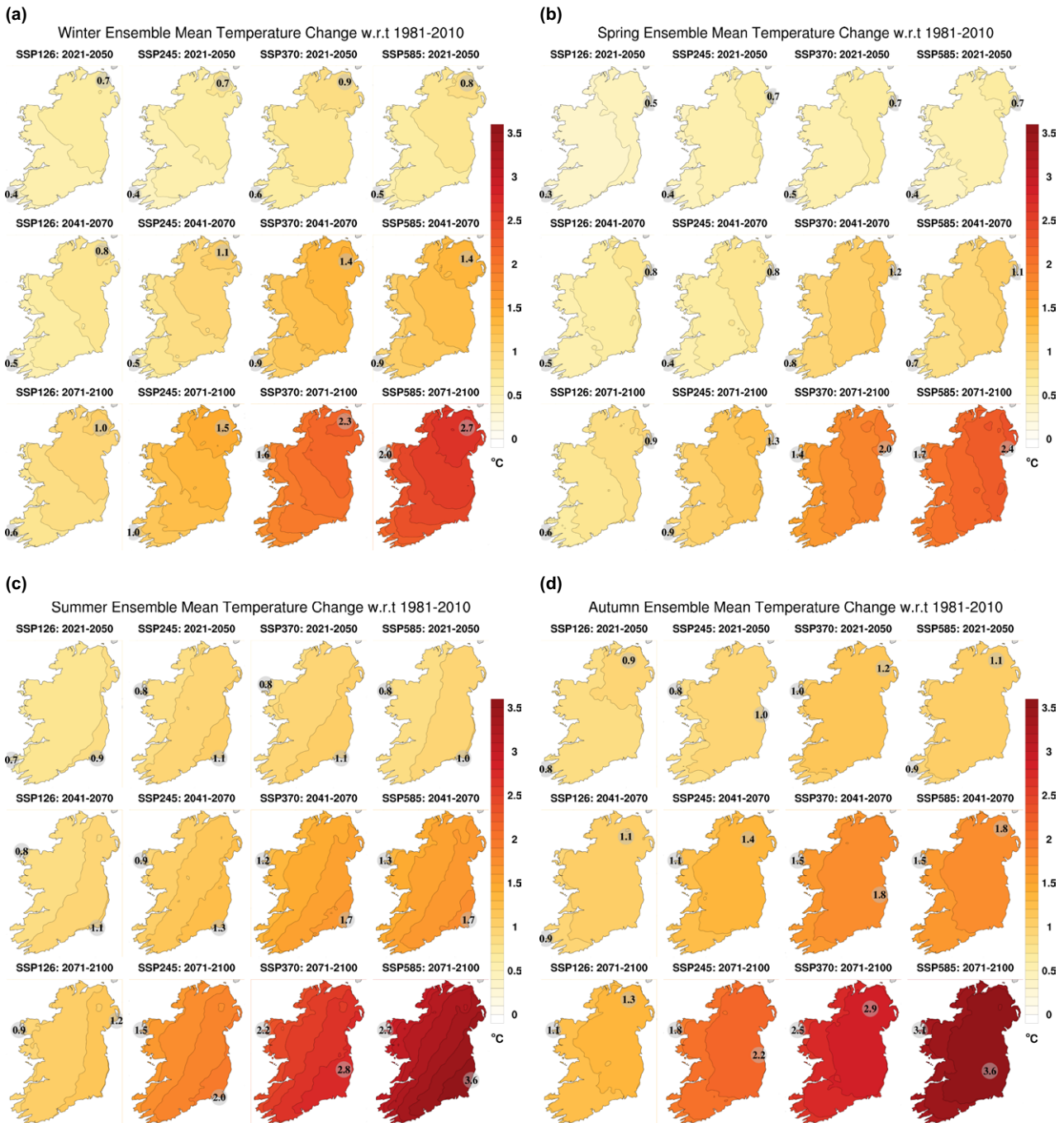
Figure 3.2. Seasonal RCM ensemble projections of mean 2 m temperature (°C) for (a) winter, (b) spring, (c) summer and (d) autumn. In each case, the future 30-year period is compared with the past period, 1981–2010. The numbers included on each plot are the minimum and maximum projected changes, displayed at their locations.

13 Henceforth, for simplicity, "SSP–RCP" will be referred to as "SSP". The individual SSP–RCP scenarios SSP1-2.6, SSP2-4.5, SSP3-7.0 and SSP5-8.5 will be referred to SSP126, SSP245, SSP370 and SSP585, respectively.

clear gradient from south-west to north-east in the projections, ranging from 0.3°C in the south-west (SSP126, 2021–2050) to 2.4°C in the north-east (SSP585, 2071–2100). The largest projected increases in temperature are noted for summer and autumn. Summer temperatures are projected to increase by 0.7°C in the west for SSP126 (2021–2050) and by 3.6°C in the south-east for SSP585 (2071–2100). Autumn temperatures are projected to increase by 0.8°C in the south-west for SSP126 (2021–2050) and by 3.6°C in the east for SSP585 (2071–2100). In summary, the temperature change gradient is from south-west to north-east in winter and spring, from north-west to south-east in summer and from west to east in autumn and over the full year. These projected changes and trends are consistent with previous studies (e.g. McGrath *et al*., 2005; McGrath and Lynch, 2008; Gleeson *et al*., 2013; Nolan, 2015; O'Sullivan *et al*., 2016; Nolan and Flanagan, 2020; O'Brien and Nolan, 2023) and all RCM–ESM–SSP simulations and future time periods assessed to date.

The absence of hatching (refer to Box 1.1, section 1.4.2, for an overview) in Figures 3.1 and 3.2 demonstrates agreement between ensemble members and assigns higher certainty to the temperature projections. To further quantify climate projection uncertainty, the mean and 33rd, 50th and 66th percentiles of annual and seasonal mean 2 m temperature projections averaged over all land points are presented in Table 3.1. For example, the annual statistics show that over 67% (P33) of the ensemble members project an annual increase in temperatures of 0.43°C and 1.99°C for the SSP126 (2021–2050) and SSP585 (2071–2100), respectively. That is to say, it is "likely" that increases in temperature will be greater than or equal to these values for these scenarios and time periods. Similarly, the 50th percentile figures (P50) provide information on the "as likely as not" projection. The 66th percentile (P66) provides information on the "unlikely" projection and can be useful for the analysis of high-impact, low-probability projections. Furthermore, the small spread (and the same sign of projections) between the statistics, as is evident across all seasons, SSPs and time periods, adds confidence to the projections.[14]

To evaluate projected changes in the future variability of temperature, changes (°C) in the standard deviation of average daily temperature were analysed.[15] The projected change in standard deviation of average daily temperature for each RCM ensemble member was calculated and the mean (of the ensemble of projections) is considered for each SSP and time period. The annual change in the standard deviation of 2 m temperature (Figure 3.3) shows small increases of between 0°C and 0.5°C. Similarly, the seasonal projected changes in the standard deviation of temperature are small (Figure 3.4); small decreases (increases) are noted for winter and spring (summer) and a mixed signal is noted for autumn. It should be noted that large increases in the mean summer temperature (Figure 3.2c) coupled with increases in the standard deviation will lead to enhanced increases in extreme high temperatures (refer to Figure 1.3d for a schematic example of such an outcome). Similarly, increases in mean winter and spring temperature (Figure 3.2a,b) coupled with a decrease in standard deviation will lead to enhanced decreases in extreme low temperatures (refer to Figure 1.3e for a schematic example of such an outcome). However, it should be noted that the projected changes in standard deviation are small for all seasons. The results suggest that, while future temperatures will increase substantially for all seasons, the shape of the temperature distribution will remain broadly similar (refer to Figure 1.3c for a schematic example of such an outcome).

3.2 Extreme Temperature Projections

Changes in the daily maximum and daily minimum temperatures are arguably of more importance, since extreme events have an abrupt and much larger impact on lives and livelihoods than a gradual change in mean values (Easterling *et al*., 2000; O'Sullivan *et al*., 2016). A sustained increase in the daily maximum temperature is associated with summer heatwaves whereas an increase in the daily minimum temperature will typically imply warmer nights. Figure 3.5a shows how the warmest 5% of daily maximum temperatures (TX95) are projected to change. A strong warming is evident, which is

---

14 It is noted that for the earlier time periods and lower SSPs, the mean is sometimes greater than P66. This is due to the large COSMO-CLM5–EC-Earth r11 outlier, as discussed in Chapter 2.

15 Refer to section 1.4.1 for an overview of the effects of changes in the standard deviation on the distribution of a climate field.

Table 3.1. Annual and seasonal 2 m temperature projections (°C). This table corresponds to the projections (°C) of Figures 3.1 and 3.2, and shows the 33rd percentile, 50th percentile, mean and 66th percentile averaged over the island of Ireland (land points). A small spread and the same sign of projection between statistics corresponds to higher certainty in the projections. Conversely, large spread corresponds to higher uncertainty

Annual 2 m temperature (°C)

Time period	SSP126				SSP245				SSP370				SSP585			
	P33	P50	Mean	P66	P33	P50	Mean	P66	P33	P50	Mean	P66	P33	P50	Mean	P66
2021–2050	0.43	0.47	0.66	0.56	0.4	0.49	0.75	0.58	0.4	0.7	0.86	0.85	0.41	0.45	0.79	0.73
2041–2070	0.48	0.54	0.81	0.66	0.49	0.6	1	0.72	0.93	1.03	1.36	1.3	0.78	0.85	1.36	1.32
2071–2100	0.32	0.58	1.01	1.26	0.84	0.88	1.57	1.91	1.61	1.8	2.29	2.46	1.99	2.43	2.85	3.26

Winter 2 m temperature (°C)

Time period	SSP126				SSP245				SSP370				SSP585			
	P33	P50	Mean	P66	P33	P50	Mean	P66	P33	P50	Mean	P66	P33	P50	Mean	P66
2021–2050	0.31	0.44	0.6	0.55	0.23	0.26	0.6	0.72	0.36	0.46	0.75	0.57	0.39	0.43	0.7	0.62
2041–2070	0.41	0.5	0.68	0.64	0.34	0.47	0.88	0.63	0.89	0.99	1.24	1.11	0.7	0.88	1.2	1.12
2071–2100	0.13	0.55	0.88	1.18	0.69	0.85	1.3	1.65	1.59	1.67	2.02	1.98	1.89	2.39	2.48	2.75

Spring 2 m temperature (°C)

Time period	SSP126				SSP245				SSP370				SSP585			
	P33	P50	Mean	P66	P33	P50	Mean	P66	P33	P50	Mean	P66	P33	P50	Mean	P66
2021–2050	0.08	0.13	0.39	0.58	0.15	0.27	0.55	0.5	0.2	0.38	0.58	0.56	0.09	0.24	0.53	0.44
2041–2070	0.21	0.24	0.63	0.51	0.15	0.19	0.67	0.4	0.57	0.67	1.03	0.87	0.4	0.54	0.93	0.66
2071–2100	0.07	0.23	0.78	0.9	0.37	0.47	1.11	1.14	1.18	1.31	1.77	1.61	1.43	1.67	2.14	2.28

Summer 2 m temperature (°C)

Time period	SSP126				SSP245				SSP370				SSP585			
	P33	P50	Mean	P66	P33	P50	Mean	P66	P33	P50	Mean	P66	P33	P50	Mean	P66
2021–2050	0.47	0.56	0.76	0.8	0.49	0.59	0.93	0.98	0.54	0.91	0.97	1.15	0.51	0.6	0.9	0.9
2041–2070	0.51	0.56	0.9	0.71	0.57	0.67	1.13	0.99	0.98	1.23	1.48	1.62	1.04	1.12	1.57	1.67
2071–2100	0.39	0.67	1.07	1.5	0.95	1.03	1.79	2.35	1.78	2.13	2.59	3.1	2.22	2.82	3.27	4.13

Autumn 2 m temperature (°C)

Time period	SSP126				SSP245				SSP370				SSP585			
	P33	P50	Mean	P66	P33	P50	Mean	P66	P33	P50	Mean	P66	P33	P50	Mean	P66
2021–2050	0.64	0.66	0.88	0.79	0.54	0.57	0.91	0.69	0.53	0.95	1.13	1.23	0.63	0.71	1.04	1.1
2041–2070	0.69	0.76	1.04	0.92	0.86	0.88	1.31	1.05	1.08	1.3	1.71	1.95	0.96	1.04	1.72	1.98
2071–2100	0.69	0.89	1.3	1.54	1.3	1.4	2.1	2.62	1.82	2.17	2.79	3.32	2.43	2.84	3.5	4.07

greater than the projected mean summer increase (Figure 3.2c), ranging from 3°C to 4°C for the end of the century under the SSP585 scenario. Warming is greater in the south than in the north.

Figure 3.5b shows how the coldest 5% of night-time temperatures (TN5) are projected to change. Again, the projected increase of TN5 is greater than the mean winter increase (Figure 3.2a), ranging from

Annual Change in St. Dev. of 2m Temperature
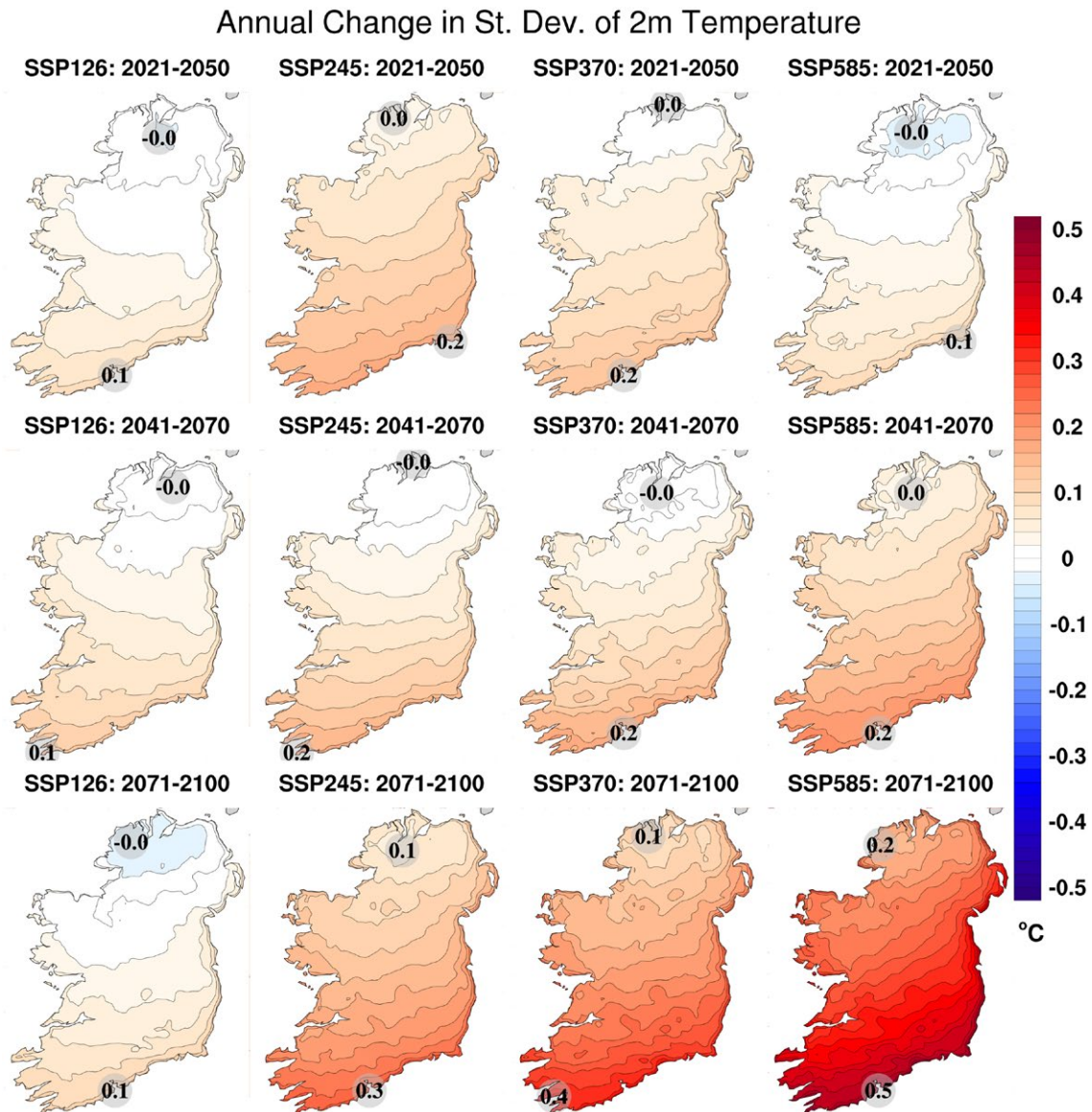
Figure 3.3. Annual projected change in the standard deviation of daily mean 2 m temperature (°C). In each case, the future 30-year period is compared with the past period, 1981–2010. The results were obtained from analysing 10 SSP126, 10 SSP245,10 SSP370 and 10 SSP585 RCM simulations. The numbers included on each plot are the minimum and maximum projected changes, displayed at their locations.

2.5°C to 3.1°C for the end of the century under the SSP585 scenario. Warming is greater in the north than in the south.

The absence of hatching in Figure 3.5, coupled with the small spread of the percentile and mean statistics presented in Table 3.2, demonstrates that the extreme temperature projections have high certainty.

3.3   Heatwaves

For the analysis of the change in number of heatwaves, we used two different definitions as described by Jacob *et al*. (2014). In the first definition (metric-1), heatwaves were considered as periods of more than 3 consecutive days exceeding the 99th percentile of the daily maximum temperature of the May to September season of the control period (1981–2010). The second definition (metric-2) was based on the WMO definition (Frich *et al*., 2002) and defined as periods of at least 5 consecutive days with daily maximum temperature exceeding the mean maximum temperature during the summer months (June, July and August) for the control period (1981–2010) by at least 5°C.
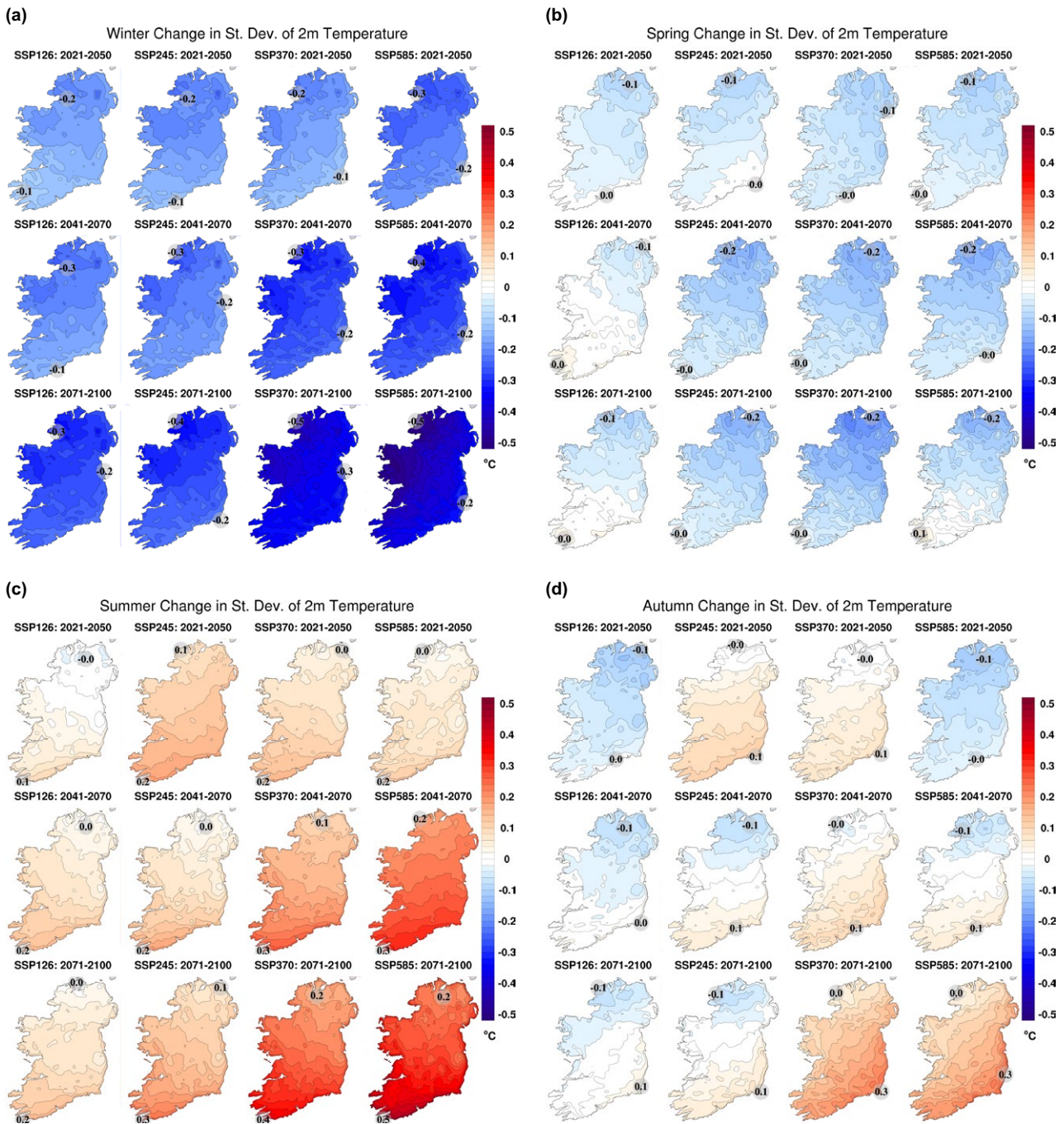
Figure 3.4. Seasonal projected change in the standard deviation of daily mean 2 m temperature (°C) for (a) winter, (b) spring, (c) summer and (d) autumn. In each case, the future 30-year period is compared with the past period, 1981–2010. The numbers included on each plot are the minimum and maximum projected changes, displayed at their locations.

The large projected increase in high summer temperatures (TX95; Figure 3.5a) suggests an increase in the number of heatwave events in the decades ahead. This is confirmed by Figure 3.6, which presents the projected change in the number of heatwave events, using the two different metrics, over each 30-year time period. The increases range from

0.5 to 5.9 for metric-1 (from 1.8 to 6 for metric-2) for SSP126 (2021–2050) and from 12 to 57 for metric-1 (from 23 to 45 for metric-2) for SSP585 (2071–2100). The heatwave projections exhibit a north-west to south-east gradient, with the largest increases in the south-east. For comparison, the observed number of heatwave events over the period 1981–2010 is

(a)

(b)
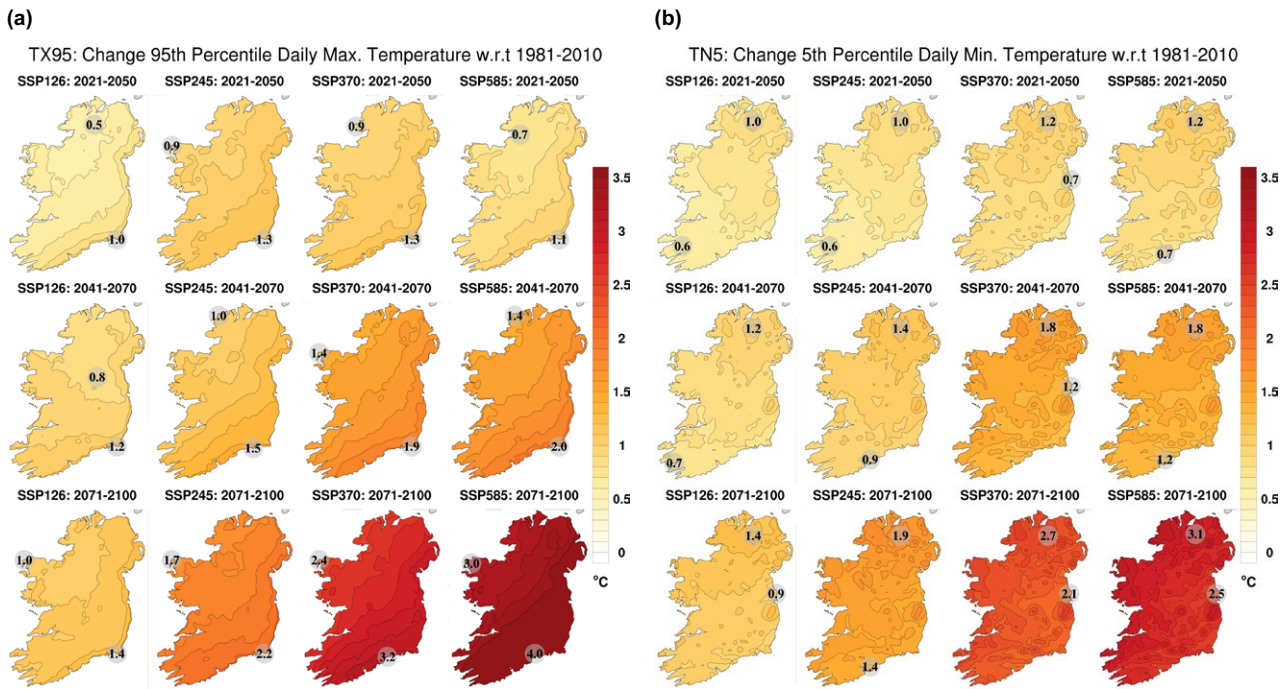
Figure 3.5. Projected changes in extreme 2 m temperature (°C). (a) TX95, top 5% of daily maximum temperatures (warm summer days) and (b) TN5, bottom 5% of daily minimum temperatures (cold winter nights). In each case, the future 30-year period is compared with the past period, 1981–2010. The numbers included on each plot are the minimum and maximum projected changes, displayed at their locations.

Table 3.2. Extreme 2 m projections (°C). This table corresponds to the projections (°C) of Figure 3.5 and presents the 33rd percentile, 50th percentile, mean and 66th percentile averaged over the island of Ireland (land points)

TX95 (°C)

Time period	SSP126				SSP245				SSP370				SSP585			
	P33	P50	Mean	P66	P33	P50	Mean	P66	P33	P50	Mean	P66	P33	P50	Mean	P66
2021–2050	0.42	0.48	0.66	0.76	0.66	0.76	1.06	1.13	0.7	1.1	1.04	1.35	0.47	0.55	0.85	0.8
2041–2070	0.4	0.86	0.95	1.17	0.72	0.85	1.2	1.16	1.18	1.47	1.63	1.84	1.25	1.38	1.66	1.69
2071–2100	0.53	0.93	1.13	1.49	1.38	1.47	1.9	2.34	2.21	2.45	2.81	3.34	2.51	3.11	3.49	4.25

TN5 (°C)

Time period	SSP126				SSP245				SSP370				SSP585			
	P33	P50	Mean	P66	P33	P50	Mean	P66	P33	P50	Mean	P66	P33	P50	Mean	P66
2021–2050	0.42	0.46	0.72	0.59	0.31	0.42	0.75	0.64	0.56	0.6	0.9	0.72	0.57	0.63	0.91	0.88
2041–2070	0.47	0.54	0.86	0.82	0.54	0.59	1.05	0.75	1.03	1.08	1.45	1.49	0.9	1.01	1.43	1.35
2071–2100	0.5	0.71	1.1	1.22	1.03	1.17	1.57	1.66	1.86	1.97	2.33	2.37	2.4	2.51	2.8	3

presented in Figure 3.7 (derived from daily maximum temperature data provided by Walsh, 2017). The projected increase in heatwaves will have a direct impact on public health and mortality, but this may be

offset by the projected decrease in frost and ice days (see section 3.4).

It is noted that the heatwave projections, presented in Figure 3.6, contain some hatching for the earlier time

(a)

(b)
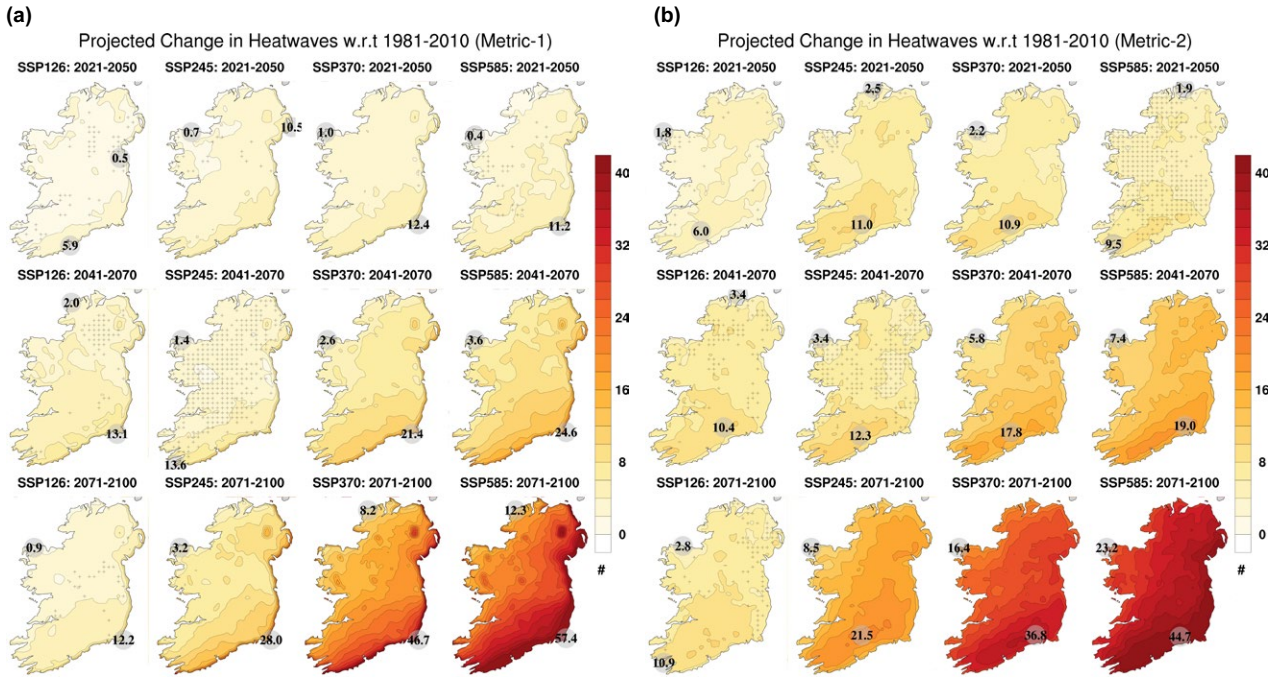
Figure 3.6. Projected changes in the number of heatwave events over 30 years for (a) heatwave metric-1 and (b) heatwave metric-2. In each case, the future 30-year period is compared with the past period, 1981–2010. The numbers included on each plot are the minimum and maximum projected changes, displayed at their locations.

(a)

(b)
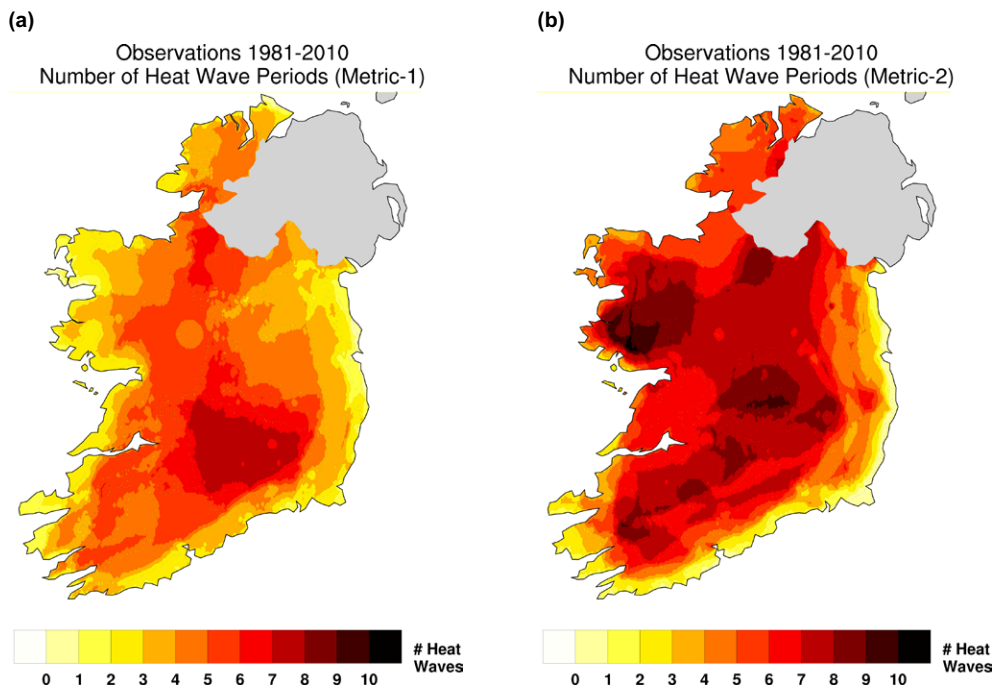
Figure 3.7. Observed number of heatwave events over the 30-year period 1981–2010 for (a) heatwave metric-1 and (b) heatwave metric-2.

periods and/or lower SSP scenarios. This is evident in Table 3.3, where the 33rd and 66th percentile statistics (averaged over all land points) have different signs

for some of the earlier 30-year time periods and/or lower SSP scenarios (e.g. 2041–2070 under SSP245). These results suggest that the heatwave projections

Table 3.3. Projections of the number of heatwave events. This table corresponds to the projections of Figure 3.6 and presents the 33rd percentile, 50th percentile, mean and 66th percentile averaged over the island of Ireland (land points)

Heatwave metric-1

Time period	SSP126				SSP245				SSP370				SSP585			
	P33	P50	Mean	P66	P33	P50	Mean	P66	P33	P50	Mean	P66	P33	P50	Mean	P66
2021–2050	−0.5	0.3	1.7	3.0	0.4	2.2	3.2	4.6	0.8	2.0	3.6	5.2	0.0	0.8	3.7	6.9
2041–2070	0.1	2.8	4.6	8.3	−1.2	−0.2	3.8	4.0	3.9	5.3	7.7	9.9	3.9	5.0	9.5	13.7
2071–2100	0.0	1.0	3.8	6.3	4.3	5.4	8.8	10.9	10.4	17.2	19.4	25.0	12.2	20.2	27.9	36.0

Heatwave metric-2

Time period	SSP126				SSP245				SSP370				SSP585			
	P33	P50	Mean	P66	P33	P50	Mean	P66	P33	P50	Mean	P66	P33	P50	Mean	P66
2021–2050	0.6	2.1	3.9	6.5	2.0	4.4	7.1	7.7	1.9	5.6	6.9	10.7	−1.4	0.4	5.8	7.6
2041–2070	0.6	6.1	7.4	11.4	−0.7	1.4	7.4	10.7	4.2	6.5	11.8	14.5	5.5	7.4	13.8	14.5
2071–2100	0.6	2.8	7.6	8.7	7.9	10.4	16.3	17.3	14.7	21.1	28.2	32.5	14.4	31.0	35.4	49.7

exhibit higher certainty for the later time periods and higher SSP scenarios.

Jacob *et al.* (2014) analysed a large ensemble of relatively low-resolution (12.5 km to 25 km) RCMs (downscaled CMIP5 under RCP scenarios) and showed small projected increases in heatwave events over Ireland (2021–2050 and 2071–2100), with a slight north-west to south-east gradient evident over

the country. These results, in addition to national projections using downscaled CMIP5-RCP data (Nolan and Flanagan, 2020), are consistent with the findings of the current report.

3.4 Frost and Ice Days

The large projected decrease in cold nights (Figure 3.5b; TN5) implies a decrease in the number
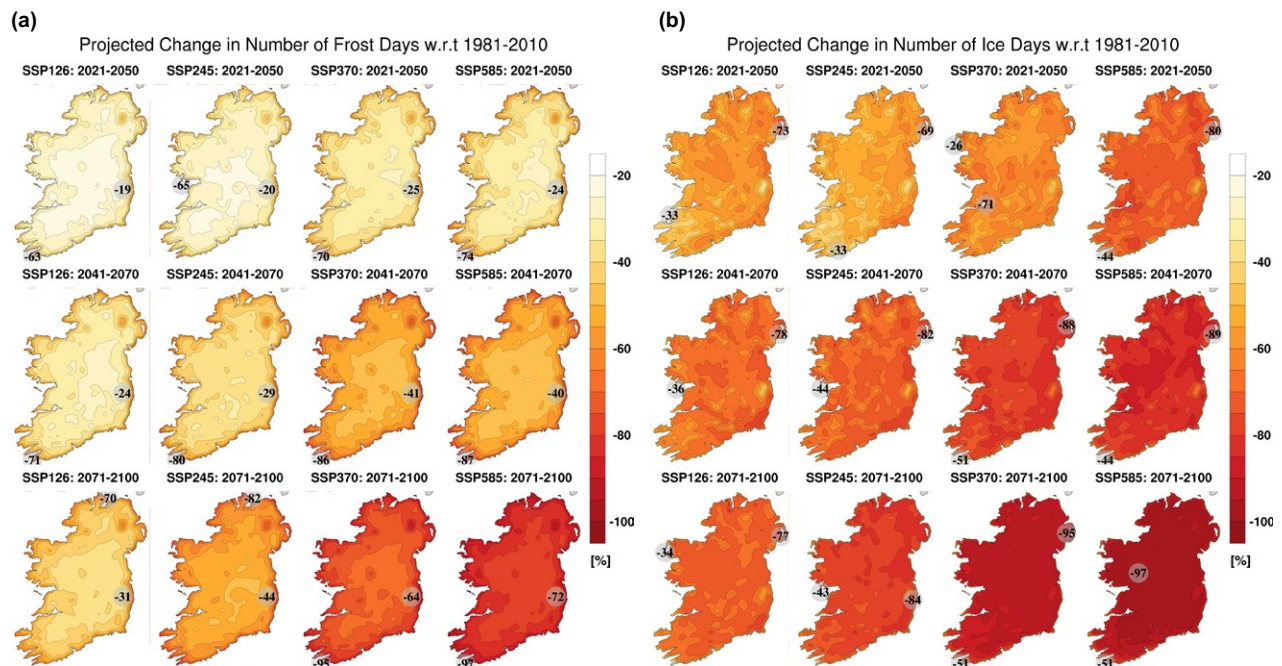
Figure 3.8. Projected changes (%) in the number of (a) frost days and (b) ice days. In each case, the future period is compared with the past period, 1981–2010. The numbers included on each plot are the minimum and maximum projected changes, displayed at their locations.

of frost and ice days over the coming decades. This is confirmed by Figure 3.8a and b, which present the projected annual change in the number of frost and ice days, respectively. Averaged over the whole country (Table 3.4), the mean projected decrease in the number of frost days (days when the minimum temperature is less than 0°C) ranges from 29% (2021–2050 under SSP126) to 82% (2071–2100 under SSP585). Similarly, the projected decrease in the number of ice days (days when the maximum temperature is less than 0°C) ranges from 57% (2021–2050 under SSP126) to 94% (2071–2100 under SSP585). The projections of frost and ice days have high certainty, as demonstrated by an absence of hatching in Figure 3.8 and a small spread between the mean and percentile statistics presented in Table 3.4.

Table 3.4. Projections (%) of the number of frost and ice days. This table corresponds to the projections (%) of Figure 3.8 and presents the 33rd percentile, 50th percentile, mean and 66th percentile averaged over the island of Ireland (land points)

Frost days (%)

Time period	SSP126				SSP245				SSP370				SSP585			
	P33	P50	Mean	P66	P33	P50	Mean	P66	P33	P50	Mean	P66	P33	P50	Mean	P66
2021–2050	−33	−29	−29	−19	−38	−30	−30	−16	−41	−38	−37	−31	−44	−39	−37	−29
2041–2070	−41	−38	−36	−25	−47	−41	−42	−29	−61	−56	−55	−49	−63	−55	−54	−46
2071–2100	−65	−54	−44	−30	−73	−65	−57	−47	−86	−78	−75	−71	−91	−89	−82	−81

Ice days (%)

Time period	SSP126				SSP245				SSP370				SSP585			
	P33	P50	Mean	P66	P33	P50	Mean	P66	P33	P50	Mean	P66	P33	P50	Mean	P66
2021–2050	−66	−61	−57	−50	−69	−62	−53	−41	−70	−63	−60	−51	−77	−72	−70	−64
2041–2070	−78	−72	−67	−57	−82	−75	−70	−60	−86	−84	−78	−77	−91	−87	−82	−78
2071–2100	−88	−82	−70	−57	−90	−84	−77	−69	−96	−95	−90	−89	−97	−97	−94	−94

(a) Observations (1981-2010) Annual Number of Frost Days

(b) Observations 1981-2010 Annual Number of Ice Days
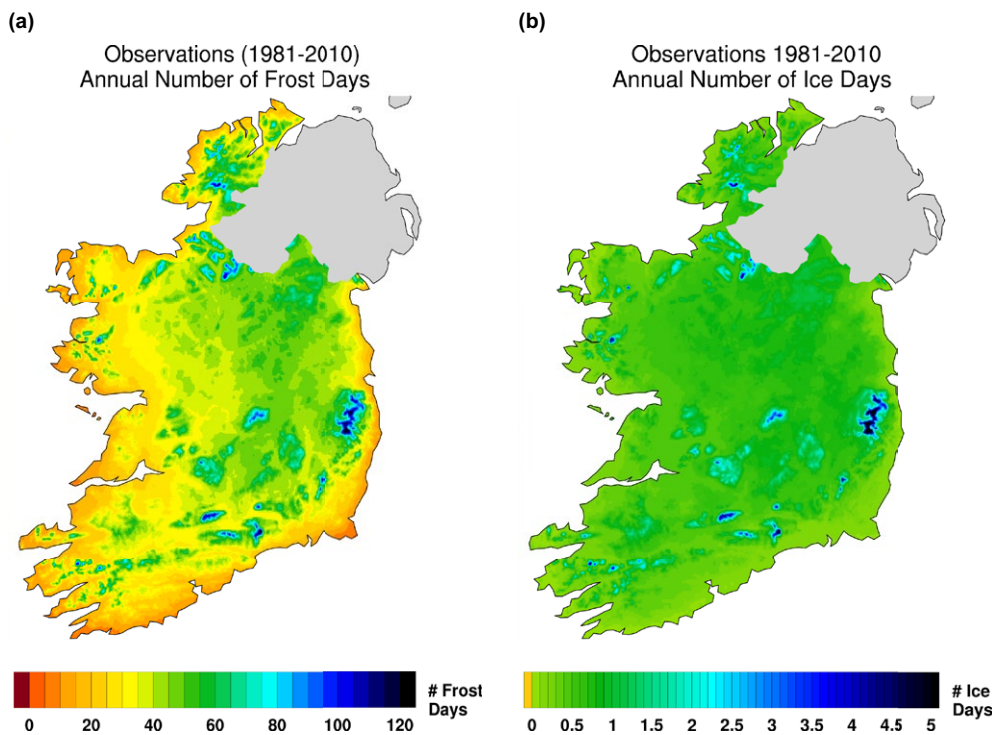
Figure 3.9. The observed mean annual number of (a) frost days and (b) ice days over the period 1981–2010.

For comparison, the observed annual mean numbers of frost and ice days for 1981–2010 are presented in Figure 3.9a and b, respectively (data from Walsh, 2017). Note that the observed number of ice days is small, particularly in coastal regions. It is worth noting that periods of frost and ice are important environmental drivers that trigger phenological phases in many plant and animal species. Changes in the occurrence of these weather types may disrupt the life cycles of these species (e.g. Williams *et al.*, 2015; Bigler and Bugmann, 2018).

3.5 Soil Temperature Projections

The growth of plants and crops is directly correlated with temperature, and projected increases under climate change will have an impact on plant biodiversity and agriculture (Sabri *et al.*, 2018). Soil temperature directly affects below-ground ecosystem processes, including root growth and respiration, decomposition, nitrogen mineralisation, and microbial (Waring and Running, 2007) and invertebrate diversity (Robinson *et al.*, 2018).

Figure 3.10 presents the spatial distribution of annual soil temperature (10 cm depth) projections
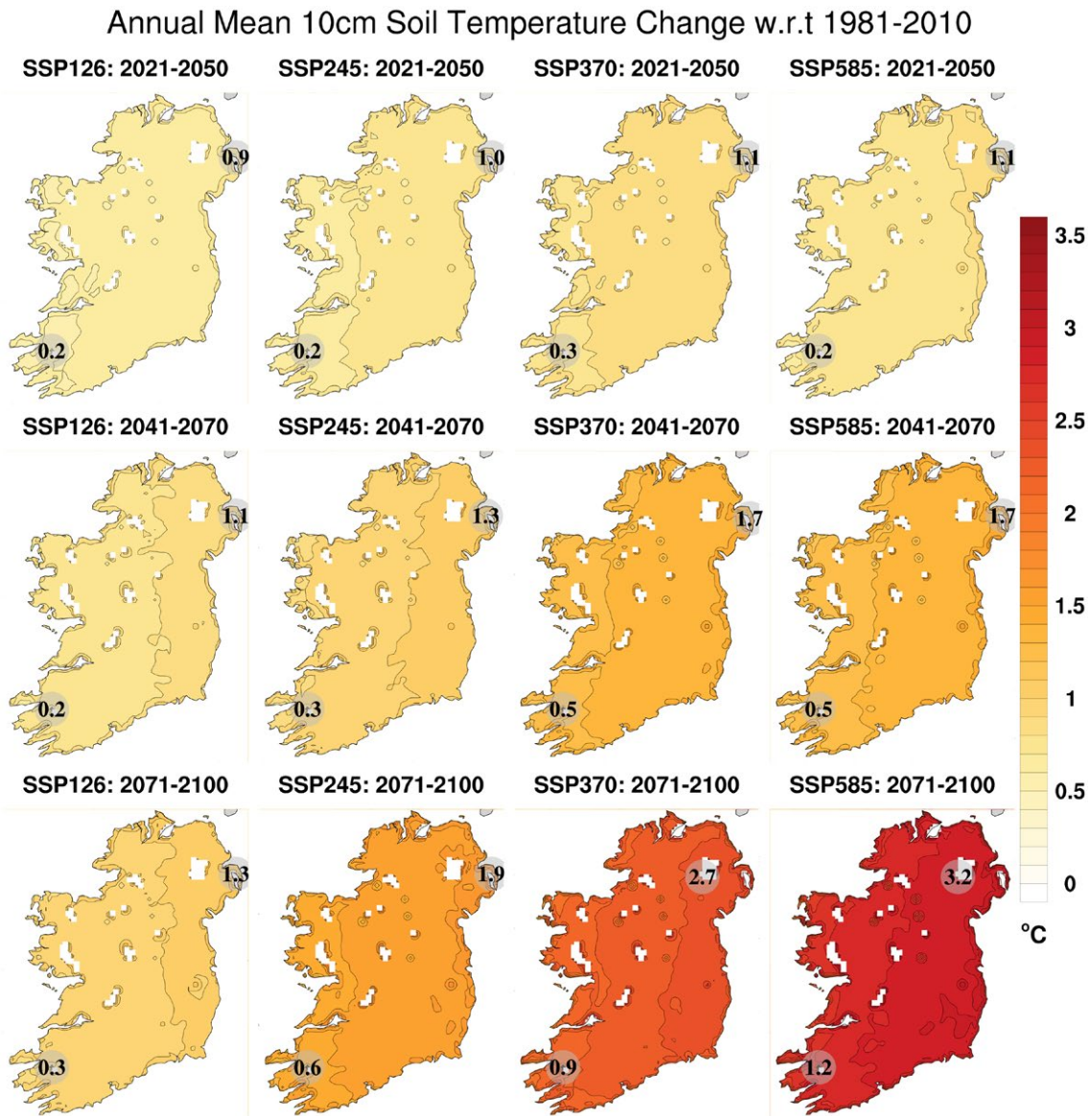
Figure 3.10. Annual RCM–CMIP6 10 cm soil temperature projections (°C). All RCM ensemble members were run with 4 km grid spacing. In each case, the future 30-year period is compared with the past period, 1981–2010. The numbers included on each plot are the minimum and maximum projected changes, displayed at their locations.

for three future 30-year time periods (2021–2050, 2041–2070 and 2071–2100) relative to 1981–2010. The mean annual soil temperature is projected to increase by 0.2–3.2°C depending on the time period and SSP scenario: 0.2–0.9°C for SSP126 (2021–2050) and 1.2–3.2°C for SSP585 (2071–2100). The soil temperature projections show a clear west-to-east gradient, with the largest increases in the east. The soil temperature projections are similar to the annual 2 m temperature projections presented in Figure 3.1, but a larger range is noted for all time periods and SSP scenarios. Averaged over the whole country (Table 3.5, first panel), the mean projected increase in soil temperature ranges from 0.6°C (2021–2050 under SSP126) to 2.8°C (2071–2100 under SSP585).

Table 3.5. Annual and seasonal 10 cm soil temperature projections (°C). This table corresponds to the projections (°C) of Figures 3.10 and 3.11, and shows the 33rd percentile, 50th percentile, mean and 66th percentile averaged over the island of Ireland (land points)

Annual 10 cm soil temperature (°C)

Time period	SSP126				SSP245				SSP370				SSP585			
	P33	P50	Mean	P66	P33	P50	Mean	P66	P33	P50	Mean	P66	P33	P50	Mean	P66
2021–2050	0.4	0.5	0.6	0.6	0.4	0.5	0.7	0.6	0.4	0.7	0.8	0.9	0.4	0.5	0.8	0.8
2041–2070	0.5	0.5	0.8	0.7	0.5	0.6	1.0	0.8	0.9	1.1	1.3	1.3	0.8	0.9	1.3	1.3
2071–2100	0.3	0.7	1.0	1.3	0.8	1.0	1.5	1.9	1.5	1.8	2.2	2.5	1.9	2.5	2.8	3.2

Winter 10 cm soil temperature (°C)

Time period	SSP126				SSP245				SSP370				SSP585			
	P33	P50	Mean	P66	P33	P50	Mean	P66	P33	P50	Mean	P66	P33	P50	Mean	P66
2021–2050	0.3	0.5	0.6	0.6	0.2	0.3	0.6	0.7	0.4	0.5	0.7	0.6	0.4	0.4	0.7	0.6
2041–2070	0.4	0.5	0.7	0.7	0.4	0.5	0.9	0.7	0.9	0.9	1.2	1.1	0.7	0.8	1.2	1.2
2071–2100	0.2	0.6	0.9	1.2	0.7	1.0	1.3	1.7	1.5	1.6	2.0	2.0	1.8	2.4	2.4	2.7

Spring 10 cm soil temperature (°C)

Time period	SSP126				SSP245				SSP370				SSP585			
	P33	P50	Mean	P66	P33	P50	Mean	P66	P33	P50	Mean	P66	P33	P50	Mean	P66
2021–2050	0.1	0.1	0.4	0.6	0.2	0.2	0.6	0.6	0.2	0.4	0.6	0.6	0.2	0.3	0.5	0.5
2041–2070	0.2	0.3	0.6	0.6	0.2	0.2	0.7	0.5	0.6	0.7	1.0	0.9	0.5	0.6	0.9	0.7
2071–2100	0.1	0.3	0.8	1.0	0.4	0.6	1.1	1.2	1.2	1.3	1.8	1.7	1.4	1.7	2.1	2.3

Summer 10 cm soil temperature (°C)

Time period	SSP126				SSP245				SSP370				SSP585			
	P33	P50	Mean	P66	P33	P50	Mean	P66	P33	P50	Mean	P66	P33	P50	Mean	P66
2021–2050	0.4	0.5	0.7	0.8	0.4	0.6	0.9	0.9	0.5	0.9	0.9	1.1	0.5	0.6	0.9	0.9
2041–2070	0.5	0.6	0.9	0.8	0.5	0.6	1.1	1.1	0.9	1.2	1.4	1.5	1.0	1.1	1.5	1.6
2071–2100	0.3	0.7	1.0	1.5	0.9	1.2	1.7	2.3	1.7	2.1	2.5	3.0	2.1	2.9	3.1	3.9

Autumn 10 cm soil temperature (°C)

Time period	SSP126				SSP245				SSP370				SSP585			
	P33	P50	Mean	P66	P33	P50	Mean	P66	P33	P50	Mean	P66	P33	P50	Mean	P66
2021–2050	0.6	0.7	0.9	0.8	0.6	0.6	0.9	0.8	0.5	1.0	1.1	1.2	0.7	0.7	1.0	1.1
2041–2070	0.7	0.8	1.0	1.0	0.9	0.9	1.3	1.1	1.1	1.4	1.7	1.9	1.0	1.1	1.7	2.0
2071–2100	0.7	1.0	1.3	1.5	1.3	1.5	2.0	2.6	1.8	2.3	2.8	3.3	2.3	2.9	3.4	4.1

The seasonal soil temperature projections are presented in Figure 3.11; winter temperatures show increases ranging from 0.2°C in the south-west to 0.8°C in the north-east for SSP126, 2021–2050 (1.1°C in the south-west to 2.8°C in the north for SSP585, 2071–2100). The patterns for spring are similar to winter, with a south-west to north-east gradient in the projections, ranging from 0.1°C in the south-west (SSP126, 2021–2050) to 2.6°C in the north-east (SSP585, 2071–2100). The largest projected increases in soil temperature are noted for summer and autumn. Summer soil temperatures are projected to increase by 0.2°C in the south-west for SSP126 (2021–2050) and by 3.7°C in the north-east for SSP585 (2071–2100).
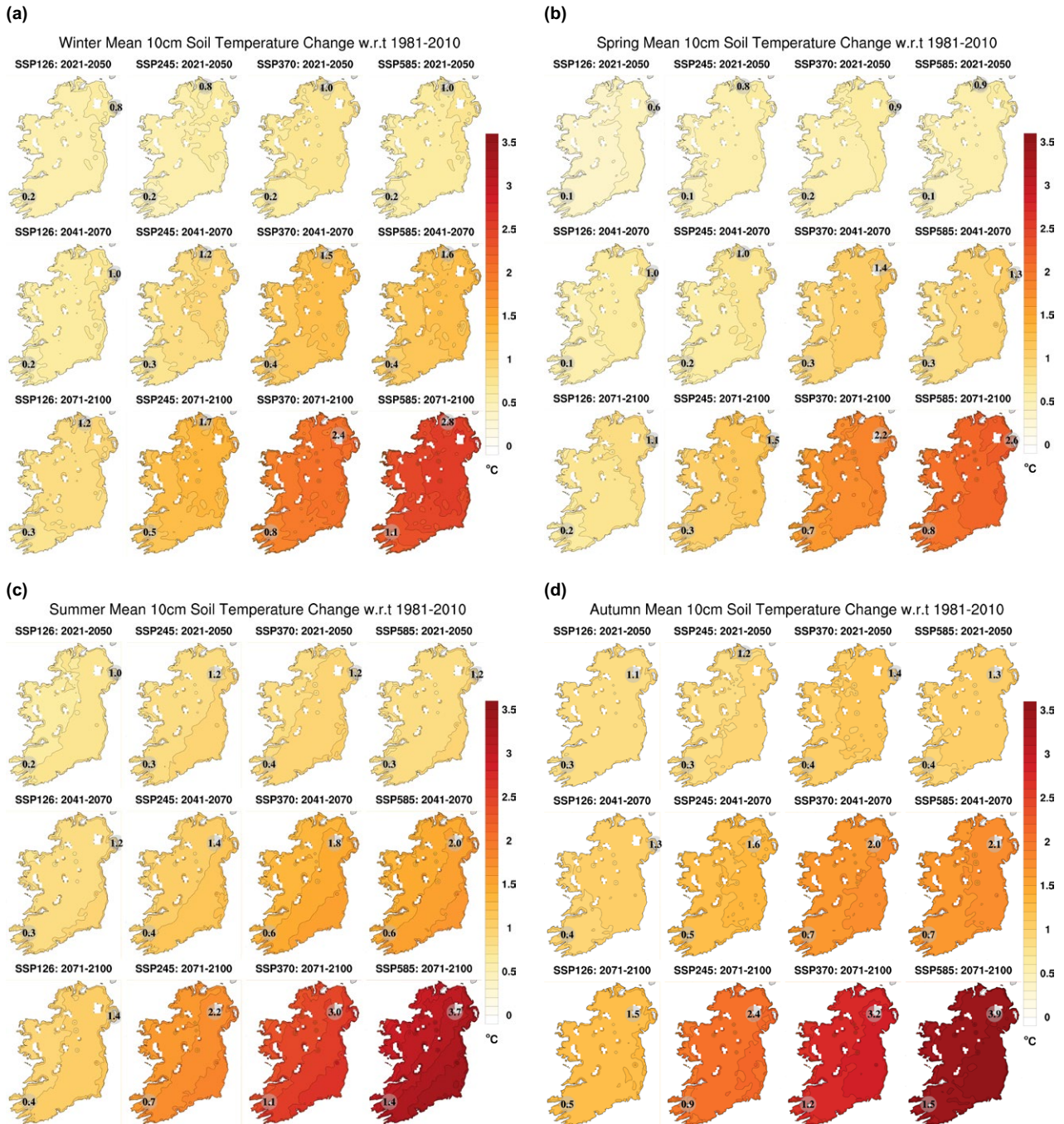
Figure 3.11. Seasonal RCM–CMIP6 10 cm soil temperature projections (°C) for (a) winter, (b) spring, (c) summer and (d) autumn. In each case, the future 30-year period is compared with the past period, 1981–2010. The numbers included on each plot are the minimum and maximum projected changes, displayed at their locations.

Autumn soil temperatures are projected to increase by 0.3°C in the south-west for SSP126 (2021–2050) and by 3.9°C in the north-east for SSP585 (2071–2100). The seasonal soil temperature projections are similar to the seasonal 2 m temperature projections presented in Figure 3.2, but a larger range is noted for all time periods and SSP scenarios.

The projections for soil temperature have low uncertainty, as demonstrated by an absence of hatching in Figures 3.10 and 3.11, and a small spread (and the same sign) between the mean and percentile statistics presented in Table 3.5.

3.6 The Growing Season

Within a period of 12 months, the thermal growing season length is officially defined as the number of days between the first occurrence of at least 6 consecutive days with a daily mean temperature >5°C and the first occurrence of at least 6 consecutive days with a daily mean temperature <5°C. Figure 3.12a shows a large projected increase in the average length of the growing season over Ireland, with values ranging from 1% to 15% for SSP126 (2021–2050) and from 3% to 39% for SSP585

(2071–2100). Averaged over the whole country (Table 3.6, first panel), the mean projected increase in the length of the growing season ranges from 6.6% (2021–2050 under SSP126) to 17.7% (2071–2100 under SSP585). Figure 3.12b, the projected change in the start of the growing season, shows that the growing season is projected to start 1–19 days early for SSP126 (2021–2050) and 4–48 days early for SSP585 (2071–2100). Averaged over the whole country (Table 3.6, second panel), the projected start (days early) of the growing season ranges from 9.2 (2021–2050 under SSP126) to 27.6 days early (2071–2100 under SSP585).

It is noted that the projections of the start of the growing season, presented in Figure 3.12b, contain some hatching for the earlier time periods and/or lower SSP scenarios. This is not so evident for the projections of the length of the growing season (Figure 3.12a). These results suggest that, for the earlier time periods and/or lower SSP scenarios, there is some disagreement between ensemble members over the degree to which the growing season is extended at the start or end of the year. In summary, the projections of the growing season length have higher certainty, as demonstrated by an absence of
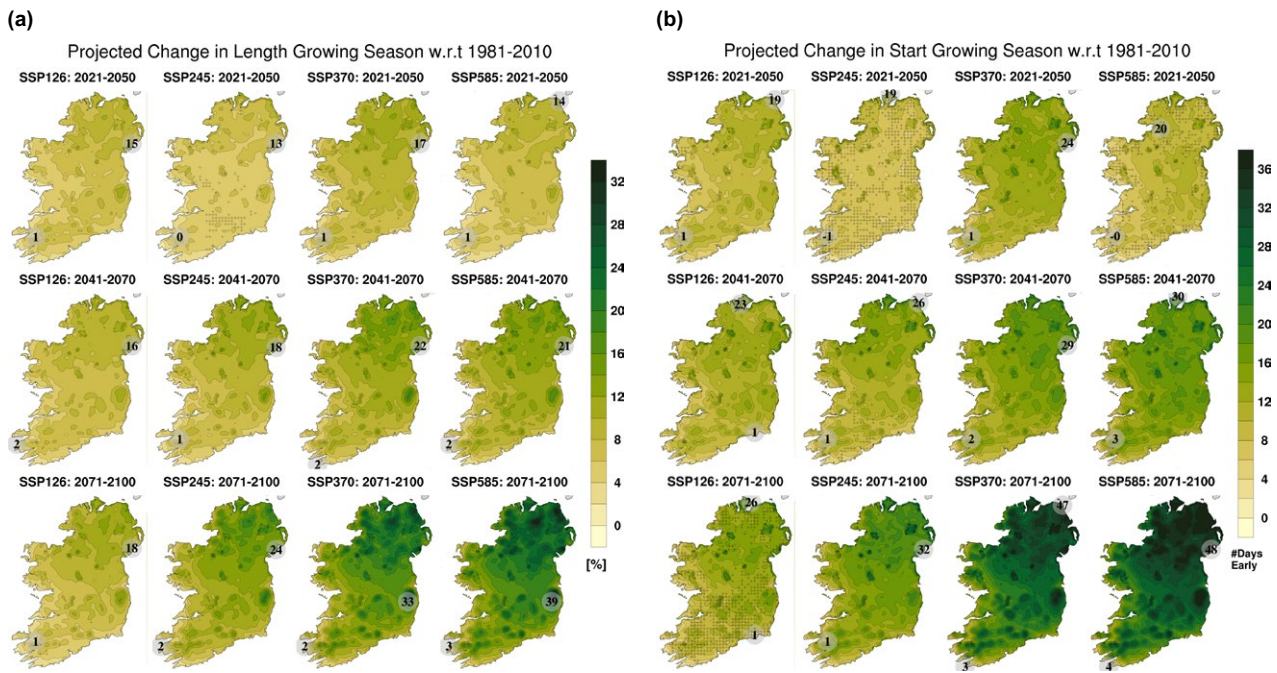
Figure 3.12. Projected changes in (a) growing season length (%) and (b) start of the growing season (number of days early). In each case, the future period is compared with the past period, 1981–2010. The numbers included on each plot are the minimum and maximum projected changes, displayed at their locations.

Table 3.6. Projected changes in length (%) and start (number of days early) of the growing season. This table corresponds to projected changes in Figure 3.12 and presents the 33rd percentile, 50th percentile, mean and 66th percentile averaged over the island of Ireland (land points)

Growing season length (%)

Time period	SSP126				SSP245				SSP370				SSP585			
	P33	P50	Mean	P66	P33	P50	Mean	P66	P33	P50	Mean	P66	P33	P50	Mean	P66
2021–2050	2.9	3.9	6.6	5.3	1.0	2.2	5.7	4.6	4.0	4.8	8.2	7.2	2.1	3.0	6.8	5.4
2041–2070	4.1	5.1	7.5	6.7	3.2	4.4	8.4	6.7	6.3	7.0	10.6	8.8	5.6	6.8	10.7	9.4
2071–2100	2.1	3.6	8.0	9.2	6.6	8.2	11.6	11.5	10.5	11.7	15.6	14.7	12.4	13.7	17.7	17.3

Growing season start (number of days early)

Time period	SSP126				SSP245				SSP370				SSP585			
	P33	P50	Mean	P66	P33	P50	Mean	P66	P33	P50	Mean	P66	P33	P50	Mean	P66
2021–2050	2.8	5.9	9.2	7.9	0.1	4.2	7.4	6.9	5.7	9.6	12.3	11.7	0.7	4.1	8.8	6.5
2041–2070	4.4	7.8	11.1	9.7	4.4	9.4	11.9	11.9	7.9	10.4	14.8	11.9	8.0	12.0	15.9	14.5
2071–2100	0.4	14.3	12.0	17.0	7.2	14.6	15.9	17.2	16.4	20.8	24.6	23.0	19.7	24.3	27.6	27.0

hatching in Figure 3.12a and a small spread between the mean and percentile statistics presented in Table 3.6. The projections of the start of the growing season are more robust for the higher SSPs and later time periods.

For comparison, the observed length and start of the growing season over the period 1981–2010

(derived from daily mean temperature data provided by Walsh, 2017) are presented in Figure 3.13a and b, respectively. It should be noted that not all geographical areas in Ireland are suitable for agriculture and/or forestry. The projections presented here (and in sections 3.7–3.9) should therefore be considered in the context of an observed landscape classification map, as presented in Figure 3.13c.
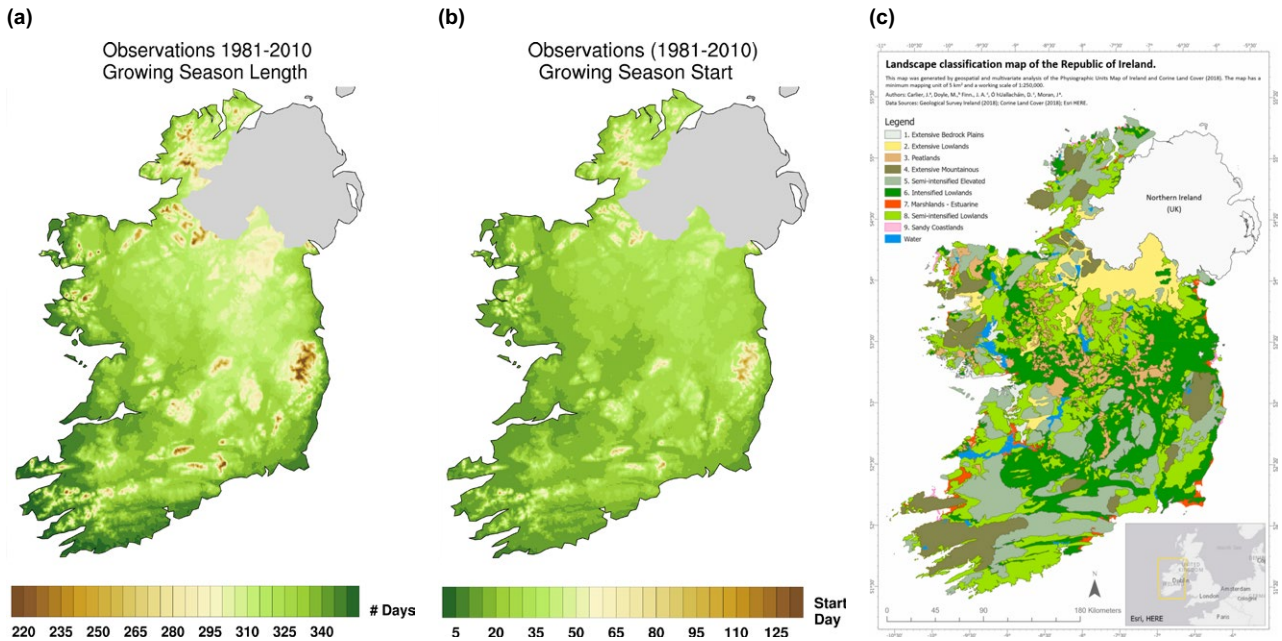
Figure 3.13. Observed growing season statistics for the period 1981–2010 for (a) mean annual length and (b) mean start day of growing season. Panel (c) presents the landscape classification map for Ireland. Source: Carlier *et al*. (2021). Reproduction licensed under the Creative Commons Attribution CC BY 4.0 licence (https://creativecommons.org/licenses/by/4.0/).

3.7 The Grazing Season

The growing season calculation is based solely on temperature and does not take into account the delay before sufficient plant cover is available to support grazing animals or the ability of animals and machinery to pass over land. The length of the grazing season, in days per year, can be approximated from the following equation (Smith, 1976; Collins and Cummins, 1996):

$$GzS = 29.3T - 0.1R + 19.5 \tag{3.1}$$

where *T* is the mean annual 2 m temperature (°C) and *R* is the mean annual rainfall (mm/year).

Figure 3.14 shows a large projected increase in the average length of the grazing season (days/year) over Ireland, with values ranging from 0 to 23 for SSP126 (2021–2050) and from 10 to 92 for SSP585 (2071–2100). Averaged over the whole country (Table 3.7), the mean projected increase in the grazing season ranges from 16.7 (2021–2050 under SSP126) to 73.9 days/year (2071–2100 under SSP585). The projections of the grazing season have high certainty, as demonstrated by an absence of hatching in Figure 3.14 and a small spread (and the same sign) between the mean and percentile statistics presented in Table 3.7.
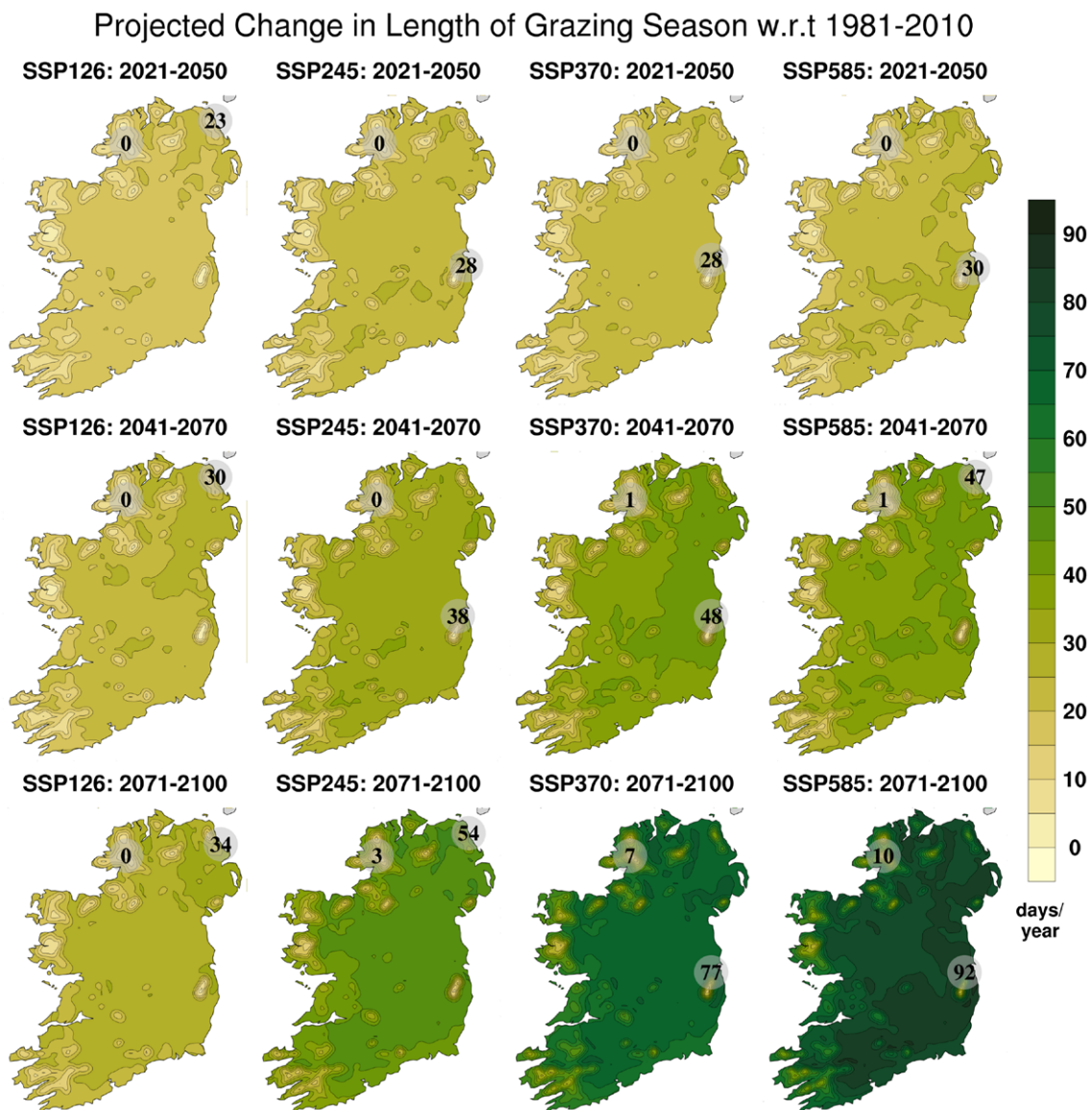
Figure 3.14. Projected changes in the length of the grazing season (days/year). In each case, the future period is compared with the past period, 1981–2010. The numbers included on each plot are the minimum and maximum projected changes, displayed at their locations.

Table 3.7. Projected changes in the length of the grazing season (days/year). This table corresponds to the projected changes in Figure 3.14, and presents the 33rd percentile, 50th percentile, mean and 66th percentile averaged over the island of Ireland (land points)

Time period	SSP126				SSP245				SSP370				SSP585			
	P33	P50	Mean	P66	P33	P50	Mean	P66	P33	P50	Mean	P66	P33	P50	Mean	P66
2021–2050	12.8	15.0	16.7	18.8	13.2	15.4	20.8	19.7	13.9	17.6	20.8	23.3	13.4	16.1	21.5	21.7
2041–2070	13.1	16.0	21.3	23.1	17.4	19.7	29.4	27.0	26.2	31.0	35.6	37.4	21.1	26.4	35.3	37.6
2071–2100	11.1	13.9	25.7	38.1	29.2	37.7	43.0	57.4	44.6	49.4	62.5	70.7	55.1	64.8	73.9	86.9

3.8 Ontario Crop Heat Units

The Ontario crop heat unit (CHU) is a variant of a degree day accumulation (see section 3.9) and is widely used to rate the suitability of regions for production of corn/maize (Collins and Cummins, 1996; Bootsma *et al*., 1999, 2007; OMAFRA, 2017). The CHU model uses separate calculations for maximum and minimum temperatures. The maximum or day-time
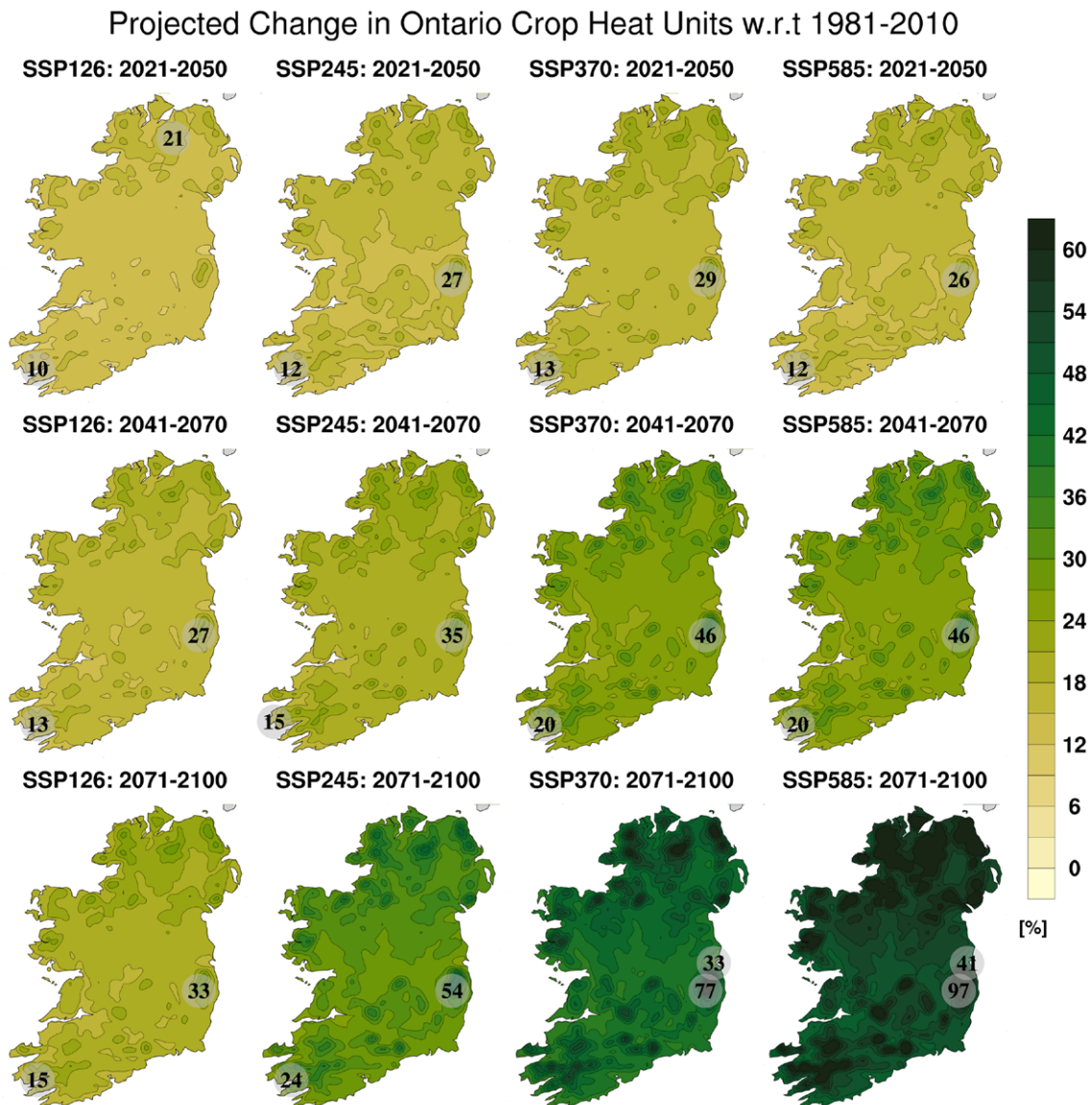
Figure 3.15. Projected changes in Ontario CHUs (%). In each case, the future period is compared with the past period, 1981–2010. The numbers included on each plot are the minimum and maximum projected changes, displayed at their locations.

Table 3.8. Projected changes in Ontario CHUs (%). This table corresponds to the projected changes in Figure 3.15, and presents the 33rd percentile, 50th percentile, mean and 66th percentile averaged over the island of Ireland

Time period	SSP126				SSP245				SSP370				SSP585			
	P33	P50	Mean	P66	P33	P50	Mean	P66	P33	P50	Mean	P66	P33	P50	Mean	P66
2021–2050	8.1	9.1	13.7	11.4	7.9	9.4	16.0	13.1	9.1	13.1	17.5	19.4	8.7	10.5	16.5	16.2
2041–2070	8.8	11.1	17.0	14.5	10.0	11.7	20.4	15.0	16.9	18.0	26.5	27.8	14.1	18.2	26.9	27.4
2071–2100	9.6	10.4	20.1	24.2	14.5	20.3	31.6	37.6	29.1	32.7	43.9	49.0	37.6	42.8	54.4	61.9

relationship (Y_{max}) uses 10°C as the base temperature and has a curvilinear response to temperature, with a maximum at 30°C; no growth occurs below 10°C and growth peaks at 30°C and declines thereafter. The minimum (or night-time) relationship uses 4.4°C as the base temperature, with the response above this being linear; Y_{min} does not specify an optimum temperature because night-time minimum temperatures very rarely exceed 25°C. Mean annual CHU values for May to September are calculated using daily values as follows:

$$Daily\ CHU = \frac{Y_{max} + Y_{min}}{2} \qquad (3.2)$$

where

$$Y_{max} = max\{3.33(T_{max}-10)-0.084(T_{max}-10)^2,0\} \qquad (3.3)$$

$$Y_{min} = max\{1.8(T_{min}-4.44),0\} \qquad (3.4)$$

and T_{min} and T_{max} are the daily minimum and maximum temperatures, respectively.

Figure 3.15 shows a large projected increase in Ontario CHUs over Ireland, with values ranging from 10% to 21% for SSP126 (2021–2050) and from 41% to 97% for SSP585 (2071–2100). Averaged over the whole country (Table 3.8), the mean projected increase in Ontario CHUs ranges from 13.7% (2021–2050 under SSP126) to 54.4% (2071–2100 under SSP585). The projections of Ontario CHUs have high certainty, as demonstrated by an absence of hatching in Figure 3.15 and a small spread (and the same sign) of the mean and percentile statistics presented in Table 3.8.

3.9 Growing Degree Days (Crops and Pests)

A degree day, an estimate of accumulated heat, is defined as the deviation (°C) from a reference temperature value (Fraisse *et al.*, 2010; Project Team ECA&D, 2013; Kendon *et al.*, 2015). Degree days represent the number of degrees by which the temperature has gone above or below a threshold. Growing degree days (GDDs) are used to predict the growth and development of plants, insects and diseases whose development is very dependent on temperature and the daily accumulation of heat. The amount of heat required to advance a plant (or pest) to the next development stage remains constant from year to year; however, the actual amount of time (days) can vary considerably because of weather conditions. Each crop, insect and disease species has a minimum base temperature (T_b) or threshold below which development does not occur (Fraisse *et al.*, 2010; OMAFRA, 2017). For example, in Europe, 5.5°C applies to wheat, barley, rye, oats and lettuce, 8°C to sunflowers and potatoes and 10°C to American maize, rice, corn and tomatoes (McMaster and Wilhelm, 1997; Miller *et al.*, 2001; Spinoni *et al.*, 2015). See Table 3.9 for a list of base temperatures for crops and pests (McMaster and Wilhelm, 1997; Johnson *et al.*, 1998; Miller *et al.*, 2001; Spinoni *et al.*, 2015).

Table 3.9. GDDs base temperature for various crops and pests

Crop or pest	Base temperature (°C)
Crop	
Wheat, barley, rye, oats and lettuce	5.5
Sunflower, potato	8
American maize, rice, corn and tomato	10
Pest	
Stalk borer	6
Corn rootworm[a]	7
Lucerne weevil	9
Black cutworm, European corn borer and standard baseline for insect and mite pests of woody plants	10

[a]Reported in the UK but not currently present in Ireland.

The GDD metric was computed using the daily mean temperature (T_M) for different base temperatures (T_b), as described by Spinoni *et al*. (2015) and Project Team ECA&D (2013):

$$GDD_{daily} = max\{(T_M - T_b), 0\} \tag{3.5}$$

$$GDD = \Sigma GDD_{daily} \tag{3.6}$$

Figure 3.16 shows that GDDs for crop base temperatures 5.5°C, 8°C and 10°C are projected to increase substantially, with the largest increases noted for the higher SSP scenarios, later time periods and higher baseline temperatures. Averaged over the whole country (Table 3.10), mean projections of GDDs (T_b = 5.5°C) range from 13.7% (2021–2050 under

(a)

(b)

(c)
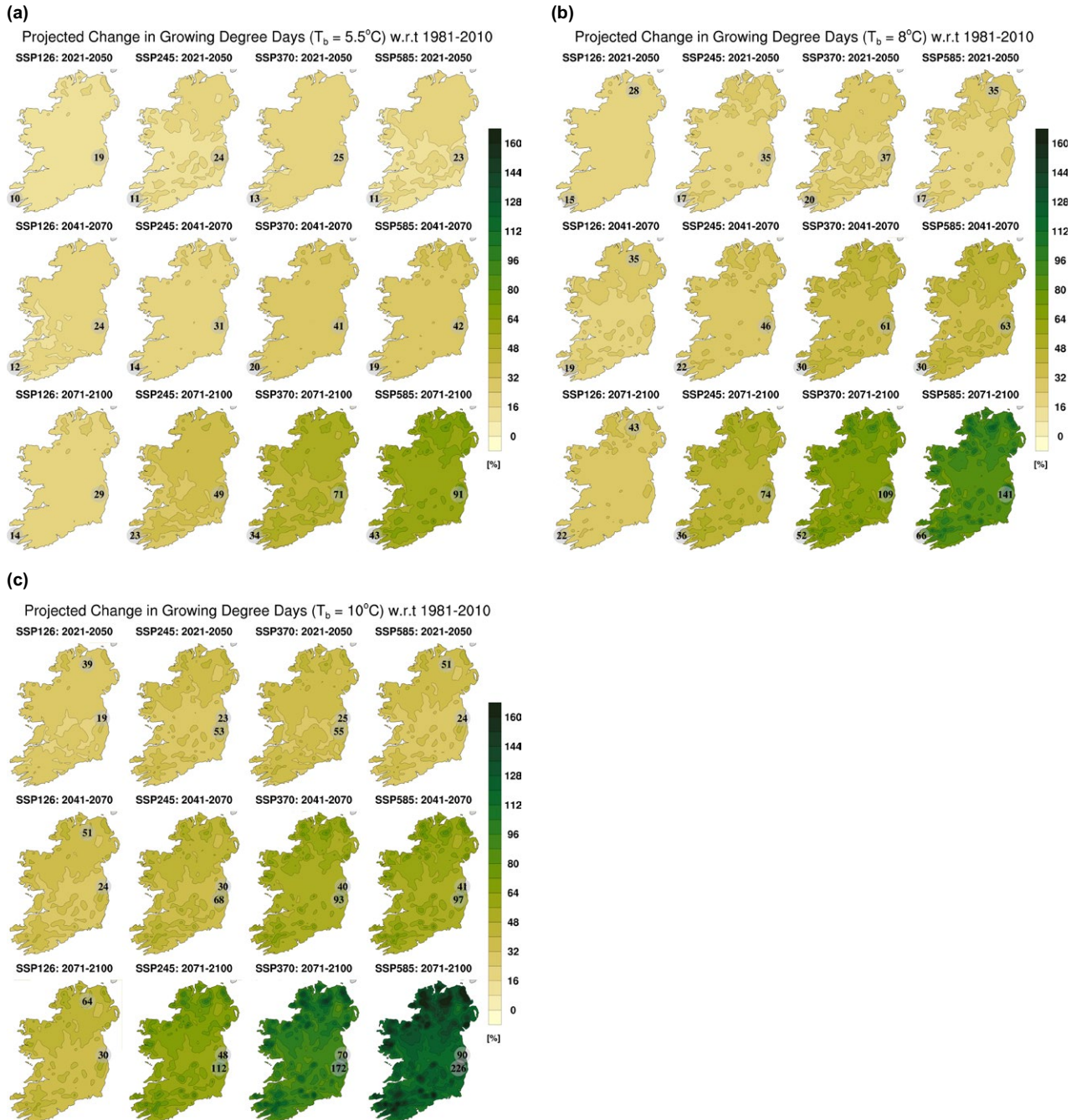
Figure 3.16. Projected changes (%) in GDDs for crop base temperatures for (a) T_b = 5.5°C (wheat, barley, rye, oats and lettuce), (b) T_b = 8°C (sunflower and potato) and (c) T_b = 10°C (American maize, rice, corn and tomato). In each case, the future 30-year period is compared with the past period, 1981–2010. The numbers included on each plot are the minimum and maximum projected changes, displayed at their locations.

Table 3.10. Projections of crop base temperatures for GDDs (%). This table corresponds to the projections in Figure 3.16, and presents the 33rd percentile, 50th percentile, mean and 66th percentile averaged over the island of Ireland (land points)

GDDs $T_b = 5.5°C$

Time period	SSP126				SSP245				SSP370				SSP585			
	P33	P50	Mean	P66	P33	P50	Mean	P66	P33	P50	Mean	P66	P33	P50	Mean	P66
2021–2050	8.4	9.0	13.7	10.6	8.0	9.0	15.9	11.2	8.1	12.8	17.7	18.2	7.9	8.6	16.3	15.1
2041–2070	8.3	10.0	17.1	13.2	9.4	10.7	21.0	13.7	16.6	18.3	27.8	27.4	14.4	16.7	28.3	27.2
2071–2100	7.1	10.0	20.8	25.0	15.0	18.0	33.1	39.2	32.0	33.5	48.2	51.5	41.3	45.4	60.8	69.2

GDDs $T_b = 8°C$

Time period	SSP126				SSP245				SSP370				SSP585			
	P33	P50	Mean	P66	P33	P50	Mean	P66	P33	P50	Mean	P66	P33	P50	Mean	P66
2021–2050	11.3	12.6	19.2	15.2	11.7	12.5	22.6	16.7	11.4	18.2	24.8	26.5	11.8	12.8	23.2	21.4
2041–2070	11.5	14.5	24.0	18.8	12.7	15.1	29.5	19.4	22.6	25.0	38.8	39.3	20.7	24.7	40.2	38.9
2071–2100	11.3	14.0	29.2	34.6	20.9	25.8	46.8	55.3	44.2	46.2	68.3	74.5	58.1	62.2	87.1	99.8

GDDs $T_b = 10°C$

Time period	SSP126				SSP245				SSP370				SSP585			
	P33	P50	Mean	P66	P33	P50	Mean	P66	P33	P50	Mean	P66	P33	P50	Mean	P66
2021–2050	14.7	17.2	26.5	21.3	16.0	17.8	32.3	25.0	16.8	24.8	34.7	37.7	16.3	18.1	32.7	29.5
2041–2070	15.3	20.2	33.6	27.0	17.0	21.7	41.5	27.9	32.0	34.3	54.8	56.2	28.8	36.8	57.6	54.8
2071–2100	16.9	18.9	40.7	47.9	28.5	37.6	66.8	78.0	60.3	66.5	98.0	108	81.2	87.8	126.1	144

SSP126) to 60.8% (2071–2100 under SSP585). Similarly, projections of GDDs ($T_b = 8°C$) range from 19.2% (2021–2050 under SSP126) to 87.1% (2071–2100 under SSP585) and projections of GDDs ($T_b = 10°C$) range from 26.5% (2021–2050 under SSP126) to 126.1% (2071–2100 under SSP585). Figure 3.17 and Table 3.11 show that the GDDs for pest base temperatures 6°C, 7°C, 9°C and 10°C are similarly projected to increase substantially. The projections of GDDs for crops and pests have high certainty, as demonstrated by an absence of hatching in Figures 3.16 and 3.17, and a small spread between the mean and percentile statistics presented in Tables 3.10 and 3.11.

The results of sections 3.5–3.9 suggest that a warming climate may present some positive opportunities for agriculture in Ireland. However, the results should be viewed while noting that a warming climate will also result in an increase in pests (Figure 3.17). Furthermore, projected increases in extreme temperatures (section 3.2), heatwaves (section 3.3), heavy precipitation (section 3.11) and dry periods/

droughts (section 3.13) will have substantial adverse effects on agriculture in Ireland.

3.10   Mean Precipitation Projections

Figure 3.18 presents the spatial distribution of mean annual change in precipitation (%) for the three future 30-year time periods (2021–2050, 2041–2070 and 2071–2100) relative to 1981–2010. There is an indication of a slight increase in the annual precipitation for 2071–2100 under SSP585. However, projected changes are small (~0%) over most of the country for all time periods and SSP scenarios. Furthermore, the abundance of hatching in Figure 3.18 (for all time periods and SSPs, except for 2071–2100 under SSP585) demonstrates disagreement between ensemble members and higher uncertainty in the annual precipitation projections. The uncertainty in the precipitation projections is further demonstrated in Table 3.12 (first panel), which presents the mean and 33rd, 50th and 66th percentiles of the ensemble of annual precipitation projections averaged over all land points. It is noted that, except for 2041–2070 under
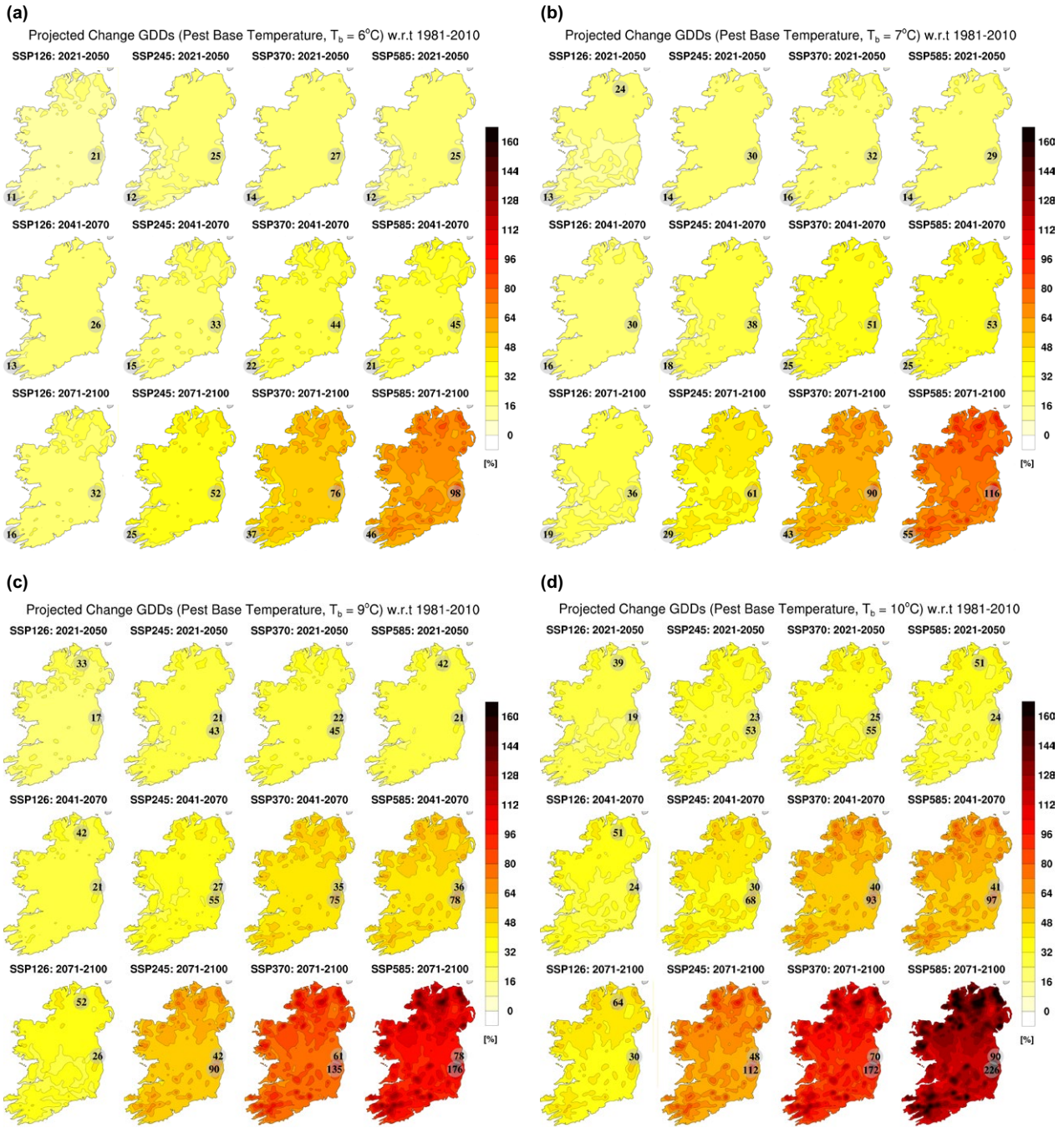
Figure 3.17. Projected changes (%) in GDDs for pest base temperatures for (a) T_b=6°C (stalk borer), (b) T_b=7°C (corn rootworm), (c) T_b=9°C (lucerne weevil) and (d) T_b=10°C (black cutworm, European corn borer and standard baseline for insect and mite pests of woody plants). In each case, the future period is compared with the past period, 1981–2010. The numbers included on each plot are the minimum and maximum projected changes, displayed at their locations.

SSP245 and 2071–2100 under SSP585, the 33rd and 66th percentile statistics have different signs. However, the spread between ensemble members is small, indicating that the ensemble members agree on small projected changes for annual precipitation, but disagree on the sign of the change.

Figure 3.19a, the winter projected change (%) in precipitation, shows an increase for the higher SSPs and later time periods. In particular, the scarcity of hatching for SSP370 and SSP585 during 2041–2100 and 2071–2100 demonstrates agreement between ensemble members and higher certainty in

Table 3.11. Projections of pest base temperatures GDD (%). This table corresponds to the projections in Figure 3.17, and presents the 33rd percentile, 50th percentile, mean and 66th percentile averaged over the island of Ireland (land points)

GDDs T_b=6°C

Time period	SSP126				SSP245				SSP370				SSP585			
	P33	P50	Mean	P66	P33	P50	Mean	P66	P33	P50	Mean	P66	P33	P50	Mean	P66
2021–2050	8.9	9.6	14.6	11.4	8.6	9.6	17.0	12.1	8.6	13.7	18.8	19.6	8.5	9.3	17.4	16.1
2041–2070	8.8	10.7	18.2	14.1	10.0	11.4	22.4	14.6	17.5	19.4	29.6	29.3	15.4	17.9	30.2	29.1
2071–2100	7.7	10.7	22.2	26.6	16.0	19.2	35.3	41.8	34.0	35.6	51.4	55.2	43.9	48.2	65.0	74.1

GDDs T_b=7°C

Time period	SSP126				SSP245				SSP370				SSP585			
	P33	P50	Mean	P66	P33	P50	Mean	P66	P33	P50	Mean	P66	P33	P50	Mean	P66
2021–2050	10.1	10.9	16.6	13.1	10.0	10.9	19.5	14.1	9.8	15.8	21.5	22.8	10.0	10.9	20.0	18.5
2041–2070	10.1	12.4	20.8	16.2	11.2	13.0	25.5	16.7	19.7	21.9	33.7	33.8	17.8	20.8	34.6	33.5
2071–2100	9.3	12.2	25.3	30.2	18.3	22.1	40.4	47.8	38.5	40.3	58.9	63.7	50.2	54.5	74.7	85.5

GDDs T_b=9°C

Time period	SSP126				SSP245				SSP370				SSP585			
	P33	P50	Mean	P66	P33	P50	Mean	P66	P33	P50	Mean	P66	P33	P50	Mean	P66
2021–2050	12.8	14.6	22.4	17.8	13.7	14.7	26.7	20.2	13.6	21.1	29.1	31.3	13.8	15.1	27.2	25.0
2041–2070	13.2	17.0	28.1	22.2	14.5	17.8	34.6	23.0	26.6	28.8	45.6	46.4	24.2	29.8	47.6	45.8
2071–2100	13.8	16.1	34.2	40.3	24.1	30.7	55.3	64.9	51.3	54.3	80.7	88.6	68.2	72.6	103.4	118

GDDs T_b=10°C

Time period	SSP126				SSP245				SSP370				SSP585			
	P33	P50	Mean	P66	P33	P50	Mean	P66	P33	P50	Mean	P66	P33	P50	Mean	P66
2021–2050	14.7	17.2	26.5	21.3	16.0	17.8	32.3	25.0	16.8	24.8	34.7	37.7	16.3	18.1	32.7	29.5
2041–2070	15.3	20.2	33.6	27.0	17.0	21.7	41.5	27.9	32.0	34.3	54.8	56.2	28.8	36.8	57.6	54.8
2071–2100	16.9	18.9	40.7	47.9	28.5	37.6	66.8	78.0	60.3	66.5	98.0	108	81.2	87.8	126.1	144

winter precipitation projections for these time periods and SSPs. This is further demonstrated by Table 3.12 (second panel), which shows that, for SSP245 (2071–2100), and SSP370 and SSP585 (2041–2070 and 2071–2100), the 33rd and 66th percentile statistics have the same sign. In summary, the projected increases in precipitation during winter have higher certainty for the higher SSPs and later time periods, with robust (i.e. P33 and P66 statistics have the same sign) mean increases (averaged over the country) ranging from 2.9% for SSP245 (2041–2070) to 9.8% for SSP585 (2071–2100).

The projections for spring precipitation have high uncertainty, as demonstrated by an abundance of

hatching in Figure 3.19b and disagreement in sign between the P33 and P66 statistics (all SSPs and time periods) of Table 3.12 (third panel).

Figure 3.19c shows a projected drying for the future summer months, which is enhanced for the higher SSPs and later time periods. The projected drying for summer has higher certainty (mid- and late-century under SSP245, SSP370 and SSP585), as demonstrated by an absence of hatching in Figure 3.19c and agreement in sign between the P33 and P66 statistics of Table 3.12 (fourth panel). In summary, the projected decreases in precipitation during summer have higher certainty for the higher SSPs and later time periods, with robust projected
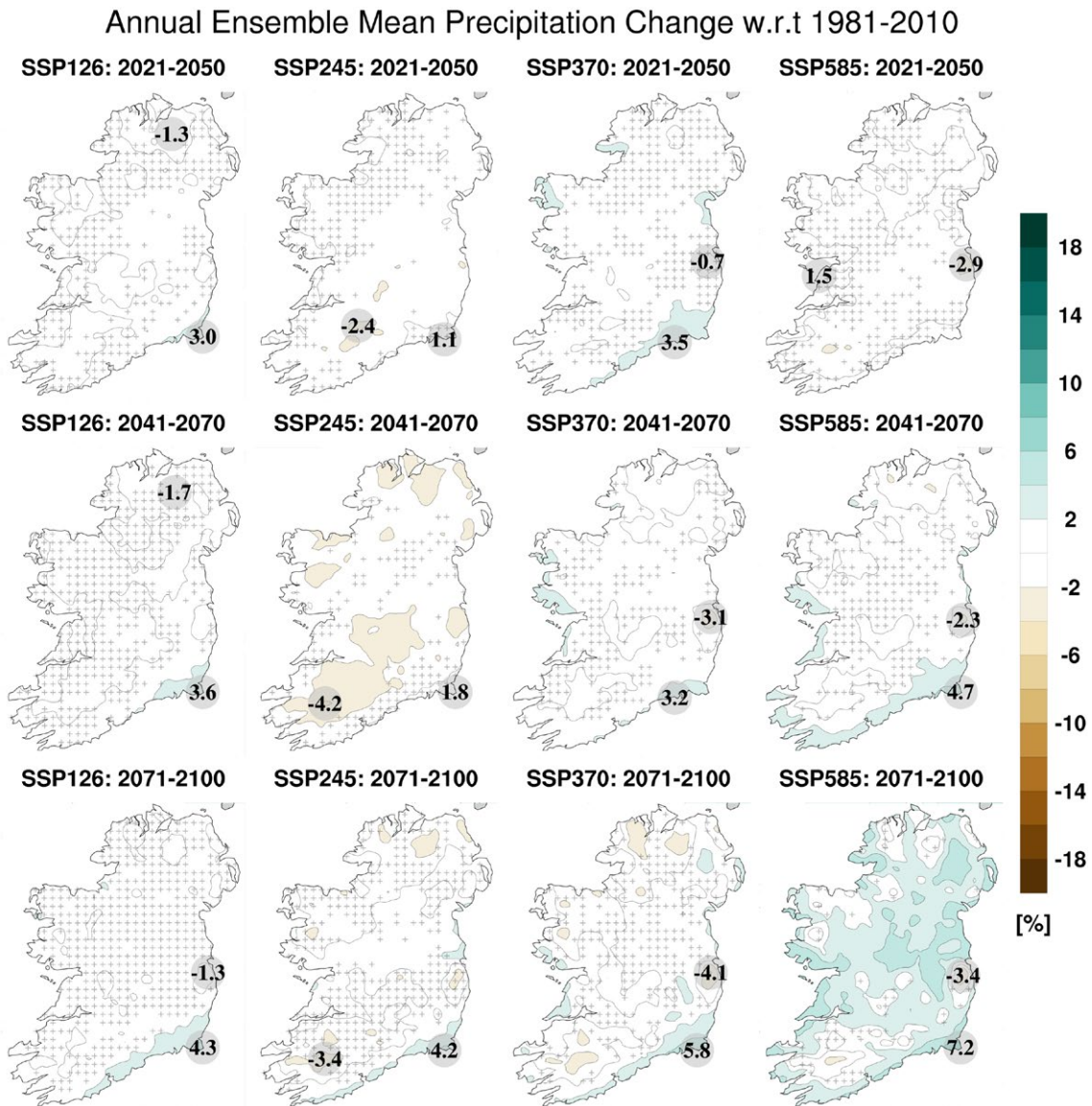
Figure 3.18. RCM–CMIP6 ensemble projections of mean annual precipitation (%). All RCM ensemble members were run with 4 km grid spacing. In each case, the future 30-year period is compared with the past period, 1981–2010. The numbers included on each plot are the minimum and maximum projected changes, displayed at their locations.

decreases (averaged over country) ranging from 0.7% for SSP126 (2071–2100) to 9.1% for SSP370 (2071–2100).

Figure 3.19d, the autumn projected change (%) in precipitation, shows an increase, which is enhanced for the higher SSPs and later time periods. In particular, the sparsity of hatching for SSP370 and SSP585 during 2041–2070 and 2071–2100 demonstrates agreement between ensemble members and higher certainty in the autumn

precipitation projections for these time periods and SSPs. This is further demonstrated by Table 3.12 (fifth panel), which shows that, for SSP370 and SSP585 (2041–2070 and 2071–2100), the 33rd and 66th percentile statistics have the same sign. In summary, the projected increases in precipitation during autumn have higher certainty for the higher SSPs and later time periods, with robust projected increases (averaged over country) ranging from 2.7% for SSP370 (2041–2070) to 5.9% for SSP585 (2071–2100).

Table 3.12. Annual and seasonal precipitation projections (%). This table corresponds to the projections in Figures 3.18 and 3.19, and shows the 33rd percentile, 50th percentile, mean and 66th percentile averaged over the island of Ireland

Annual precipitation (%)

Time period	SSP126				SSP245				SSP370				SSP585			
	P33	P50	Mean	P66	P33	P50	Mean	P66	P33	P50	Mean	P66	P33	P50	Mean	P66
2021–2050	−1.7	−1.0	0.3	0.7	−2.3	−1.4	−0.6	0.3	−0.7	0.0	1.2	1.6	−1.3	−0.4	−0.3	1.0
2041–2070	−2.1	−1.2	0.0	1.7	−3.4	−2.4	−1.5	−0.4	−1.0	−0.4	0.6	0.8	−0.7	0.1	0.7	1.4
2071–2100	−1.4	−0.6	0.8	1.7	−1.1	0.2	0.0	2.5	−1.1	−0.2	0.3	1.4	1.2	2.0	2.7	3.5

Winter precipitation (%)

Time period	SSP126				SSP245				SSP370				SSP585			
	P33	P50	Mean	P66	P33	P50	Mean	P66	P33	P50	Mean	P66	P33	P50	Mean	P66
2021–2050	−2.1	−0.7	−0.2	2.3	−2.3	−1.2	1.0	2.6	−0.3	1.0	1.4	3.2	−0.9	0.1	0.2	1.7
2041–2070	−2.6	−1.5	0.3	1.4	−2.4	−1.4	−0.5	0.9	1.0	2.2	3.2	5.1	1.5	2.4	3.1	4.7
2071–2100	−1.4	−0.3	2.0	4.6	0.2	1.9	2.9	5.3	2.2	3.4	4.0	5.8	6.5	9.3	9.8	13

Spring precipitation (%)

Time period	SSP126				SSP245				SSP370				SSP585			
	P33	P50	Mean	P66	P33	P50	Mean	P66	P33	P50	Mean	P66	P33	P50	Mean	P66
2021–2050	−2.2	−0.6	0.7	2.3	−6.6	−3.3	−2.3	0.8	−0.6	0.8	2.8	4.0	−5.0	−4.1	−2.8	−2.0
2041–2070	−5.2	−3.4	−1.3	1.1	−6.0	−4.6	−4.0	−1.0	−1.5	0.4	1.0	3.4	−3.5	−2.1	−0.5	1.2
2071–2100	−3.1	−1.7	−1.0	0.9	−6.5	−5.4	−3.4	−2.0	−6.3	−0.2	−1.4	4.0	−4.5	−2.3	−1.1	2.2

Summer precipitation (%)

Time period	SSP126				SSP245				SSP370				SSP585			
	P33	P50	Mean	P66	P33	P50	Mean	P66	P33	P50	Mean	P66	P33	P50	Mean	P66
2021–2050	−4.1	−2.4	1.0	0.9	−7.9	−6.4	−4.3	−3.2	−11	−8.8	−2.9	−0.9	−7.3	−5.6	1.0	2.1
2041–2070	−5.3	−3.0	−0.6	1.7	−12	−8.7	−5.3	−3.8	−13	−11	−5.8	−3.0	−14	−12	−5.2	−4.3
2071–2100	−6.8	−5.1	−0.7	−0.9	−11	−8.7	−6.5	−4.1	−16	−13	−9.1	−8.2	−12	−9.6	−7.7	−5.5

Autumn precipitation (%)

Time period	SSP126				SSP245				SSP370				SSP585			
	P33	P50	Mean	P66	P33	P50	Mean	P66	P33	P50	Mean	P66	P33	P50	Mean	P66
2021–2050	−1.4	0.1	0.9	3.1	−1.3	0.0	2.4	2.9	1.9	3.3	3.5	6.1	−3.0	−1.7	1.7	5.9
2041–2070	−1.6	0.4	2.0	5.1	−0.2	1.2	3.2	4.5	0.9	2.3	2.7	4.7	1.8	3.3	4.5	6.8
2071–2100	0.8	2.2	3.1	4.9	−0.8	4.3	5.1	9.8	1.3	2.6	5.6	5.8	4.2	5.3	5.9	7.4

The precipitation projections are consistent with previous RCM climate projection studies for Ireland (e.g. McGrath *et al.*, 2005; McGrath and Lynch, 2008; Gleeson *et al.*, 2013; Nolan, 2015; Nolan *et al.*, 2017; Nolan and Flanagan, 2020; O'Brien and Nolan, 2023).

3.11 Projections of Heavy Precipitation Events

Changes in the occurrence of heavy rainfall events are of particular importance because of the link with flooding (e.g. Wang *et al.*, 2006; Steele-Dunne *et al.*, 2008; Morrissey *et al.*, 2021). In this section,
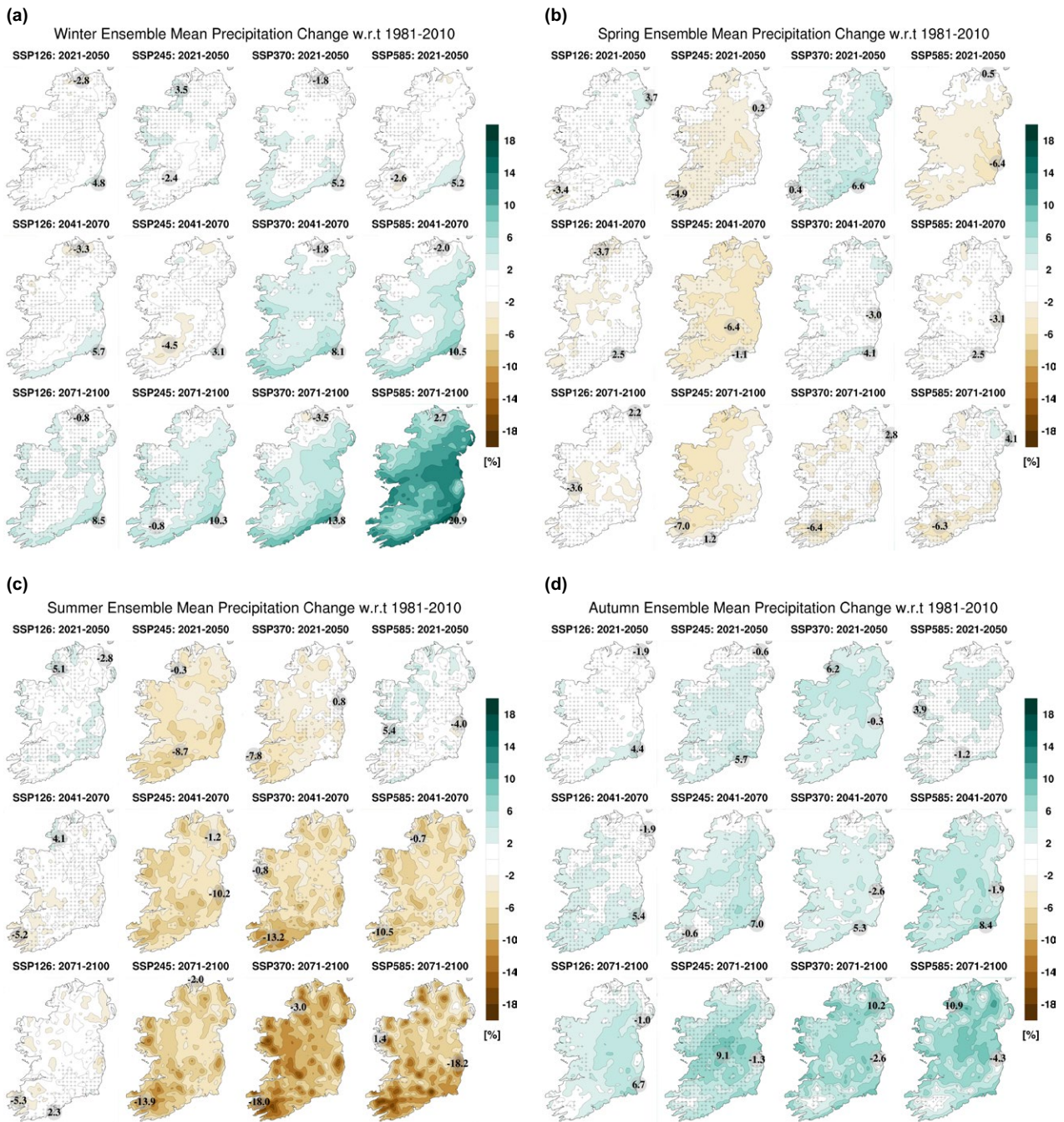
Figure 3.19. Seasonal RCM ensemble projections of mean precipitation (%) for (a) winter, (b) spring, (c) summer and (d) autumn. In each case, the future 30-year period is compared with the past period, 1981–2010. The numbers included on each plot are the minimum and maximum projected changes, displayed at their locations.

projections of heavy precipitation (R20 mm and R30 mm) are presented. The R20 mm and R30 mm metrics are defined as the number of days with precipitation greater than 20 mm and 30 mm, respectively. The projected increase in R20 mm and R30 mm should be considered in the context of historical values. Figure 3.20 presents the observed

annual R20 mm and R30 mm indices, averaged over the 30-year period 1981–2010 (derived from daily precipitation data provided by Walsh, 2016). The observed seasonal R20 mm indices are presented in Figure 3.21. The seasonal R30 mm figures (not shown) present a similar (but smaller in magnitude) geographical trend.

(a)

Observations 1981-2010
Annual No. Days Precipitation > 20 mm/day

(b)

Observations 1981-2010
Annual No. Days Precipitation > 30 mm/day
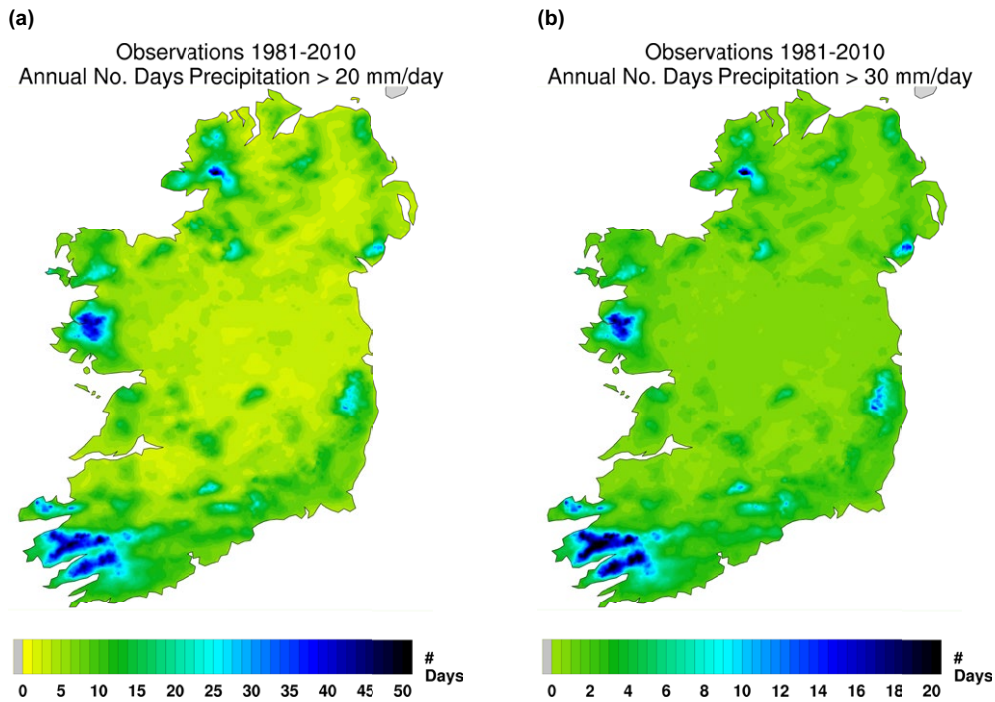
Figure 3.20. The observed annual number of (a) days with precipitation > 20 mm (R20 mm) and (b) days with precipitation > 30 mm (R30 mm) averaged over the 30-year period 1981–2010. Note the different scales for each figure.

(a)

Observations 1981-2010
Winter No. Days Precipitation > 20 mm/day

(b)

Observations 1981-2010
Spring No. Days Precipitation > 20 mm/day

(c)

Observations 1981-2010
Summer No. Days Precipitation > 20 mm/day

(d)

Observations 1981-2010
Autumn No. Days Precipitation > 20 mm/day
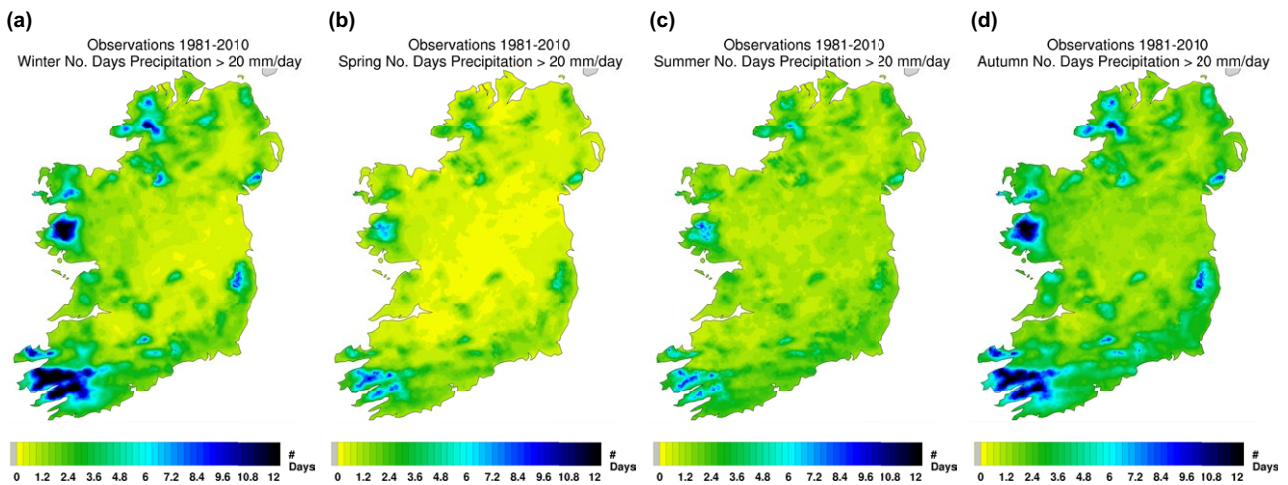
Figure 3.21. The observed number of days with precipitation > 20 mm (R20 mm) averaged over the 30-year period 1981–2010 for (a) winter, (b) spring, (c) summer and (d) autumn.

Figure 3.22a indicates an increase (%) in the annual R20 mm index, with the largest increases noted for the higher SSPs and later time periods. The scarcity of hatching in Figures 3.22a (in particular for the higher SSPs and later time periods) demonstrates agreement between ensemble members and higher certainty in the annual projections of R20 mm. The certainty in the annual projections of R20 mm is further demonstrated by Table 3.13 (first panel), which presents the mean and 33rd, 50th and 66th percentiles of the ensemble of annual R20 mm projections averaged over all land points. It is noted that the 33rd and 66th percentile statistics have the same sign for all SSPs and time periods. The projected increase in R20 mm (averaged over the country) ranges from 10% for SSP585 (2021–2050) to 40.7% for SSP585 (2071–2100).
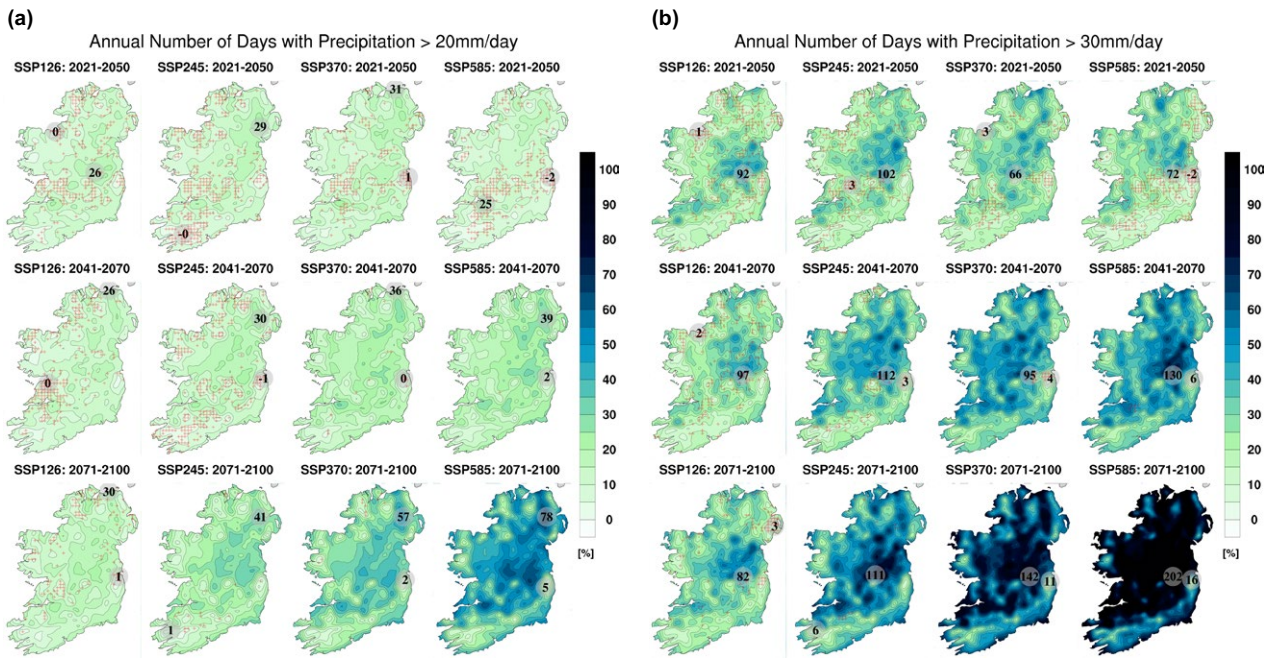
Figure 3.22. Projected changes (%) in the annual number of days with precipitation greater than (a) 20 mm/day (R20 mm) and (b) 30 mm/day (R30 mm). In each case, the future 30-year period is compared with the past period, 1981–2010. The numbers included on each plot are the minimum and maximum projected changes, displayed at their locations.

The annual projections of the more extreme R30 mm index, presented in Figure 3.22b and Table 3.14 (first panel), are enhanced in comparison with the R20 mm projections, but otherwise exhibit a similar trend. The projected increase in annual R30 mm (averaged over the country) ranges from 22.1% for SSP126 (2021–2050) to 89% for SSP585 (2071–2100).

Figure 3.23a, the winter projected change (%) in R20 mm, shows a robust increase for the higher SSPs and later time periods. In particular, the scarcity of hatching for SSP370 and SSP585 during 2041–2100 and 2071–2100 demonstrates agreement between ensemble members and higher certainty in winter R20 mm projections for these time periods and SSPs. This is further demonstrated by Table 3.13 (second panel), which shows that, for SSP245 (2071–2100), SSP370 (2041–2070 and 2071–2100) and SSP585 (2021–2050, 2041–2070 and 2071–2100), the 33rd and 66th percentile statistics have the same sign. In summary, the projected increases in winter R20 mm have higher certainty for the higher SSPs and/or later time periods, with robust increases (averaged over the country) ranging from 11.4% for SSP585 (2021–2050) to 52.5% for SSP585 (2071–2100). The projected increases in winter R30 mm (Figure 3.24a

and Table 3.14, second panel) are enhanced compared with the winter R20 mm projections, but otherwise exhibit a similar trend, with robust projected increases (averaged over the country) ranging from 26% for SSP245 (2021–2050) to 109% for SSP585 (2071–2100).

Figure 3.23b, the spring projected change (%) in R20 mm, shows a slight increase in the number of wet days. However, the projections have higher uncertainty, as demonstrated by an abundance of hatching for the earlier time periods and lower SSPs. The scarcity of hatching for SSP370 and SSP585 during 2071–2100 demonstrates agreement between ensemble members and higher certainty in spring R20 mm projections for the end of the century under these SSPs. This is confirmed by Table 3.13 (third panel), which shows robust increases (averaged over the country) ranging from 14% for SSP126 (2021–2050) to 32% for SSP585 (2071–2100). The projected increases in spring R30 mm (Figure 3.24b and Table 3.14, third panel) are enhanced compared with the R20 mm projections, but otherwise exhibit a similar trend, with robust projections (averaged over the country) ranging from 39% for SSP370 (2041–2070) to 76% for SSP585 (2071–2100).

Table 3.13. Annual and seasonal projections of R20 mm (%). This table corresponds to the projections of R20 mm (%) in Figures 3.22a and 3.23, and shows the 33rd percentile, 50th percentile, mean and 66th percentile averaged over the island of Ireland

Annual R20 mm (%)

Time period	SSP126				SSP245				SSP370				SSP585			
	P33	P50	Mean	P66	P33	P50	Mean	P66	P33	P50	Mean	P66	P33	P50	Mean	P66
2021–2050	2.3	5.3	10.7	11.6	2.0	5.0	10.7	12.6	3.5	6.0	12.1	12.4	2.7	5.5	10.0	12
2041–2070	2.9	5.9	11.0	13.3	3.1	6.2	12.6	15.2	8.0	10.8	17.5	17.5	11	14	19.1	21
2071–2100	4.5	8.2	14.0	16.2	10.7	14.7	21.0	26.6	16.8	21.4	28.2	33.4	29	34	40.7	44

Winter R20 mm (%)

Time period	SSP126				SSP245				SSP370				SSP585			
	P33	P50	Mean	P66	P33	P50	Mean	P66	P33	P50	Mean	P66	P33	P50	Mean	P66
2021–2050	−2.1	2.5	9.6	12.3	−0.4	4.7	12.2	17.2	−3.1	1.1	8.6	10.9	2.2	6.4	11.4	16
2041–2070	−0.3	4.2	10.1	14.3	−0.7	4.7	11.8	16.8	7.5	11.9	19.6	22.7	8.9	14	21.7	26
2071–2100	0.0	4.5	13.6	15.9	9.9	15.1	22.2	27.9	18.3	23.7	30.7	35.6	36	43	52.5	58

Spring R20 mm (%)

Time period	SSP126				SSP245				SSP370				SSP585			
	P33	P50	Mean	P66	P33	P50	Mean	P66	P33	P50	Mean	P66	P33	P50	Mean	P66
2021–2050	1.1	7.5	14.0	20.8	−2.1	3.3	11.2	15.3	2.8	8.9	18.4	22.5	−6.9	−1.6	4.8	10
2041–2070	−2.9	4.1	12.8	20.1	−6.6	−1.1	6.5	10.8	2.6	9.0	16.9	23.1	4.4	10	17.9	23
2071–2100	0.8	6.8	14.2	19.8	−2.6	4.5	14.9	20.7	8.6	17.3	24.0	34.9	14	21	32.0	37

Summer R20 mm (%)

Time period	SSP126				SSP245				SSP370				SSP585			
	P33	P50	Mean	P66	P33	P50	Mean	P66	P33	P50	Mean	P66	P33	P50	Mean	P66
2021–2050	−0.6	4.8	17.1	17.0	−6.6	−1.6	8.1	9.6	−7.4	−2.0	12.5	12.6	−4.4	2.4	16.6	21
2041–2070	−1.4	4.3	15.2	17.6	−7.2	−0.7	9.0	14.4	−5.1	1.1	13.9	16.8	−8.4	−1.9	14.6	15
2071–2100	−4.4	1.1	13.3	13.8	−2.6	5.5	14.2	21.8	−3.3	4.9	18.3	24.7	9.2	17	29.9	36

Autumn R20 mm (%)

Time period	SSP126				SSP245				SSP370				SSP585			
	P33	P50	Mean	P66	P33	P50	Mean	P66	P33	P50	Mean	P66	P33	P50	Mean	P66
2021–2050	4.3	8.4	11.9	17.2	5.4	10.1	16.3	21.2	7.8	12.5	17.9	23.1	1.8	6.9	13.4	21
2041–2070	4.3	8.8	14.3	19.2	11.9	16.5	24.4	29.3	12.1	16.7	23.8	28.7	17	21	26.9	32
2071–2100	10.0	15.1	20.5	26.4	20.4	26.7	33.2	39.6	24.4	30.0	40.9	44.5	37	42	47.6	54

The summer projected changes in R20 mm, as presented in Figure 3.23c, have high uncertainty for all SSPs and time periods except for 2071–2100 under SSP585. This uncertainty in the summer R20 mm projections is further demonstrated in Table 3.13 (fourth panel), where the P33 and P66 percentile statistics have different signs for all SSPs and time periods except for 2071–2100 under SSP585 (29.9% increase averaged over the country). The projected increases in summer R30 mm have higher certainty, as is evidenced by less hatching in Figure 3.24c and better agreement in sign between the P33 and P66 statistics of Table 3.14 (fourth panel). Averaged over the country, robust summer projections of

Table 3.14. Annual and seasonal projections of R30 mm (%). This table corresponds to the projections in Figures 3.22b and 3.24, and shows the 33rd percentile, 50th percentile, mean and 66th percentile averaged over the island of Ireland

Annual R30 mm (%)

Time period	SSP126				SSP245				SSP370				SSP585			
	P33	P50	Mean	P66	P33	P50	Mean	P66	P33	P50	Mean	P66	P33	P50	Mean	P66
2021–2050	5.4	11.1	22.1	24.5	6.8	12.6	24.0	27.2	8.9	14.1	24.8	26.9	6.4	12	22.3	24
2041–2070	7.5	13.4	24.0	27.5	12.0	18.3	31.9	35.3	17.6	23.3	38.5	37.7	20	27	41	42
2071–2100	10.6	16.6	29.1	32.4	21.0	29.4	45.3	53.9	36.0	45.5	62.0	69.7	56	68	89	94

Winter R30 mm (%)

Time period	SSP126				SSP245				SSP370				SSP585			
	P33	P50	Mean	P66	P33	P50	Mean	P66	P33	P50	Mean	P66	P33	P50	Mean	P66
2021–2050	–3	6	26	29	1	10	26	33	–3	6	21	26	4	13	30	37
2041–2070	–3	6	24	29	5	16	34	42	14	25	44	51	15	26	47	52
2071–2100	3	13	32	37	15	26	47	52	29	40	60	68	66	81	109	118

Spring R30 mm (%)

Time period	SSP126				SSP245				SSP370				SSP585			
	P33	P50	Mean	P66	P33	P50	Mean	P66	P33	P50	Mean	P66	P33	P50	Mean	P66
2021–2050	–5	8	31	38	–2	10	37	40	2	14	43	47	–12	–1	19	25
2041–2070	–5	9	34	40	–5	6	31	32	0	13	39	44	2	15	39	45
2071–2100	1	13	40	43	–7	7	37	42	18	34	60	70	26	41	76	78

Summer R30 mm (%)

Time period	SSP126				SSP245				SSP370				SSP585			
	P33	P50	Mean	P66	P33	P50	Mean	P66	P33	P50	Mean	P66	P33	P50	Mean	P66
2021–2050	4	14	37	38	–2	7	26	28	–2	8	33	33	–1	9	31	37
2041–2070	5	15	37	40	–2	9	28	33	4	14	40	40	0	11	38	38
2071–2100	0	9	32	31	8	20	40	48	13	27	53	61	30	46	78	85

Autumn R30 mm (%)

Time period	SSP126				SSP245				SSP370				SSP585			
	P33	P50	Mean	P66	P33	P50	Mean	P66	P33	P50	Mean	P66	P33	P50	Mean	P66
2021–2050	7	15	23	32	9	18	33	40	12	20	32	39	5	15	29	37
2041–2070	8	16	28	36	23	32	50	57	23	32	50	55	32	42	58	65
2071–2100	15	24	38	45	36	47	68	75	50	62	87	93	71	84	106	117

R30 mm range from 32% (SSP126, 2071–2100) to 78% (SSP585, 2071–2100).

Figure 3.23d indicates an increase in autumn R20 mm, with the largest increases noted for the higher SSPs and later time periods. The scarcity of hatching in Figure 3.23d (in particular for the higher SSPs and later time periods) demonstrates agreement between ensemble members and higher certainty in the projections. The certainty in the autumn R20 mm projections is further demonstrated by Table 3.13 (fifth panel), where it is noted that the 33rd and 66th percentile statistics have the same sign for all SSPs and time periods. The projected increase in autumn R20 mm (averaged over the country) ranges from 11.9% for SSP126 (2021–2050) to 47.6% for

(a) Winter Number of Days with Precipitation > 20 mm/day

(b) Spring Number of Days with Precipitation > 20 mm/day

(c) Summer Number of Days with Precipitation > 20 mm/day

(d) Autumn Number of Days with Precipitation > 20 mm/day
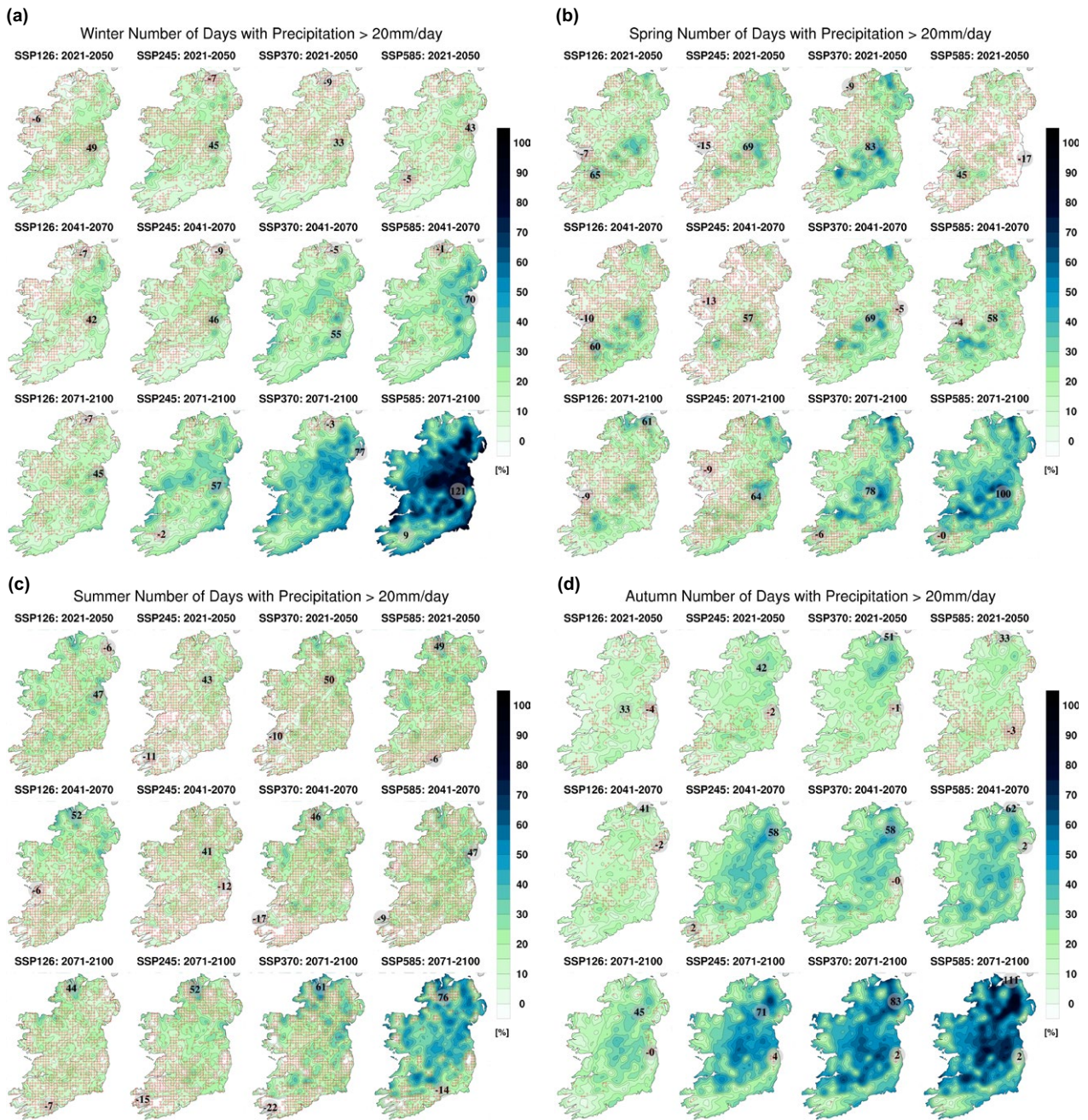
Figure 3.23. Seasonal projected changes (%) in the annual number of days with precipitation greater than 20 mm/day (R20 mm) for (a) winter, (b) spring, (c) summer and (d) autumn. In each case, the future 30-year period is compared with the past period, 1981–2010. The numbers included on each plot are the minimum and maximum projected changes, displayed at their locations.

SSP585 (2071–2100). The projections of autumn R30 mm, presented in Figure 3.24d and Table 3.14 (fifth panel), are enhanced compared with the R20 mm projections, but otherwise exhibit a similar trend. The projected increase in autumn R30 mm (averaged over the country) ranges from 23% for SSP126 (2021–2050) to 106% for SSP585 (2071–2100).

The increased frequency of heavy precipitation is well marked in winter and autumn and over the full year, particularly for the higher SSPs and later time periods, but regional details are not reliable because of a large spread in the ensembles.

The projected increases in heavy rainfall events are in line with previous RCM studies for Ireland, which showed large projected increases in intense rainfall by mid-century, particularly during the winter and autumn months (e.g. Gleeson *et al*., 2013; Nolan, 2015; Nolan *et al*., 2017; Nolan and Flanagan 2020).

51

(a) Winter Number of Days with Precipitation > 30mm/day

(b) Spring Number of Days with Precipitation > 30mm/day

(c) Summer Number of Days with Precipitation > 30mm/day

(d) Autumn Number of Days with Precipitation > 30mm/day
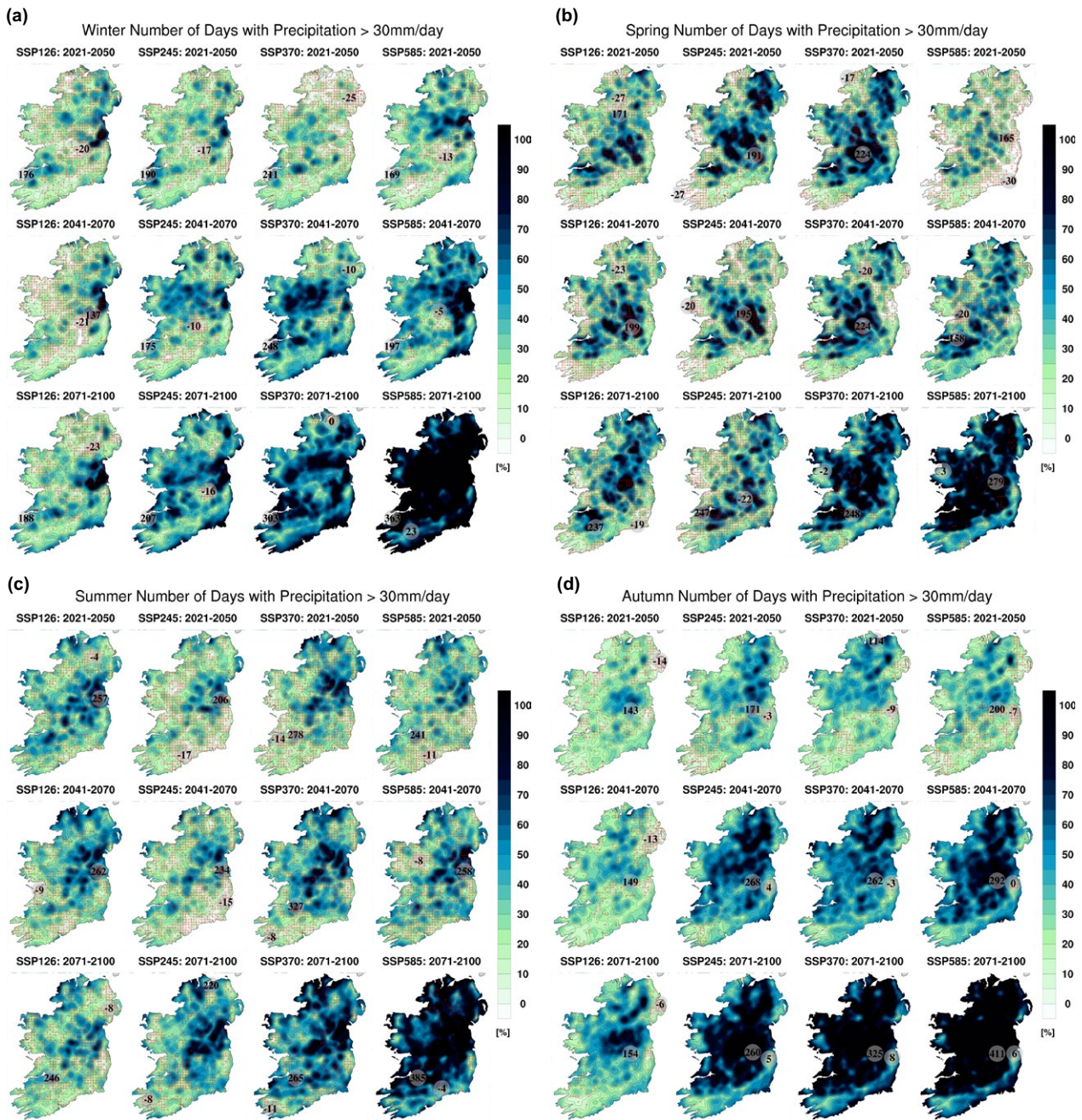
Figure 3.24. Seasonal projected changes (%) in the annual number of days with precipitation greater than 30 mm/day (R30 mm) for (a) winter, (b) spring, (c) summer and (d) autumn. In each case, the future 30-year period is compared with the past period, 1981–2010. The numbers included on each plot are the minimum and maximum projected changes, displayed at their locations.

3.12 Projections of Simple Daily Intensity Index

The Simple Daily Intensity Index (SDII) is the average precipitation on wet days (days with precipitation ≥ 1 mm) during the period of interest. Analysing SDII projections provides an insight into how future wet days will change under climate change.

Figure 3.25, the spatial distribution of mean annual change in SDII (%), shows an increase in SDII projections for all SSPs and time periods, with projected increases enhanced for the higher SSPs and later time periods. The largest projected increases are noted in the south-east (up to 17% for 2071–2100 under SSP585). The scarcity of

Annual Simple Daily Intensity Projections
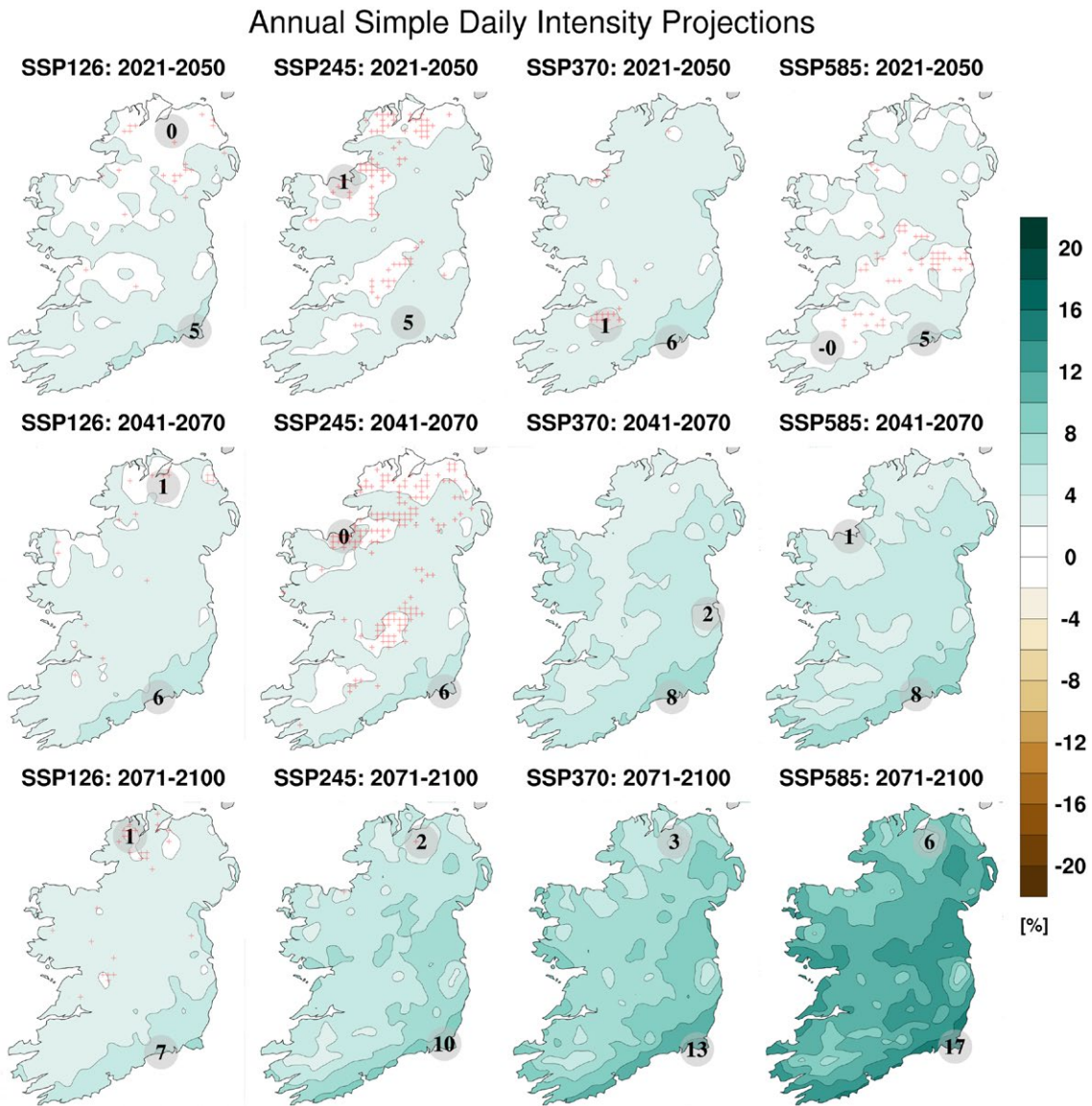
Figure 3.25. RCM–CMIP6 ensemble projections of SDII of precipitation (%). All RCM ensemble members were run with 4 km grid spacing. In each case, the future 30-year period is compared with the past period, 1981–2010. The numbers included on each plot are the minimum and maximum projected changes, displayed at their locations.

hatching in Figure 3.25 (for all time periods and SSPs) demonstrates agreement between ensemble members and higher certainty in the annual SDII projections. The higher certainty in the annual SDII projections is further demonstrated in Table 3.15 (first panel), which presents the mean and 33rd, 50th and 66th percentiles of the ensemble of annual SDII projections averaged over all land points. It is noted that the 33rd and 66th percentile statistics have the same sign for all SSPs and time periods, with projected increases ranging from 2.3% (SSP126, 2021–2050) to 11.1% (SSP585, 2071–2100).

Figure 3.26a, the projected change (%) in winter SDII, shows a robust increase for the higher SSPs and later time periods. In particular, the scarcity of hatching for SSP245 (2071–2100) and SSP370 and SSP585 (2041–2100 and 2071–2100) demonstrates agreement between ensemble members and higher certainty in winter SDII projections for these time periods and SSPs. This is further demonstrated by Table 3.15 (second panel), which shows that the projected increases in winter SDII have higher certainty (i.e. P33 and P66 have the same sign) for the higher SSPs and/or later time periods, with robust projected

Table 3.15. Annual and seasonal projections of SDII of precipitation (%). This table corresponds to the projections in Figures 3.25 and 3.26, and shows the 33rd percentile, 50th percentile, mean and 66th percentile averaged over the island of Ireland

Annual SDII (%)

Time period	SSP126				SSP245				SSP370				SSP585			
	P33	P50	Mean	P66	P33	P50	Mean	P66	P33	P50	Mean	P66	P33	P50	Mean	P66
2021–2050	0.6	1.3	2.3	3.0	0.3	1.0	2.4	3.3	0.9	1.7	2.9	3.8	0.7	1.6	2.3	3.5
2041–2070	1.0	1.6	2.8	3.7	0.2	1.1	2.7	4.3	2.3	3.0	4.3	5.0	3.0	3.9	4.6	5.9
2071–2100	1.0	2.1	3.3	5.0	2.8	3.8	5.4	8.3	5.1	6.5	7.6	10.4	8.5	9.7	11.1	13

Winter SDII (%)

Time period	SSP126				SSP245				SSP370				SSP585			
	P33	P50	Mean	P66	P33	P50	Mean	P66	P33	P50	Mean	P66	P33	P50	Mean	P66
2021–2050	–0.8	0.2	1.6	2.3	–0.1	1.0	2.5	3.5	–0.7	0.3	2.0	3.2	0.9	1.7	2.4	3.6
2041–2070	0.6	1.5	2.4	3.3	–1.3	–0.1	1.8	3.7	2.0	2.8	4.0	5.0	2.9	3.7	4.6	5.7
2071–2100	0.3	1.4	3.0	4.7	2.6	3.8	4.7	7.0	4.4	5.6	6.7	8.5	8.2	9.5	11.0	13

Spring SDII (%)

Time period	SSP126				SSP245				SSP370				SSP585			
	P33	P50	Mean	P66	P33	P50	Mean	P66	P33	P50	Mean	P66	P33	P50	Mean	P66
2021–2050	–0.2	0.9	1.3	2.7	–1.7	–0.7	0.3	1.5	–0.2	0.7	1.7	2.5	–2.5	–1.3	–0.4	1.0
2041–2070	–1.0	0.4	1.3	3.5	–2.3	–1.4	–0.3	0.6	–0.5	0.4	1.3	2.5	0.2	1.3	2.0	3.3
2071–2100	–0.2	1.1	1.6	3.3	–1.2	0.3	1.4	3.6	1.8	3.4	3.5	6.0	3.4	4.7	5.4	7.4

Summer SDII (%)

Time period	SSP126				SSP245				SSP370				SSP585			
	P33	P50	Mean	P66	P33	P50	Mean	P66	P33	P50	Mean	P66	P33	P50	Mean	P66
2021–2050	0.4	2.0	4.2	5.5	–1.2	0.3	1.9	3.5	–0.8	0.8	3.5	4.8	–1.3	0.8	3.3	6.5
2041–2070	–0.2	1.3	3.6	5.2	–1.0	0.8	2.5	5.2	0.3	2.5	4.4	7.0	–0.9	1.3	3.7	6.3
2071–2100	–1.3	0.8	3.0	4.9	–0.1	2.2	4.8	8.2	1.8	5.4	7.3	11.6	7.2	9.8	12.1	16

Autumn SDII (%)

Time period	SSP126				SSP245				SSP370				SSP585			
	P33	P50	Mean	P66	P33	P50	Mean	P66	P33	P50	Mean	P66	P33	P50	Mean	P66
2021–2050	1.9	2.8	3.2	4.8	1.8	3.0	4.2	5.8	2.5	3.6	5.2	6.4	1.1	2.7	4.0	6.7
2041–2070	1.7	2.8	4.3	6.0	2.7	4.2	6.4	8.4	4.3	5.7	7.2	9.4	5.6	6.9	7.8	9.7
2071–2100	3.0	4.3	5.4	7.2	6.9	8.3	10.1	11.7	8.0	9.9	12.4	14.2	12	14	15.4	18

increases (averaged over the country) ranging from 2.4% for SSP126 (2041–2070) to 11% for SSP585 (2071–2100).

Figure 3.26b, the projected change (%) in spring SDII, shows small (~0%) changes for the lower SSPs and/or earlier time periods (small increases otherwise). The

spring SDII projections have high uncertainty for lower SSPs and earlier time periods, as demonstrated by an abundance of hatching in Figure 3.26b. The spring SDII projections have higher certainty for SSP370 (2071–2100) and SSP585 (2041–2070 and 2071–2100), as demonstrated by an absence of hatching in Figure 3.26b and agreement in sign between the

(a)

Winter Simple Daily Intensity Projections

(b)

Spring Simple Daily Intensity Projections

(c)

Summer Simple Daily Intensity Projections

(d)

Autumn Simple Daily Intensity Projections
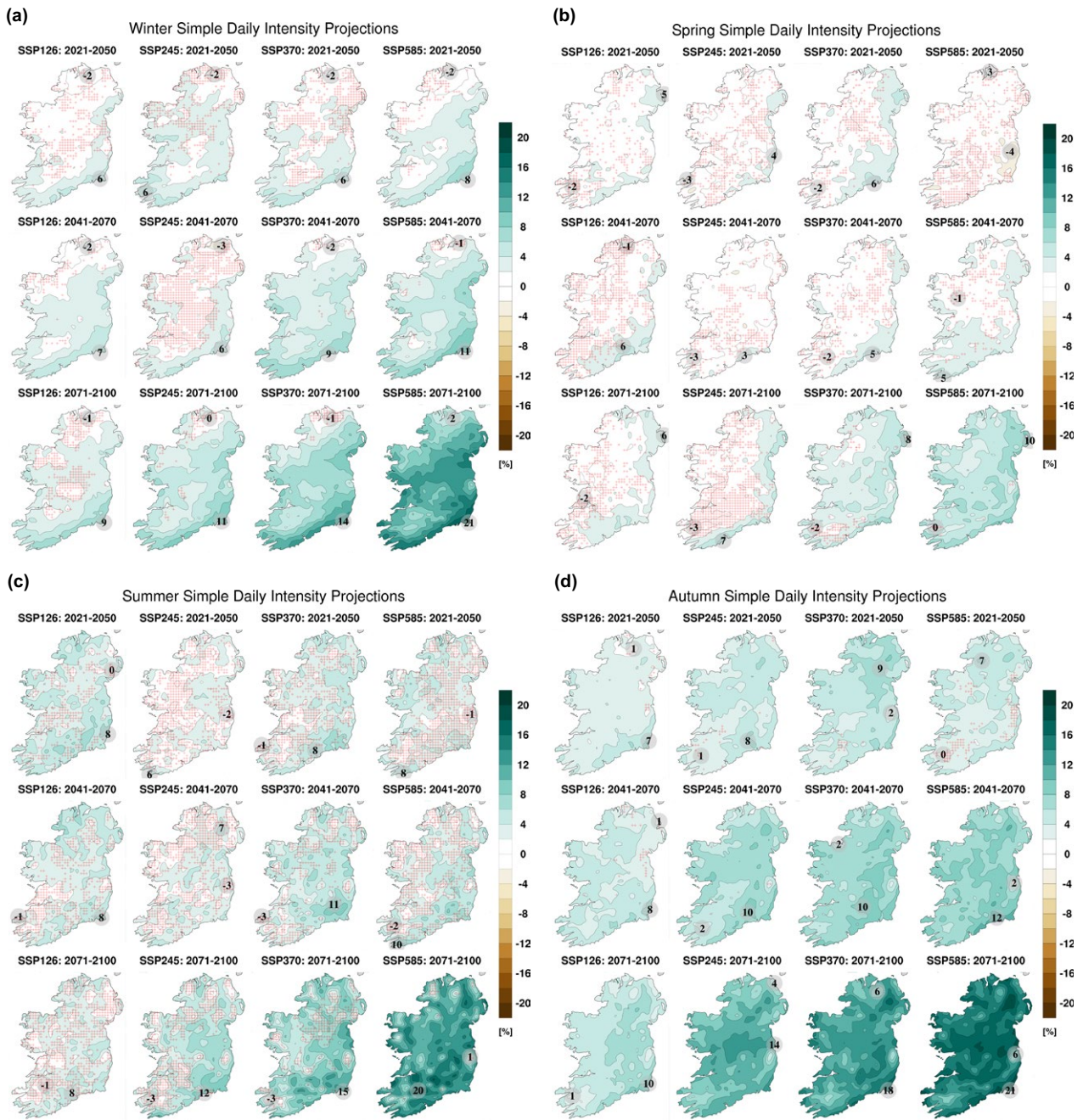
Figure 3.26. Seasonal RCM ensemble projections of SDII (%) for (a) winter, (b) spring, (c) summer and (d) autumn. In each case, the future 30-year period is compared with the past period, 1981–2010. The numbers included on each plot are the minimum and maximum projected changes, displayed at their locations.

P33 and P66 statistics of Table 3.15 (third panel). Averaged over the whole country, robust projections of increases in spring SDII are 3.5% for SSP370 (2071–2100), 2% for SSP585 (2041–2070) and 5.4% for SSP585 (2071–2100).

Figure 3.26c, the projected change (%) in summer SDII, shows an increase (or small change), which is enhanced for the higher SSPs and later time periods.

However, the abundance of hatching demonstrates high uncertainty in summer SDII projections for the earlier time periods and lower SSPs. The summer SDII projections have higher certainty for SSP370 (2041–2070 and 2071–2100) and SSP585 (2071–2100), as demonstrated by an absence of hatching in Figure 3.26c and agreement in sign between the P33 and P66 statistics of Table 3.15 (fourth panel).

Averaged over the whole country, robust projected increases in summer SDII are 4.4% for SSP370 (2041–2070), 7.3% for SSP370 (2071–2100) and 12.1% for SSP585 (2071–2100).

Figure 3.26d, the projected change (%) in autumn SDII, shows an increase for all SSPs and time periods, with projected increases enhanced for the higher SSPs and later time periods. The largest projected increases are noted in the south-east (up to 21% for

Observed Annual SDII 1981-2010

Figure 3.27. The observed annual SDII (mm), 1981–2010.

2071–2100 under SSP585). The scarcity of hatching in Figure 3.26d (for all time periods and SSPs) demonstrates agreement between ensemble members and higher certainty in the autumn SDII projections. The higher certainty in the autumn SDII projections is further demonstrated in Table 3.15 (fifth panel), where the 33rd and 66th percentile statistics have the same sign for all SSPs and time periods, with projected increases ranging from 3.2% (SSP126, 2021–2050) to 15.4% (SSP585, 2071–2100).

For comparison, the observed mean annual and seasonal SDII projections over the period 1981–2010 (derived from daily precipitation data provided by Walsh, 2016) are presented in Figures 3.27 and 3.28, respectively.

3.13 Dry Periods

To quantify the potential impact of climate change on future drought events, the change in the number of dry periods was analysed. A dry period is defined as at least 5 consecutive days (i.e. 5 days or more) for which the daily precipitation is less than 1 mm. The observed annual number of dry periods, averaged over the 30-year period 1981–2010, is presented in Figure 3.29a. Similarly, the seasonal number of dry periods is presented in Figure 3.30.

Figure 3.31, the annual projected change (%) in dry periods, shows an increase (or small change), which is enhanced for the higher SSPs and later time periods. The annual dry period projections have higher certainty for the later time periods and/or higher SSPs, as demonstrated by an absence of hatching

Figure 3.28. The observed SDII (mm), 1981–2010, for (a) winter, (b) spring, (c) summer and (d) autumn.

(a)

Observations 1981-2010
Mean Annual Number of Dry Periods

(b)

Observations 1981-2010
Mean Annual Max. Length of Dry Period
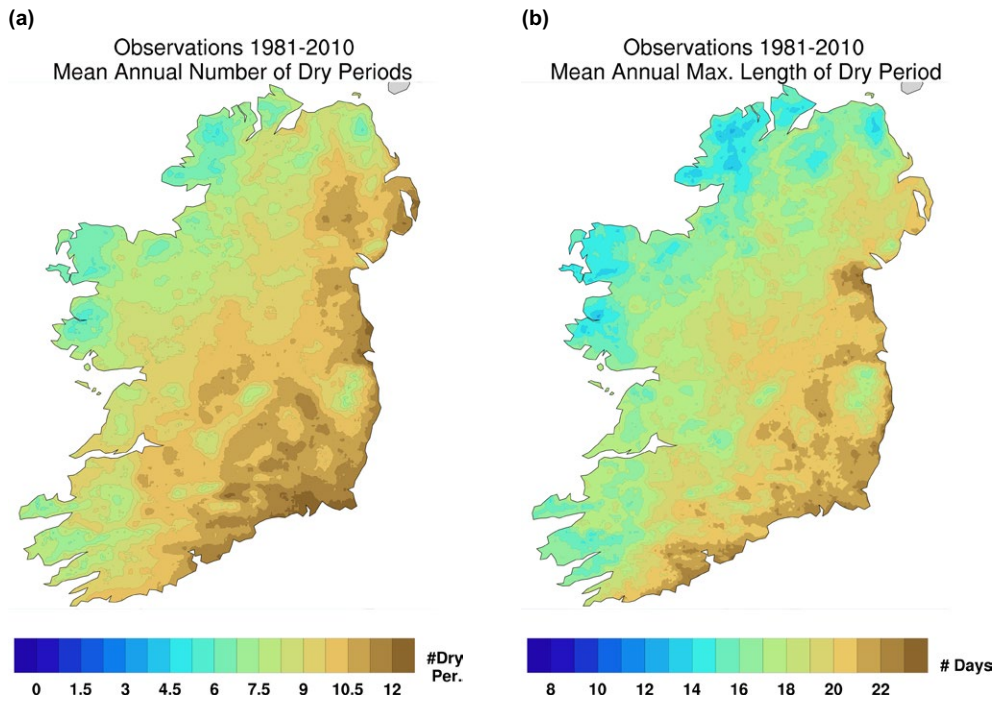
Figure 3.29. (a) The observed number of annual dry periods (5 consecutive days or more for which the daily precipitation is less than 1 mm) and (b) the largest annual number of consecutive dry days, averaged over the 30-year period 1981–2010.

(a)

Observations 1981-2010
Mean Winter Number of Dry Periods

(b)

Observations 1981-2010
Mean Spring Number of Dry Periods

(c)

Observations 1981-2010
Mean Summer Number of Dry Periods

(d)

Observations 1981-2010
Mean Autumn Number of Dry Periods
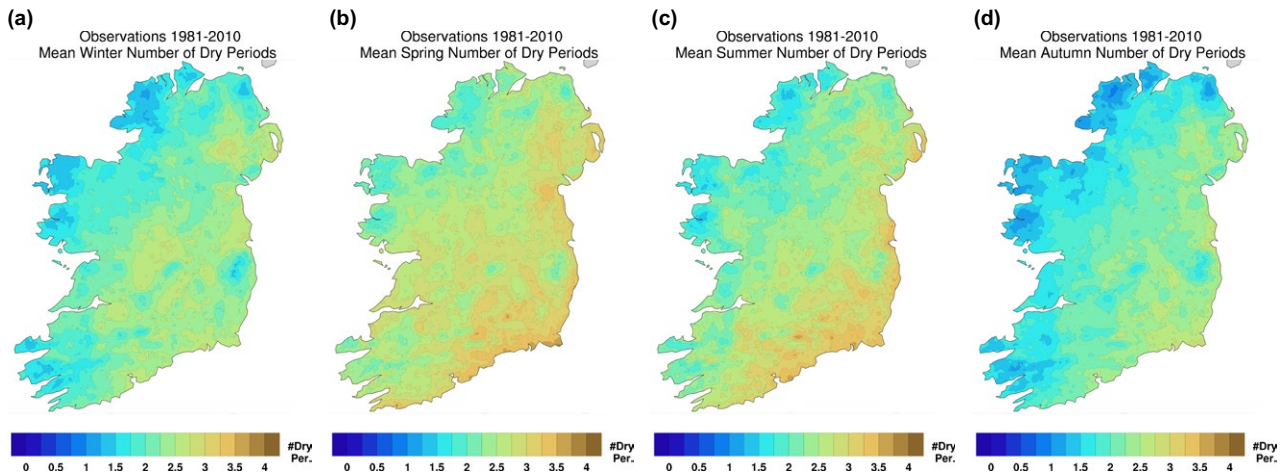
Figure 3.30. Observed seasonal number of dry periods averaged over the 30-year period 1981–2010 for (a) winter, (b) spring, (c) summer and (d) autumn.

in Figure 3.31 and agreement in sign between the P33 and P66 statistics of Table 3.16 (first panel). Averaged over the whole country, robust (i.e. P33 and P66 have the same sign) projections of increases in mean annual dry periods range from 3.2% for SSP126 (2021–2050) to 9.5% for SSP585 (2071–2100).

The projections of winter dry periods are very uncertain, as demonstrated by an abundance of hatching in Figure 3.32a and disagreement in sign,

and large spread, between the percentile statistics (all SSPs and time periods) in Table 3.16 (second panel). The large changes noted in the mean projections of Figure 3.32a for the earlier time periods and lower SSPs are due to ensemble outliers, as is evident from the large spread of the mean and percentile statistics of Table 3.16 (second panel).

The projections of increases (or small changes) in spring dry periods also have high uncertainty,

Annual 5-Day Dry Periods (< 1mm/day) Projections
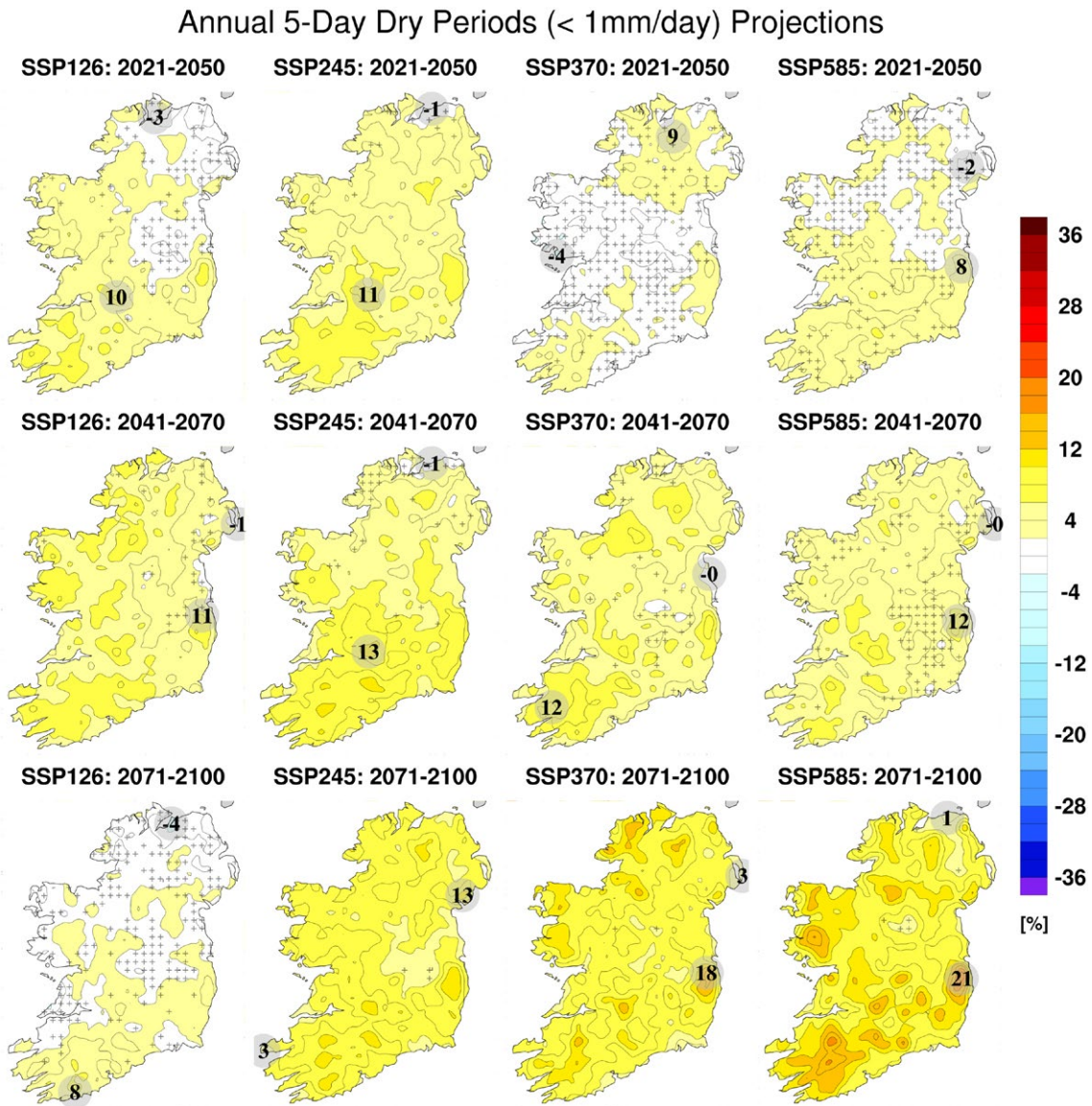
Figure 3.31. Annual RCM–CMIP6 ensemble projections of the number of dry periods (%). All RCM ensemble members were run with 4 km grid spacing. In each case, the future 30-year period is compared with the past period, 1981–2010. The numbers included on each plot are the minimum and maximum projected changes, displayed at their locations.

in particular for 2021–2050 and 2041–2070, as demonstrated by an abundance of hatching in Figure 3.32b and disagreement in sign between the percentile statistics of Table 3.16 (third panel). Averaged over the whole country, robust (i.e. P33 and P66 have the same sign) projections of increases in spring dry periods range from 5% for SSP126 (2041–2070) to 7.1% for SSP585 (2071–2100).

The largest projected increases in dry periods are noted for summer (Figure 3.32c), which are enhanced for the higher SSPs and later time periods. The summer dry period projections have higher

certainty for the later time periods and/or higher SSPs, as demonstrated by an absence of hatching in Figure 3.32c and agreement in sign between the P33 and P66 statistics of Table 3.16 (fourth panel). Averaged over the whole country, robust (i.e. P33 and P66 have the same sign) projections of increases in summer dry periods range from 6.3% for SSP370 (2021–2050) to 20% for SSP585 (2071–2100).

The projections of autumn dry periods have high uncertainty for the earlier time periods, as demonstrated by an abundance of hatching in Figure 3.32d and disagreement in sign between

Table 3.16. Annual and seasonal projections of dry periods (%). This table corresponds to the projections in Figures 3.31 and 3.32, and shows the 33rd percentile, 50th percentile, mean and 66th percentile averaged over the island of Ireland

Annual dry periods (%)

Time periods	SSP126				SSP245				SSP370				SSP585			
	P33	P50	Mean	P66	P33	P50	Mean	P66	P33	P50	Mean	P66	P33	P50	Mean	P66
2021–2050	1.0	2.5	3.2	5.3	2.5	3.8	4.7	6.5	–1.0	0.9	1.5	4.6	–0.6	1.2	2.7	4.9
2041–2070	2.2	3.7	5.2	6.8	3.1	5.0	6.1	8.6	2.5	4.1	5.1	7.4	1.1	2.9	4.2	6.7
2071–2100	–0.2	1.3	2.0	4.3	3.9	5.6	7.6	9.4	4.7	6.4	8.3	10.4	5.3	7.8	9.5	13

Winter dry periods (%)

Time periods	SSP126				SSP245				SSP370				SSP585			
	P33	P50	Mean	P66	P33	P50	Mean	P66	P33	P50	Mean	P66	P33	P50	Mean	P66
2021–2050	3.8	8.9	12.3	20.4	2.2	6.9	9.2	15.5	–1.8	3.8	5.2	14.2	0.8	6.1	8.0	16
2041–2070	4.8	8.6	11.5	16.3	0.2	4.6	8.8	14.0	–0.5	3.9	8.3	13.9	–4.1	0.2	2.3	9.4
2071–2100	–4.3	1.2	4.8	11.4	–4.9	–1.1	1.7	6.6	–4.0	–0.2	2.8	7.8	–5.9	0.1	2.8	12

Spring dry periods (%)

Time periods	SSP126				SSP245				SSP370				SSP585			
	P33	P50	Mean	P66	P33	P50	Mean	P66	P33	P50	Mean	P66	P33	P50	Mean	P66
2021–2050	–3.9	–0.9	0.6	5.2	–0.4	2.7	4.7	8.9	–7.1	–4.5	–4.1	0.4	–0.9	2.7	4.2	9.7
2041–2070	0.9	3.5	5.0	8.8	–0.8	2.0	4.4	8.4	–6.5	–3.4	–0.4	3.3	–1.7	1.5	4.0	8.4
2071–2100	–1.3	1.3	2.2	6.2	1.4	4.8	6.8	11.9	–0.4	2.5	7.6	9.3	0.3	3.7	7.1	11

Summer dry periods (%)

Time periods	SSP126				SSP245				SSP370				SSP585			
	P33	P50	Mean	P66	P33	P50	Mean	P66	P33	P50	Mean	P66	P33	P50	Mean	P66
2021–2050	–1.2	2.0	2.9	7.1	2.0	4.8	6.8	10.2	0.8	4.0	6.3	10.9	–3.3	–0.4	1.4	5.2
2041–2070	–0.6	2.2	4.6	8.7	3.6	7.3	10.0	14.4	4.4	8.1	12.0	16.1	4.7	8.1	11.0	15
2071–2100	–3.3	0.0	1.1	6.1	6.5	9.5	12.3	16.0	11.2	14.8	16.9	22.2	12	16	20	25

Autumn dry periods (%)

Time periods	SSP126				SSP245				SSP370				SSP585			
	P33	P50	Mean	P66	P33	P50	Mean	P66	P33	P50	Mean	P66	P33	P50	Mean	P66
2021–2050	–3.6	–0.8	3.4	5.9	–4.9	–1.5	4.1	8.4	–1.7	1.3	3.2	7.1	–3.6	–0.6	1.7	5.6
2041–2070	–1.6	1.4	4.4	8.3	–2.6	0.0	5.0	7.0	1.3	4.1	5.5	9.3	–5.2	–1.4	1.0	6.3
2071–2100	–2.8	0.4	4.5	8.9	1.9	5.1	9.3	12.7	0.1	3.1	5.5	9.2	3.6	6.7	8.0	13

the percentile statistics of Table 3.16 (fifth panel). Averaged over the whole country, robust (i.e. P33 and P66 have the same sign) projections of increases in autumn dry periods are 9.3% for SSP245 (2071–2100), 5.5% for SSP370 (2041–2070 and 2071–2100) and 8% for SSP585 (2071–2100).

The observed mean annual longest dry period (1981–2010) is presented in Figure 3.29b. For this metric, the longest consecutive dry period was noted for each year and the average was calculated over the 30-year period of interest. The projected change (%) in the mean annual longest dry period is presented in
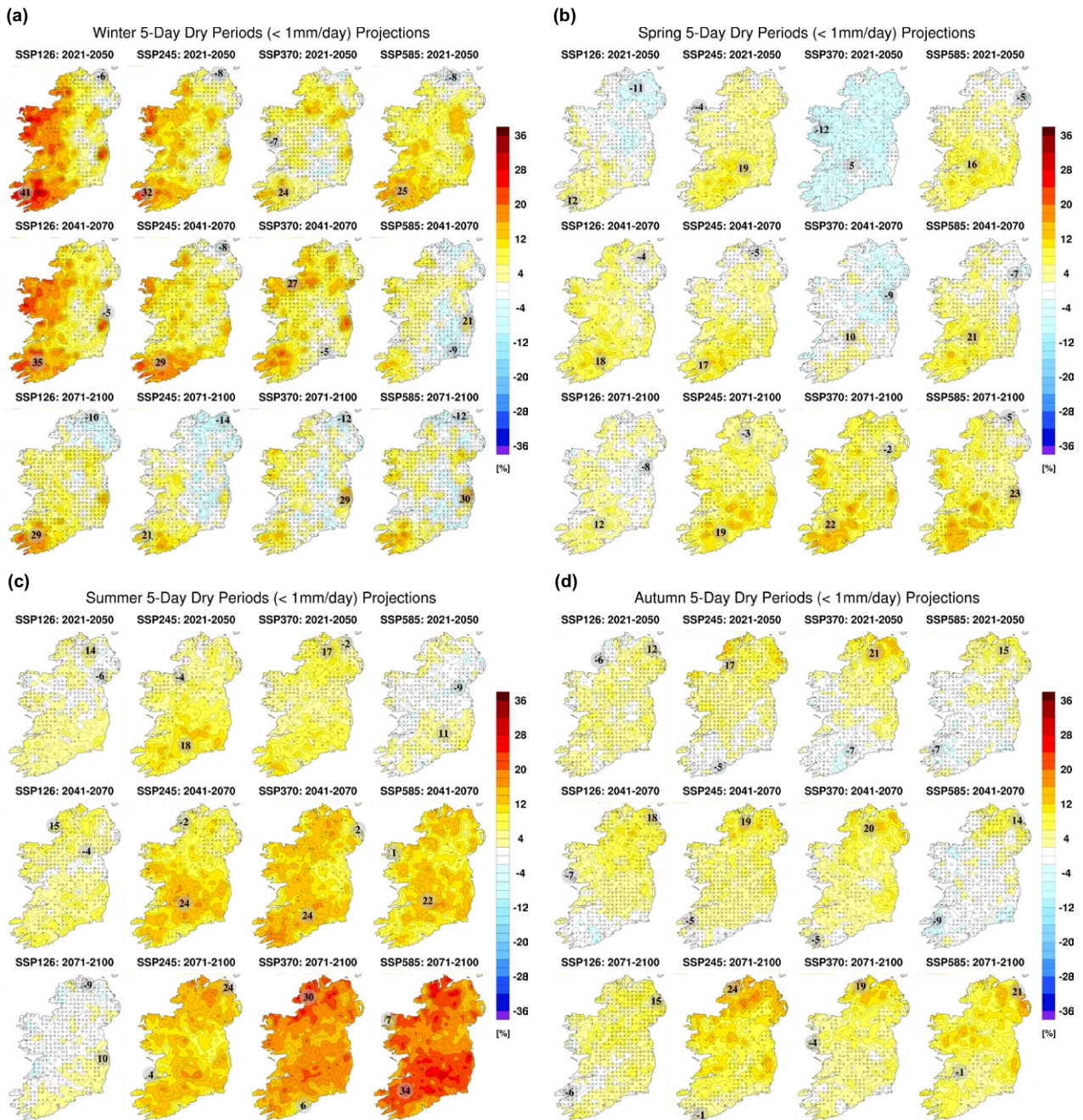
Figure 3.32. Projected changes (%) in the number of dry periods for (a) winter, (b) spring, (c) summer and (d) autumn. In each case, the future 30-year period is compared with the past period, 1981–2010. The numbers included on each plot are the minimum and maximum projected changes, displayed at their locations.

Figure 3.33. The seasonal projections of longest dry periods (per year) are presented in Figure 3.34. The projections of longest dry periods are similar to the projections of dry periods; general increases are noted for all seasons, with the largest increases projected for summer (and spring), which are enhanced for the higher SSPs and later time periods. Averaged over the whole country, robust (i.e. P33 and P66 have the same sign) projections of average annual longest dry period (Table 3.17, first panel) range from 4.1% for SSP245 (2021–2050) to 15% for SSP370 (2071–2100). The corresponding robust seasonal projections of

Annual Mean Longest Dry Period (< 1mm/day) Projections
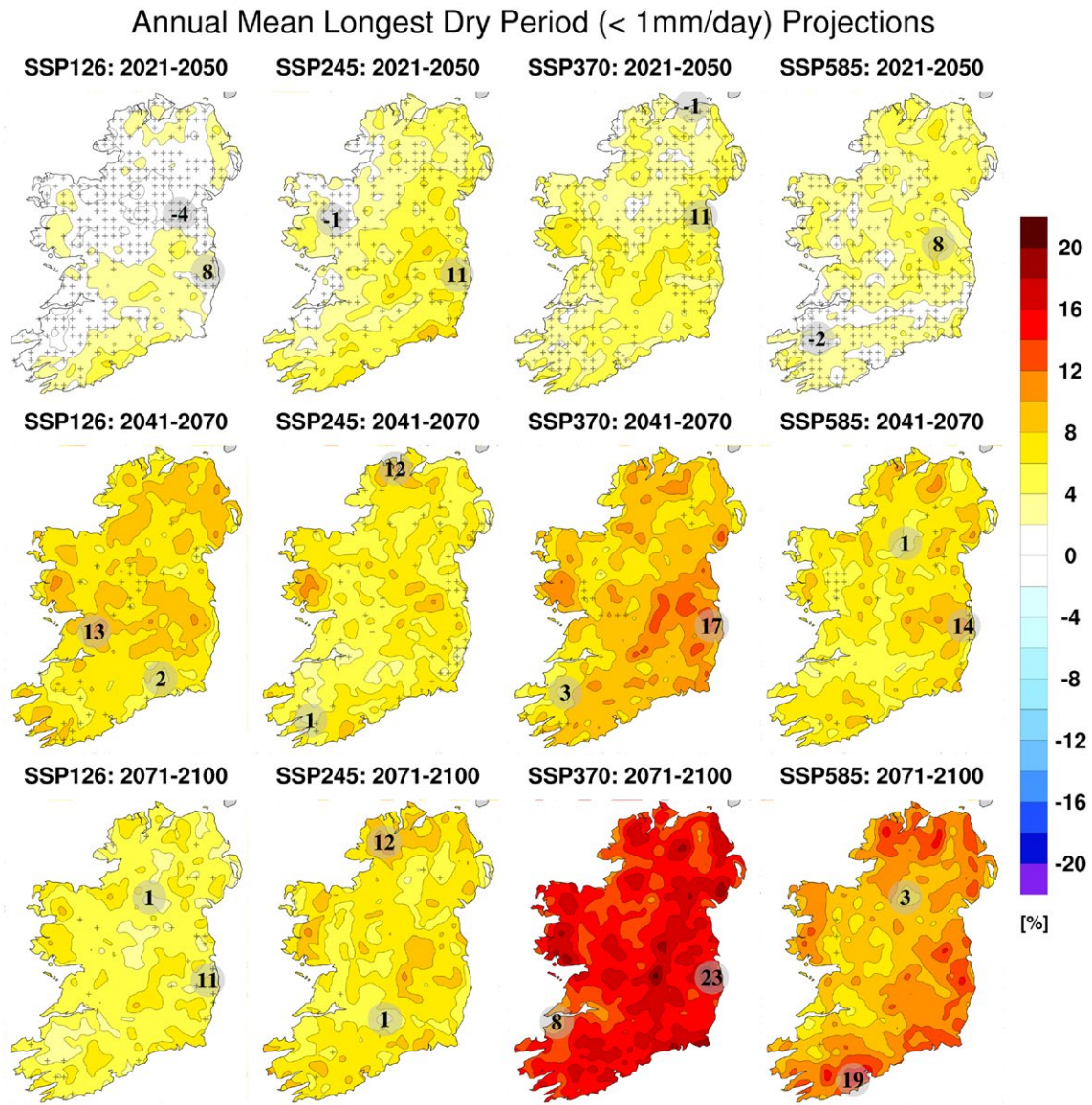
Figure 3.33. Annual RCM–CMIP6 ensemble projections of the mean annual longest dry period (%). All RCM ensemble members were run with 4 km grid spacing. In each case, the future 30-year period is compared with the past period, 1981–2010. The numbers included on each plot are the minimum and maximum projected changes, displayed at their locations.

average longest dry period range from 2.6% (SSP585, 2071–2100) to 7.4% (SSP126, 2041–2070) for winter (Table 3.17, second panel), from 3.4% (SSP585, 2021–2050) to 16% (SSP370, 2071–2100) for spring (Table 3.17, third panel), from 6.3% (SSP126, 2071–2100) to 15.8% (SSP370, 2071–2100) for summer (Table 3.17, fourth panel) and from 2.9% (SSP245, 2041–2070) to 6% (SSP585, 2021–2050) for autumn (Table 3.17, fifth panel).

3.14   Changes in the Variability of the Precipitation Climate

To evaluate projected changes in the future variability of precipitation, changes (%) in the standard deviation of daily total precipitation were analysed.[16] The projected change in standard deviation of daily precipitation for each RCM ensemble member was calculated and the mean (of the ensemble of

---

16 Refer to section 1.4.1 for an overview of the effects of changes in the standard deviation on the distribution of a climate field.
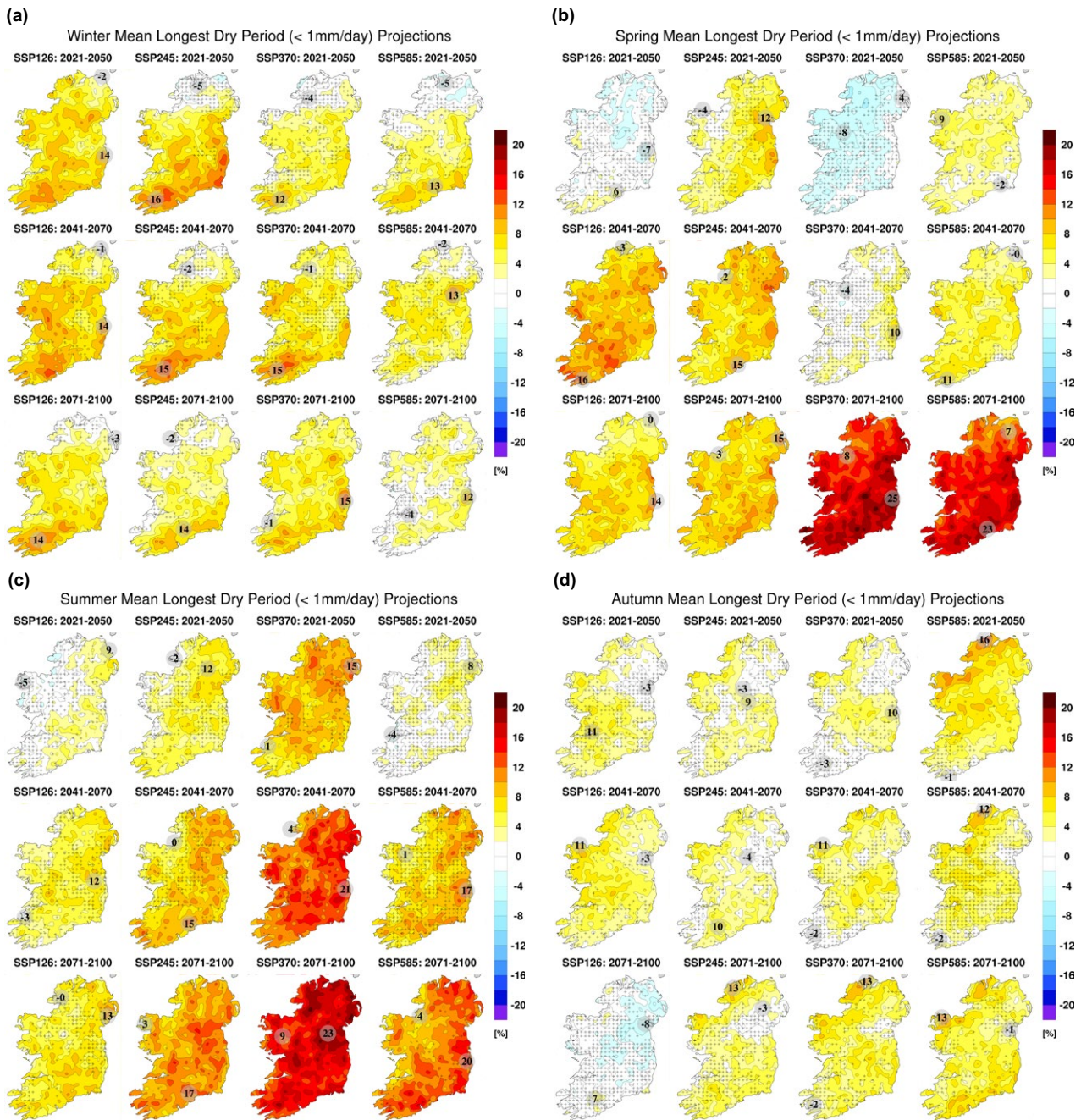
Figure 3.34. Projected changes (%) in the mean seasonal longest dry period (%) for (a) winter, (b) spring, (c) summer and (d) autumn. In each case, the future 30-year period is compared with the past period, 1981–2010. The numbers included on each plot are the minimum and maximum projected changes, displayed at their locations.

projections) was considered for each SSP and time period.

The projected precipitation changes, presented in sections 3.10–3.13, exhibit high uncertainty compared with the temperature projections of section 3.1. This is partially due to the precipitation projections varying greatly between ensemble members, much more so than for the temperature projections. The

uncertainty in the precipitation projections is also caused by projected changes in the mean and/or variability. The relative projected changes in the mean and variability can enhance or diminish the uncertainty (and magnitude of the climate change signal). Taking projections of annual precipitation (Figure 3.18) as an example, the uncertainty and small (~0%) projected changes can be partly attributed to

Table 3.17. Annual and seasonal projections of the mean longest dry period per year (%). This table corresponds to the projections in Figures 3.33 and 3.34, and shows the 33rd percentile, 50th percentile, mean and 66th percentile averaged over the island of Ireland

Annual longest dry period (%)

Time period	SSP126				SSP245				SSP370				SSP585			
	P33	P50	Mean	P66	P33	P50	Mean	P66	P33	P50	Mean	P66	P33	P50	Mean	P66
2021–2050	−1.1	0.8	1.7	4.7	0.6	2.7	4.1	7.0	−0.1	2.8	4.2	8.4	−0.6	1.7	3.3	6.5
2041–2070	3.3	6.1	7.5	11.4	2.6	5.4	6.1	10.1	4.0	6.3	8.8	11.8	2.9	4.9	6.8	9.4
2071–2100	2.8	4.7	5.2	8.4	4.2	5.8	6.8	9.1	10.3	12.7	15.0	18.0	5.4	7.3	10.2	12

Winter longest dry period (%)

Time period	SSP126				SSP245				SSP370				SSP585			
	P33	P50	Mean	P66	P33	P50	Mean	P66	P33	P50	Mean	P66	P33	P50	Mean	P66
2021–2050	4.4	6.2	7.0	9.7	2.7	5.6	6.3	11.0	−0.2	2.4	3.9	7.5	0.3	3.2	3.4	7.7
2041–2070	1.5	3.9	7.4	9.8	1.8	4.7	6.6	10.8	−0.2	2.6	6.3	10.4	−0.2	2.6	4.5	9.3
2071–2100	3.3	5.7	5.6	10.2	1.2	3.2	4.2	7.3	2.7	4.5	5.8	8.3	0.3	2.6	2.6	6.6

Spring longest dry period (%)

Time period	SSP126				SSP245				SSP370				SSP585			
	P33	P50	Mean	P66	P33	P50	Mean	P66	P33	P50	Mean	P66	P33	P50	Mean	P66
2021–2050	−4.7	−2.5	−0.5	2.3	0.0	3.5	4.7	9.5	−5.1	−2.5	−3.2	1.9	0.9	2.6	3.4	6.0
2041–2070	4.1	7.2	9.0	13.2	3.4	6.7	7.6	13.1	−4.2	−0.5	1.8	7.3	1.4	3.4	5.0	7.7
2071–2100	3.8	6.1	6.6	10.2	4.9	7.0	8.0	11.0	8.8	11.9	16.0	19.5	9.3	13	14.8	20

Summer longest dry period (%)

Time period	SSP126				SSP245				SSP370				SSP585			
	P33	P50	Mean	P66	P33	P50	Mean	P66	P33	P50	Mean	P66	P33	P50	Mean	P66
2021–2050	−1.3	1.0	1.7	5.3	−0.3	2.2	4.6	8.0	2.2	7.3	8.8	16.7	−6.1	−2.6	1.9	4.9
2041–2070	−0.1	4.8	5.0	10.9	1.3	6.9	8.0	15.2	4.7	9.5	12.5	18.9	−1.1	3.0	8.0	13
2071–2100	0.6	4.0	6.3	11.1	6.4	9.6	10.2	15.6	9.4	14.8	15.8	22.9	3.5	6.5	11.2	15

Autumn longest dry period (%)

Time period	SSP126				SSP245				SSP370				SSP585			
	P33	P50	Mean	P66	P33	P50	Mean	P66	P33	P50	Mean	P66	P33	P50	Mean	P66
2021–2050	−1.2	1.7	3.0	7.5	−1.3	1.2	2.6	6.3	−1.2	0.9	2.4	5.2	2.9	5.5	6.0	11
2041–2070	1.3	3.6	4.4	8.3	0.2	2.4	2.9	6.4	−0.5	2.5	3.7	8.0	−4.1	−0.4	4.4	8.4
2071–2100	−7.2	−4.3	−1.1	3.7	−0.8	2.2	3.7	8.2	0.4	3.3	4.9	8.9	1.2	5.0	5.4	11

a projected increase in the variability of the future Irish precipitation climate, resulting in an increase in both dry periods and heavy rainfall events. This is clearly demonstrated in Figure 3.35, which presents the annual projected change in the standard deviation of daily precipitation (the corresponding seasonal figures are presented in Figure 3.36). It is noted that the variability of precipitation is projected to increase over the full year (and all seasons). The large projected changes in the standard deviation of annual precipitation, coupled with small changes in the mean (Figure 3.18), imply an increase in both dry periods and heavy rainfall events (i.e. the tails of precipitation distribution will become more
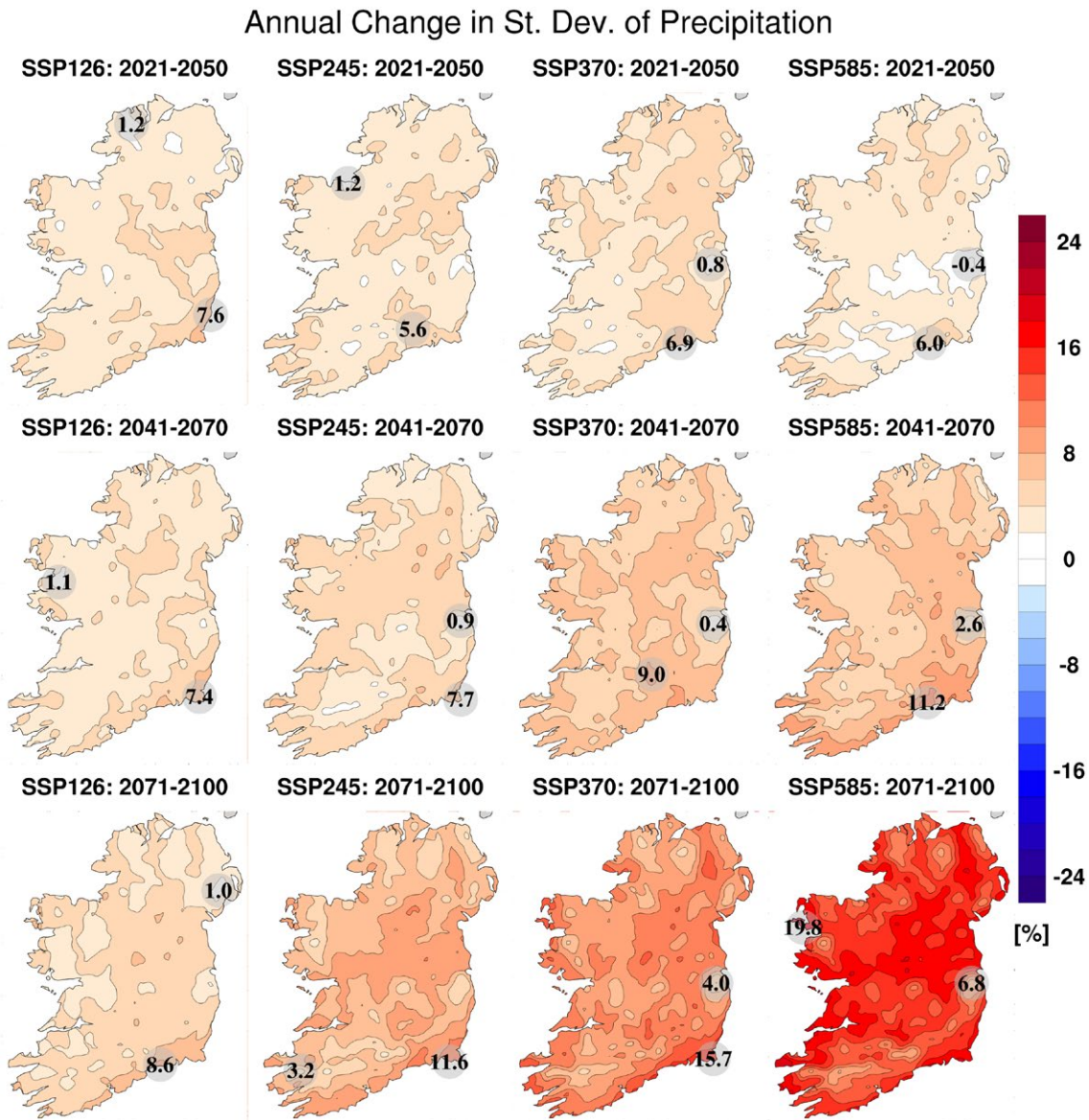
Figure 3.35. Annual projected change (%) in the standard deviation of daily precipitation. In each case, the future 30-year period is compared with the past period, 1981–2010. The numbers included on each plot are the minimum and maximum projected changes, displayed at their locations.

pronounced; see Figure 1.3a for a schematic example of such an outcome. This is confirmed by the large projected changes in intense rainfall events and dry periods shown in sections 3.11 and 3.13, respectively. An overview of the annual and seasonal precipitation projections of sections 3.10–3.13 is presented in Table 3.18. Note that this simple analysis focuses on the more robust projections of the higher SSPs and later time periods.

The projections of increased variability of the precipitation climate will have adverse implications for society (e.g. droughts, flooding, water management and housing) and sectors of the economy such as agriculture. Furthermore, the increase in frequency of both droughts and heavy rainfall events could be detrimental to the potential gains of a warming climate to the agricultural sector, as discussed in sections 3.5–3.9.

3.15 Snowfall Projections

Figure 3.37 shows that total annual snowfall is projected to decrease substantially over Ireland,
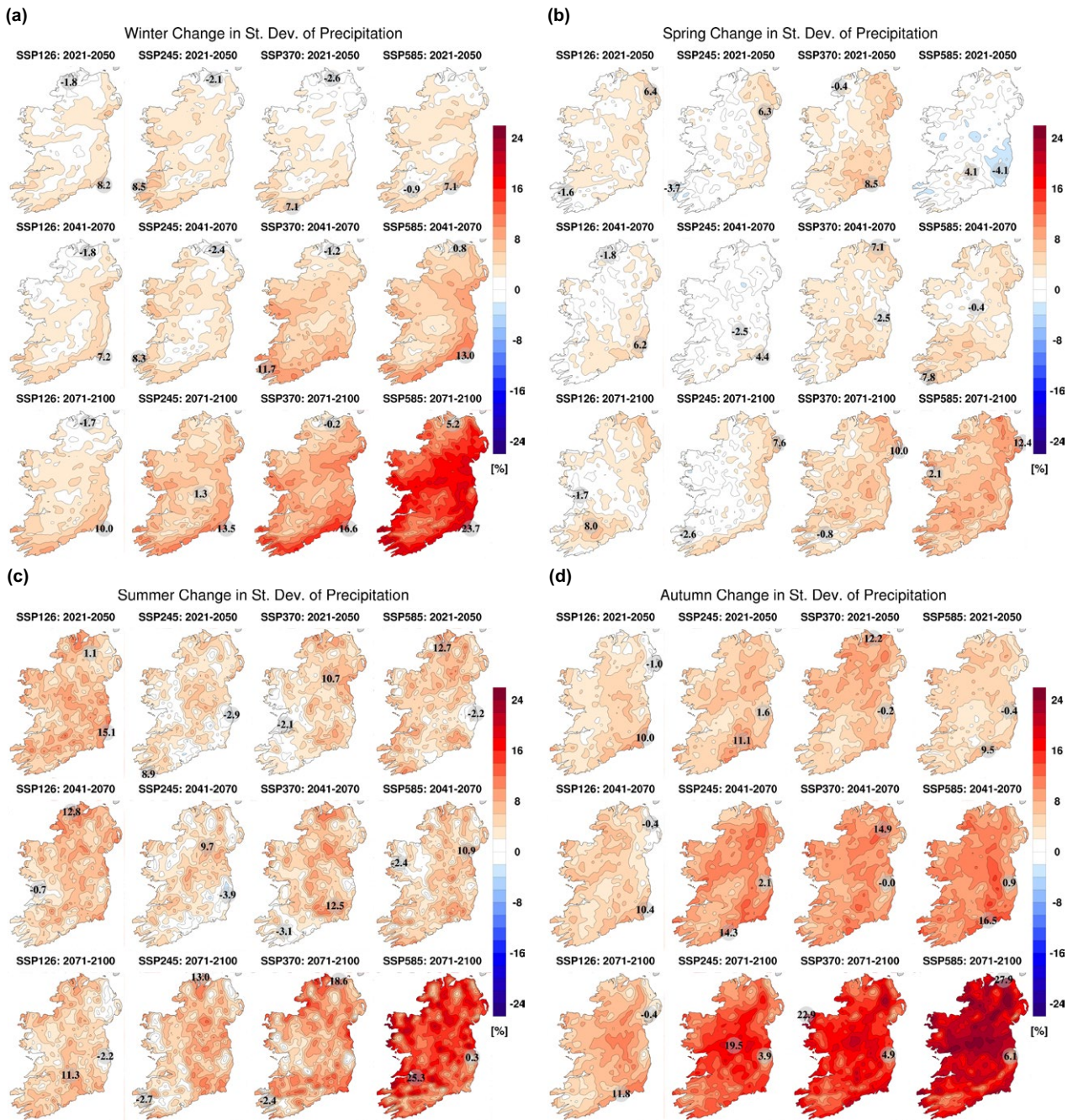
Figure 3.36. Seasonal projected change in the standard deviation of daily precipitation for (a) winter, (b) spring, (c) summer and (d) autumn. In each case, the future 30-year period is compared with the past period, 1981–2010. The numbers included on each plot are the minimum and maximum projected changes, displayed at their locations.

with decreases ranging from 18–47% for SSP126 (2021–2050) to 70–93% for SSP585 (2071–2100). Averaged over the whole country (Table 3.19), the mean projected decrease in snowfall ranges from 31% (2021–2050 under SSP126) to 84% (2071–2100 under SSP585). The projections of snowfall have high certainty, as demonstrated by an absence of hatching

in Figure 3.37 and a small spread (and the same sign) between the mean and percentile statistics presented in Table 3.19. For reference, the "observed" mean annual snowfall (mm) in the period 1981–2010, as resolved by a high-resolution (1.5 km) downscaled ERA-Interim climate simulation, is presented in Figure 3.38.

Table 3.18. Overview of projections of the annual and seasonal precipitation climate (sections 3.10 to 3.13). For each, an example of a schematic is provided to illustrate the relative changes in the mean and variability, and the resulting impacts on the distribution of precipitation

Projection	Mean	Standard deviation	R20 mm	R30 mm	SDII	Dry periods	Corresponding schematic
Annual	Small (~0%) change, high uncertainty	Increase	Increase	Increase	Increase	Increase	Figure 1.3a
Winter	Increase	Increase	Increase	Increase	Increase	~0% change, high uncertainty	Figure 1.3d
Spring	Small (~0%) change, high uncertainty	Small increase	Small increase	Increase	Small increase, higher uncertainty	Small increase, high uncertainty	Less pronounced version of Figure 1.3a
Summer	Decrease	Increase	Small increase, higher uncertainty	Increase	Small increase, higher uncertainty	Large increase	Figure 1.3g
Autumn	Increase	Increase	Increase	Increase	Increase	Small increase, high uncertainty	Figure 1.3d
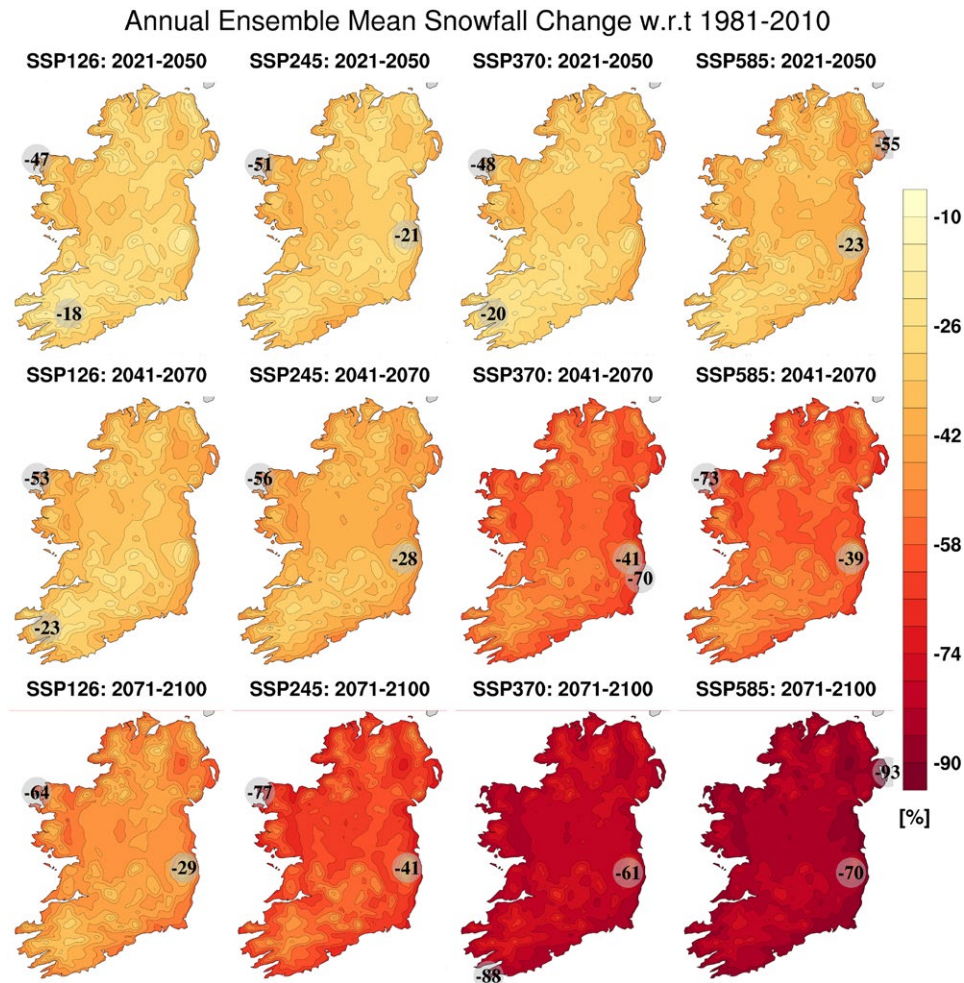
Figure 3.37. Annual RCM–CMIP6 ensemble mean projections of snowfall (%). In each case, the future 30-year period is compared with the past period, 1981–2010. The numbers included on each plot are the minimum and maximum projected changes, displayed at their locations.

Table 3.19. Annual projections of snowfall (%). This table corresponds to the projections in Figure 3.37 and shows the 33rd percentile, 50th percentile, mean and 66th percentile averaged over the island of Ireland

Time period	SSP126				SSP245				SSP370				SSP585			
	P33	P50	Mean	P66	P33	P50	Mean	P66	P33	P50	Mean	P66	P33	P50	Mean	P66
2021–2050	−35	−32	−31	−22	−44	−36	−33	−18	−41	−36	−33	−22	−41	−35	−37	−26
2041–2070	−44	−38	−36	−25	−57	−42	−40	−19	−60	−56	−56	−50	−63	−55	−56	−45
2071–2100	−69	−57	−47	−26	−82	−74	−61	−45	−90	−81	−79	−72	−93	−89	−84	−78
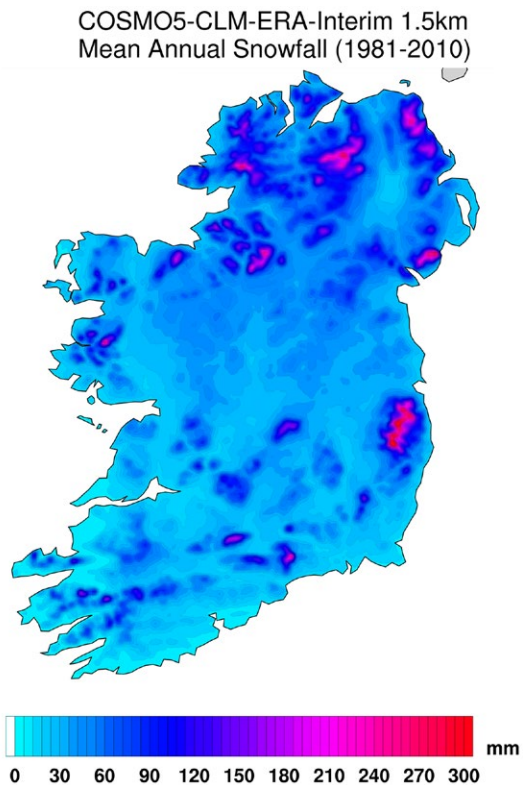
Figure 3.38. Mean annual snowfall (mm/year) 1981–2010 as resolved by a COSMO-CLM5–ERA-Interim 1.5 km resolution simulation. Refer to Flanagan *et al*. (2019) and Flanagan and Nolan (2020) for overviews of the climate simulation configuration and validation results.
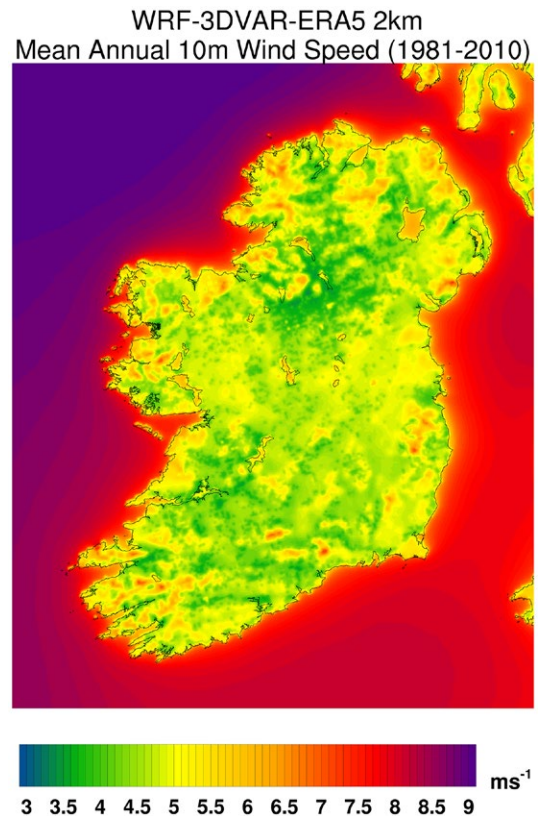
Figure 3.39. Annual mean 10 m wind speed (m s⁻¹) as resolved by a WRF-3DVAR–ERA5 simulation with 2 km grid spacing (1981–2010). For details of this downscaled reanalysis dataset see, for example, McGrath and Nolan (2024).

3.16   Changes in 10 m Wind Speed Projections

In this section, the projected changes in 10 m wind speed are assessed. For reference, the "observed" mean annual 10 m wind speed (m s⁻¹) for 1981–2010, as resolved by a high-resolution (2 km) downscaled reanalysis climate simulation (WRF-3DVAR–ERA5), is presented in Figure 3.39.

Figure 3.40 presents the spatial distribution of 10 m wind speed projections. For the purpose of offshore wind energy and shipping applications, the analyses of wind speed cover all land points and a small portion of the surrounding sea. The mean annual 10 m wind speed is projected to decrease by 0.5–4.6% depending on the location, time period and SSP scenario with reductions of 0.7—1.7% for SSP126 (2021–2050) and 2–4.6% for SSP585 (2071–2100).
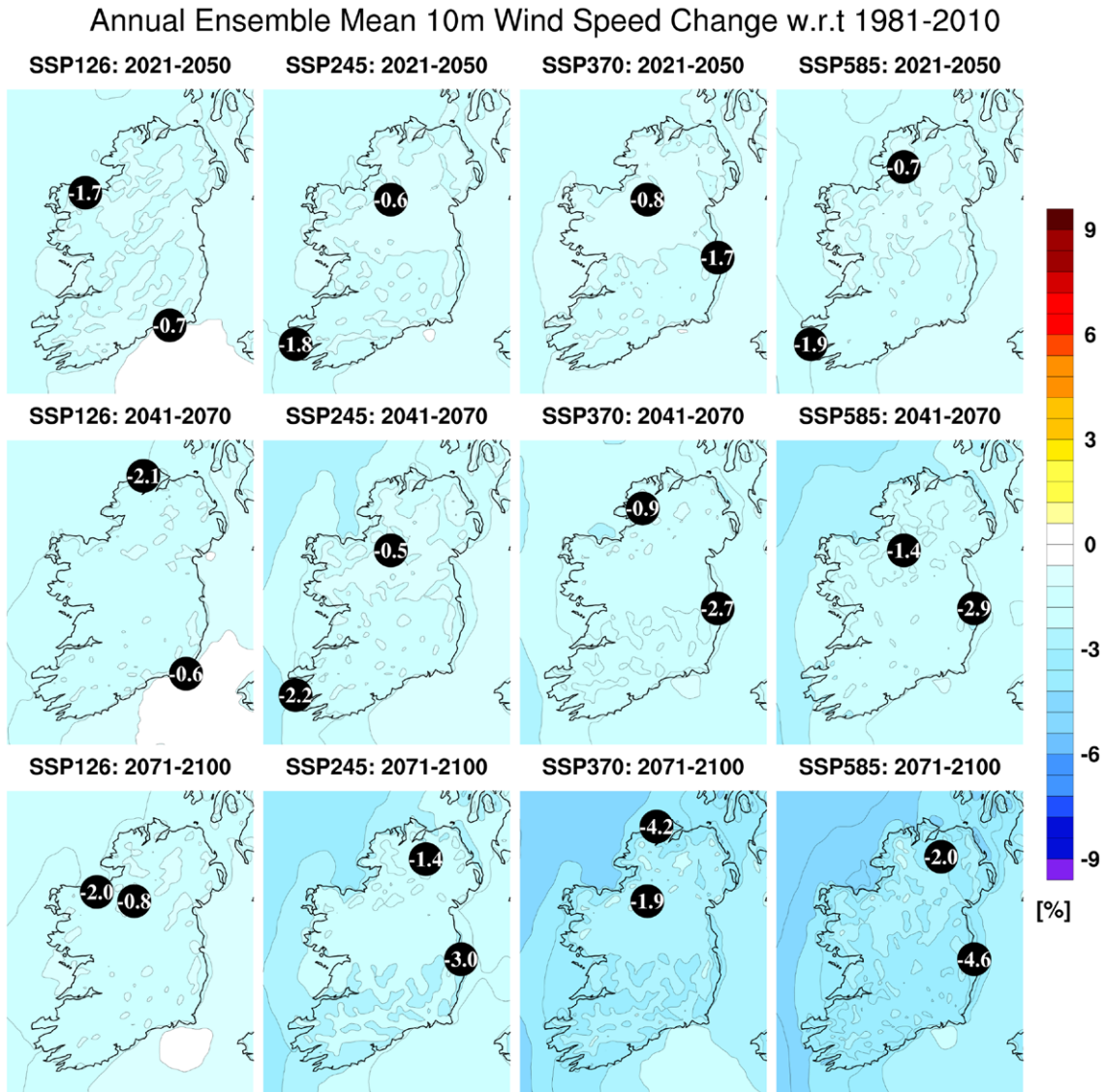
Figure 3.40. RCM–CMIP6 ensemble projections of annual 10 m wind speed (%). All RCM ensemble members were run with 4 km grid spacing. In each case, the future 30-year period is compared with the past period, 1981–2010. The numbers included on each plot are the minimum and maximum projected changes, displayed at their locations.

Averaged over the whole country (Table 3.20, first panel), the mean projected decrease in annual 10 m wind speed ranges from 1.2% (2021–2050 under SSP126) to 3.2% (2071–2100 under SSP585). The projected decreases in annual 10 m wind speed have high certainty, as demonstrated by an absence of hatching in Figure 3.40 (for all time periods and SSPs) and agreement in sign (and small spread) between the mean and percentile statistics of Table 3.20 (first panel).

Figure 3.41a, the projected change in winter 10 m wind speed (%), shows small decreases or small

(~0%) changes. Figure 3.41a contains some hatching, indicating uncertainty in the projections over limited areas. However, Table 3.20 (second panel) shows an agreement in sign (and small spread) between the percentile and mean statistics for most of the SSPs and time periods, indicating high certainty in the projection of small decreases (or small changes) in winter wind speeds.

Figure 3.41b, the projected change in spring 10 m wind speed (%), shows small (~0%) changes or decreases, which are enhanced for the higher SSPs and later time periods. The spring 10 m wind speed

Table 3.20. Annual and seasonal projections of 10 m wind speed (%). This table corresponds to the projections in Figures 3.40 and 3.41, and shows the 33rd percentile, 50th percentile, mean and 66th percentile averaged over the island of Ireland

Annual 10 m wind speed (%)

Time period	SSP126				SSP245				SSP370				SSP585			
	P33	P50	Mean	P66	P33	P50	Mean	P66	P33	P50	Mean	P66	P33	P50	Mean	P66
2021–2050	−1.8	−1.2	−1.2	−0.4	−1.8	−1.2	−1.2	−0.9	−2.1	−1.8	−1.2	−0.3	−1.6	−1.4	−1.3	−1.0
2041–2070	−2.0	−1.7	−1.5	−0.7	−1.7	−1.4	−1.3	−0.8	−2.6	−2.2	−1.7	−0.7	−1.9	−1.7	−2.0	−1.3
2071–2100	−1.8	−1.3	−1.4	−0.9	−2.4	−2.0	−2.2	−1.5	−3.4	−3.2	−2.9	−2.7	−3.7	−3.4	−3.2	−2.2

Winter 10 m wind speed (%)

Time period	SSP126				SSP245				SSP370				SSP585			
	P33	P50	Mean	P66	P33	P50	Mean	P66	P33	P50	Mean	P66	P33	P50	Mean	P66
2021–2050	−2.1	−1.7	−1.6	−0.8	−1.6	−1.2	−0.6	−0.2	−2.1	−0.9	−0.8	0.0	−1.6	−1.3	−1.6	−0.8
2041–2070	−1.8	−1.6	−1.4	−0.7	−1.3	−0.8	−0.7	0.1	−1.8	−1.1	−0.7	−0.1	−2.4	−1.7	−1.4	−0.3
2071–2100	−2.1	−1.8	−1.5	−1.4	−1.9	−1.4	−1.1	−0.1	−2.5	−1.8	−1.2	−0.6	−0.7	−0.4	−0.8	0.4

Spring 10 m wind speed (%)

Time period	SSP126				SSP245				SSP370				SSP585			
	P33	P50	Mean	P66	P33	P50	Mean	P66	P33	P50	Mean	P66	P33	P50	Mean	P66
2021–2050	−1.8	−1.5	−0.7	−0.4	−1.6	−1.4	−1.3	−1.0	−1.6	−1.3	−1.0	−0.6	−2.0	−1.7	−1.2	−0.9
2041–2070	−2.3	−1.8	−1.6	−0.5	−2.0	−1.8	−1.6	−1.1	−1.4	−1.1	−1.0	−0.6	−2.7	−2.3	−1.8	−0.9
2071–2100	−2.6	−2.3	−2.0	−1.6	−3.6	−3.2	−2.9	−2.2	−3.3	−3.0	−2.8	−2.3	−3.4	−2.9	−3.1	−2.2

Summer 10 m wind speed (%)

Time period	SSP126				SSP245				SSP370				SSP585			
	P33	P50	Mean	P66	P33	P50	Mean	P66	P33	P50	Mean	P66	P33	P50	Mean	P66
2021–2050	−2.6	−2.4	−2.1	−1.8	−2.9	−2.7	−2.5	−2.1	−3.5	−2.9	−2.9	−2.1	−2.5	−2.0	−1.9	−1.4
2041–2070	−2.2	−2.0	−1.9	−1.5	−3.5	−3.1	−3.1	−2.4	−4.7	−4.1	−3.9	−3.2	−4.8	−4.5	−4.3	−3.9
2071–2100	−2.6	−2.2	−2.0	−1.3	−4.6	−4.3	−4.3	−3.7	−7.0	−6.6	−6.6	−6.0	−9.3	−8.8	−7.9	−6.8

Autumn 10 m wind speed (%)

Time period	SSP126				SSP245				SSP370				SSP585			
	P33	P50	Mean	P66	P33	P50	Mean	P66	P33	P50	Mean	P66	P33	P50	Mean	P66
2021–2050	−0.8	−0.2	−0.5	1.2	−1.3	−0.9	−0.7	0.6	−1.5	−0.8	−0.4	0.9	−1.8	−1.4	−0.5	1.2
2041–2070	−0.2	0.3	−0.8	0.8	0.0	0.3	−0.3	0.8	−2.3	−2.0	−1.5	−0.7	−1.1	−0.7	−0.8	0.5
2071–2100	0.1	0.4	0.0	1.2	−1.5	−1.2	−0.9	−0.3	−1.8	−1.5	−1.8	−1.0	−2.7	−2.3	−2.0	−1.0

projections have high certainty, as demonstrated by a scarcity of hatching in Figure 3.41b and agreement in sign between the P33 and P66 statistics of Table 3.20 (third panel). Averaged over the whole country (see Table 3.20, third panel), the mean projected decrease in spring 10 m wind speed ranges from 0.7% (2021–2050 under SSP126) to 3.1% (2071–2100 under SSP585).
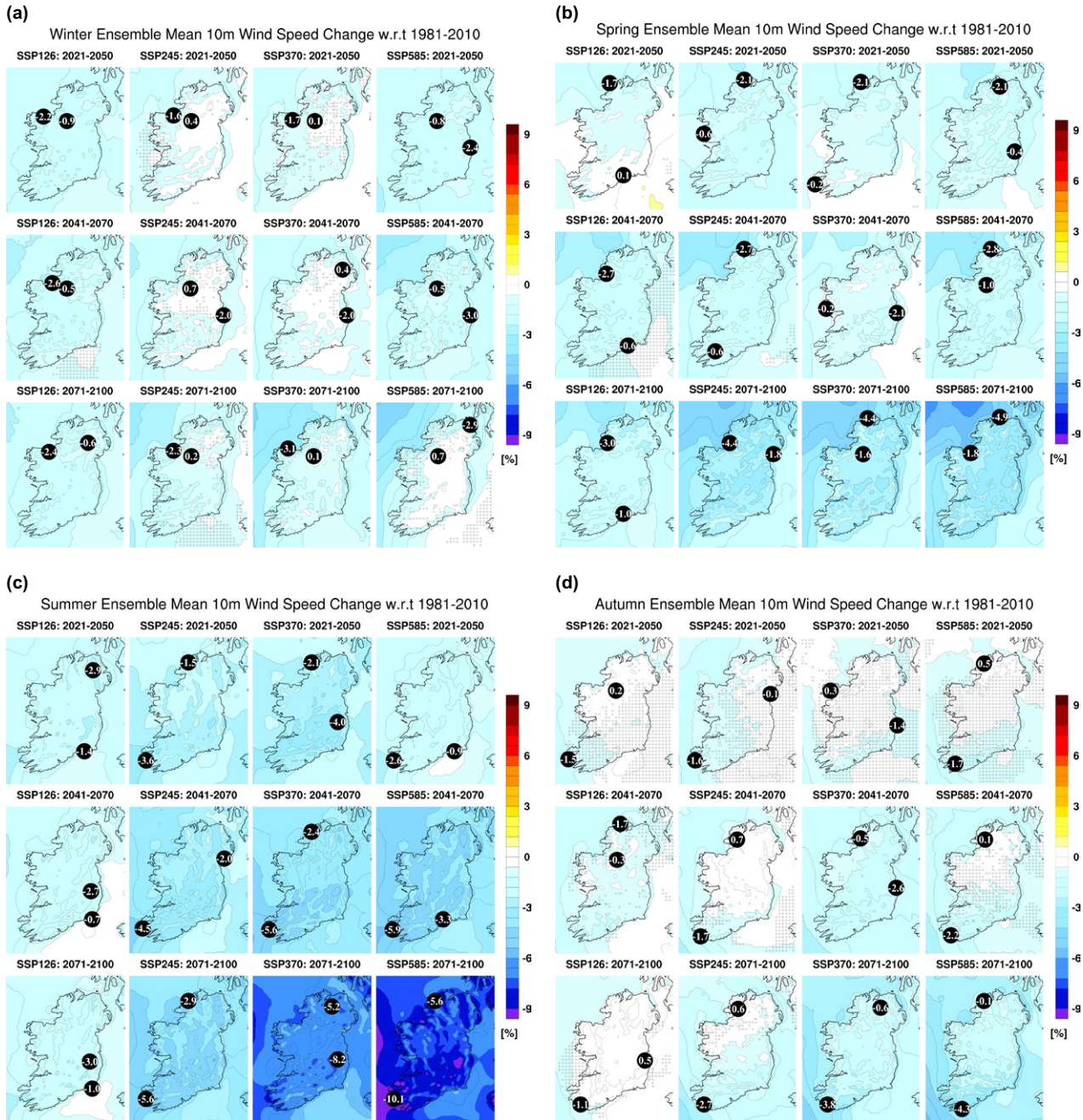
Figure 3.41. Seasonal RCM ensemble projections of 10 m wind speed (%) for (a) winter, (b) spring, (c) summer and (d) autumn. In each case, the future 30-year period is compared with the past period, 1981–2010. The numbers included on each plot are the minimum and maximum projected changes, displayed at their locations.

The largest projected decreases in 10 m wind speed are noted for summer (Figure 3.41c), which are enhanced for the higher SSPs and later time periods. The summer 10 m wind speed projections have high certainty (for all time periods and SSPs), as demonstrated by an absence of hatching in Figure 3.41c and agreement in sign between the

P33 and P66 statistics of Table 3.20 (fourth panel). Averaged over the whole country (see Table 3.20, fourth panel), the mean projected decrease in summer wind speed ranges from 1.9% (2041–2070 under SSP126) to 7.9% (2071–2100 under SSP585).

Figure 3.41d, the projected change in autumn 10 m wind speed, shows small (~0%) changes for

Annual Change in St. Dev. of 10m Wind Speed
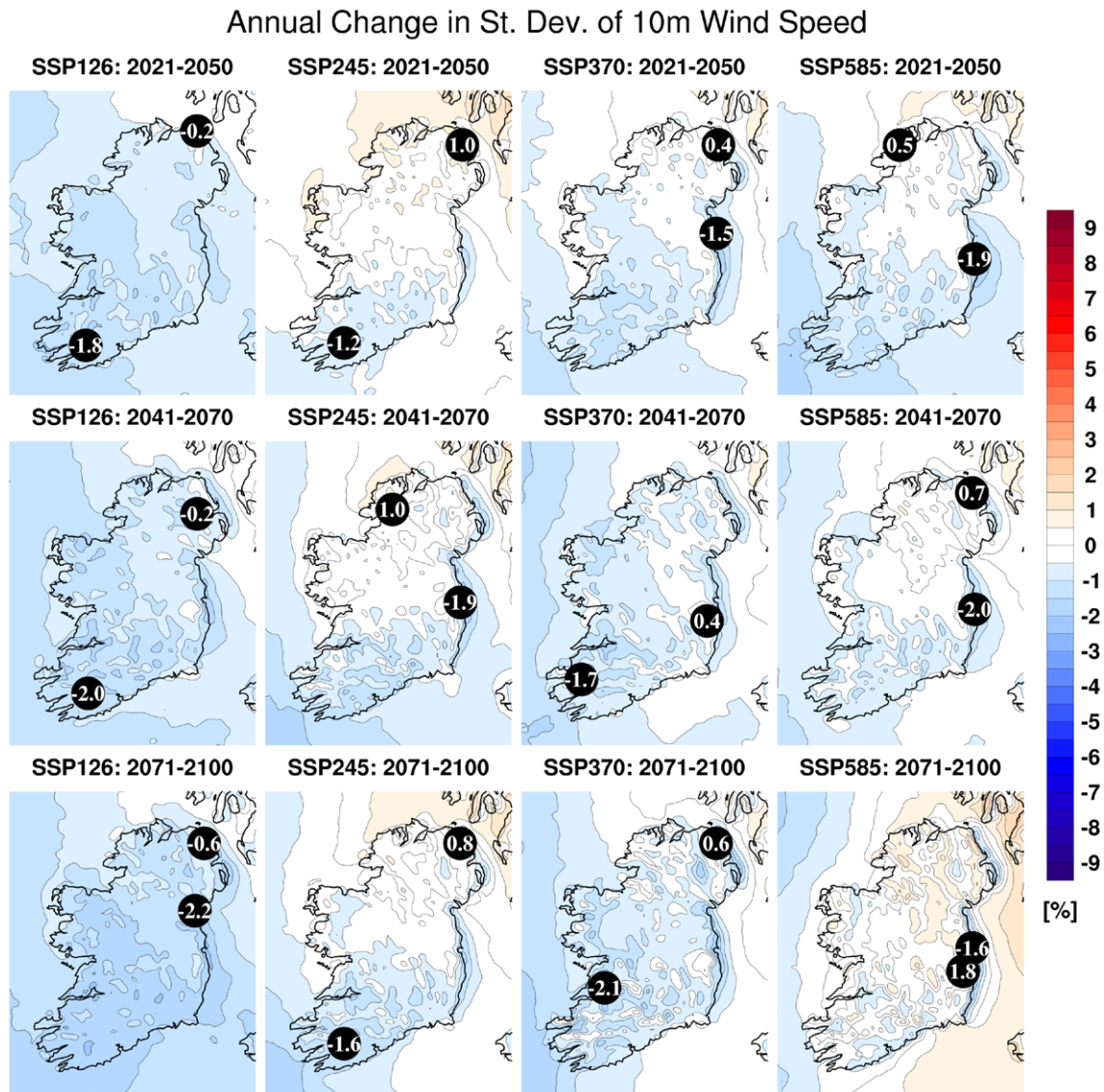
Figure 3.42. Annual projected change (%) in the standard deviation of 10 m wind speed. In each case, the future 30-year period is compared with the past period, 1981–2010. The numbers included on each plot are the minimum and maximum projected changes, displayed at their locations.

the lower SSPs and/or earlier time periods (small decreases otherwise). Table 3.20 (fifth panel) shows that while some uncertainty is evident in the projections for the lower SSPs and/or earlier time periods, the spread between ensemble members is small, indicating that the ensemble members agree on small projected changes but disagree on the sign of change. The autumn wind speed projections have higher certainty for the higher SSPs and later time periods, as demonstrated by an absence of hatching in Figure 3.41d and agreement in sign between the P33 and P66 statistics of Table 3.20 (fifth panel).

Averaged over the whole country, robust projections of decreases in autumn wind speed range from 0.9% for SSP245 (2071–2100) to 2% for SSP585 (2071–2100).

To evaluate projected changes in the future variability of 10 m wind speed, changes (%) in the standard deviation of mean daily 10 m wind speed were analysed.[17] The projected change (%) in standard deviation of average daily wind speed for each RCM ensemble member was calculated and the mean (of the ensemble of projections) was considered for each SSP and time period. The annual change in the standard deviation of 10 m wind speed (Figure 3.42)

---

17 Refer to section 1.4.1 for an overview of the effects of changes in the standard deviation on the distribution of a climate field.

shows small changes. The seasonal projected changes in the standard deviation of 10 m wind speed, presented in Figure 3.43, show small changes for winter, spring and autumn, with large decreases noted for summer. It should be noted that large decreases in the mean summer 10 m wind speed

(Figure 3.41c), coupled with large decreases in the standard deviation, imply a shift to the left of the wind speed distribution and a substantial decrease in the frequency of higher wind speeds (refer to Figure 1.3h for a schematic example of such an outcome). Similarly, decreases in mean annual, winter, spring
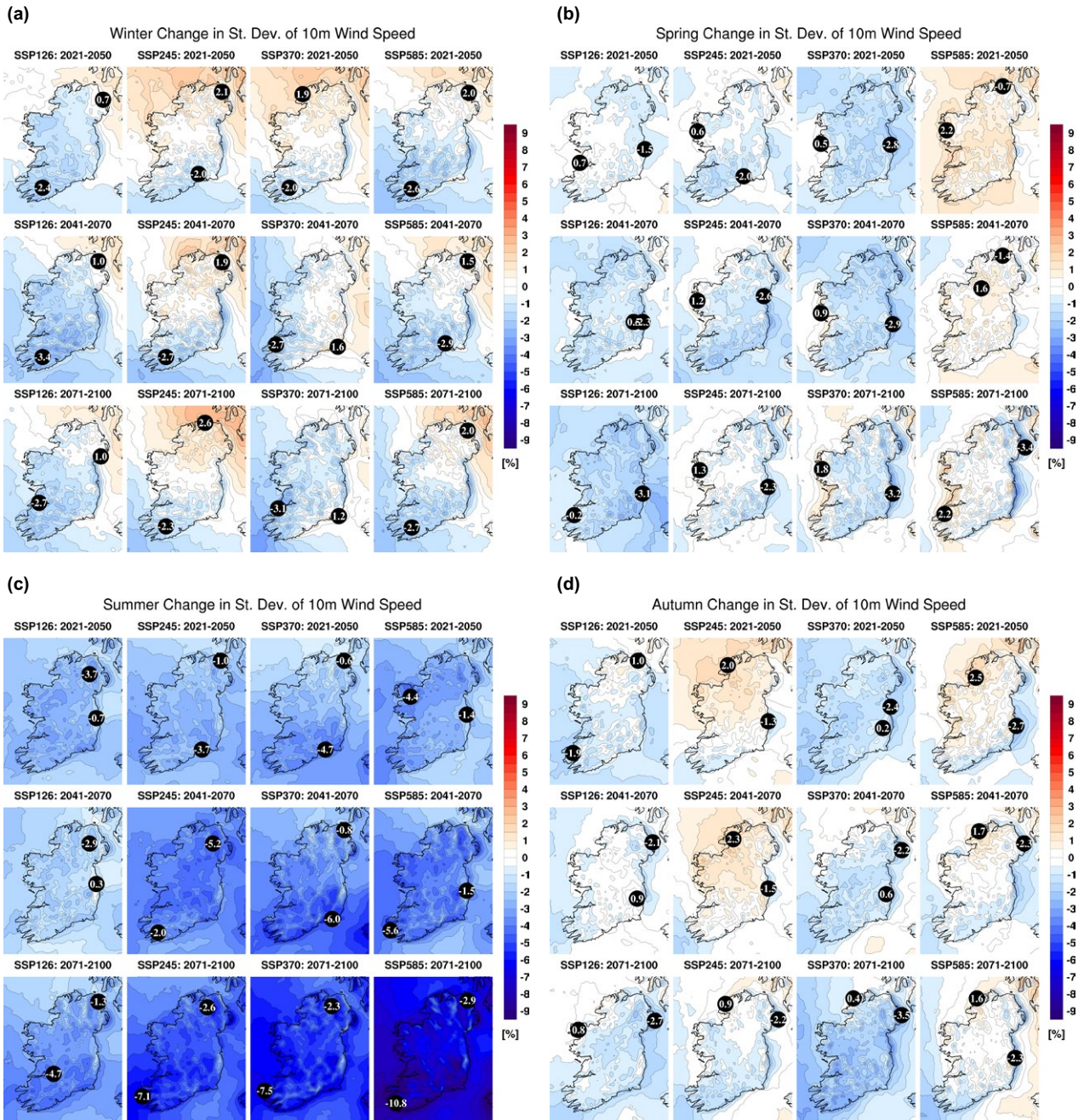
Figure 3.43. Seasonal projected change (%) in the standard deviation of 10 m wind speed for (a) winter, (b) spring, (c) summer and (d) autumn. In each case, the future 30-year period is compared with the past period, 1981–2010. The numbers included on each plot are the minimum and maximum projected changes, displayed at their locations.

and autumn wind speeds (Figures 3.40 and 3.41), coupled with a small change (~0%) in the standard deviation, imply a shift to the left of the wind speed distribution and a decrease in the frequency of higher wind speeds (refer to Figure 1.3f for a schematic example of such an outcome).

Previous work has demonstrated that, since near-surface wind direction is closely correlated to the local topography, regional climate projections of 10 m

wind direction over Ireland (onshore) do not show any significant change (Nolan *et al*., 2012, 2014; Nolan, 2015). Future work will investigate the impact of climate change on offshore wind direction.

3.17   Specific Humidity Projections

Figure 3.44 shows that mean annual near-surface (2 m) specific humidity (the amount of water vapour
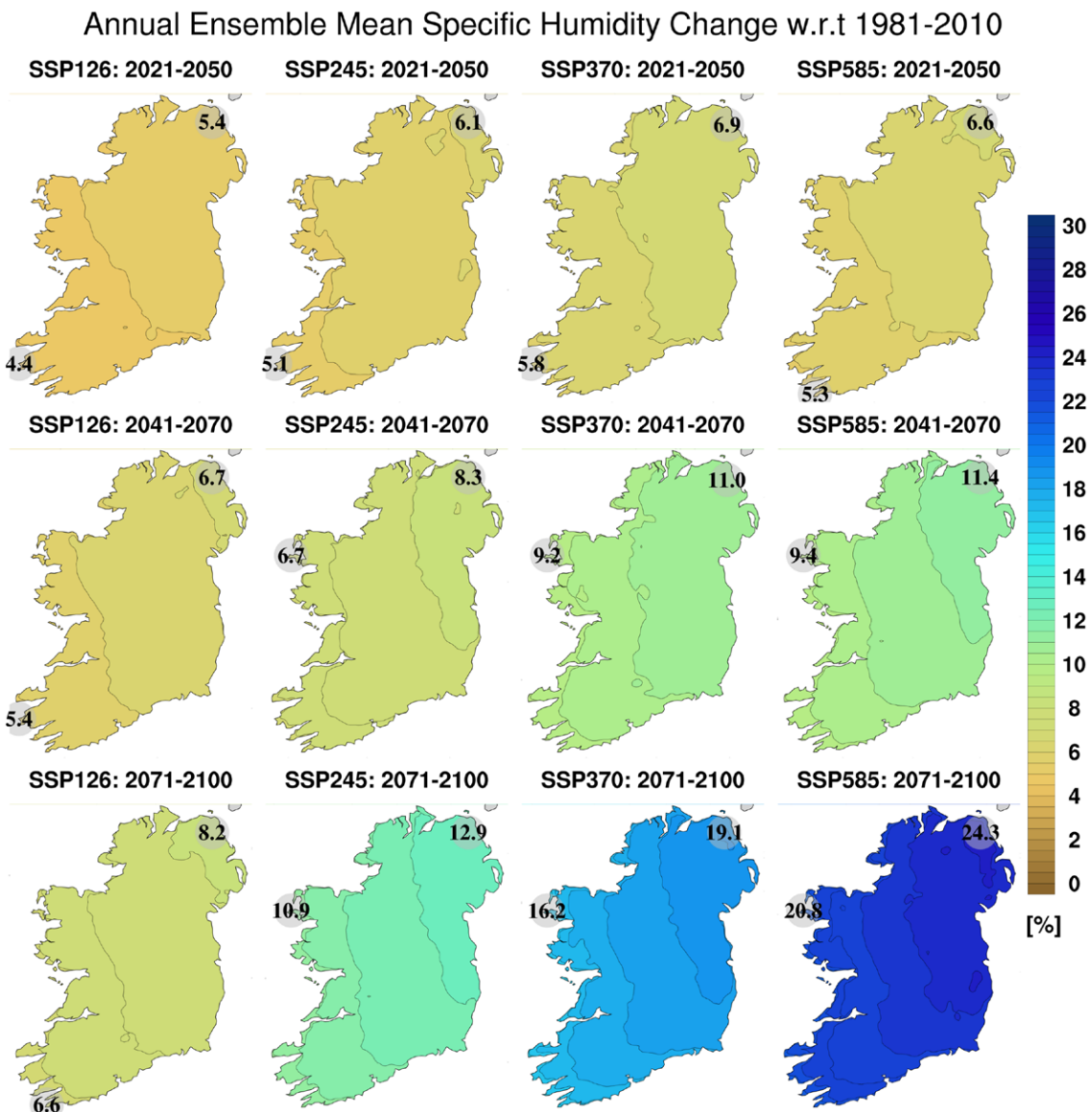
Figure 3.44. RCM–CMIP6 ensemble projections of annual near-surface (2 m) specific humidity (%). All RCM ensemble members were run with 4 km grid spacing. In each case, the future 30-year period is compared with the past period, 1981–2010. The numbers included on each plot are the minimum and maximum projected changes, displayed at their locations.

in the atmosphere calculated as the ratio of the mass of water vapour to the total mass of the air parcel) is projected to increase substantially, with increases enhanced for the higher SSPs and later time periods. There exists a clear south-west to north-east gradient in the projections, with the largest increases in the north. The annual specific humidity is projected to increase by 4.4–5.4% for SSP126 (2021–2050) and by 20.8–24.3% for SSP585 (2071–2100). Averaged over the whole country (Table 3.21, first panel), the mean projected increase in annual specific humidity ranges from 5% (2021–2050 under SSP126) to 23% (2071–2100 under SSP585).

Table 3.21. Annual and seasonal projections of near-surface (2 m) specific humidity (%). This table corresponds to the projections in Figures 3.44 and 3.45, and shows the 33rd percentile, 50th percentile, mean and 66th percentile averaged over the island of Ireland

Annual near-surface (2 m) specific humidity (%)

Time period	SSP126				SSP245				SSP370				SSP585			
	P33	P50	Mean	P66	P33	P50	Mean	P66	P33	P50	Mean	P66	P33	P50	Mean	P66
2021–2050	3.4	4.0	5.0	4.5	3.3	4.1	5.7	4.7	3.2	5.1	6.5	7.4	3.4	3.9	6.1	6.5
2041–2070	4.1	4.4	6.1	4.7	3.8	5.5	7.8	6.3	7.0	8.0	10.5	10.7	6.6	6.9	10.7	11
2071–2100	2.9	4.7	7.6	9.5	6.5	6.9	12.2	15.0	12.4	14.3	18.1	19.8	16	20	23	27

Winter near-surface (2 m) specific humidity (%)

Time period	SSP126				SSP245				SSP370				SSP585			
	P33	P50	Mean	P66	P33	P50	Mean	P66	P33	P50	Mean	P66	P33	P50	Mean	P66
2021–2050	1.8	3.2	4.1	4.1	1.3	1.6	4.0	5.1	2.6	3.1	5.1	3.8	2.4	2.8	4.8	4.7
2041–2070	2.9	3.1	4.7	4.8	2.2	3.3	6.2	4.7	6.4	6.9	8.7	7.7	5.1	5.8	8.6	8.5
2071–2100	0.7	3.8	5.9	8.2	4.3	6.1	9.2	12.8	11.1	11.9	14.7	14.9	13	18	18.5	21

Spring near-surface (2 m) specific humidity (%)

Time period	SSP126				SSP245				SSP370				SSP585			
	P33	P50	Mean	P66	P33	P50	Mean	P66	P33	P50	Mean	P66	P33	P50	Mean	P66
2021–2050	0.7	0.9	3.0	4.5	2.0	2.3	4.1	4.0	2.3	3.9	4.7	5.6	0.9	2.7	4.0	3.4
2041–2070	2.1	2.3	4.6	3.8	1.7	2.1	5.0	3.2	5.0	5.3	8.0	7.2	3.5	5.1	7.3	6.2
2071–2100	1.3	2.3	5.9	6.8	2.8	3.5	8.3	8.5	9.8	11.6	13.7	12.5	11	15	16.9	18

Summer near-surface (2 m) specific humidity (%)

Time period	SSP126				SSP245				SSP370				SSP585			
	P33	P50	Mean	P66	P33	P50	Mean	P66	P33	P50	Mean	P66	P33	P50	Mean	P66
2021–2050	3.9	4.3	6.1	6.5	4.3	4.8	7.2	8.2	4.0	5.4	7.3	9.3	4.4	4.7	7.1	8.5
2041–2070	4.1	4.8	7.0	5.9	4.8	7.0	9.0	8.8	7.7	8.8	11.6	13.3	8.2	8.8	12.4	14
2071–2100	3.6	5.3	8.3	11.5	7.4	7.8	14.0	17.9	14.0	15.9	20.5	24.6	18	22	26.9	34

Autumn near-surface (2 m) specific humidity (%)

Time period	SSP126				SSP245				SSP370				SSP585			
	P33	P50	Mean	P66	P33	P50	Mean	P66	P33	P50	Mean	P66	P33	P50	Mean	P66
2021–2050	4.6	4.7	6.2	5.4	3.7	3.9	6.5	4.4	3.9	6.9	8.1	8.7	4.8	5.0	7.6	8.4
2041–2070	4.8	5.4	7.4	6.4	5.7	6.5	9.6	8.0	7.8	9.7	12.4	13.8	7.2	7.6	12.8	15
2071–2100	4.9	6.7	9.4	10.4	9.5	9.9	15.4	18.8	13.5	16.2	21.4	25.0	18	22	27.2	32

(a)

(b)

(c)

(d)
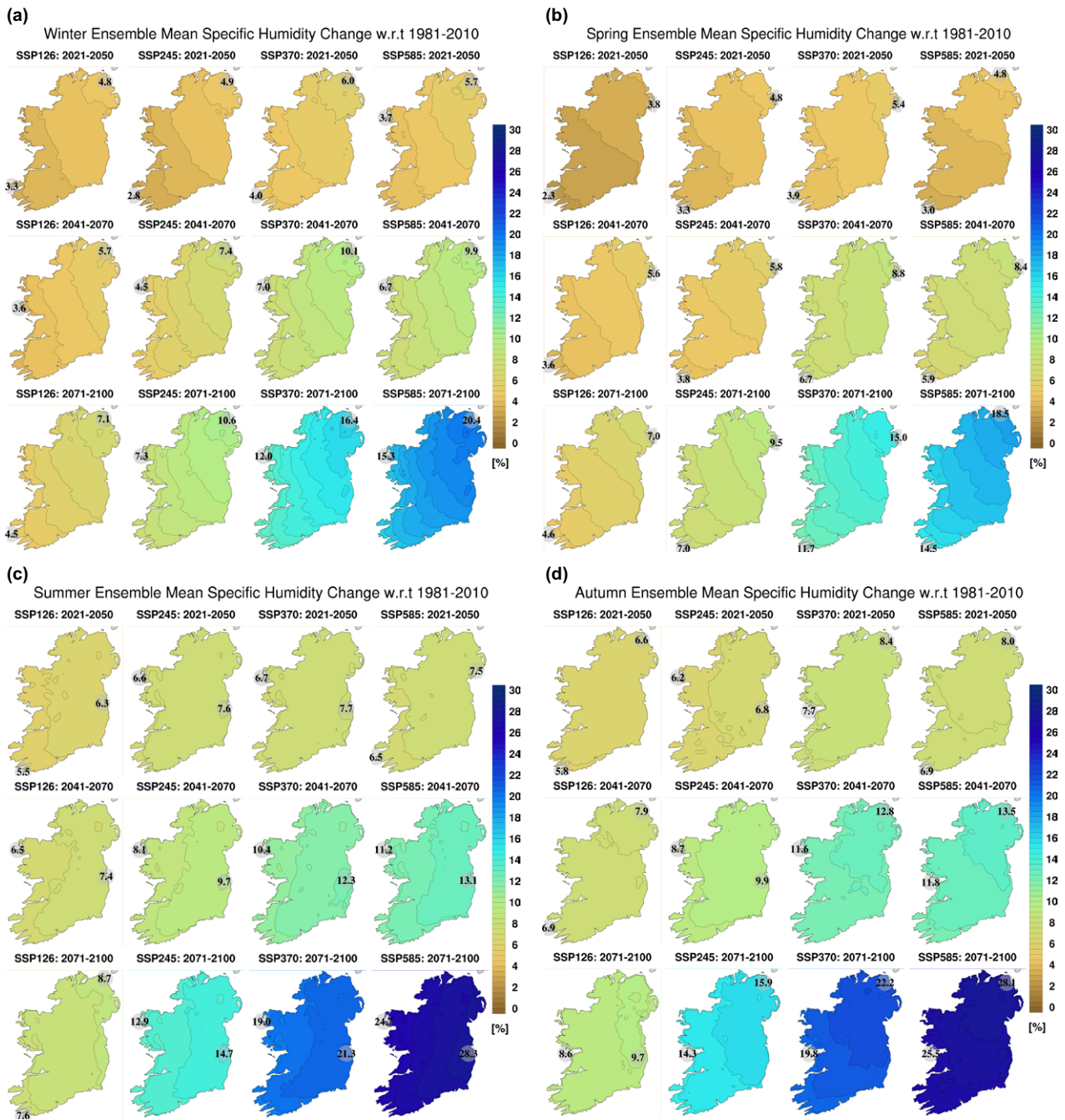
Figure 3.45. Seasonal RCM ensemble projections of near-surface (2 m) specific humidity (%) for (a) winter, (b) spring, (c) summer and (d) autumn. In each case, the future 30-year period is compared with the past period, 1981–2010. The numbers included on each plot are the minimum and maximum projected changes, displayed at their locations.

Specific humidity is projected to increase for all seasons (Figure 3.45), with increases enhanced for the higher SSPs and later time periods. The largest increases are noted for the summer and autumn months. Averaged over the whole country, mean projected increases in specific humidity for winter (Table 3.21, second panel) range from 4.1% (SSP245, 2021–2050) to 18.5% (SSP585, 2071–2100), for spring (Table 3.21, third panel) range from 3% (SSP126, 2021–2050) to 16.9% (SSP585, 2071–2100), for summer (Table 3.21, fourth panel) range from 6.1% (SSP126, 2021–2050) to 26.9% (SSP585, 2071–2100) and for autumn (Table 3.21, fifth panel) range from 6.2% (SSP126, 2021–2050) to 27.2% (SSP585, 2071–2100).

The projections of annual and seasonal specific humidity have high certainty, as demonstrated by an absence of hatching in Figures 3.44 and 3.45 and a small spread (and the same sign) between the mean and percentile statistics presented in Table 3.21.

For reference, the "observed" mean annual specific humidity (g g^{-1}), as resolved by a high-resolution (1.5 km) downscaled ERA-Interim climate simulation, is presented in Figure 3.46a.

Specific humidity has direct effects on animal and human health. An increase in specific humidity will amplify the adverse effects of increases in extreme temperatures (section 3.2) and heatwaves (section 3.3) and lead to higher mortality by limiting heat loss through evaporative cooling (Coffel *et al*., 2017). The link between climate and viruses such as influenza is well established. For example, epidemiological studies indicate that low levels of specific humidity (e.g. Shaman *et al*., 2010, 2011; Noti *et al*., 2013; Tamerius *et al*., 2013) and temperature (e.g. Ianevski *et al*., 2019) are associated with greater influenza mortality. Barreca and Shimshack (2012) showed that

the humidity–influenza relation is non-linear with lower specific humidity levels resulting in "greater influenza mortality at mean daily specific humidity levels below 6 g/kg" and that "incremental changes in humidity do not significantly affect influenza mortality when mean daily specific humidity exceeds a 6 g/kg threshold". Similar links between ultraviolet (UV) radiation and influenza are well established; for example, Sagripanti and Lytle (2007) found that "inactivation of viruses in the environment by solar UV radiation plays a role in the seasonal occurrence of influenza pandemics".

Although research on the effects of climate on COVID-19 is at an early stage and provides some conflicting results, some clear trends emerge on the role of the local climate, especially for temperature and humidity. A systematic review of research found a negative association between temperature and humidity and COVID-19 mortality in the majority of studies (Romero Starke *et al*., 2021). A more recent study recommends a city-level time-series approach to evaluate the association between meteorological exposures and COVID-19 incidence at the global scale (Nottmeyer

(a)
COSMO5-CLM-ERA-Interim 1.5km (1981-2010)
Mean Annual Specific Humidity

(b)
COSMO5-CLM-ERA-Interim 1.5km (1981-2010)
Mean Annual Relative Humidity
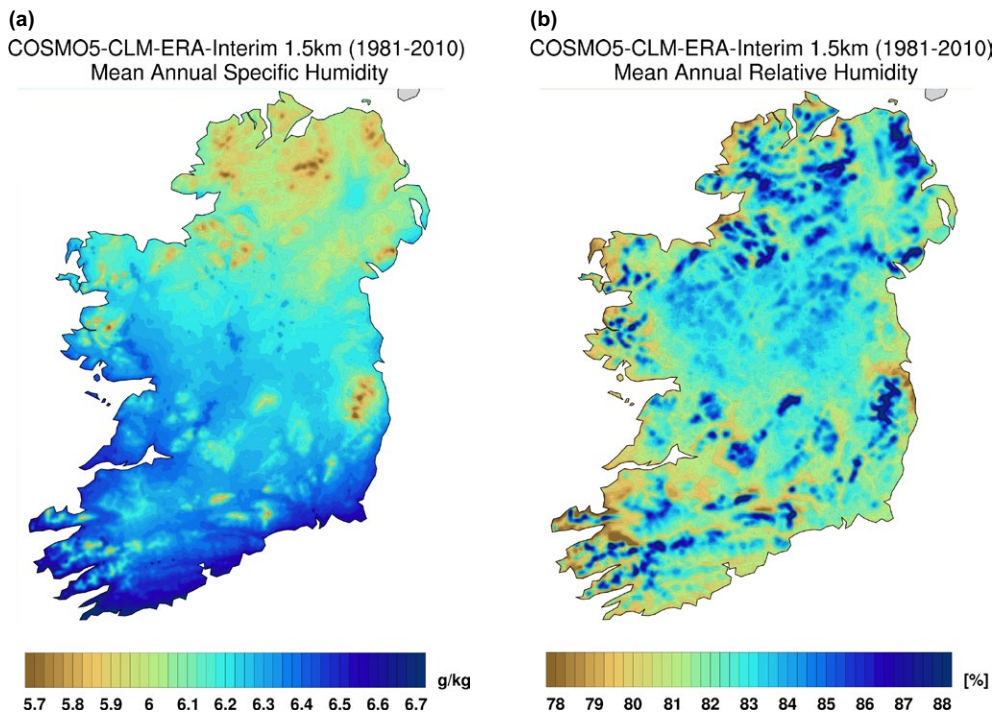
Figure 3.46. Annual mean 2 m (a) specific humidity (g g^{-1}) and (b) relative humidity (%) as resolved by a COSMO-CLM5–ERA-Interim 1.5 km simulation (1981–2010). Refer to Flanagan *et al*. (2019) and Flanagan and Nolan (2020) for an overview of the climate simulation configuration and validation results.

et al., 2023). The study indicates that "there is a tendency of a higher risk of COVID-19 cases at low temperature or absolute humidity levels, which aligns to an extent with available mechanistic explanations and previous literature basis". Other studies have indicated that regions with higher levels of UV light were strongly associated with lower COVID-19 growth rates (e.g. Asher *et al.*, 2021; Carleton *et al.*, 2021; Nicastro *et al.*, 2021) under the main hypothesis that UV light could cause the inactivation of viruses in the air and on surfaces. However, other studies have demonstrated no significant trend (e.g. Nottmeyer *et al.*, 2023) or a non-linear association, with low and high levels of radiation associated with lower risk, which may be attributed to "the effects of weather-dependent human behaviour change" (Donzelli *et al.*, 2022).

In Ireland, temperature (section 3.1) and humidity are projected to increase, which has the potential to alleviate future outbreaks of influenza and COVID-19. Conversely, surface radiation is projected to decrease (see section 3.19 and Nolan and Flanagan, 2020), which may exacerbate future outbreaks. However, more research is required at a national level to quantify the impacts of climate change on influenza and COVID-19.

3.18 Relative Humidity Projections

Relative humidity is the ratio of the amount of water vapour present in the air to the greatest amount possible at the same temperature. Warm air can hold substantially more moisture than cold air, meaning that the relative humidity of cold air is far higher than that of warm air for equal absolute humidity levels. Relative humidity is expressed as a percentage, with 0% corresponding to totally dry air and 100% to totally saturated air (leading to increased probability of precipitation). Relative humidity is a measure of how "saturated" the air is (i.e. how much water vapour the air contains compared with the maximum it could contain) whereas specific humidity (section 3.17) is a measure of the "moisture content" of the air (i.e. how much water vapour there is in relation to the total mass of water vapour and air combined). For reference, "observed" mean annual relative humidity (%), as resolved by a high-resolution (1.5 km) downscaled

ERA-Interim climate simulation, is presented in Figure 3.46b.

The general consensus in the scientific literature is that specific humidity will increase over land and oceans whereas relative humidity will decrease over land in a warming climate. The IPCC AR6 report concluded that "a *very likely* decrease in relative humidity has occurred over much of the global land area since 2000, particularly over mid-latitude regions of the Northern Hemisphere, with increases at northern high latitudes" (IPCC, 2021). Observations since the 1970s show a *very likely* increase in near-surface specific humidity over both land and oceans (IPCC, 2021). Byrne and O'Gorman (2018) showed that the observed decreases in relative humidity over land in recent decades (1979–2016) are more closely linked to the warming of the land surface, which is more pronounced than that of the ocean surface. Declining relative humidity over land, and increasing specific humidity over land and ocean, is also the dominant feature of future climate projections. The CMIP6 multi-model ensemble projects (*medium confidence*) general decreases in near-surface relative humidity over a large fraction of land areas (with exceptions such as India, which shows no changes or small increases) but moderate increases over the ocean (IPCC, 2021). There is *high confidence* in continued increases in global mean near-surface specific humidity over land (IPCC, 2021).

Figure 3.47, projections of the mean annual near-surface (2 m) relative humidity, shows small changes (~0%) or small projected increases, which are enhanced for the higher SSPs and later time periods. There exists a south-east to west gradient in the projections, with the largest increases in the north-west. Averaged over the whole country, the mean projected increase in annual relative humidity (Table 3.22, first panel) ranges from 0.23% (2021–2050 under SSP245) to 0.91% (2071–2100 under SSP585). The projections of annual relative humidity have higher certainty, as demonstrated by an absence of hatching in Figure 3.47 and a small spread (and the same sign) between the mean and percentile statistics presented in Table 3.22 (first panel).

Figure 3.48a, the projected change in winter relative humidity, shows very small (and uncertain) changes
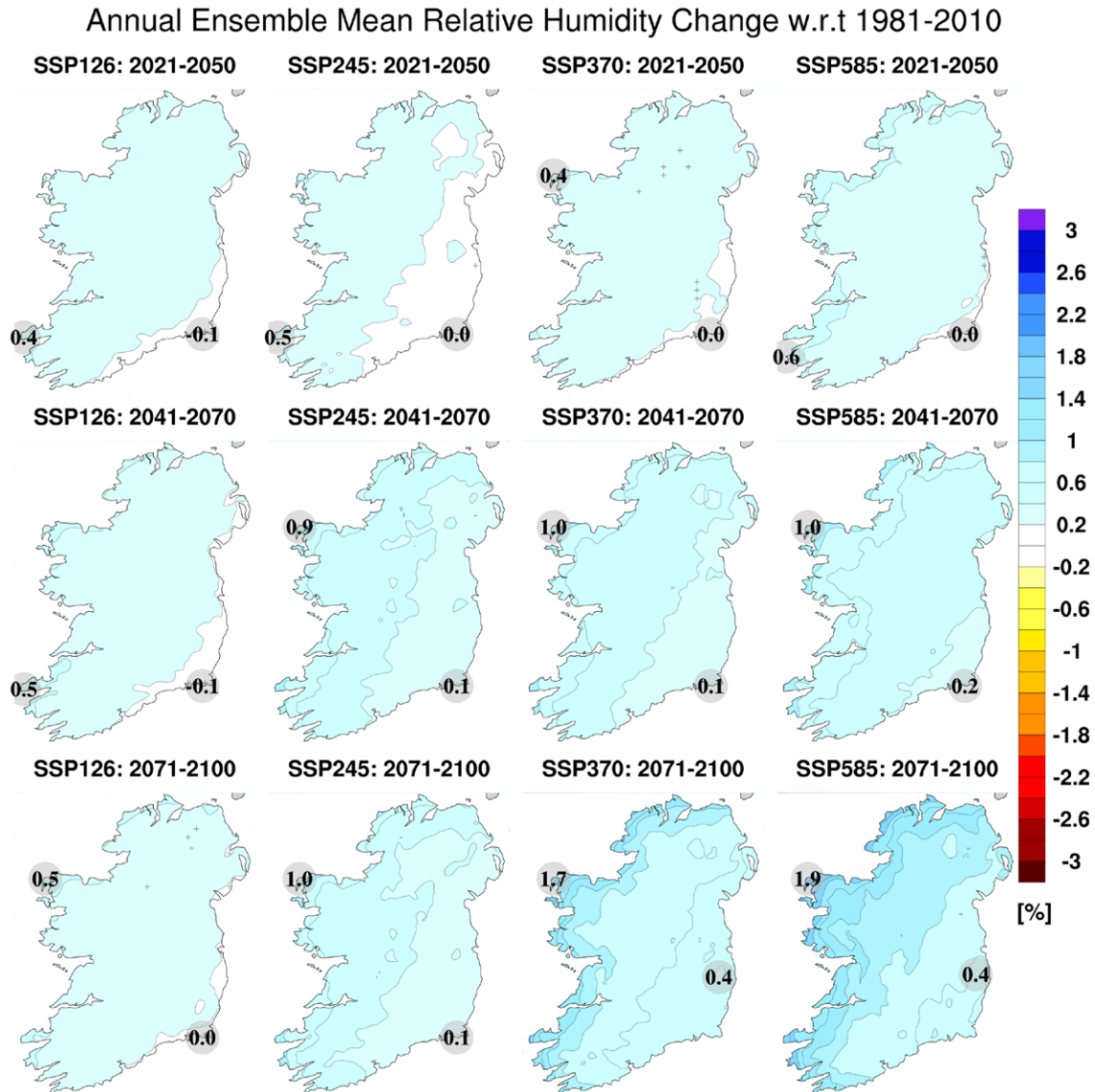
Figure 3.47. RCM–CMIP6 ensemble projections of annual near-surface relative humidity (%). Note that relative humidity has the unit "%". The projection metric is a (future–past) difference (%) as opposed to a percentage change. All RCM ensemble members were run with 4 km grid spacing. In each case, the future 30-year period is compared with the past period, 1981–2010. The numbers included on each plot are the minimum and maximum projected changes, displayed at their locations.

for all SSPs and time periods. Table 3.22 (second panel) shows that, while uncertainty is evident in the winter projections for the lower SSPs and/or earlier time periods, the spread between ensemble members is small, indicating that the ensemble members agree on small projected changes but disagree on the sign of change.

Figure 3.48b and c show that relative humidity is projected to increase for spring and summer with enhanced increases for the higher SSPs and later time periods. Averaged over the whole country,

projected increases in relative humidity during spring (Table 3.22, third panel) range from 0.23% (SSP126, 2021–2050) to 1.07% (SSP585, 2071–2100). Summer (Table 3.22, fourth panel) projected increases range from 0.46% (SSP370, 2021–2050) to 1.81% (SSP585, 2071–2100). The projections of spring and summer relative humidity have higher certainty, as demonstrated by a scarcity of hatching in Figure 3.48b and c, and a small spread (and the same sign) between the mean and percentile statistics presented in Table 3.22.

Table 3.22. Annual and seasonal projections of near-surface (2 m) relative humidity (%). This table corresponds to the projections in Figures 3.47 and 3.48, and shows the 33rd percentile, 50th percentile, mean and 66th percentile averaged over the island of Ireland

Annual near-surface (2 m) relative humidity (%)

Time period	SSP126				SSP245				SSP370				SSP585			
	P33	P50	Mean	P66	P33	P50	Mean	P66	P33	P50	Mean	P66	P33	P50	Mean	P66
2021–2050	0.23	0.26	0.28	0.34	0.22	0.29	0.23	0.41	0.18	0.29	0.27	0.4	0.32	0.38	0.33	0.49
2041–2070	0.19	0.23	0.28	0.35	0.32	0.39	0.45	0.56	0.38	0.52	0.47	0.64	0.44	0.52	0.55	0.71
2071–2100	0.21	0.28	0.28	0.39	0.35	0.43	0.44	0.55	0.62	0.7	0.73	0.88	0.76	0.84	0.91	1.11

Winter near-surface (2 m) relative humidity (%)

Time period	SSP126				SSP245				SSP370				SSP585			
	P33	P50	Mean	P66	P33	P50	Mean	P66	P33	P50	Mean	P66	P33	P50	Mean	P66
2021–2050	−0.13	0.03	0.03	0.22	−0.03	0.08	−0.02	0.24	0	0.06	−0.04	0.16	0	0.09	0.07	0.25
2041–2070	0.03	0.14	0.06	0.31	0.17	0.24	0.14	0.4	0.04	0.13	0.05	0.32	0.09	0.19	0.11	0.4
2071–2100	−0.13	0.01	−0.09	0.21	0.01	0.11	−0.01	0.25	0.05	0.26	0.13	0.51	0.11	0.25	0.13	0.44

Spring near-surface (2 m) relative humidity (%)

Time period	SSP126				SSP245				SSP370				SSP585			
	P33	P50	Mean	P66	P33	P50	Mean	P66	P33	P50	Mean	P66	P33	P50	Mean	P66
2021–2050	0.13	0.21	0.23	0.35	0.15	0.25	0.28	0.44	0.25	0.41	0.49	0.82	0.11	0.25	0.26	0.45
2041–2070	0.17	0.26	0.24	0.4	0.3	0.38	0.4	0.56	0.45	0.57	0.66	0.93	0.45	0.54	0.66	0.83
2071–2100	0.2	0.3	0.35	0.56	0.3	0.39	0.45	0.58	0.66	0.77	0.92	1.08	0.83	0.94	1.07	1.23

Summer near-surface (2 m) relative humidity (%)

Time period	SSP126				SSP245				SSP370				SSP585			
	P33	P50	Mean	P66	P33	P50	Mean	P66	P33	P50	Mean	P66	P33	P50	Mean	P66
2021–2050	0.45	0.56	0.67	0.8	0.45	0.65	0.62	0.87	0.19	0.34	0.46	0.74	0.44	0.68	0.68	0.98
2041–2070	0.33	0.4	0.64	0.76	0.52	0.67	0.91	1.27	0.7	0.85	0.96	1.27	0.63	0.85	0.98	1.26
2071–2100	0.36	0.52	0.66	0.86	0.71	0.81	0.99	1.18	0.9	1.19	1.32	1.66	1.29	1.62	1.81	2.28

Autumn near-surface (2 m) relative humidity (%)

Time period	SSP126				SSP245				SSP370				SSP585			
	P33	P50	Mean	P66	P33	P50	Mean	P66	P33	P50	Mean	P66	P33	P50	Mean	P66
2021–2050	0.13	0.18	0.18	0.29	−0.05	0	0.05	0.15	−0.03	0.05	0.14	0.18	0.16	0.23	0.31	0.42
2041–2070	0.03	0.13	0.18	0.36	0.22	0.32	0.33	0.45	−0.06	0.13	0.21	0.42	0.34	0.42	0.45	0.55
2071–2100	0.08	0.15	0.2	0.33	0.14	0.23	0.33	0.42	0.44	0.49	0.56	0.64	0.48	0.55	0.6	0.7

Figure 3.48d, the projected change in autumn relative humidity, shows small (~0%) changes for the lower SSPs and/or earlier time periods (small increases otherwise). Table 3.22 (fifth panel) shows that, while some uncertainty is evident in the autumn projections, the spread between ensemble members is small, indicating that the ensemble members agree on small projected changes but disagree on the sign of change. The autumn relative humidity projections have higher certainty for the higher SSPs and later time periods, as demonstrated by an absence of hatching
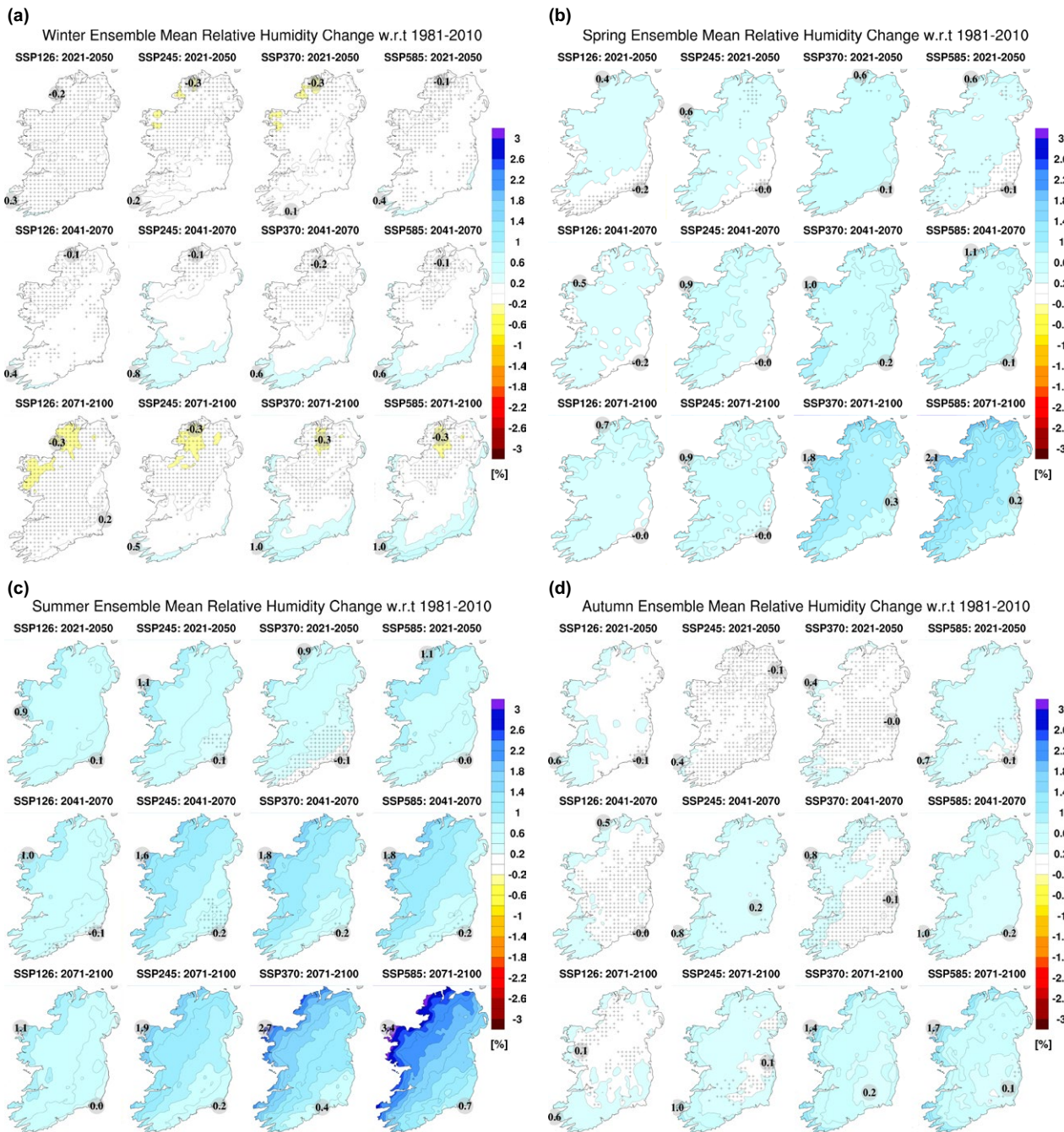
Figure 3.48. Seasonal RCM ensemble projections of near-surface relative humidity (%) for (a) winter, (b) spring, (c) summer and (d) autumn. In each case, the future 30-year period is compared with the past period, 1981–2010. The numbers included on each plot are the minimum and maximum projected changes, displayed at their locations.

in Figure 3.48d and agreement in sign between the P33 and P66 statistics of Table 3.22 (fifth panel).

The projections of relative humidity are somewhat contrary to the general consensus in the scientific literature that relative humidity will decrease over land (and moderately increase over the ocean) in a warming climate. The projections of the current

study, of small projected increases (or ~0% change) in relative humidity for all seasons, may be partly attributed to the large influence of the North Atlantic Ocean on the Irish climate.

Relative humidity is an important climate field that has a direct impact on many sectors, including public health, agriculture and the built environment. For

example, the link between low relative (and specific) humidity and greater influenza mortality is well established (e.g. Noti *et al*., 2013). The incidence of Lyme borreliosis (Lyme disease), a vector-borne illness caused by the bacterium *Borrelia* and spread by ticks, increases with high relative humidity; ticks require a minimum 80% humidity to avoid drying out during the early stages of life (Cullen, 2010) and air temperatures greater than 6°C during host questing (Süss *et al*., 2008). Potato crop failures in Ireland can occur when high relative humidity and temperatures combine to provide the warm, wet conditions in which the *Phytophthora infestans* fungus (potato blight) thrives (Collins and Cummins, 1996; Cucak *et al*., 2019). Changes in relative humidity will have an impact on the built and archaeological heritage of Ireland, affecting deterioration mechanisms such as salt weathering, mould growth and corrosion (Daly, 2019). Relative humidity is also an important field for derived variables, such as fire risk indexes; the risk of wildfire decreases with increasing relative humidity (e.g. Dowdy *et al*., 2010).
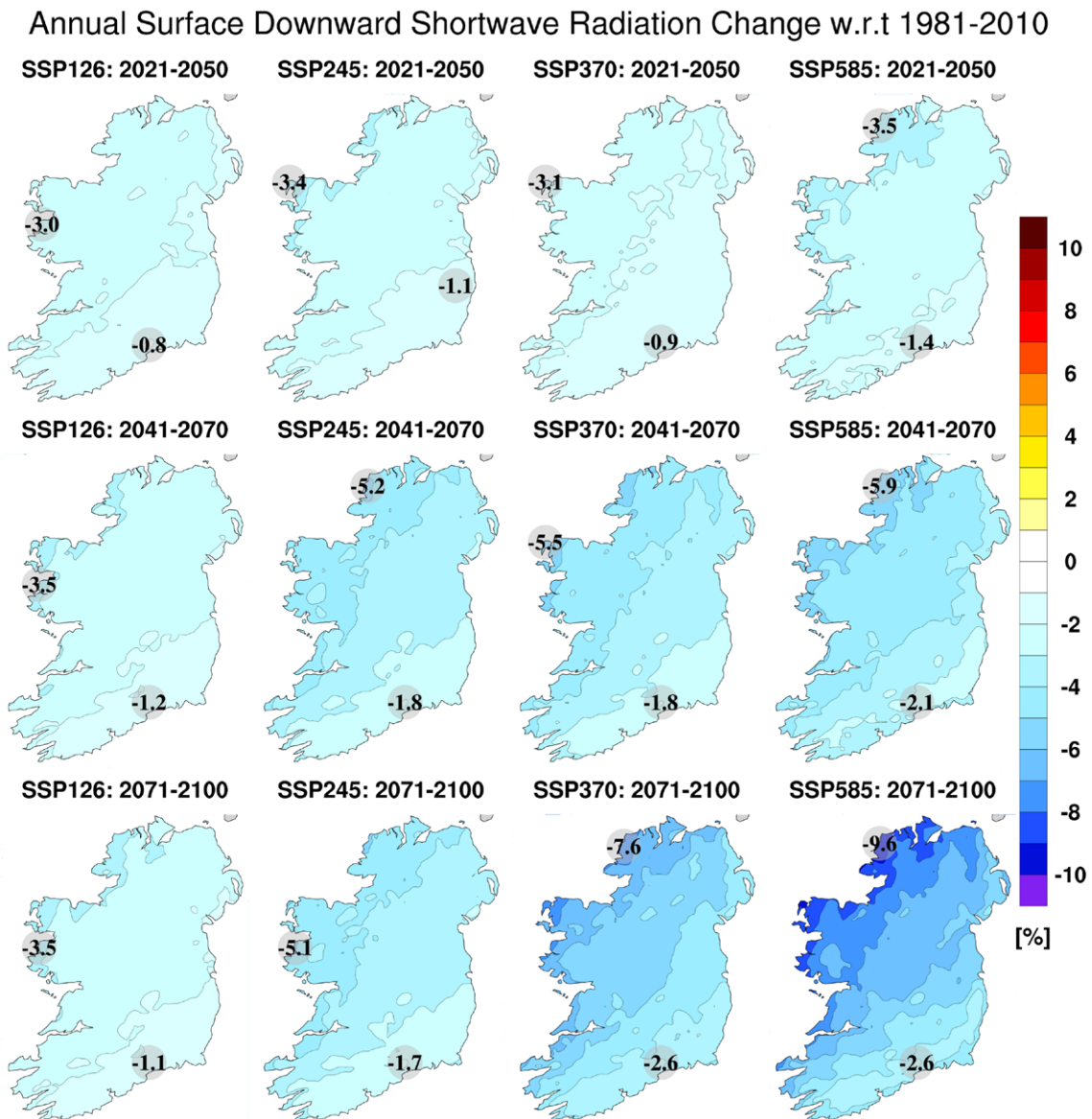
Figure 3.49. Annual RCM–CMIP6 ensemble mean projections of surface downwards shortwave radiation (%). All RCM ensemble members were run with 4 km grid spacing. In each case, the future 30-year period is compared with the past period, 1981–2010. The numbers included on each plot are the minimum and maximum projected changes, displayed at their locations.

3.19 Surface Shortwave Radiation and Cloud Cover

Figure 3.49, projections of the mean annual surface downwards shortwave radiation (SWR), shows decreases, which are enhanced for the higher SSPs and later time periods. There exists a south-east to north-west gradient in the projections, with the largest increases in the north-west. The annual surface SWR is projected to decrease by 0.8–3% for SSP126 (2021–2050) and by 2.6–9.6% for SSP585 (2071–2100). Averaged over the whole country, the mean projected decrease in annual SWR (Table 3.23, first panel) ranges from 2% (2021–2050 under SSP370) to 6.1% (2071–2100 under SSP585).

Table 3.23. Annual and seasonal projections of surface downwards SWR (%). This table corresponds to the projections in Figures 3.49 and 3.50, and shows the 33rd percentile, 50th percentile, mean and 66th percentile averaged over the island of Ireland

Annual SWR (%)

Time period	SSP126				SSP245				SSP370				SSP585			
	P33	P50	Mean	P66	P33	P50	Mean	P66	P33	P50	Mean	P66	P33	P50	Mean	P66
2021–2050	–2.7	–2.4	–2.1	–1.5	–3.6	–2.4	–2.3	–1.6	–2.3	–2.0	–2.0	–1.2	–3.6	–3.1	–2.5	–2.1
2041–2070	–3.0	–2.7	–2.3	–1.5	–4.4	–3.7	–3.5	–2.3	–4.7	–4.0	–3.8	–2.7	–6.2	–4.1	–4.1	–2.9
2071–2100	–3.0	–2.3	–2.4	–1.6	–5.2	–3.9	–3.6	–2.5	–7.3	–4.8	–5.1	–3.7	–8.7	–6.1	–6.1	–4.4

Winter SWR (%)

Time period	SSP126				SSP245				SSP370				SSP585			
	P33	P50	Mean	P66	P33	P50	Mean	P66	P33	P50	Mean	P66	P33	P50	Mean	P66
2021–2050	–3.3	–2.6	–2.6	–1.6	–3.4	–2.8	–2.6	–1.8	–3.8	–3.1	–2.7	–1.9	–3.9	–3.4	–2.7	–1.7
2041–2070	–4.0	–3.4	–3.3	–2.4	–5.5	–5.2	–4.8	–4.4	–7.0	–6.3	–5.3	–4.3	–5.8	–5.3	–4.5	–4.0
2071–2100	–3.1	–2.8	–2.5	–1.7	–5.7	–5.2	–4.9	–4.4	–8.5	–8.1	–7.1	–6.7	–9.3	–8.8	–7.8	–7.6

Spring SWR (%)

Time period	SSP126				SSP245				SSP370				SSP585			
	P33	P50	Mean	P66	P33	P50	Mean	P66	P33	P50	Mean	P66	P33	P50	Mean	P66
2021–2050	–2.4	–2.1	–1.6	–1.4	–2.6	–2.2	–2.1	–1.5	–3.0	–2.5	–2.5	–1.7	–2.7	–2.3	–2.0	–1.5
2041–2070	–2.7	–2.3	–1.9	–1.5	–2.9	–2.6	–2.9	–2.1	–4.6	–3.6	–4.1	–2.7	–5.3	–3.9	–4.5	–3.3
2071–2100	–2.7	–2.3	–2.3	–1.6	–4.1	–3.8	–3.3	–2.8	–6.2	–5.4	–5.2	–3.9	–6.0	–5.4	–5.8	–4.4

Summer SWR (%)

Time period	SSP126				SSP245				SSP370				SSP585			
	P33	P50	Mean	P66	P33	P50	Mean	P66	P33	P50	Mean	P66	P33	P50	Mean	P66
2021–2050	–3.5	–3.0	–2.6	–1.6	–5.4	–3.2	–3.2	–1.7	–2.8	–2.2	–1.7	–0.1	–5.2	–4.1	–3.3	–2.7
2041–2070	–4.4	–3.4	–3.1	–1.6	–6.0	–5.0	–4.3	–2.5	–4.5	–3.9	–4.1	–2.6	–6.9	–4.0	–4.3	–2.4
2071–2100	–4.2	–3.4	–2.9	–2.1	–6.1	–3.5	–4.1	–2.6	–7.1	–4.9	–5.3	–3.1	–8.4	–7.0	–7.2	–4.4

Autumn SWR (%)

Time period	SSP126				SSP245				SSP370				SSP585			
	P33	P50	Mean	P66	P33	P50	Mean	P66	P33	P50	Mean	P66	P33	P50	Mean	P66
2021–2050	–2.4	–1.8	–1.3	–0.8	–0.9	–0.5	–0.3	0.4	–1.6	–1.2	–0.9	–0.1	–2.4	–2.0	–1.7	–1.3
2041–2070	–1.7	–1.3	–1.0	–0.6	–3.7	–3.1	–2.5	–2.1	–3.0	–2.4	–1.5	–0.5	–4.0	–3.1	–2.8	–1.8
2071–2100	–2.1	–1.6	–1.1	–0.3	–2.5	–1.8	–2.3	–0.7	–4.4	–4.0	–3.4	–2.7	–4.5	–3.5	–3.5	–2.6

(a)

Winter Surface Downward Shortwave Radiation Change w.r.t 1981-2010

(b)

Spring Surface Downward Shortwave Radiation Change w.r.t 1981-2010

(c)

Summer Surface Downward Shortwave Radiation Change w.r.t 1981-2010

(d)

Autumn Surface Downward Shortwave Radiation Change w.r.t 1981-2010
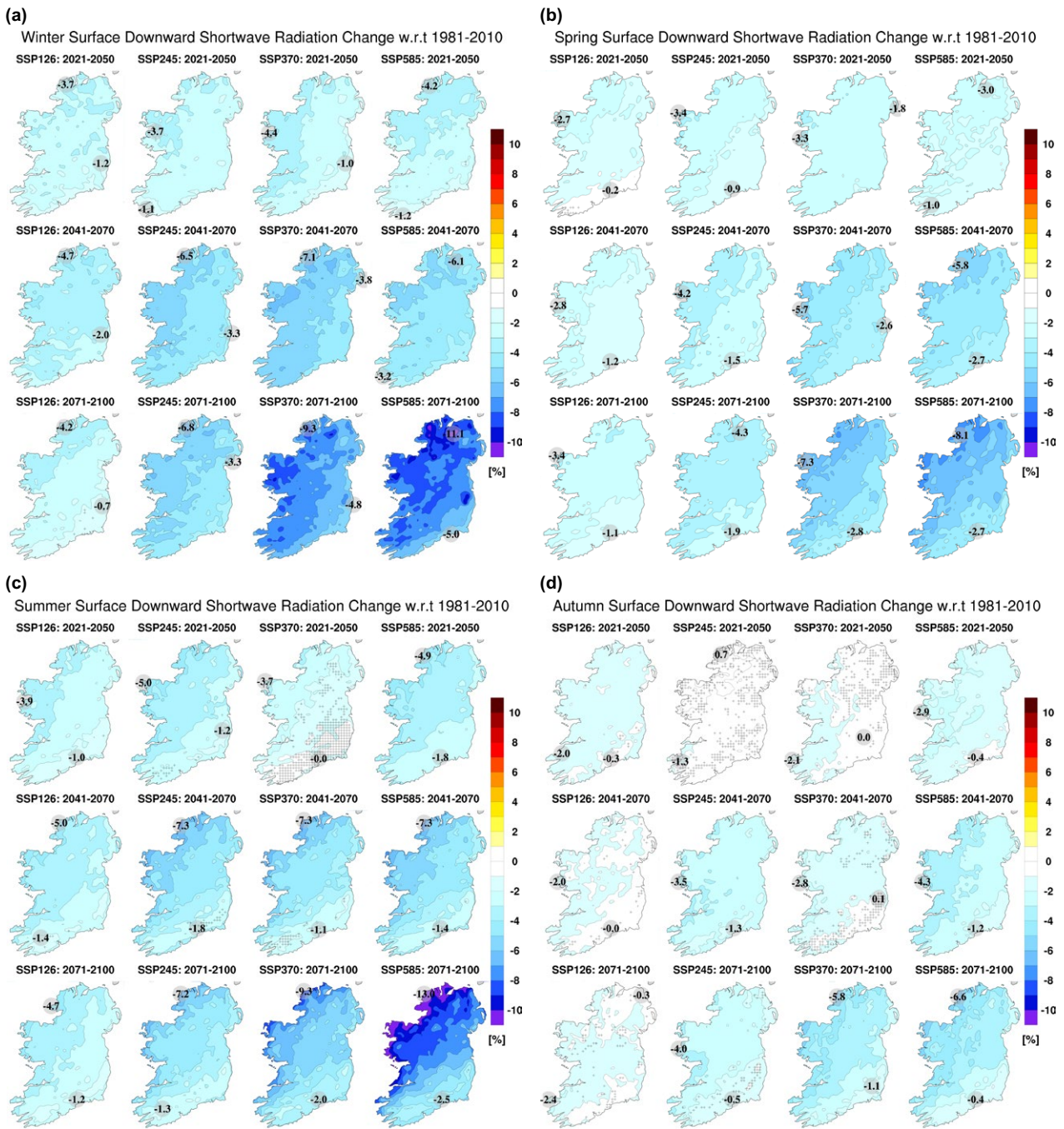
Figure 3.50. Seasonal RCM ensemble mean projections of surface downwards SWR (%) for (a) winter, (b) spring, (c) summer and (d) autumn. In each case, the future 30-year period is compared with the past period, 1981–2010. The numbers included on each plot are the minimum and maximum projected changes, displayed at their locations.

The seasonal projections of SWR are presented in Figure 3.50. Projections of SWR are small (~0%) for autumn during 2021–2050 (Figure 3.50d). Otherwise, SWR is projected to decrease for all seasons, with decreases enhanced for the higher SSPs and later time periods. The largest decreases are noted for the winter and summer months. Averaged over the whole country, robust projected decreases in SWR for winter (Table 3.23, second panel) range from 2.5%

(SSP126, 2071–2100) to 7.8% (SSP585, 2071–2100), for spring (Table 3.23, third panel) range from 1.6% (SSP126, 2021–2050) to 5.8% (SSP585, 2071–2100), for summer (Table 3.23, fourth panel) range from 1.7% (SSP370, 2021–2050) to 7.2% (SSP585, 2071–2100) and for autumn (Table 3.23, fifth panel) range from 0.9% (SSP370, 2021–2050) to 3.5% (SSP585, 2071–2100).

Except for autumn during 2021–2050, the projections of decreases in annual and seasonal surface downwards SWR have low uncertainty, as demonstrated by a scarcity of hatching in Figures 3.49 and 3.50 and a small spread (and the same sign) between the mean and percentile statistics presented in Table 3.23.

The radiation projections are in line with similar Irish (Nolan and Flanagan, 2020) and European studies. Jerez *et al*. (2015) analysed an ensemble

of EURO-CORDEX RCM projections (over Europe) and found that the ensemble mean pattern of change for mean surface-downwelling SWR (2070–2099 vs 1970–1999 climatologies under RCP8.5) shows "positive signals (about 5 W/m²) in Southern Mediterranean regions" and "negative signals northwards (about −10 W/m², down to −20 W/m² in the northernmost areas)". Bartók *et al*. (2017) also analysed a EURO-CORDEX RCP85 ensemble and found that "the multi-model mean of RCMs indicates a decrease in surface solar radiation of −0.60 W/m² per
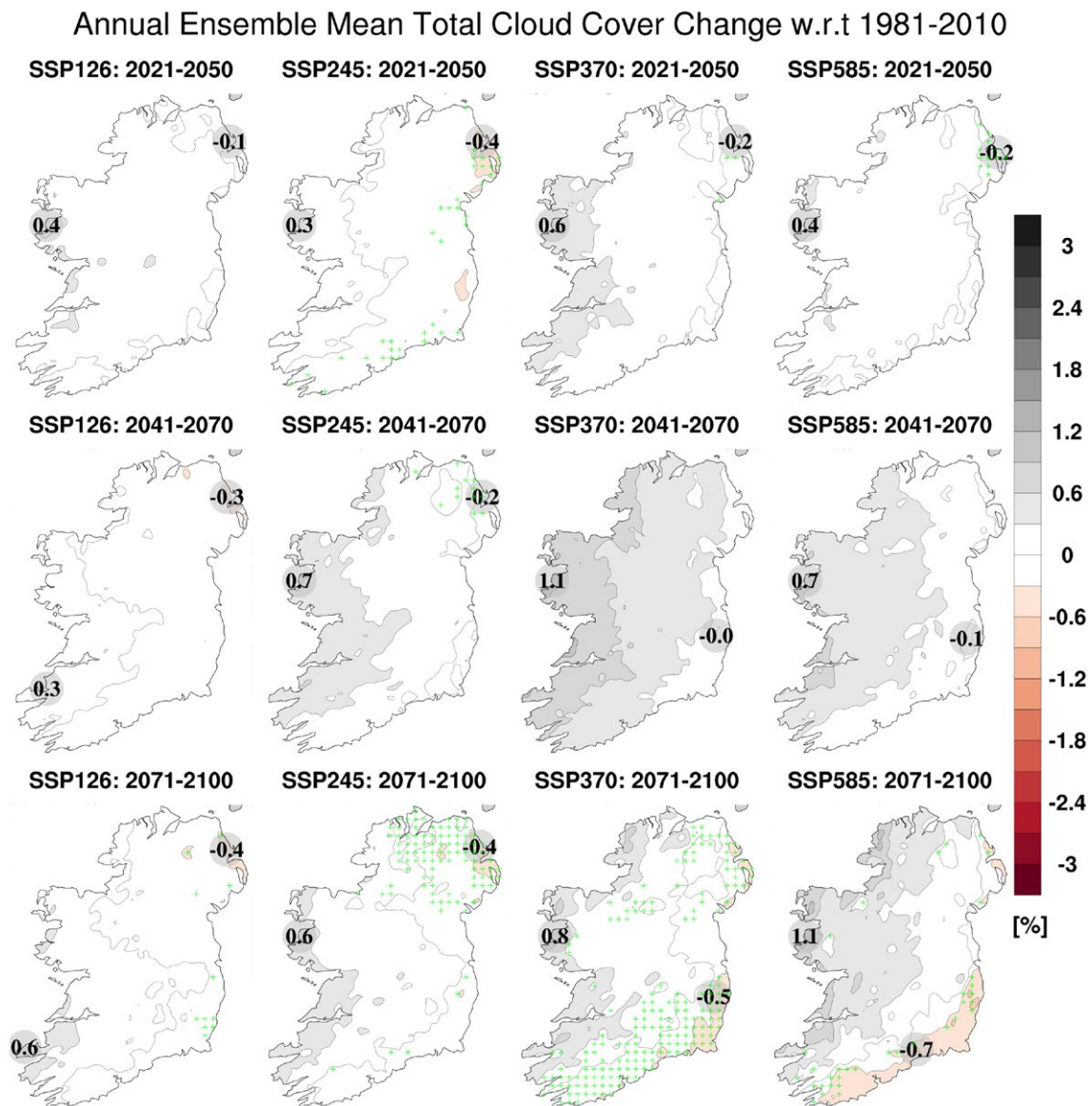
Figure 3.51. Annual RCM–CMIP6 ensemble mean projections of total cloud cover (%). Note that cloud cover has the unit "%". The projection metric is a (future–past) difference (%) as opposed to a percentage change. All RCM ensemble members were run with 4 km grid spacing. In each case, the future 30-year period is compared with the past period, 1981–2010. The numbers included on each plot are the minimum and maximum projected changes, displayed at their locations.

decade over Europe" for the period 2006–2100. The authors proposed that the reduction of surface solar radiation in the RCMs "can be attributed to increasing atmospheric absorption in line with the increase of water vapour content" (Bartók *et al*., 2017).

The annual and seasonal projected changes in cloud cover (%) are presented in Figures 3.51 and 3.52, respectively. The corresponding percentile and mean projection statistics, averaged over the country, are presented in Table 3.24. While the projected
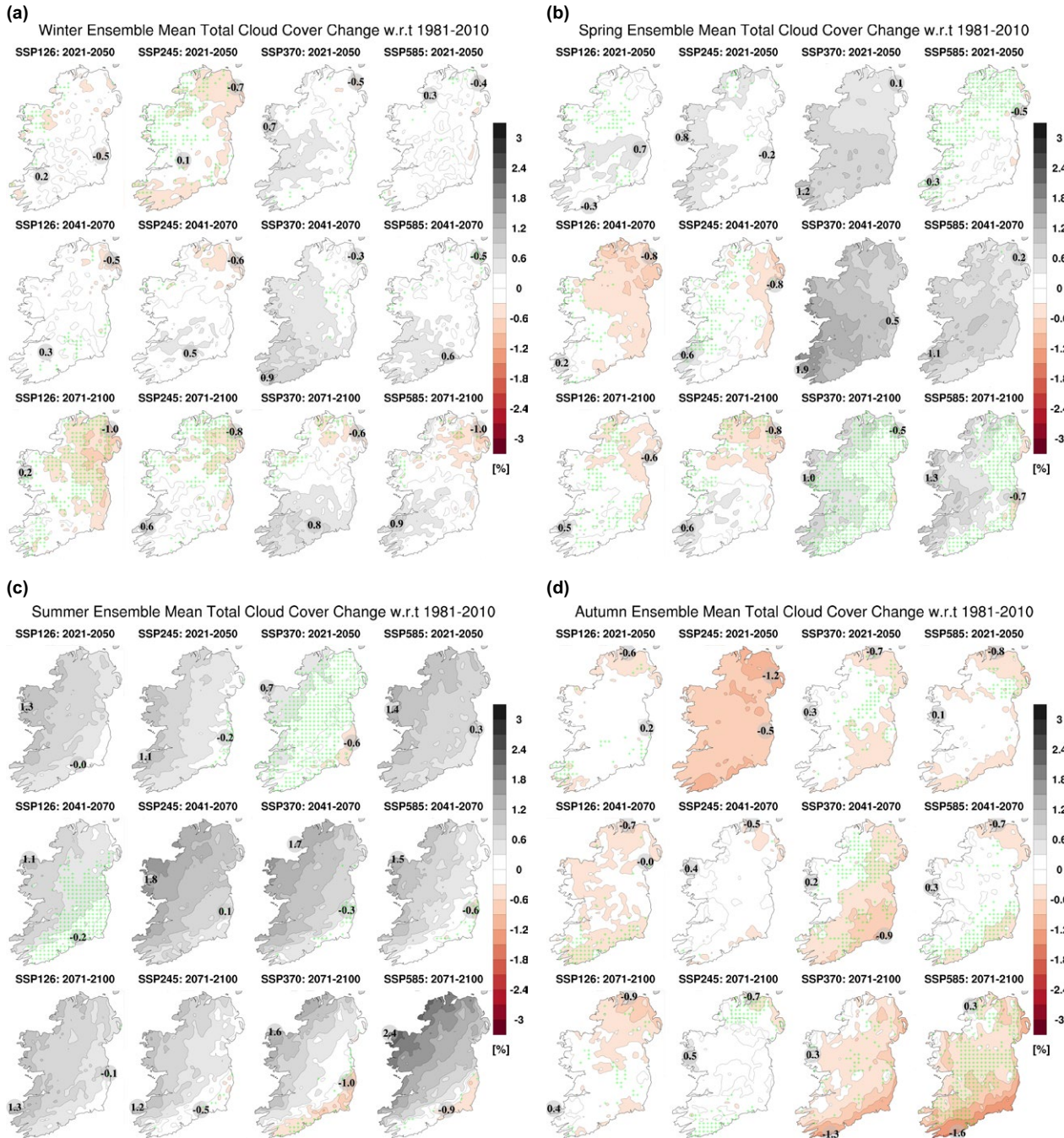
Figure 3.52. Seasonal RCM ensemble mean projections of total cloud cover (%) for (a) winter, (b) spring, (c) summer and (d) autumn. Note that cloud cover has the unit "%". The projection metric is a (future–past) difference (%) as opposed to a percentage change. In each case, the future 30-year period is compared with the past period, 1981–2010. The numbers included on each plot are the minimum and maximum projected changes, displayed at their locations.

Table 3.24. Annual and seasonal projections of cloud cover (%). This table corresponds to the projections in Figures 3.43 and 3.44, and shows the 33rd percentile, 50th percentile, mean and 66th percentile averaged over the island of Ireland

Annual cloud cover (%)

Time period	SSP126				SSP245				SSP370				SSP585			
	P33	P50	Mean	P66	P33	P50	Mean	P66	P33	P50	Mean	P66	P33	P50	Mean	P66
2021–2050	0.25	0.33	0.13	0.49	–0.05	0.42	–0.07	0.65	0.19	0.37	0.17	0.82	0.05	0.34	0.11	0.8
2041–2070	–0.04	0.15	–0.05	0.52	0.07	0.64	0.22	1.1	0.21	0.62	0.5	1.51	0.39	0.79	0.3	1.15
2071–2100	–0.09	0.49	0.01	0.77	–0.22	0.6	0.07	1	–0.34	0.72	0.11	1.25	0.03	0.98	0.2	1.36

Winter cloud cover (%)

Time period	SSP126				SSP245				SSP370				SSP585			
	P33	P50	Mean	P66	P33	P50	Mean	P66	P33	P50	Mean	P66	P33	P50	Mean	P66
2021–2050	–0.33	–0.13	–0.11	0.4	–0.55	–0.27	–0.27	0.55	–0.05	0.26	0.17	0.78	–0.16	0.11	–0.06	0.52
2041–2070	–0.11	0.28	–0.02	0.7	0.16	0.36	0.02	0.83	0.06	0.56	0.37	1.41	0.03	0.25	0.16	1.26
2071–2100	–0.55	–0.19	–0.29	0.73	–0.44	0.1	–0.09	0.93	0.24	0.7	0.17	1.3	0.26	0.57	0.03	1.12

Spring cloud cover (%)

Time period	SSP126				SSP245				SSP370				SSP585			
	P33	P50	Mean	P66	P33	P50	Mean	P66	P33	P50	Mean	P66	P33	P50	Mean	P66
2021–2050	–0.31	0.2	0.15	0.58	–0.01	0.28	0.25	0.79	0.12	0.53	0.62	1.15	–0.6	–0.18	–0.07	0.55
2041–2070	–0.74	–0.42	–0.35	0.19	–0.62	–0.14	–0.08	0.42	0.84	1.08	1.09	1.59	0.41	0.68	0.65	1.24
2071–2100	–0.38	0.12	–0.12	0.59	–0.56	–0.2	–0.08	0.48	–0.98	0.28	0.3	1.68	–0.41	0.16	0.34	1.44

Summer cloud cover (%)

Time period	SSP126				SSP245				SSP370				SSP585			
	P33	P50	Mean	P66	P33	P50	Mean	P66	P33	P50	Mean	P66	P33	P50	Mean	P66
2021–2050	0.38	0.65	0.67	1.23	0.78	1.16	0.55	1.65	–0.81	0.32	0.13	1.15	0.62	1.31	0.82	1.91
2041–2070	–0.37	0.31	0.46	1.48	0.99	1.59	1.02	2.35	0.34	1.22	0.89	1.88	0.87	1.18	0.55	1.55
2071–2100	0.85	1.21	0.69	1.6	0.62	0.99	0.5	1.36	0.56	1.03	0.41	1.76	1.06	1.45	1.04	2.41

Autumn cloud cover (%)

Time period	SSP126				SSP245				SSP370				SSP585			
	P33	P50	Mean	P66	P33	P50	Mean	P66	P33	P50	Mean	P66	P33	P50	Mean	P66
2021–2050	–0.14	0.15	–0.21	0.75	–1.0	–0.8	–0.82	–0.41	–0.42	–0.18	–0.23	0.44	–0.19	0.12	–0.24	0.47
2041–2070	–0.24	0.02	–0.31	0.56	–0.13	0	–0.09	0.35	–0.74	–.41	–0.39	0.57	–0.39	–0.16	–0.15	0.84
2071–2100	–0.41	–0.15	–0.25	0.41	–0.24	0.07	–0.03	0.82	–0.68	–0.11	–0.46	0.37	–1.1	–0.38	–0.62	0.54

changes in cloud cover are small, a correlation is noted between the projected changes in cloud cover and SWR. This correlation is evident, for example, in the annual SWR (Figure 3.49) and cloud cover (Figure 3.51) projections, which both exhibit a similar south-west to north-east gradient for the higher SSPs and later time periods. This correlation is strongest for summer, with projections of SWR (Figure 3.50c) and cloud cover (Figure 3.52c) exhibiting a similar south-west to north-east gradient for all SSPs and time periods. While the dominant driver of decreases in SWR is an increase in water vapour, the above

analysis shows that changes in cloud cover also have an impact.

3.20   Solar Photovoltaic Power

To assess the impact of climate change on solar power in Ireland, solar photovoltaic (PV) power, at time *t,* was evaluated using the following method outlined in Jerez *et al*. (2015) and Mavromatakis *et al*. (2010):

$$PV(t) = P_R(t)\frac{SW(t)}{SW_S} \qquad (3.7)$$

where *SW* refers to surface-downwelling SWR (Wm⁻²) and SW_s refers to surface-downwelling SWR at standard test conditions ($SW_s = 1000\,W\,m^{-2}$), and the nominal capacity of a PV device is determined as its measured power output. P_R is the "performance ratio", formulated to account for changes of the PV cells' efficiency as a result of changes in their temperature as:

$$P_R(t) = 1 + \gamma(T_{cell}(t) - T_s) \qquad (3.8)$$

where T_{cell} is the PV cell temperature, $T_s = 25°C$ (standard test conditions) and $\gamma = -0.005°C^{-1}$,
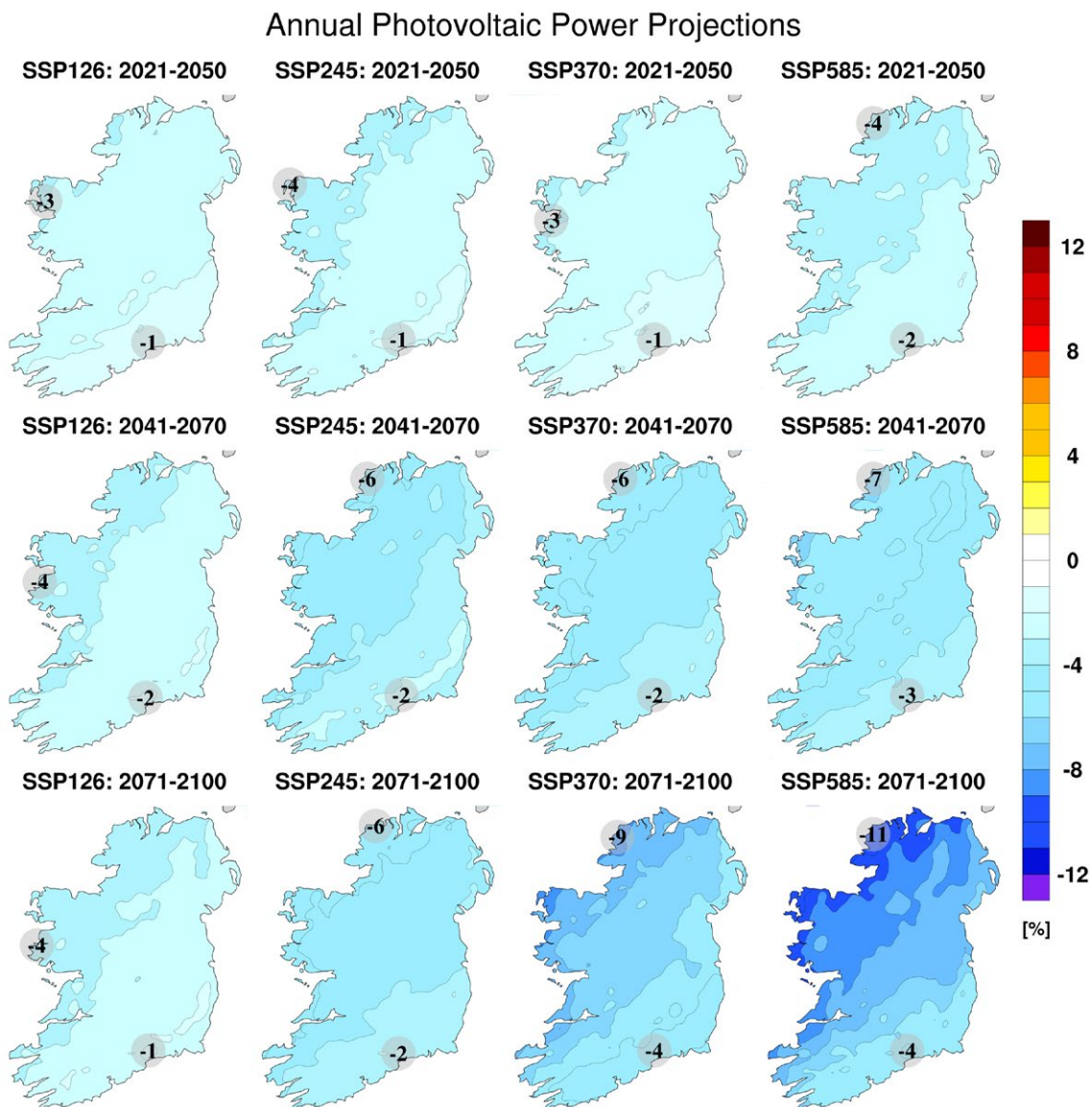
Figure 3.53. Annual RCM–CMIP6 ensemble mean projections of solar PV power (%). All RCM ensemble members were run with 4 km grid spacing. In each case, the future 30-year period is compared with the past period, 1981–2010. The numbers included on each plot are the minimum and maximum projected changes, displayed at their locations.

considering the typical response of monocrystalline silicon solar panels (Tonui and Tripanagnostopoulos, 2008). T_{cell} is modelled considering the effects of surface temperature, T (°C), SW (W m^{-2}) and wind speed, W (m s^{-1}), on it as:

$$T_{cell}(t) = c_1 + c_2 T + c_3 SW + c_4 W \qquad (3.9)$$

where $c_1 = 4.3$°C, $c_2 = 0.943$, $c_3 = 0.028$°C m^2 W^{-1}, and $c_4 = -1.528$ s m^{-1}, as recommended by Jerez *et al.* (2015) and Tonui and Tripanagnostopoulos (2008).

The projections of the mean annual PV power (Figure 3.53) show decreases, which are enhanced for the higher SSPs and later time periods. There

Table 3.25. Annual and seasonal projections of PV power (%). This table corresponds to the projections in Figures 3.53 and 3.54, and shows the 33rd percentile, 50th percentile, mean and 66th percentile averaged over the island of Ireland

Annual PV power (%)

Time period	SSP126				SSP245				SSP370				SSP585			
	P33	P50	Mean	P66	P33	P50	Mean	P66	P33	P50	Mean	P66	P33	P50	Mean	P66
2021–2050	–2.9	–2.5	–2.3	–1.8	–3.8	–2.6	–2.7	–1.9	–2.6	–2.3	–2.4	–1.7	–3.7	–3.2	–2.9	–2.4
2041–2070	–3.2	–2.9	–2.8	–2.1	–4.7	–4.0	–4.0	–2.8	–5.2	–4.5	–4.4	–3.4	–6.4	–5.0	–4.8	–3.3
2071–2100	–3.2	–2.6	–2.8	–2.1	–5.6	–5.0	–4.4	–3.2	–8.1	–5.9	–6.2	–4.7	–9.7	–7.8	–7.5	–5.5

Winter PV power (%) power

Time period	SSP126				SSP245				SSP370				SSP585			
	P33	P50	Mean	P66	P33	P50	Mean	P66	P33	P50	Mean	P66	P33	P50	Mean	P66
2021–2050	–3.6	–2.9	–2.9	–1.9	–3.6	–3.1	–2.9	–2.1	–4.0	–3.5	–3.0	–2.3	–4.1	–3.6	–3.1	–2.2
2041–2070	–4.3	–3.8	–3.6	–2.8	–5.8	–5.5	–5.1	–4.7	–7.4	–6.7	–5.8	–4.8	–6.1	–5.7	–5.1	–4.7
2071–2100	–3.6	–3.2	–3.0	–2.2	–6.3	–5.7	–5.5	–4.9	–9.3	–8.8	–7.9	–7.5	–10	–9.6	–8.8	–8.3

Spring PV power (%)

Time period	SSP126				SSP245				SSP370				SSP585			
	P33	P50	Mean	P66	P33	P50	Mean	P66	P33	P50	Mean	P66	P33	P50	Mean	P66
2021–2050	–2.6	–2.3	–1.8	–1.7	–2.8	–2.4	–2.4	–1.8	–3.3	–2.9	–2.7	–2.1	–2.8	–2.5	–2.2	–1.9
2041–2070	–3.1	–2.7	–2.2	–1.9	–3.3	–3.0	–3.2	–2.4	–4.9	–4.2	–4.6	–3.3	–5.8	–4.5	–4.9	–3.7
2071–2100	–3.3	–2.9	–2.7	–2.1	–4.7	–4.3	–3.9	–3.3	–6.8	–6.0	–6.1	–4.8	–7.1	–6.5	–6.8	–5.6

Summer PV power (%)

Time period	SSP126				SSP245				SSP370				SSP585			
	P33	P50	Mean	P66	P33	P50	Mean	P66	P33	P50	Mean	P66	P33	P50	Mean	P66
2021–2050	–3.7	–3.2	–2.9	–2.0	–5.6	–3.4	–3.6	–1.9	–3.2	–2.5	–2.2	–0.8	–5.5	–4.4	–3.8	–2.7
2041–2070	–4.7	–3.7	–3.5	–1.9	–6.3	–5.4	–4.8	–2.9	–5.1	–4.5	–4.8	–3.4	–7.5	–4.8	–5.1	–2.9
2071–2100	–4.5	–3.8	–3.4	–2.2	–6.7	–4.6	–5.0	–3.3	–8.3	–6.3	–6.6	–4.0	–10	–8.9	–8.8	–5.7

Autumn PV power (%)

Time period	SSP126				SSP245				SSP370				SSP585			
	P33	P50	Mean	P66	P33	P50	Mean	P66	P33	P50	Mean	P66	P33	P50	Mean	P66
2021–2050	–2.6	–2.1	–1.7	–1.2	–1.4	–1.1	–0.8	–0.1	–2.0	–1.6	–1.4	–0.8	–2.7	–2.4	–2.2	–1.8
2041–2070	–2.1	–1.7	–1.6	–1.2	–4.2	–3.7	–3.2	–2.8	–3.4	–3.0	–2.3	–1.6	–4.9	–3.9	–3.6	–2.3
2071–2100	–2.8	–2.2	–1.7	–1.0	–3.8	–3.1	–3.3	–1.8	–5.7	–5.1	–4.8	–4.3	–5.8	–5.1	–5.2	–4.2

exists a clear south-east to north-west gradient in the projections, with the largest increases in the north-west. The annual PV power is projected to decrease by 1–3% for SSP126 (2021–2050) and by 4–11% for SSP585 (2071–2100). Averaged over the whole country (Table 3.25, first panel), the mean projected decrease in annual PV power ranges from 2.3% (2021–2050 under SSP126) to 7.5% (2071–2100 under SSP585).

PV power is projected to decrease for all seasons (Figure 3.54), with decreases enhanced for the higher SSPs and later time periods. The largest decreases are noted for the winter and summer months (Figure 3.54a and c). Averaged over the whole country, projected decreases in PV for winter (Table 3.25, second panel) range from 2.9% (SSP126, 2021–2050) to 8.8% (SSP585, 2071–2100), for spring (Table 3.25, third panel) range from 1.8% (SSP126, 2021–2050) to
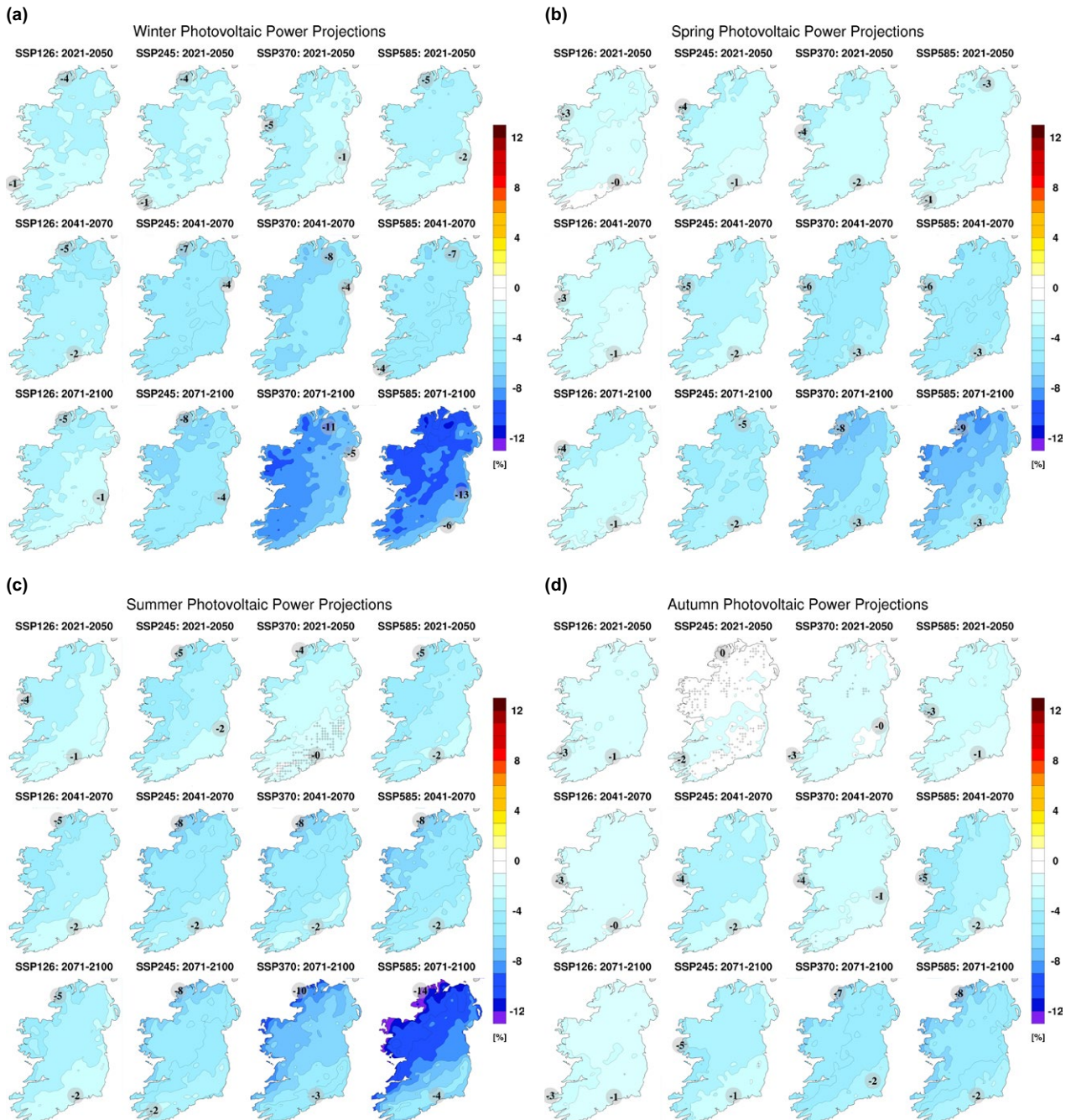
Figure 3.54. Seasonal RCM ensemble mean projections of solar PV power (%) for (a) winter, (b) spring, (c) summer and (d) autumn. In each case, the future 30-year period is compared with the past period, 1981–2010. The numbers included on each plot are the minimum and maximum projected changes, displayed at their locations.

6.8% (SSP585, 2071–2100), for summer (Table 3.25, fourth panel) range from 2.2% (SSP370, 2021–2050) to 8.8% (SSP585; 2071–2100) and for autumn (Table 3.25, fifth panel) range from 0.8% (SSP245, 2021–2050) to 5.2% (SSP585, 2071–2100). The projected decreases in annual and seasonal PV power have high certainty, as demonstrated by a scarcity of hatching in Figures 3.53 and 3.54 and a small spread

(and the same sign) between the mean and percentile statistics presented in Table 3.25.

The results are consistent with similar high-resolution RCM studies for Ireland (Nolan and Flanagan, 2020) and with those of Jerez *et al*. (2015), who analysed the effects of climate change on PV in Europe using an ensemble of EURO-CORDEX datasets.
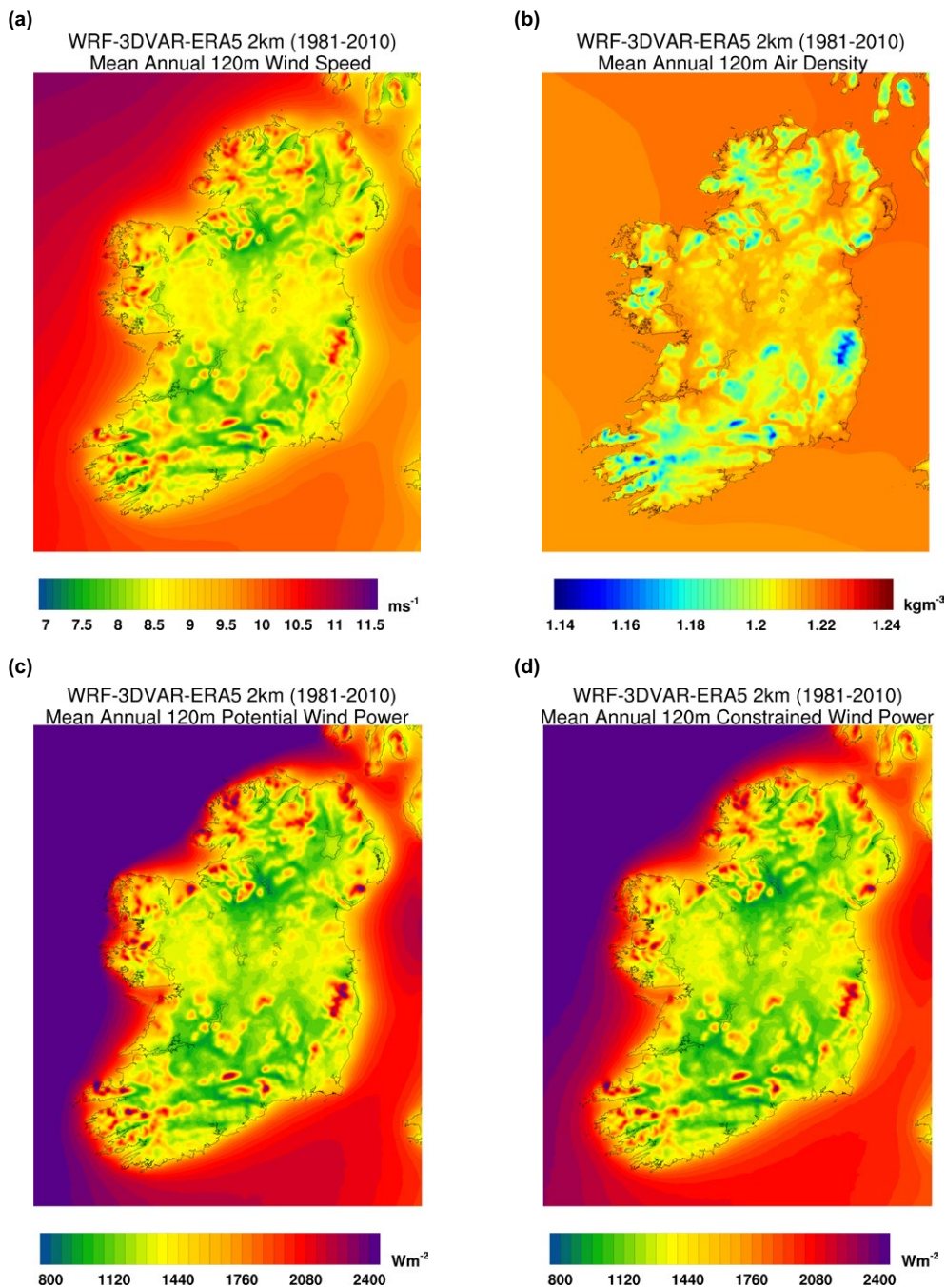
Figure 3.55. Annual mean 120 m (a) wind speed, (b) air density, (c) potential wind power and (d) constrained wind power as resolved by a WRF-3DVAR–ERA5 simulation (1981–2010). For details on this reanalysis dataset see, for example, McGrath and Nolan (2024).

3.21 Wind Power and Air Density at Turbine Height

In this section, the effects of climate change on wind power at turbine height (120 m) are analysed. A wind turbine obtains its power input by converting the force of the wind into a torque (turning force) acting on the rotor blades. The amount of energy that the wind transfers to the rotor depends on the density of the air, the rotor area and the wind speed. The mean power density P in the wind (W m^{-2}), which is equal to the average kinetic energy flux per unit area to

the flow (Troen and Petersen, 1989), is given by the formula:

$$P = \frac{1}{2N} \sum_{i=1}^{N} \rho_i v_i^3 \qquad (3.10)$$

where ρ is the density of the air (kg m^{-3}), v is the wind speed (m s^{-1}) and N is the number of data values. For the current study, the ρ and v variables have 3 hour temporal resolution and N is the number of 3 hour data values over the 30-year time period of interest ($N \approx 87,660$).
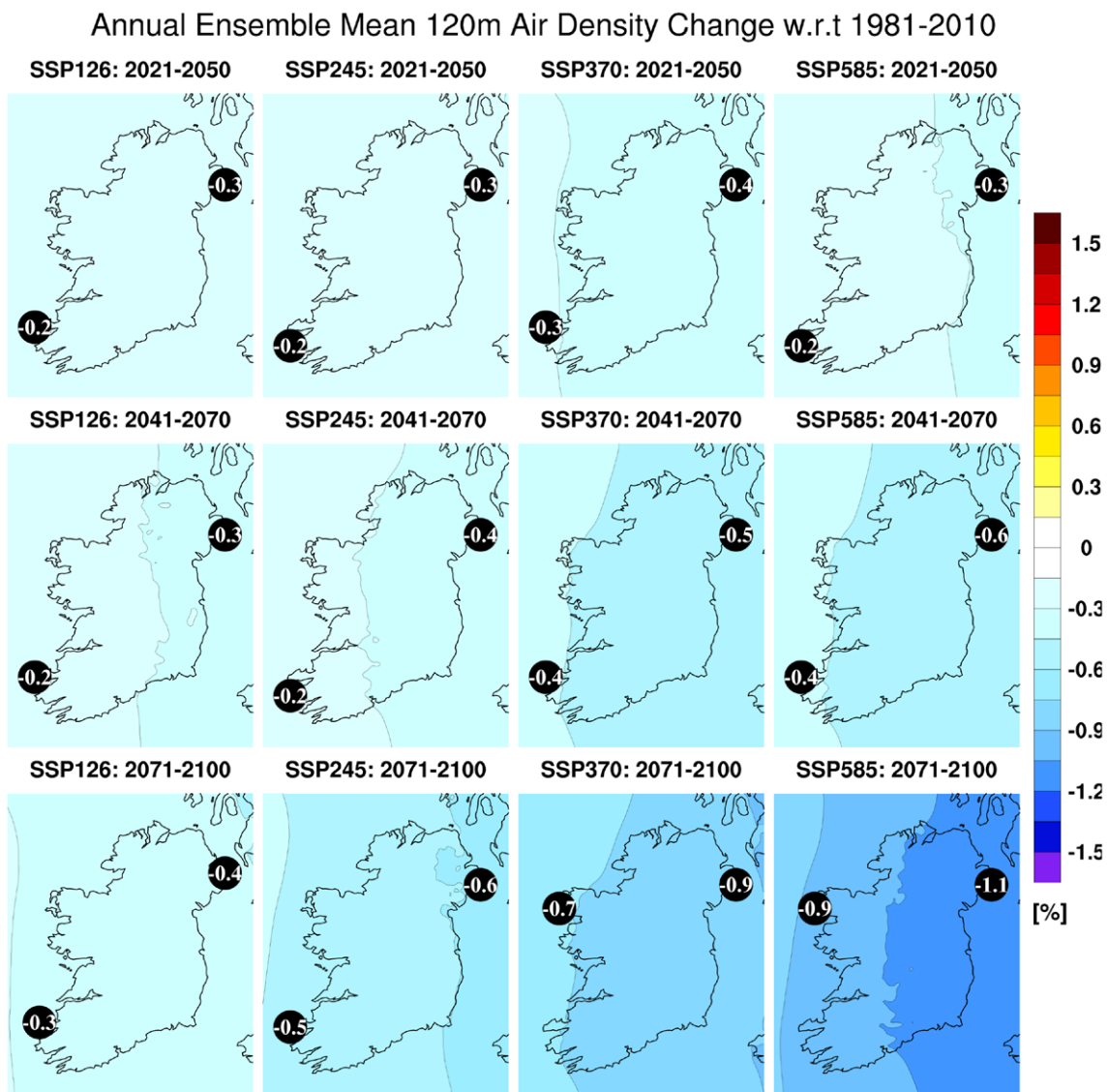
Figure 3.56. Annual RCM–CMIP6 turbine height (120 m) air density (%). All RCM ensemble members were run with 4 km grid spacing. In each case, the future 30-year period is compared with the past period, 1981–2010. The numbers included on each plot are the minimum and maximum projected changes over Ireland, displayed at their locations.

Wind turbines typically work within a certain range of wind speeds: the *cut-in* speed at which the turbine starts to generate power and the *cut-out* speed at which the turbine is turned off to prevent structural damage. In this section, we consider *cut-in* and *cut-out* speeds of $3\,m\,s^{-1}$ and $25\,m\,s^{-1}$, respectively, for a typical 5 MW offshore wind turbine (Ulazia *et al*., 2019). We analysed projected changes in *energetically useful*

wind power by calculating the "constrained wind power" for wind speeds within these limits as:

$$P_{constrained} = \frac{1}{2N} \sum_{i=1}^{N} \rho_i v_i^3 \qquad (3.11)$$

such that

$$\rho_i v_i^3 = 0 \text{ if } v_i < 3\,m\,s^{-1} \text{ or } v_i > 25\,m\,s^{-1} \qquad (3.12)$$
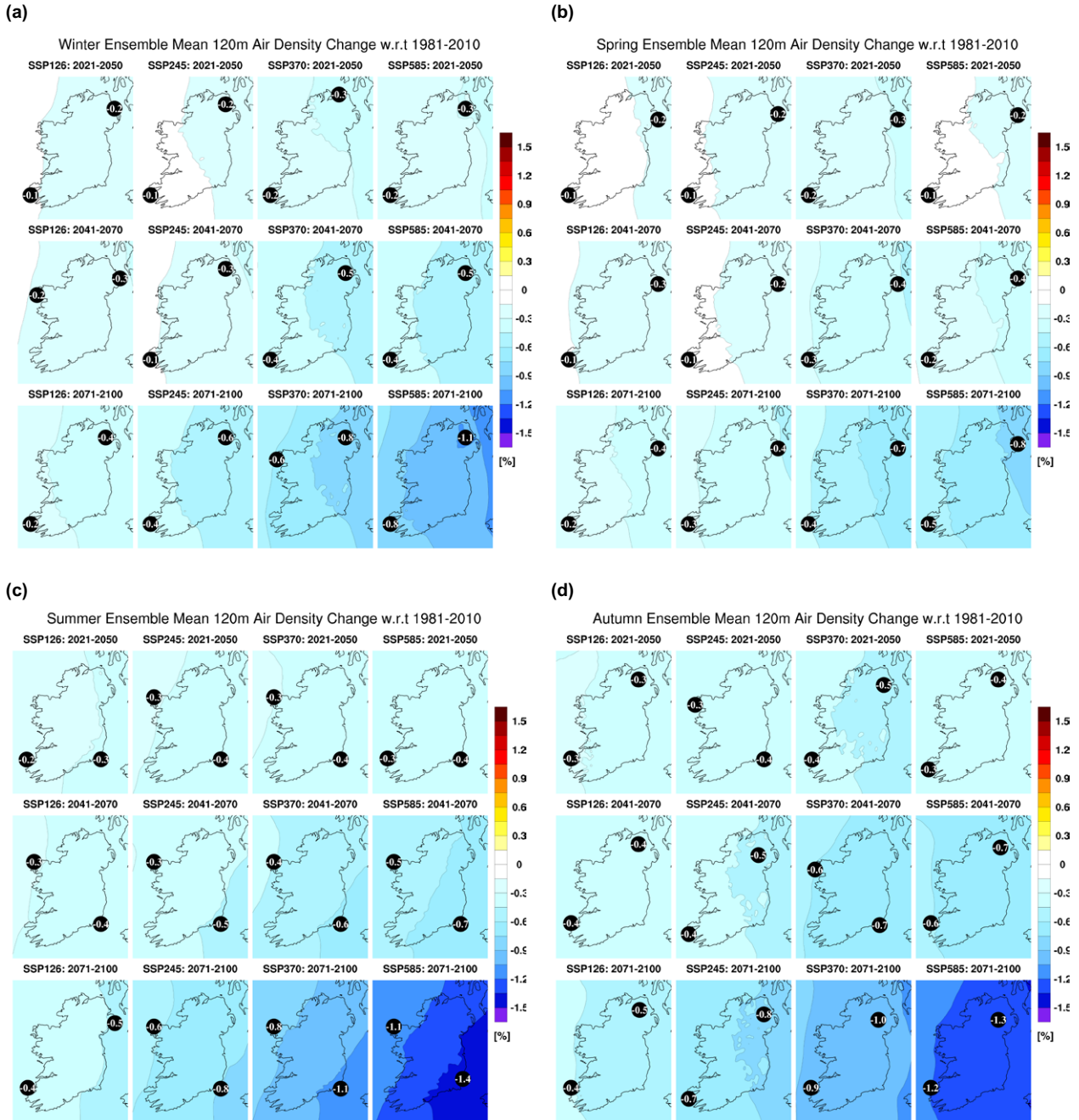
Figure 3.57. Seasonal RCM ensemble mean turbine height (120 m) air density (%) for (a) winter, (b) spring, (c) summer and (d) autumn. In each case, the future 30-year period is compared with the past period, 1981–2010. The numbers included on each plot are the minimum and maximum projected changes over Ireland, displayed at their locations.

For reference, relevant mean annual "observed" wind statistics at 120 m turbine height, as resolved by a high-resolution (2 km) downscaled reanalysis climate simulation (WRF-3DVAR–ERA5) 1981–2010, are presented in Figure 3.55: (a) wind speed (m s⁻¹), (b) air density (kg m⁻³), (c) potential (i.e. not constrained) wind power (W m⁻²) and (d) constrained wind power (W m⁻²).

The potential wind power provides an upper bound on the energy content of the wind available if wind turbines become more efficient (i.e. the range within the *cut-in* and *cut-out* limits is increased).

The annual and seasonal projected changes in 120 m air density (%) are presented in Figures 3.56 and 3.57,

Table 3.26. Annual and seasonal projections of 120 m air density (%). This table corresponds to the projections in Figures 3.56 and 3.57, and shows the 33rd percentile, 50th percentile, mean and 66th percentile averaged over the island of Ireland

Annual 120 m air density (%)

Time period	SSP126				SSP245				SSP370				SSP585			
	P33	P50	Mean	P66	P33	P50	Mean	P66	P33	P50	Mean	P66	P33	P50	Mean	P66
2021–2050	–0.1	–0.1	–0.2	–0.1	–0.2	–0.1	–0.3	–0.1	–0.3	–0.3	–0.3	–0.1	–0.3	–0.2	–0.3	–0.1
2041–2070	–0.2	–0.2	–0.3	–0.1	–0.2	–0.2	–0.3	–0.1	–0.5	–0.4	–0.5	–0.3	–0.5	–0.4	–0.5	–0.2
2071–2100	–0.5	–0.4	–0.4	–0.1	–0.7	–0.6	–0.6	–0.2	–0.9	–0.8	–0.8	–0.6	–1.3	–1.1	–1.1	–0.7

Winter 120 m air density (%)

Time period	SSP126				SSP245				SSP370				SSP585			
	P33	P50	Mean	P66	P33	P50	Mean	P66	P33	P50	Mean	P66	P33	P50	Mean	P66
2021–2050	–0.1	–0.1	–0.2	0.0	–0.2	0.0	–0.2	0.0	–0.2	–0.2	–0.3	–0.2	–0.3	–0.3	–0.3	–0.1
2041–2070	–0.2	–0.1	–0.2	–0.1	–0.2	–0.1	–0.2	0.0	–0.4	–0.3	–0.5	–0.3	–0.4	–0.4	–0.5	–0.3
2071–2100	–0.3	–0.3	–0.3	–0.1	–0.6	–0.6	–0.5	–0.1	–0.7	–0.7	–0.7	–0.5	–0.9	–0.9	–1.0	–0.7

Spring 120 m air density (%)

| Time period	SSP126				SSP245				SSP370				SSP585			
	P33	P50	Mean	P66	P33	P50	Mean	P66	P33	P50	Mean	P66	P33	P50	Mean	P66
2021–2050	–0.1	–0.1	–0.1	0.0	–0.2	–0.1	–0.2	–0.1	–0.3	–0.2	–0.3	–0.1	–0.1	0.0	–0.1	0.0
2041–2070	–0.2	–0.1	–0.2	–0.1	–0.1	0.0	–0.2	0.0	–0.3	–0.3	–0.4	–0.2	–0.2	–0.2	–0.3	–0.1
2071–2100	–0.3	–0.3	–0.3	–0.1	–0.5	–0.4	–0.4	–0.1	–0.6	–0.5	–0.6	–0.4	–0.8	–0.7	–0.7	–0.5

Summer 120 m air density (%)

Time period	SSP126				SSP245				SSP370				SSP585			
	P33	P50	Mean	P66	P33	P50	Mean	P66	P33	P50	Mean	P66	P33	P50	Mean	P66
2021–2050	–0.3	–0.2	–0.3	–0.2	–0.4	–0.3	–0.3	–0.2	–0.5	–0.4	–0.4	–0.1	–0.5	–0.4	–0.4	–0.1
2041–2070	–0.3	–0.2	–0.3	–0.1	–0.4	–0.3	–0.4	–0.1	–0.7	–0.5	–0.5	–0.3	–0.7	–0.6	–0.6	–0.3
2071–2100	–0.6	–0.5	–0.4	–0.1	–1.0	–0.8	–0.7	–0.3	–1.3	–1.0	–1.0	–0.6	–1.7	–1.4	–1.3	–0.8

Autumn 120 m air density (%)

Time period	SSP126				SSP245				SSP370				SSP585			
	P33	P50	Mean	P66	P33	P50	Mean	P66	P33	P50	Mean	P66	P33	P50	Mean	P66
2021–2050	–0.2	–0.2	–0.3	–0.2	–0.2	–0.2	–0.3	–0.1	–0.4	–0.4	–0.5	–0.3	–0.3	–0.3	–0.4	–0.2
2041–2070	–0.3	–0.3	–0.4	–0.3	–0.3	–0.3	–0.4	–0.2	–0.7	–0.6	–0.6	–0.4	–0.6	–0.5	–0.7	–0.3
2071–2100	–0.5	–0.4	–0.5	–0.2	–0.9	–0.7	–0.7	–0.4	–1.2	–1.0	–1.0	–0.6	–1.6	–1.4	–1.3	–0.9

respectively. The corresponding percentile and mean projection statistics, averaged over the country, are presented in Table 3.26. The projections show a robust small decrease (≤ 1.1%) in 120 m air density over the full year and in all seasons. The projected decreases are enhanced for the later time periods and higher SSPs. The projected decreases in the annual and seasonal air density have low uncertainty, as demonstrated by an absence of hatching in Figures 3.56 and 3.57, and a small spread (and the same sign) between the mean and percentile statistics presented in Table 3.26.

Figure 3.58, projections of the mean annual *constrained wind power* at 120 m, shows decreases,

which are enhanced for the higher SSPs and later time periods. The annual constrained wind power (over Ireland) is projected to decrease by 3.6–5.8% for SSP126 (2021–2050) and by 6.9–10.8% for SSP585 (2071–2100). Averaged over the whole country (Table 3.27, first panel), the mean projected decrease in annual constrained wind power ranges from 4.1% (2021–2050 under SSP245) to 8.6% (2071–2100 under SSP585).

Except for autumn (which shows uncertainty in the projections for earlier time periods and lower SSPs), the 120 m constrained wind power is projected to decrease for all seasons (Figure 3.59), with decreases enhanced for the higher SSPs and later time periods.
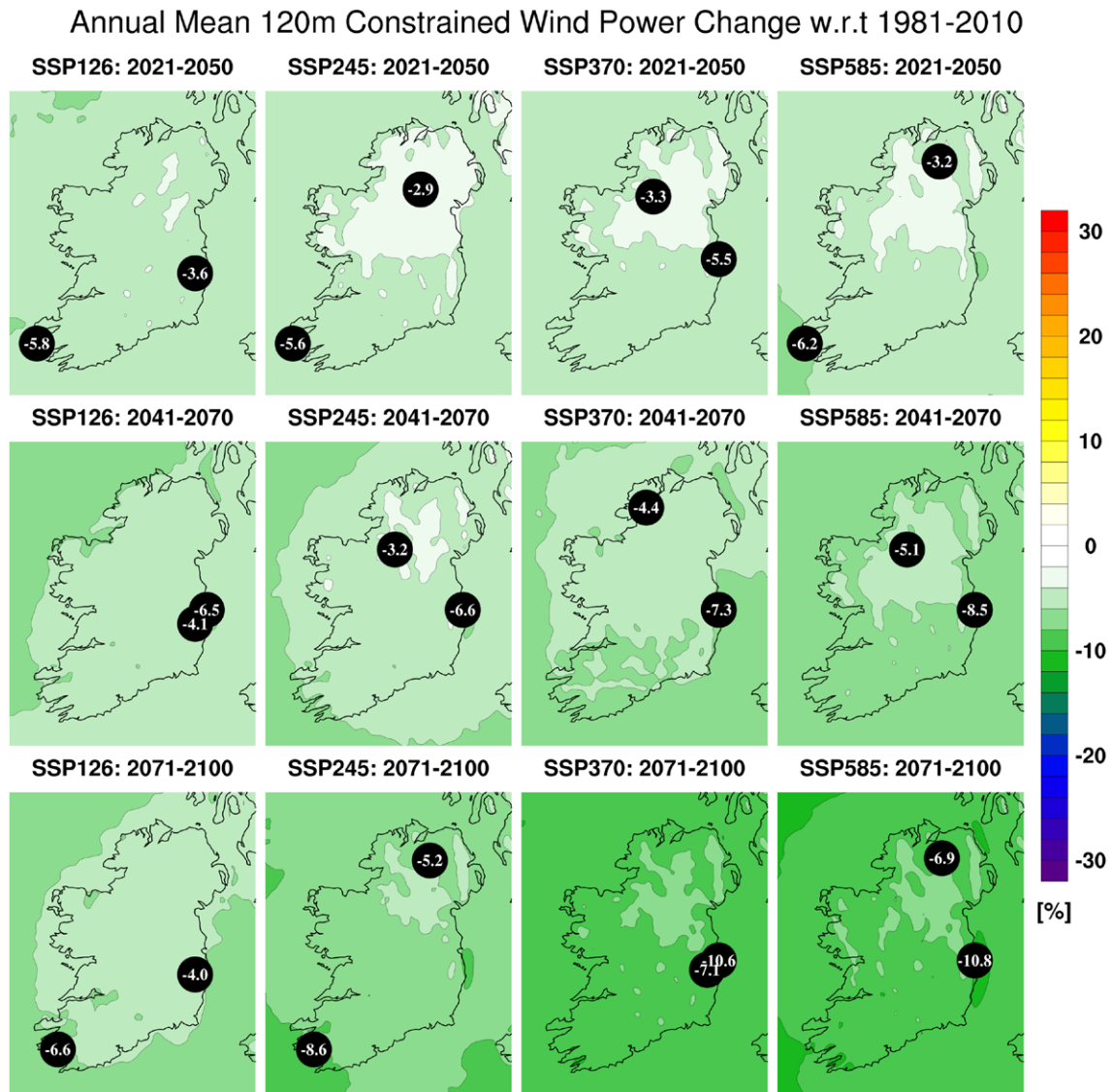

Figure 3.58. Annual projected change (%) in turbine height (120 m) constrained wind power. All RCM ensemble members were run with 4 km grid spacing. In each case, the future 30-year period is compared with the past period, 1981–2010. The numbers included on each plot are the minimum and maximum projected changes over Ireland, displayed at their locations.

Table 3.27. Annual and seasonal projections of 120 m constrained wind power (%). This table corresponds to projections in Figures 3.58 and 3.59, and shows the 33rd percentile, 50th percentile, mean and 66th percentile averaged over the island of Ireland

Annual 120 m constrained wind power (%)

Time period	SSP126				SSP245				SSP370				SSP585			
	P33	P50	Mean	P66	P33	P50	Mean	P66	P33	P50	Mean	P66	P33	P50	Mean	P66
2021–2050	−5.6	−4.2	−4.6	−2.7	−5.3	−4.7	−4.1	−2.9	−5.6	−4.8	−4.3	−2.6	−5.4	−4.7	−4.4	−3.7
2041–2070	−5.9	−5.4	−5.2	−3.8	−5.7	−5.0	−4.7	−3.9	−7.0	−5.6	−5.5	−4.3	−7.6	−6.0	−6.2	−4.7
2071–2100	−6.3	−5.7	−5.3	−4.1	−8.7	−6.9	−6.7	−4.5	−9.7	−9.0	−8.5	−8.0	−10	−9.0	−8.6	−7.0

Winter 120 m constrained wind power (%)

Time period	SSP126				SSP245				SSP370				SSP585			
	P33	P50	Mean	P66	P33	P50	Mean	P66	P33	P50	Mean	P66	P33	P50	Mean	P66
2021–2050	−6.6	−5.7	−5.4	−3.9	−4.8	−3.9	−3.2	−2.3	−5.3	−3.7	−3.4	−1.3	−5.8	−5.2	−4.9	−3.5
2041–2070	−6.7	−6.0	−5.5	−4.9	−5.9	−4.7	−3.7	−1.9	−6.4	−4.3	−3.9	−1.9	−9.1	−6.3	−5.7	−3.1
2071–2100	−6.9	−6.2	−5.4	−4.8	−7.2	−5.4	−5.0	−2.3	−8.4	−7.7	−6.0	−5.2	−6.5	−5.1	−5.0	−2.6

Spring 120 m constrained wind power (%)

Time period	SSP126				SSP245				SSP370				SSP585			
	P33	P50	Mean	P66	P33	P50	Mean	P66	P33	P50	Mean	P66	P33	P50	Mean	P66
2021–2050	−5.5	−4.9	−3.3	−3.1	−5.1	−4.5	−4.5	−3.5	−5.6	−4.8	−4.2	−2.8	−5.9	−4.8	−3.9	−2.8
2041–2070	−7.9	−6.3	−5.5	−2.4	−6.2	−5.3	−5.4	−4.1	−5.3	−4.5	−4.2	−2.9	−8.1	−6.6	−5.5	−3.4
2071–2100	−8.4	−7.8	−6.6	−5.3	−10	−8.7	−7.9	−6.2	−9.4	−8.6	−7.9	−6.7	−8.6	−7.3	−8.2	−5.7

Summer 120 m constrained wind power (%)

Time period	SSP126				SSP245				SSP370				SSP585			
	P33	P50	Mean	P66	P33	P50	Mean	P66	P33	P50	Mean	P66	P33	P50	Mean	P66
2021–2050	−8.8	−8.2	−7.6	−6.5	−9.7	−9.1	−8.6	−7.5	−11	−10	−9.7	−8.2	−8.8	−7.8	−7.3	−5.8
2041–2070	−8.0	−7.6	−7.1	−6.6	−13	−12	−11.2	−8.8	−14	−13	−12.9	−11	−15	−14	−13.6	−12
2071–2100	−11	−9.8	−8.4	−7.1	−15	−14	−14	−13	−20	−20	−20	−18	−27	−25	−23.3	−22

Autumn 120 m constrained wind power (%)

Time period	SSP126				SSP245				SSP370				SSP585			
	P33	P50	Mean	P66	P33	P50	Mean	P66	P33	P50	Mean	P66	P33	P50	Mean	P66
2021–2050	−3.5	−1.8	−2.8	0.4	−4.7	−2.8	−2.6	−1.1	−4.8	−2.9	−2.8	−1.1	−6.1	−4.7	−2.5	1.1
2041–2070	−3.2	−1.8	−3.4	−0.1	−2.9	−1.7	−2.2	−0.2	−6.6	−5.9	−5.3	−4.4	−5.2	−3.2	−3.9	−1.8
2071–2100	−4.1	−1.9	−2.4	0.2	−7.0	−5.4	−4.2	−2.5	−8.2	−7.3	−6.9	−5.4	−8.6	−7.8	−6.6	−4.4

The largest decreases are noted for the summer months (Figure 3.59c). Averaged over the whole country, robust projected decreases in constrained wind power for winter (Table 3.27, second panel) range from 3.2% (SSP245, 2021–2050) to 6% (SSP370, 2071–2100), for spring (Table 3.27, third panel) range from 3.3% (SSP126, 2021–2050) to 8.2% (SSP585, 2071–2100), for summer (Table 3.27, fourth panel)

range from 7.1% (SSP126, 2041–2070) to 23.3% (SSP585, 2071–2100) and for autumn (Table 3.27, fifth panel) range from 2.2% (SSP245, 2041–2070) to 6.9% (SSP370, 2071–2100).

Except for autumn (for earlier time periods and lower SSPs), the projected decreases in annual and seasonal 120 m constrained wind power have high
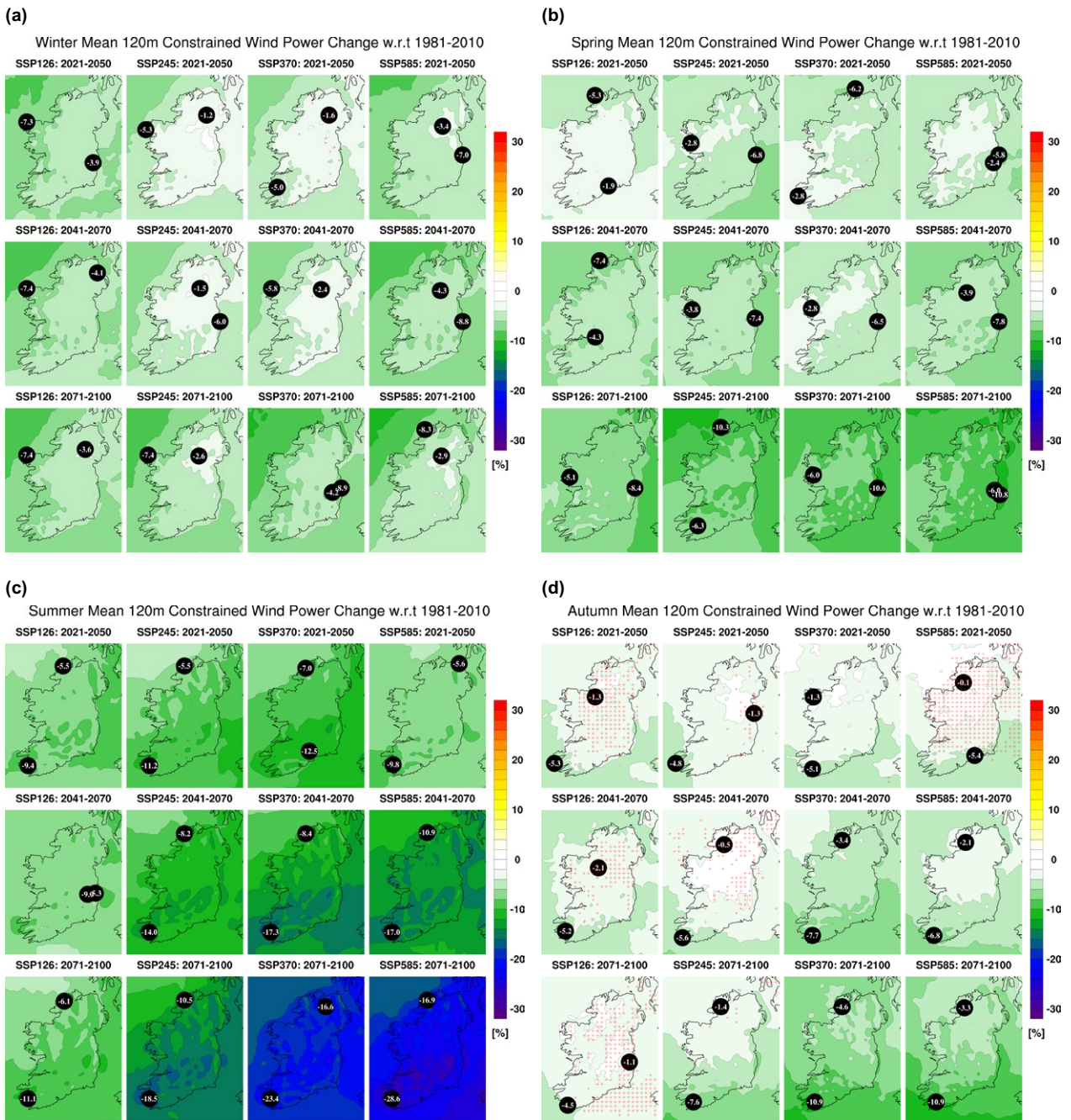
Figure 3.59. Seasonal projected change (%) in turbine height (120 m) constrained wind power for (a) winter, (b) spring, (c) summer and (d) autumn. In each case, the future 30-year period is compared with the past period, 1981–2010. The numbers included on each plot are the minimum and maximum projected changes over Ireland, displayed at their locations.

certainty, as demonstrated by a scarcity of hatching in Figures 3.58 and 3.59 and a small spread (and the same sign) between the mean and percentile statistics presented in Table 3.27.

The *potential wind power*, presented in Figure 3.60 (annual), Figure 3.61 (seasonal) and Table 3.28,

is also projected to decrease annually and for all seasons. It is noted that that projections of decreases in *constrained wind power* are enhanced compared with the corresponding *potential wind power* projected decreases (annual, Figure 3.58 vs Figure 3.60; seasonal, Figure 3.59 vs Figure 3.61 and Table 3.27 vs
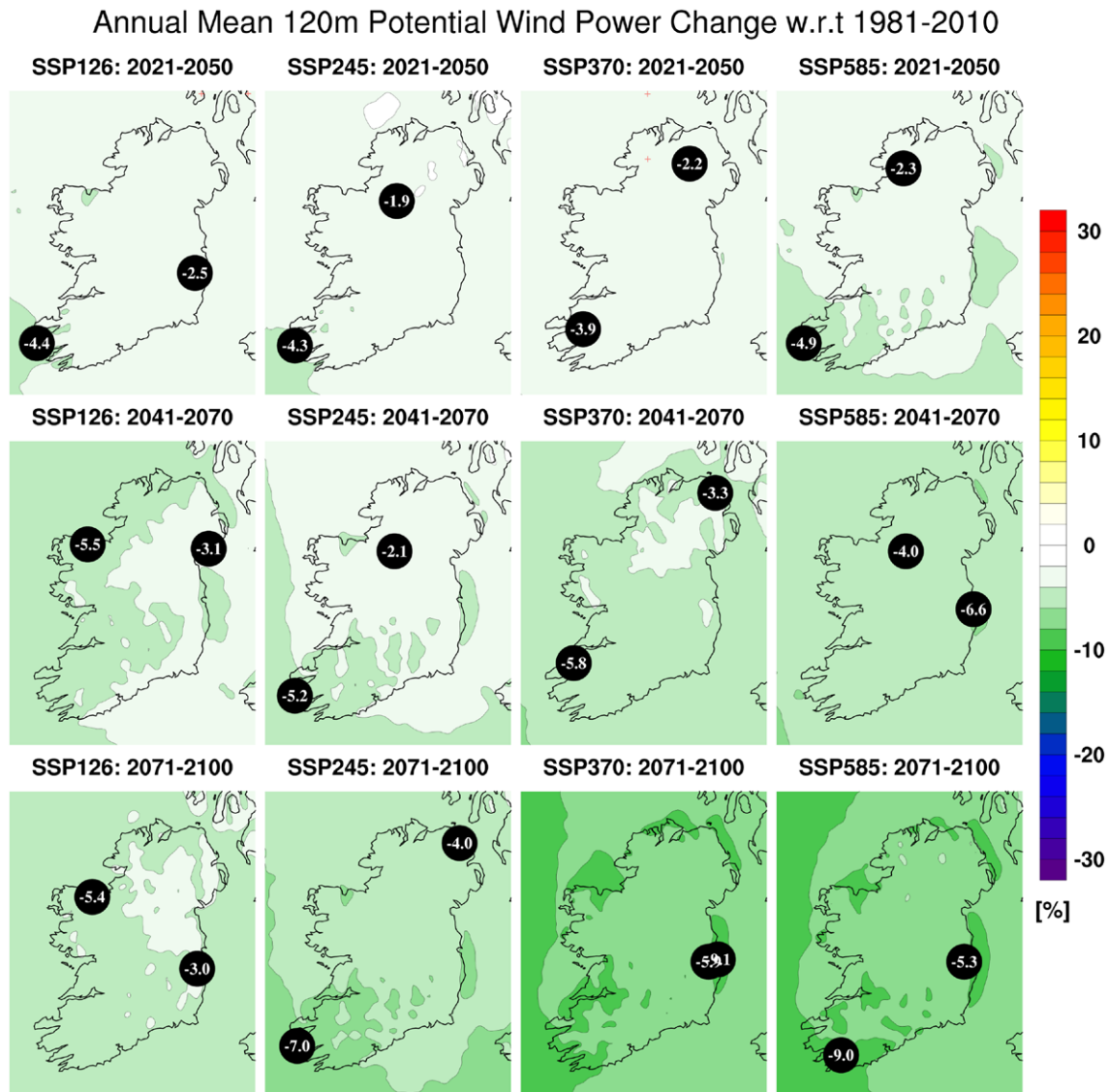
Figure 3.60. Annual projected change (%) in turbine height (120 m) potential wind power (%). All RCM ensemble members were run with 4 km grid spacing. In each case, the future 30-year period is compared with the past period, 1981–2010. The numbers included on each plot are the minimum and maximum projected changes over Ireland, displayed at their locations.

Table 3.28), indicating that if wind turbines become more efficient (i.e. the range within the cut-in and cut-out limits is increased), the impact of climate change on wind power will be less pronounced.

A preliminary analysis has shown that the main driver of the projected decreases in constrained wind power is projected decreases in wind speed, with decreases in air density having less of an impact. Future work will quantify the individual components through a sensitivity analysis. The projected changes in wind power are in line with previous RCM studies

for Ireland, which showed projected decreases in wind power for all seasons (Nolan, 2015; Nolan and Flanagan, 2020), all seasons except winter (e.g. Doddy Clarke *et al*., 2022), and during summer and over the full year (Nolan *et al*., 2012, 2014).

3.22 Heating and Cooling Degree Days

A degree day, an estimate of accumulated heat, is defined as the deviation (°C) from a base temperature value (Fraisse *et al*., 2010; Kalogirou, 2013; Project Team ECA&D, 2013; Kendon *et al*., 2015). Heating
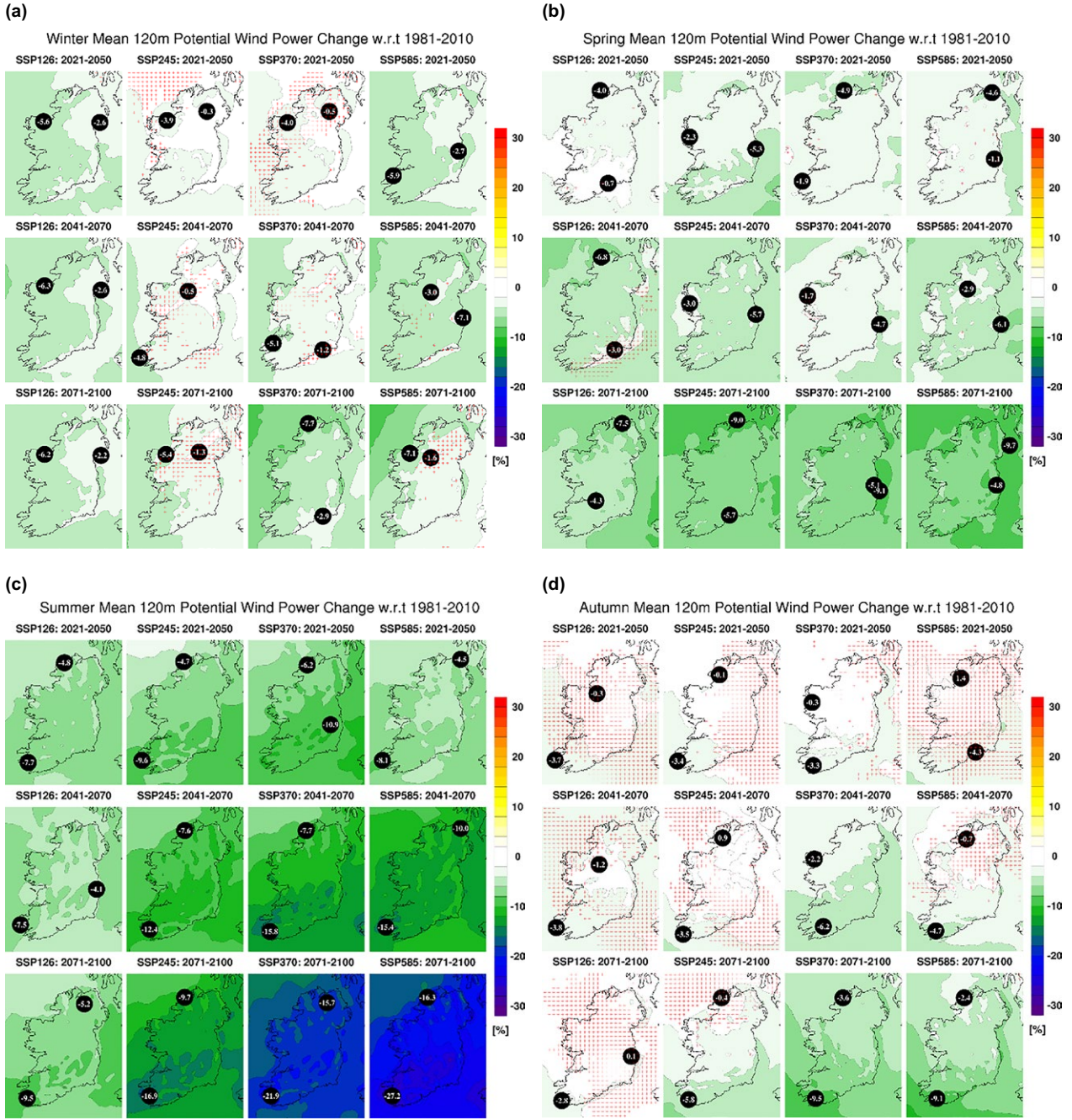
Figure 3.61. Seasonal RCM ensemble mean turbine height (120 m) potential wind power (%) for (a) winter, (b) spring, (c) summer and (d) autumn. In each case, the future 30-year period is compared with the past period, 1981–2010. The numbers included on each plot are the minimum and maximum projected changes over Ireland, displayed at their locations.

degree days (HDDs) are used to estimate the amount of energy required for residential or commercial space heating during the cold season. Conversely, cooling degree days (CDDs) are used to estimate the amount of air conditioning usage during the warm season. The HDD value was computed using a base temperature of 15.5°C (i.e. a temperature below which heating is required) and the daily mean temperature (T_M), as

described by Spinoni *et al*. (2015) and Project Team ECA&D (2013):

$$HDD_{daily} = max\{(15.5°C - T_M), 0\} \tag{3.13}$$

$$HDD = \Sigma HDD_{daily} \tag{3.14}$$

The CDD value was computed using a base temperature of 22°C (i.e. a temperature above which

Table 3.28. Annual and seasonal projections of 120 m potential wind power (%). This table corresponds to the projections in Figures 3.60 and 3.61, and shows the 33rd percentile, 50th percentile, mean and 66th percentile averaged over the island of Ireland

Annual 120 m potential wind power (%)

Time period	SSP126				SSP245				SSP370				SSP585			
	P33	P50	Mean	P66	P33	P50	Mean	P66	P33	P50	Mean	P66	P33	P50	Mean	P66
2021–2050	−3.5	−2.6	−3.4	−1.5	−3.7	−3.1	−2.9	−2.2	−5.5	−4.8	−3.1	−1.8	−4.4	−4.0	−3.4	−2.9
2041–2070	−5.2	−4.4	−4.1	−3.1	−4.7	−4.3	−3.5	−1.9	−6.3	−5.2	−4.5	−2.2	−5.5	−5.0	−5.0	−2.7
2071–2100	−4.8	−4.1	−4.2	−3.3	−6.6	−5.0	−5.4	−3.5	−8.6	−8.3	−7.5	−7.0	−8.9	−8.5	−7.4	−4.9

Winter 120 m potential wind power (%)

Time period	SSP126				SSP245				SSP370				SSP585			
	P33	P50	Mean	P66	P33	P50	Mean	P66	P33	P50	Mean	P66	P33	P50	Mean	P66
2021–2050	−4.7	−3.8	−4.2	−2.2	−3.4	−2.6	−2.0	−1.3	−5.0	−3.3	−2.2	0.3	−4.9	−4.0	−4.2	−2.7
2041–2070	−5.2	−4.5	−4.4	−3.5	−4.6	−3.8	−2.6	0.1	−5.2	−4.0	−3.0	−0.4	−7.3	−5.3	−4.5	−0.7
2071–2100	−5.5	−5.0	−4.3	−4.0	−4.9	−3.0	−3.4	0.1	−8.0	−7.2	−5.0	−4.4	−4.6	−4.0	−3.6	−0.6

Spring 120 m potential wind power (%)

Time period	SSP126				SSP245				SSP370				SSP585			
	P33	P50	Mean	P66	P33	P50	Mean	P66	P33	P50	Mean	P66	P33	P50	Mean	P66
2021–2050	−5.1	−3.8	−2.2	−1.5	−4.6	−3.8	−3.6	−2.1	−4.6	−3.7	−3.0	−1.7	−4.1	−3.2	−2.6	−1.1
2041–2070	−7.5	−6.1	−4.6	−0.9	−5.3	−4.7	−4.4	−3.4	−3.9	−3.2	−3.1	−1.7	−6.7	−6.0	−4.3	−1.9
2071–2100	−8.1	−6.6	−5.7	−4.2	−9.7	−8.8	−7.1	−4.5	−8.4	−7.5	−6.9	−5.9	−6.9	−5.9	−7.5	−4.8

Summer 120 m potential wind power (%)

Time period	SSP126				SSP245				SSP370				SSP585			
	P33	P50	Mean	P66	P33	P50	Mean	P66	P33	P50	Mean	P66	P33	P50	Mean	P66
2021–2050	−7.8	−7.1	−6.4	−5.6	−8.5	−7.8	−7.3	−6.4	−9.5	−8.7	−8.5	−7.3	−7.4	−6.5	−6.1	−4.6
2041–2070	−6.5	−5.9	−5.9	−5.0	−12	−10	−10.1	−7.9	−13	−11	−11.8	−10	−13	−12	−12.5	−11
2071–2100	−9.3	−8.0	−7.2	−5.7	−14	−13	−13.4	−11	−19	−18	−18.8	−17	−27	−25	−22.3	−20

Autumn 120 m potential wind power (%)

Time period	SSP126				SSP245				SSP370				SSP585			
	P33	P50	Mean	P66	P33	P50	Mean	P66	P33	P50	Mean	P66	P33	P50	Mean	P66
2021–2050	−1.7	−0.6	−1.6	2.1	−3.4	−2.3	−1.4	0.7	−3.7	−2.6	−1.6	−0.5	−5.4	−4.4	−1.4	3.0
2041–2070	−1.0	−0.1	−2.3	1.3	−1.1	0.0	−0.7	1.4	−5.2	−4.7	−4.2	−3.4	−3.3	−2.0	−2.4	−0.1
2071–2100	−2.3	−0.3	−1.3	1.3	−5.4	−4.1	−2.9	−1.5	−7.0	−6.3	−6.0	−4.4	−7.4	−6.5	−5.4	−3.8

air conditioning is required) and the daily mean temperature (T_M):

$$CDD_{daily} = max\{(T_M - 22°C), 0\} \qquad (3.15)$$

$$CDD = \Sigma CDD_{daily} \qquad (3.16)$$

The projections of HDDs (Figure 3.62) show that over the coming decades there will be a greatly reduced requirement for heating in Ireland. The annual heating requirement is projected to decrease by 7–11% for SSP126 (2021–2050) and by 29–38% for SSP585 (2071–2100). Averaged over the whole country (Table 3.29), the mean projected decrease in
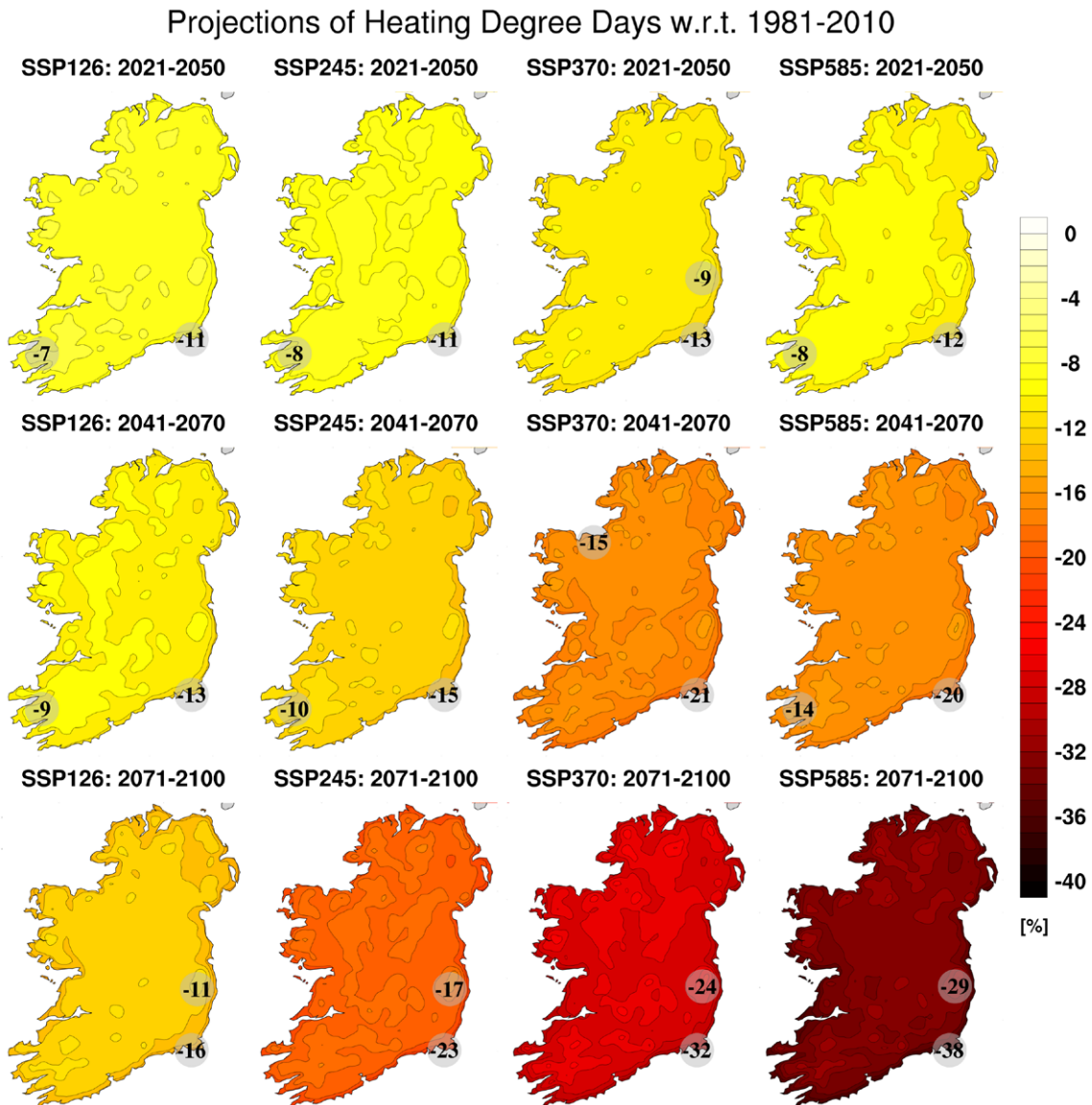
Projections of Heating Degree Days w.r.t. 1981-2010

Figure 3.62. Annual RCM–CMIP6 ensemble projections of HDDs (%). In each case, the future 30-year period is compared with the past period, 1981–2010.

Table 3.29. Annual projections of HDDs (%). This table corresponds to the projections in Figure 3.62 and shows the 33rd percentile, 50th percentile, mean and 66th percentile averaged over the island of Ireland

Time period	SSP126				SSP245				SSP370				SSP585			
	P33	P50	Mean	P66	P33	P50	Mean	P66	P33	P50	Mean	P66	P33	P50	Mean	P66
2021–2050	−7.4	−7.0	−8.4	−5.2	−7.7	−6.3	−9.1	−4.7	−11.1	−10.9	−10.7	−4.8	−10.7	−10.2	−10.0	−5.0
2041–2070	−7.9	−7.7	−10.2	−7.2	−9.2	−8.9	−12.4	−5.7	−16.9	−16.7	−17.0	−11.1	−18.0	−17.2	−16.6	−9.3
2071–2100	−17.2	−16.9	−12.8	−3.8	−25.2	−24.5	−19.3	−10.2	−30.3	−29.9	−27.3	−18.9	−38.9	−37.9	−32.9	−23.2

HDDs ranges from 8.4% (2021–2050 under SSP126) to 32.9% (2071–2100 under SSP585). CDDs are projected to slightly increase (not shown), particularly over the south-east and midlands, suggesting a very small increase in air conditioning requirements in the coming decades. However, the amounts are small compared with HDDs and therefore have a negligible effect on the projected changes in the total energy demand (TED = HDD + CDD). It is noted that the projections of TED (Table 3.30) are very similar to the projections of HDDs (Table 3.29), demonstrating the negligible effect of increases in CDDs on TED.

Table 3.30. Annual projections of TED (%). This table shows the 33rd percentile, 50th percentile, mean and 66th percentile averaged over the island of Ireland

Time period	SSP126				SSP245				SSP370				SSP585			
	P33	P50	Mean	P66	P33	P50	Mean	P66	P33	P50	Mean	P66	P33	P50	Mean	P66
2021–2050	–7.4	–7.0	–8.3	–5.2	–7.7	–6.2	–9.1	–4.7	–11.0	–10.8	–10.7	–4.7	–10.6	–10.2	–10.0	–5.0
2041–2070	–7.9	–7.7	–10.2	–7.2	–9.2	–8.9	–12.4	–5.7	–16.8	–16.5	–16.9	–11.1	–17.7	–17.2	–16.5	–9.2
2071–2100	–17.2	–16.8	–12.8	–3.8	–24.9	–24.5	–19.2	–10.2	–29.7	–29.4	–27.1	–18.8	–37.7	–37.2	–32.4	–23.1

The projected decreases in the annual and seasonal HDDs (and TED) have high certainty, as demonstrated by an absence of hatching in Figures 3.62 and a small spread (and the same sign) between the mean and percentile statistics presented in Tables 3.29 and 3.30.

The projected changes in heating and cooling energy demand are in line with previous RCM studies for Ireland. Nolan and Flanagan (2020) analysed an ensemble of downscaled CMIP5 simulations and found a greatly reduced requirement for heating by mid-century (2041–2060), with decreases of 12–17% and 15–21% for the RCP4.5 and RCP8.5 scenarios, respectively. Projections of CDDs showed a small (but negligible) increase by mid-century (Nolan and Flanagan, 2020). Semmler *et al*. (2010) found that mid-century (2021–2060) heating demand is projected to decrease by ~10% for the A1B and A2 emissions scenarios. The authors found a small projected increase in summer CDDs, which may enhance the currently weak demand for air conditioning towards the end of the century (Semmler *et al*., 2010). However, the "main influence of a warming climate will be reflected in a decrease in energy requirements for commercial and domestic heating in Ireland" (Semmler *et al*., 2010).

3.23   Driving Rain

The "driving rain" metric ($m^2 s^{-1} year^{-1}$) can be approximated from the following equation (Collins and Cummins, 1996; Walsh, 2010):

$$DR = W \times R \tag{3.17}$$

where W is the mean annual 10 m wind speed ($m s^{-1}$) and R is the mean annual rainfall ($m year^{-1}$).[18]

The driving rain metric is a useful parameter for agriculture, built environment and transport applications.

Figure 3.63, projections of the mean annual driving rain, shows small changes (~0%) or small projected decreases. However, the projections are small and exhibit high uncertainty, as demonstrated by an abundance of hatching in Figure 3.63 and disagreement in sign between the mean and percentile statistics presented in Table 3.31 (first panel).

Figure 3.64, the projected change in seasonal driving rain, shows increases for winter (later time periods and higher SSPs), a weak and uncertain decrease for spring, decreases for summer, which are enhanced for higher SSPs and later time periods, and a weak increase for autumn. Averaged over the country, robust projected increases for winter driving rain (Table 3.31, second panel) range from 1.7% (SSP585, 2041–2070) to 9% (SSP585, 2071–2100). Robust spring projected decreases (Table 3.31, third panel) range from 3% (SSP126, 2071–2100) to 6.2% (SSP245, 2071–2100). Robust summer projected decreases (Table 3.31, fourth panel) range from 1.2% (SSP126, 2021–2050) to 15.2% (SSP370, 2071–2100). The projections for autumn (Table 3.31, fifth panel) are more uncertain for the early- and mid-century time periods, with robust projected increases of ~3.8% for SSP370 and SSP585 in the period 2071–2100.

The higher certainty in the summer projections of driving rain is attributed to the robust projected decreases in both summer precipitation (Figure 3.19c) and wind speed (Figure 3.41c). Conversely, the uncertainty exhibed for winter and autumn is attributed to opposing signs in the projections of precipitation (increases; Figure 3.19a and d) and wind speed (decreases; Figure 3.41a and d).

---

18 Future work will implement the updated International Organization for Standardization (ISO) definition of driving rain used by Met Éireann (Mateus and Coonan, 2022).
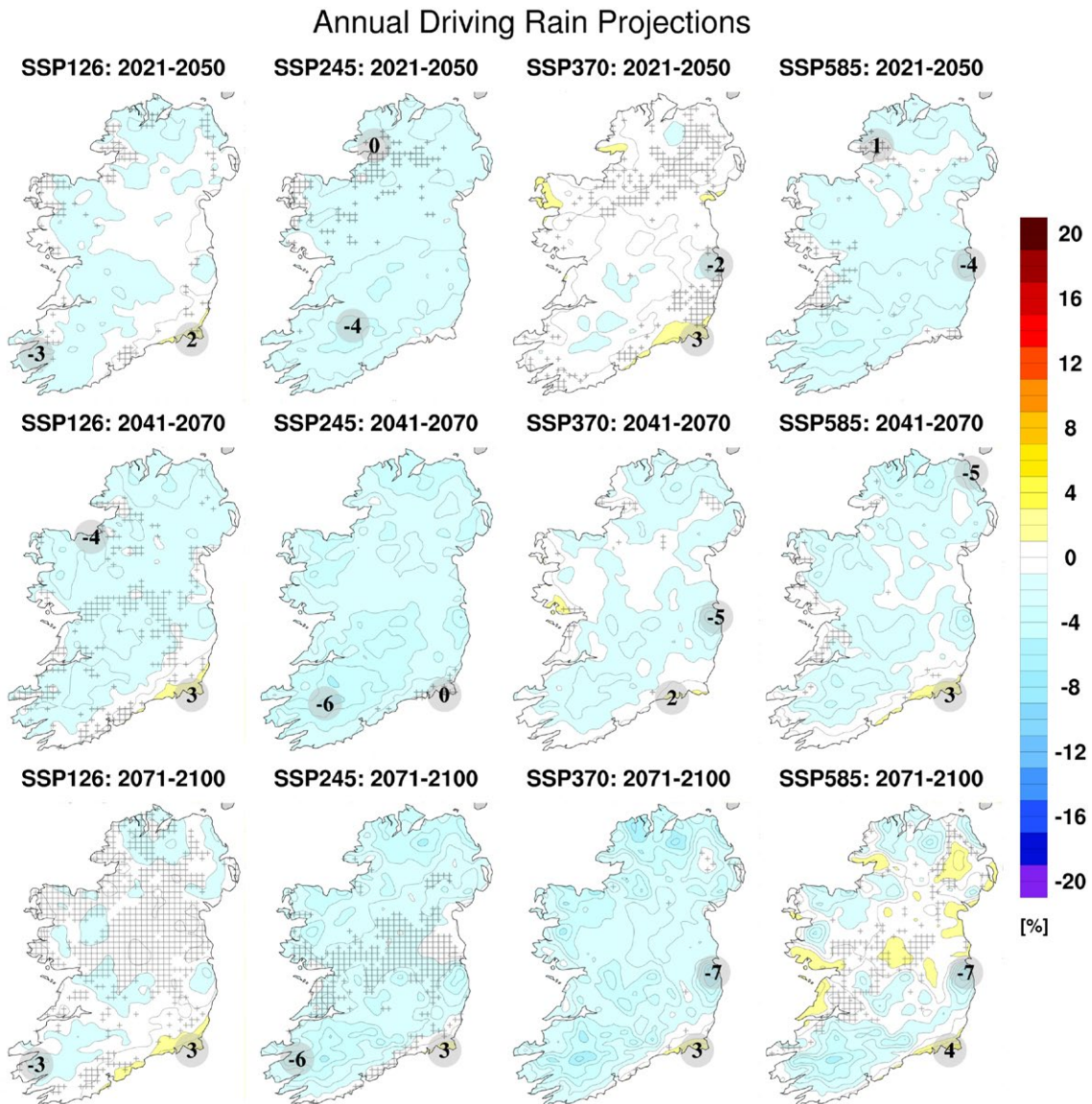
Figure 3.63. Annual RCM–CMIP6 ensemble projections of driving rain (%). All RCM ensemble members were run with 4 km grid spacing. In each case, the future 30-year period is compared with the past period, 1981–2010. The numbers included on each plot are the minimum and maximum projected changes, displayed at their locations.

The projected changes in driving rain are in line with previous RCM studies for Ireland. Nolan and Flanagan (2020) analysed an ensemble of downscaled CMIP5 simulations and found that by mid-century the frequency of driving rain events is projected to decrease for summer and over the full year. For winter months, under the RCP8.5 scenario, small increases are projected (Nolan and Flanagan, 2020).

3.24 Evapotranspiration

Figure 3.65, projections of the mean annual evapotranspiration, shows increases, which are

enhanced for the higher SSPs and later time periods. There exists a clear north-west to south-east gradient in the projections, with the largest increases in the south-east. Averaged over the whole country, robust projected increases in annual evapotranspiration (Table 3.32, first panel) range from 3.6% (2041–2070 under SSP370) to 8.1% (2071–2100 under SSP585).

The seasonal projections of evapotranspiration, presented in Figure 3.66, show that evapotranspiration is projected to increase (or small ~0% change) for all seasons, with increases enhanced for the higher

Table 3.31. Annual and seasonal projections of driving rain (%). This table corresponds to the projections in Figures 3.63 and 3.64, and shows the 33rd percentiles, 50th percentile, mean and 66th percentile averaged over the island of Ireland

Annual driving rain (%)

Time period	SSP126				SSP245				SSP370				SSP585			
	P33	P50	Mean	P66	P33	P50	Mean	P66	P33	P50	Mean	P66	P33	P50	Mean	P66
2021–2050	−2.8	−2.2	−0.9	−0.3	−3.5	−2.5	−1.8	−0.6	−1.9	−1.3	−0.1	0.3	−2.5	−1.7	−1.6	−0.4
2041–2070	−3.6	−2.8	−1.5	0.2	−4.3	−3.5	−2.9	−1.9	−2.4	−1.9	−1.1	−0.8	−2.7	−2.0	−1.3	−0.5
2071–2100	−2.9	−2.0	−0.6	1.1	−3.0	−1.6	−2.2	0.2	−4.0	−3.3	−2.6	−1.8	−2.0	−1.4	−0.6	0.2

Winter driving rain (%)

Time period	SSP126				SSP245				SSP370				SSP585			
	P33	P50	Mean	P66	P33	P50	Mean	P66	P33	P50	Mean	P66	P33	P50	Mean	P66
2021–2050	−3.2	−1.9	−1.8	0.5	−3.6	−1.8	0.4	4.3	−1.1	0.0	0.6	2.2	−2.3	−1.4	−1.3	0.4
2041–2070	−4.0	−2.9	−1.1	0.3	−2.6	−1.6	−1.2	0.4	0.7	2.0	2.5	4.7	0.5	1.5	1.7	3.5
2071–2100	−3.6	−2.5	0.5	3.6	−1.1	0.2	1.8	3.5	0.8	2.2	2.7	4.5	6.2	8.6	9.0	12

Spring driving rain (%)

Time period	SSP126				SSP245				SSP370				SSP585			
	P33	P50	Mean	P66	P33	P50	Mean	P66	P33	P50	Mean	P66	P33	P50	Mean	P66
2021–2050	−2.4	−0.6	0.0	2.0	−8.7	−4.3	−3.6	−0.3	−1.8	−0.5	1.8	3.1	−6.6	−5.6	−4.0	−3.4
2041–2070	−6.1	−4.1	−2.8	0.8	−7.2	−5.8	−5.5	−2.4	−2.7	−0.6	0.0	2.7	−5.2	−4.1	−2.3	−1.6
2071–2100	−4.6	−3.1	−3.0	−0.4	−8.9	−7.8	−6.2	−4.5	−8.9	−3.6	−4.0	1.1	−8.1	−4.9	−4.2	−0.6

Summer driving rain (%)

Time period	SSP126				SSP245				SSP370				SSP585			
	P33	P50	Mean	P66	P33	P50	Mean	P66	P33	P50	Mean	P66	P33	P50	Mean	P66
2021–2050	−6.0	−4.3	−1.2	−1.4	−10	−8.6	−6.6	−5.2	−14	−11	−5.7	−2.6	−8.9	−7.1	−1.0	1.0
2041–2070	−6.9	−4.8	−2.6	−0.3	−14	−12	−8.2	−7.3	−17	−14	−9.5	−5.6	−17	−16	−9.4	−8.0
2071–2100	−8.2	−6.4	−2.7	−2.4	−15	−13	−10.5	−8.7	−21	−19	−15.2	−15	−19	−17	−15.0	−14

Autumn driving rain (%)

Time period	SSP126				SSP245				SSP370				SSP585			
	P33	P50	Mean	P66	P33	P50	Mean	P66	P33	P50	Mean	P66	P33	P50	Mean	P66
2021–2050	−2.9	−0.5	0.6	4.1	−2.9	−1.1	1.7	3.5	2.1	3.9	3.2	7.2	−3.9	−2.3	1.3	4.2
2041–2070	−2.7	0.3	1.2	6.0	−1.0	0.8	3.0	4.7	−0.3	1.1	1.1	3.5	0.9	2.6	3.7	6.5
2071–2100	0.2	1.9	3.2	5.4	−3.7	1.2	4.2	11.3	−0.8	0.6	3.8	3.6	2.0	3.4	3.8	6.0

SSPs and later time periods. The largest increases are noted for the winter and autumn months. The smallest increases are noted for summer, in particular for 2021–2050 and 2041–2070. Averaged over the whole country, robust projected increases in evapotranspiration (Table 3.32) for winter (second panel) range from 4.1% (SSP370, 2021–2050) to 11.9% (SSP585, 2071–2100), for spring (third panel) range from 5.2% (SSP370, 2071–2100) to 6.7% (SSP585, 2071–2100), for summer (fourth panel) range from 4.7% (SSP370, 2071–2100) to 5.4% (SSP585, 2071–2100) and for autumn (fifth panel) range from 3.6% (SSP126, 2021–2050) to 14.5% (SSP585, 2071–2100).
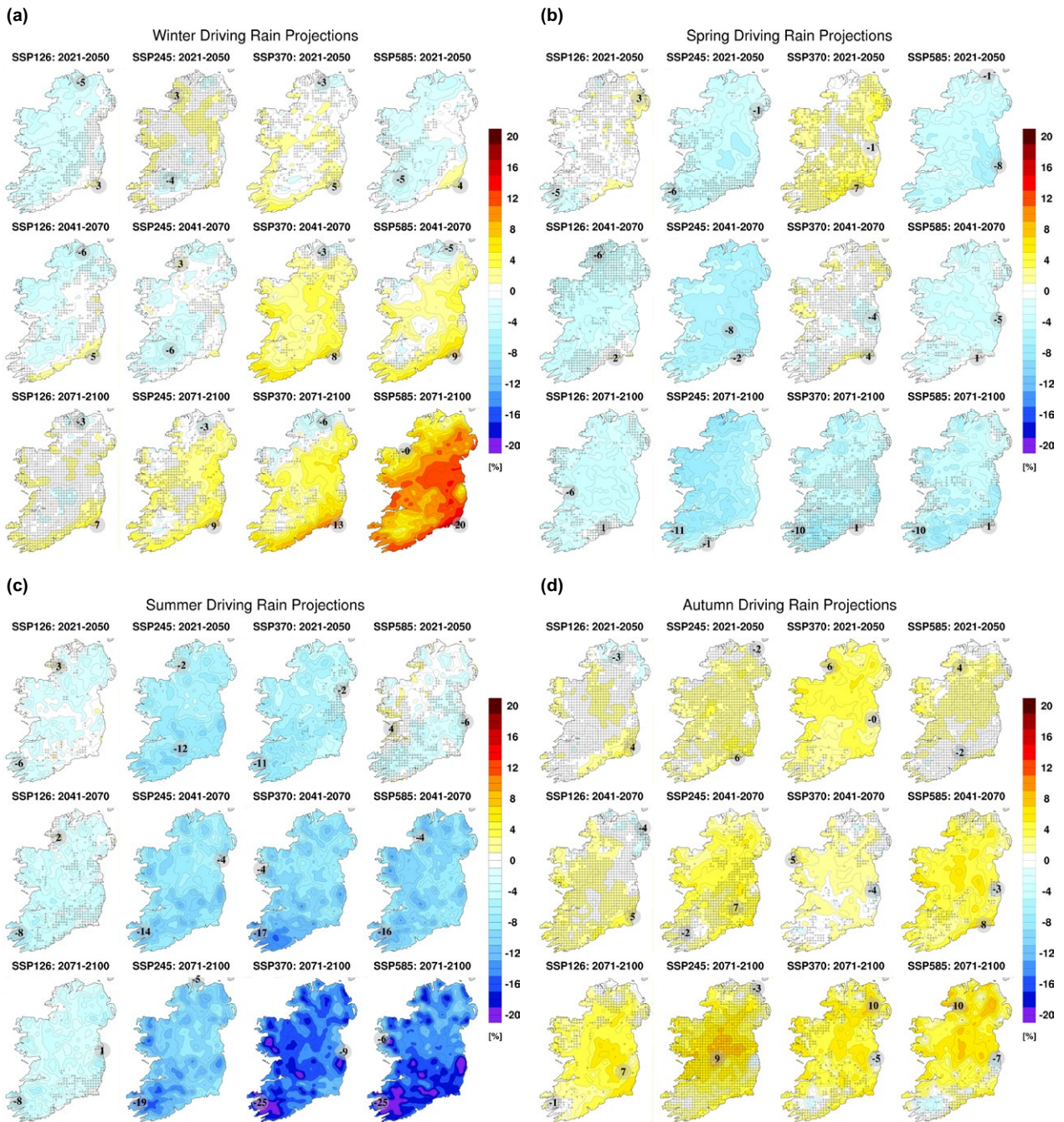
Figure 3.64. Seasonal RCM ensemble mean projections of driving rain (%) for (a) winter, (b) spring, (c) summer and (d) autumn. In each case, the future 30-year period is compared with the past period, 1981–2010. The numbers included on each plot are the minimum and maximum projected changes, displayed at their locations.

The projections of increases in annual and seasonal evapotranspiration have higher certainty for the higher SSPs and later time periods, as is evident from an absence of hatching (Figures 3.65 and 3.66) and agreement in sign between the statistics of Table 3.32. The projected increases in autumn evapotranspiration have high certainty for all SSPs and time periods.

The projected increase in evapotranspiration may offset flooding events arising from the expected increases in heavy rainfall events (see section 3.11) and intensity of wet days (see section 3.12). For reference, "observed" annual evapotranspiration (mm day^{-1}), derived from a high-resolution (1.5 km) downscaled ERA-Interim climate simulation, is

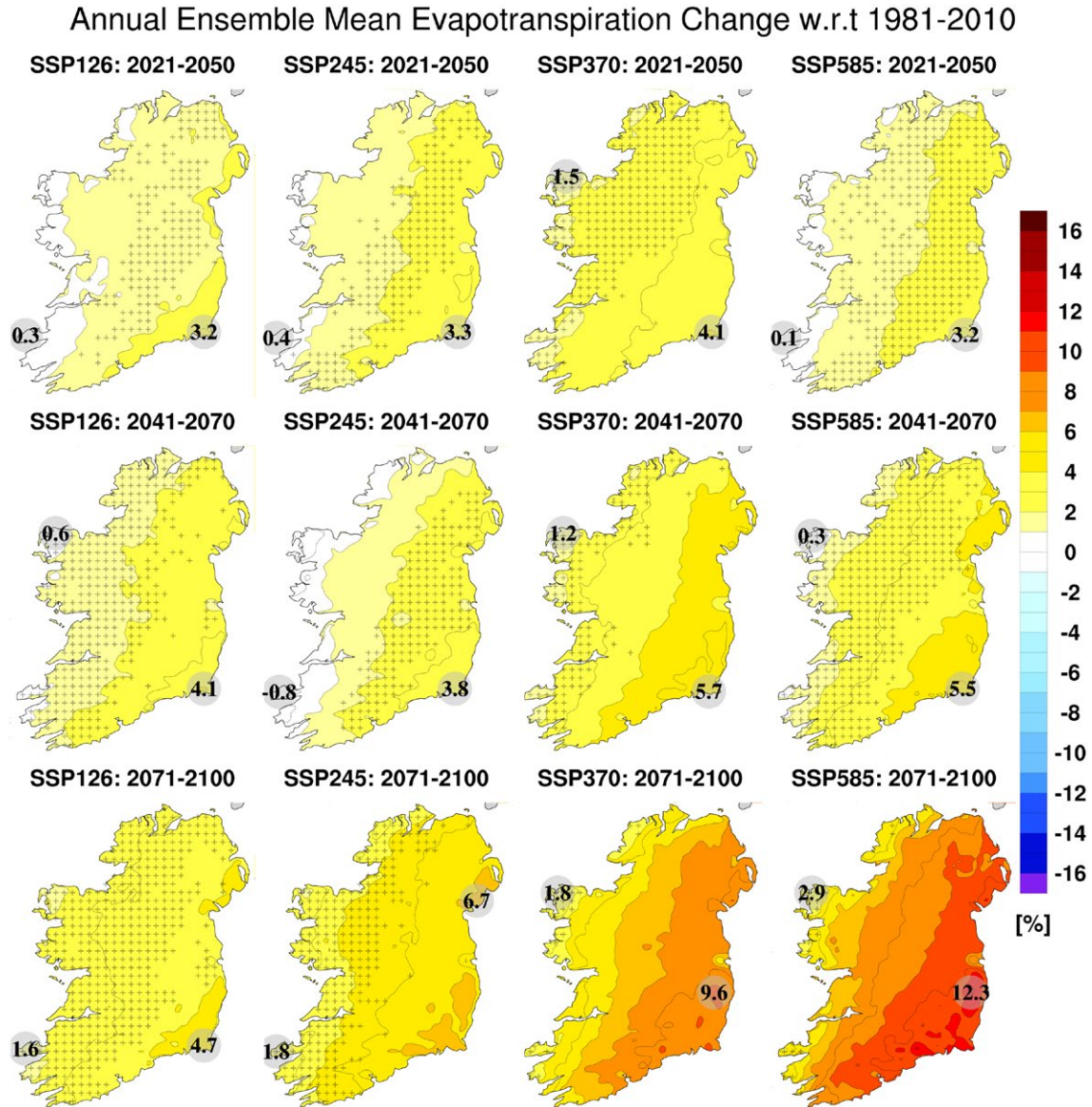## Annual Ensemble Mean Evapotranspiration Change w.r.t 1981-2010

Figure 3.65. Annual RCM–CMIP6 projections of evapotranspiration (%). All RCM ensemble members were run with 4 km grid spacing. In each case, the future 30-year period is compared with the past period, 1981–2010. The numbers included on each plot are the minimum and maximum projected changes, displayed at their locations.

presented in Figure 3.67. Refer to Werner *et al.* (2019) for validations and additional maps and information.[19]

Evapotranspiration was calculated using the output of RCMs following the Penman–Monteith FAO-56 method (Allen *et al.*, 1998) of Zotarelli *et al.* (2010). A mathematical description is provided below.

$$ET_{sz} = \frac{0.408\Delta(R_n - G) + \gamma \dfrac{C_n}{T_{mean} + 273} u_2(e_s - e_a)}{\Delta + \gamma(1 + C_d u_2)} \quad (3.18)$$

- ET_{sz} is the reference evaporation, mm day^{-1};
- R_n is the net surface radiation, MJ m^{-2} d^{-1} (see equation 3.19);
- G is the surface sensible heat flux, MJ m^{-2} d^{-1} (see equation 3.20);
- T_{mean} is the mean daily 2 m temperature, °C;
- u_2 is the mean daily 2 m wind speed, m s^{-1} (see equation 3.21);

---

19 In summary, Werner *et al.* (2019) compared modelled evapotranspiration with observational data at 22 stations throughout Ireland and found that the COSMO-CLM5 RCM resolved evapotranspiration to "within 10% of values calculated from station measurements for all stations analysed".

Table 3.32. Annual and seasonal projections of evapotranspiration (%). This table corresponds to the projections in Figures 3.65 and 3.66, and shows the 33rd percentile, 50th percentile, mean and 66th percentile averaged over Ireland

Annual evapotranspiration (%)

Time period	SSP126				SSP245				SSP370				SSP585			
	P33	P50	Mean	P66	P33	P50	Mean	P66	P33	P50	Mean	P66	P33	P50	Mean	P66
2021–2050	–1.0	–0.3	1.5	0.6	–1.1	–0.5	1.9	0.7	–0.4	0.5	2.7	2.9	–2.0	–1.0	1.8	0.9
2041–2070	–0.9	–0.4	2.1	2.5	–1.7	–1.4	1.8	0.1	0.4	0.8	3.6	4.1	–1.1	–0.3	3.1	3.0
2071–2100	–1.2	–0.5	3.2	4.7	–0.6	1.3	4.7	7.3	2.3	2.9	6.4	8.5	3.5	4.3	8.1	11.5

Winter evapotranspiration (%)

Time period	SSP126				SSP245				SSP370				SSP585			
	P33	P50	Mean	P66	P33	P50	Mean	P66	P33	P50	Mean	P66	P33	P50	Mean	P66
2021–2050	–2.1	–0.4	1.6	2.3	–2.0	–0.7	2.7	4.8	0.2	0.6	4.1	1.7	–0.4	0.3	1.9	1.8
2041–2070	–1.0	–0.3	2.0	1.9	–1.3	–0.7	2.6	1.1	2.0	2.7	5.9	4.4	–0.6	0.5	4.4	4.5
2071–2100	–1.8	2.1	4.5	6.0	0.7	2.2	6.0	5.7	5.1	6.2	9.4	8.9	7.3	9.0	11.9	12.1

Spring evapotranspiration (%)

Time period	SSP126				SSP245				SSP370				SSP585			
	P33	P50	Mean	P66	P33	P50	Mean	P66	P33	P50	Mean	P66	P33	P50	Mean	P66
2021–2050	–1.0	–0.7	1.1	0.6	–1.4	–0.7	1.4	0.7	–1.4	–0.7	1.3	1.0	–2.2	–1.1	1.6	3.1
2041–2070	–0.5	0.4	2.1	1.9	–1.5	–1.1	1.5	0.0	–0.3	1.2	2.7	2.8	–1.6	–0.8	1.6	1.8
2071–2100	–1.8	–1.2	2.8	4.4	–0.7	0.2	3.4	5.7	0.8	1.5	5.2	7.7	2.9	3.5	6.7	9.6

Summer evapotranspiration (%)

Time period	SSP126				SSP245				SSP370				SSP585			
	P33	P50	Mean	P66	P33	P50	Mean	P66	P33	P50	Mean	P66	P33	P50	Mean	P66
2021–2050	–1.5	–0.8	0.8	0.2	–2.1	–1.6	1.0	1.0	–1.5	0.4	2.1	4.0	–3.3	–2.0	1.0	–0.5
2041–2070	–1.9	–1.2	1.1	2.7	–3.3	–2.4	0.5	–0.4	–2.0	0.4	1.9	2.8	–2.0	–1.2	2.4	2.9
2071–2100	–2.5	–1.7	2.0	3.0	–1.0	–0.4	3.2	6.6	0.5	1.7	4.7	6.7	0.5	2.0	5.4	10.2

Autumn evapotranspiration (%)

Time period	SSP126				SSP245				SSP370				SSP585			
	P33	P50	Mean	P66	P33	P50	Mean	P66	P33	P50	Mean	P66	P33	P50	Mean	P66
2021–2050	1.2	1.8	3.6	3.3	1.6	2.3	4.6	4.1	3.5	4.4	5.8	6.6	0.8	1.4	4.0	3.1
2041–2070	0.6	1.4	4.4	5.4	1.5	2.2	5.1	4.5	3.4	4.1	7.6	10.0	2.9	3.6	6.3	6.9
2071–2100	3.0	3.8	6.4	8.3	5.2	7.1	9.4	12.7	5.1	6.1	10.8	14.9	9.3	10.7	14.5	17.2

- e_s is the saturation vapour pressure (daily average), kPa (see equation 3.22);
- e_a is the actual vapour pressure (daily average), kPa (see equation 3.23);
- Δ is the slope of the vapour pressure curve, kPa°C^{-1} (see equation 3.24);

- γ is the psychrometric constant, kPa°C^{-1} (see equation 3.25);
- C_n is the reference crop type constant numerator;
- C_d is the reference crop type constant denominator.

(a)
Winter Ensemble Mean Evapotranspiration Change w.r.t 1981-2010

(b)
Spring Ensemble Mean Evapotranspiration Change w.r.t 1981-2010

(c)
Summer Ensemble Mean Evapotranspiration Change w.r.t 1981-2010

(d)
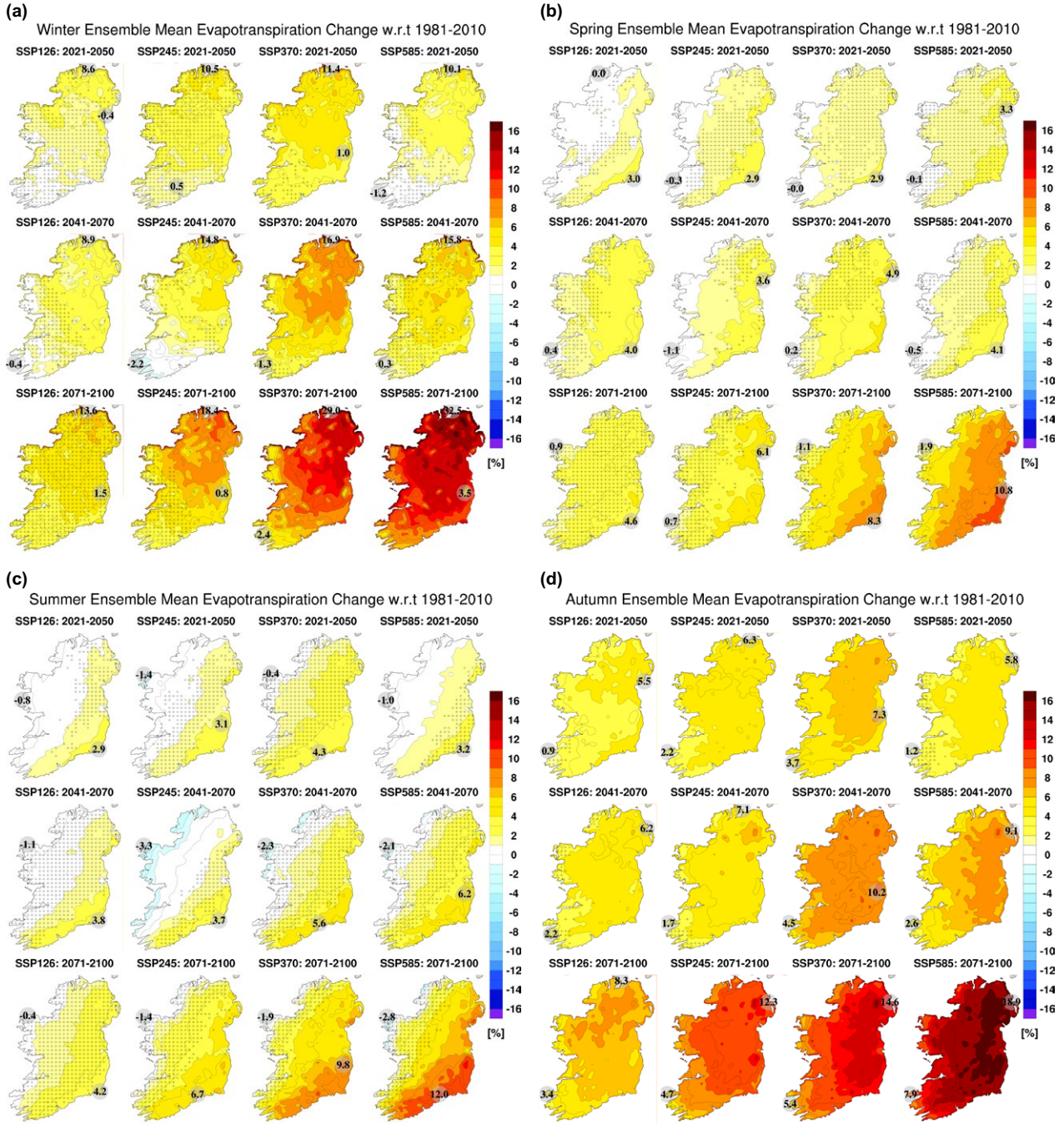Autumn Ensemble Mean Evapotranspiration Change w.r.t 1981-2010

Figure 3.66. Seasonal RCM ensemble mean evapotranspiration (%) for (a) winter, (b) spring, (c) summer and (d) autumn. In each case, the future 30-year period is compared with the past period, 1981–2010. The numbers included on each plot are the minimum and maximum projected changes, displayed at their locations.

For the calculation below, $C_n = 900$ and $C_d = 0.34$ were used.

$$R_n = 0.0864(R_{ns} - R_{nl}) \tag{3.19}$$

R_{ns} and R_{nl} are the mean daily surface shortwave and longwave net radiation in units of $W\,m^{-2}$.

$$G = 0.0864\,SH \tag{3.20}$$

SH is the mean daily surface sensible heat flux in units of $W\,m^{-2}$.

$$u_2 = u_{10}\frac{4.87}{\ln(67.8 \times 10 - 5.42)} \tag{3.21}$$

u_{10} is the 10 m wind speed, $m\,s^{-1}$.

$$e_s = 0.6108e^{\left(\frac{17.27T}{T+237.3}\right)} \tag{3.22}$$

T is the 2 m temperature, °C.

$$e_a = 0.6108 \, e^{\left(\frac{17.27 T_d}{T_d + 237.3}\right)} \quad \text{(3.23)}$$

T_d is the 2 m dew point temperature, °C.

$$\Delta = \frac{4098.2 \, e_s}{(T_{mean} + 237.3)^2} \quad \text{(3.24)}$$

$$\gamma = 0.000000665 \, P \quad \text{(3.25)}$$

where P is the mean daily surface pressure, *Pa*.

CLM-ERAInterim Annual ET (1981-2015), 1.5km
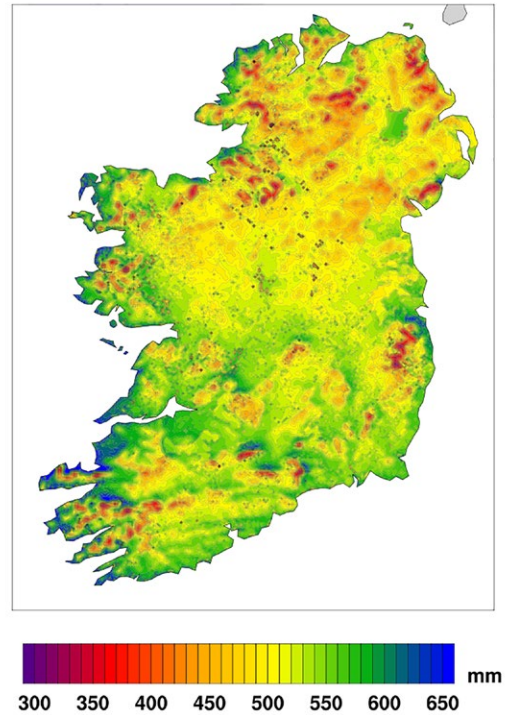
Figure 3.67. "Observed" annual evapotranspiration FAO-56 (1981–2015), as resolved by COSMO-CLM5–ERA-Interim 1.5 km simulation. Please refer to Werner *et al.* (2019) for an overview of the climate simulation configuration and agri-climate validation results.

4 Global Climate Modelling and Ireland's Contribution to CMIP6

A second main component of the project involved simulating the global climate using the EC-Earth ESM. Note that, since there is an overlap between this research and a previous EPA project (Nolan and McKinstry, 2020), and the results have been published (e.g. Jones *et al*., 2021; Döscher *et al*., 2022), a short summary is presented below.

The following EC-Earth (v 3.3) CMIP6 contributions were completed[20] (approximately 3600 years of simulated data in total):

- 7 × EC-Earth AOGCM/Veg Historical simulations 1850–2014;
- 28 × EC-Earth AOGCM/Veg ScenarioMIP 2015–2100 simulations; 7 × SSP126, 7 × SSP245, 7 × SSP370 and 7 × SSP585.

The EC-Earth simulations were run on the ICHEC and ECMWF supercomputers. While the main motivation for completing these EC-Earth simulations was to contribute to CMIP6, consideration was given to the choice of configurations to maximise the utility for Irish research. Since the climate of Ireland and north-west Europe is dominated by the Atlantic Ocean and its interaction with the atmosphere, all CMIP6 contributions were performed with the AOGCM configuration (Döscher *et al*., 2022). Since agriculture is an important industry in Ireland, 40% of the CMIP6 contributions used the EC-Earth3-Veg configuration (Döscher *et al*., 2022), which extends the EC-Earth3 AOGCM by inclusion of the interactively coupled dynamic global vegetation model LPJ-GUESS (Smith *et al*., 2014). Finally, model-level data were archived for three historical and 12 future simulations, allowing for international (e.g. CORDEX) and national regional downscaling (e.g. Chapter 3) using RCMs.

The EC-Earth ensemble members were validated by comparing the seven historical ensemble members with CRU observational and ECMWF ERA5 reanalysis datasets. Comprehensive validations and assessments of the projections of EC-Earth temperature, precipitation, 10 m wind speed, mean sea level pressure, total cloud cover, snowfall, sea surface temperature and sea ice fraction were completed (e.g. Nolan and McKinstry, 2020). See Döscher *et al*. (2022) for a more comprehensive overview of the EC-Earth model, validations and CMIP6 experiments. The validations confirm that the CMIP6 EC-Earth model accurately simulates the global climate and outperforms the CMIP5 version for the majority of variables analysed.

The full CMIP6 Scenario-MIP ensemble was analysed to assess where the CMIP6 EC-Earth contributions fit within the full ensemble. Figure 4.1 presents the global annual 2 m temperature anomaly (1850–2100) with respect to the pre-industrial 50-year mean 1850–1900. The mean of the full CMIP6 ensemble is presented alongside the individual EC-Earth ensemble members. A total of 206 (SSP126), 192 (SSP245), 183 (SSP370) and 203 (SSP585) CMIP6 ensemble members were analysed.

The research of the current project also contributed to the CMIP6 CovidMIP modelling experiment, an international collaboration of climate institutes. The aim of CovidMIP is to investigate whether the COVID-19-induced reductions in emissions have had any impact on the Earth's climate (Jones *et al*., 2021). As part of the current project an ensemble of EC-Earth–COVID simulations (approximately 500 years of simulated data in total) were run and the data shared with the international research community.

The EC-Earth–CMIP6 simulations constitute Ireland's contribution to CMIP6, and their results informed the IPCC AR6 Working Group 1 report published in August 2021. The datasets (~1.5 PB in size) were standardised, quality controlled, validated and shared with the international research community on the

---

20 Note that approximately 50% of these simulations were completed as part of the EPA report *EC-Earth Global Climate Simulations: Ireland's Contributions to CMIP6* (Nolan and McKinstry, 2020).
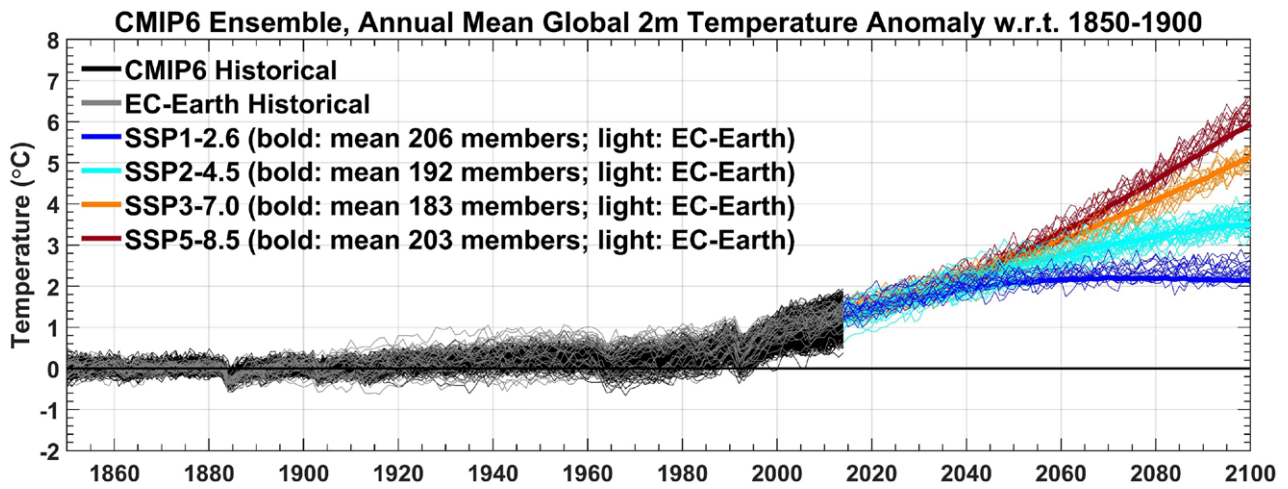
Figure 4.1. The CMIP6 global annual 2 m temperature anomaly with respect to the 50-year mean 1850–1900. The EC-Earth ensemble members are presented alongside the CMIP6 mean to assess where the EC-Earth simulations fit within the full CMIP6 ensemble.

ICHEC Earth System Grid Federation (ESGF) node (EC-Earth Consortium, 2019). Model-level data were archived allowing for international (e.g. CORDEX) and national regional downscaling using RCMs. The results will continue to inform follow-on IPCC AR6 interim reports, as well as international and national research for the next decade.

5   Global Warming Threshold Scenario Projections

In this section, the SSP–RCP scenario-based national projections of the current report are supplemented with global warming threshold (GWT) scenario projections. These alternative scenarios have garnered substantial interest since the 2015 Paris Agreement (a United Nations treaty in which 195 nations pledged to tackle climate change), which aims to limit global warming to "well below" 2°C by the end of the century, and "pursue efforts" to keep warming within the safer limit of 1.5°C (UN, 2015).

Figure 5.1 presents preliminary 2 m temperature projections for Ireland for various GWTs (1.5°C, 2°C, 2.5°C, 3°C, 3.5°C and 4°C). For example, the projections under the "2°C GWT scenario" show temperature projections over Ireland in a world that is 2°C warmer than the period 1850–1900. Similarly, seasonal GWT scenario projections are presented in Figure 5.2. The GWT scenario projections were assessed using the RCM–CMIP6-SSP scenario projections of the current report and the ensemble of
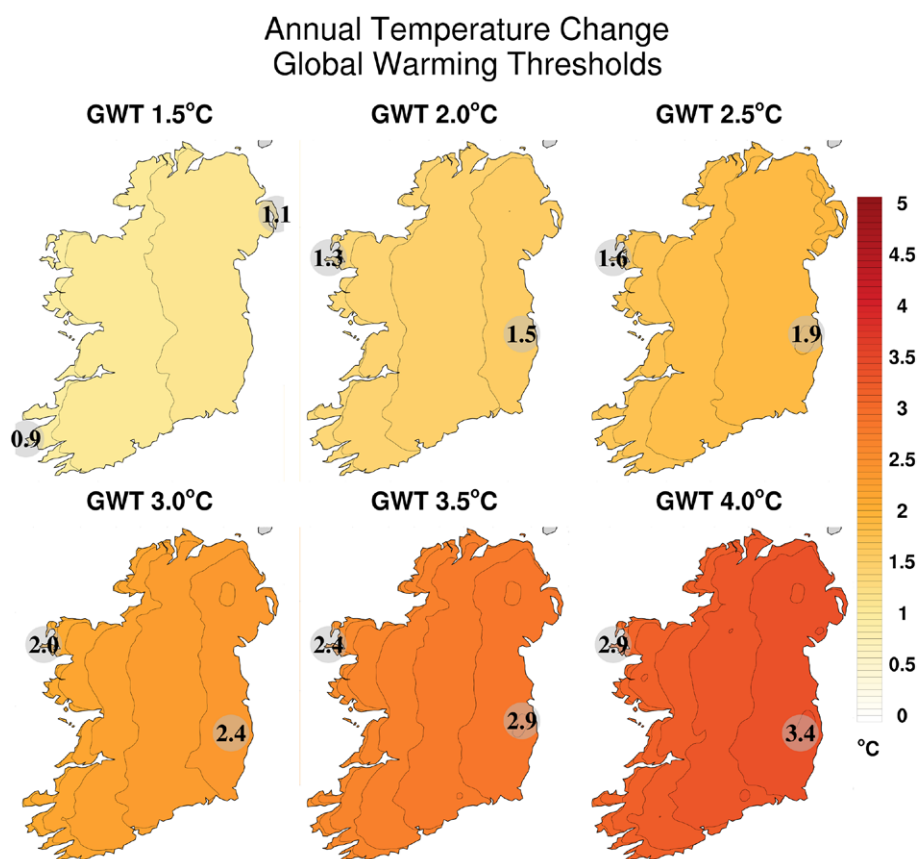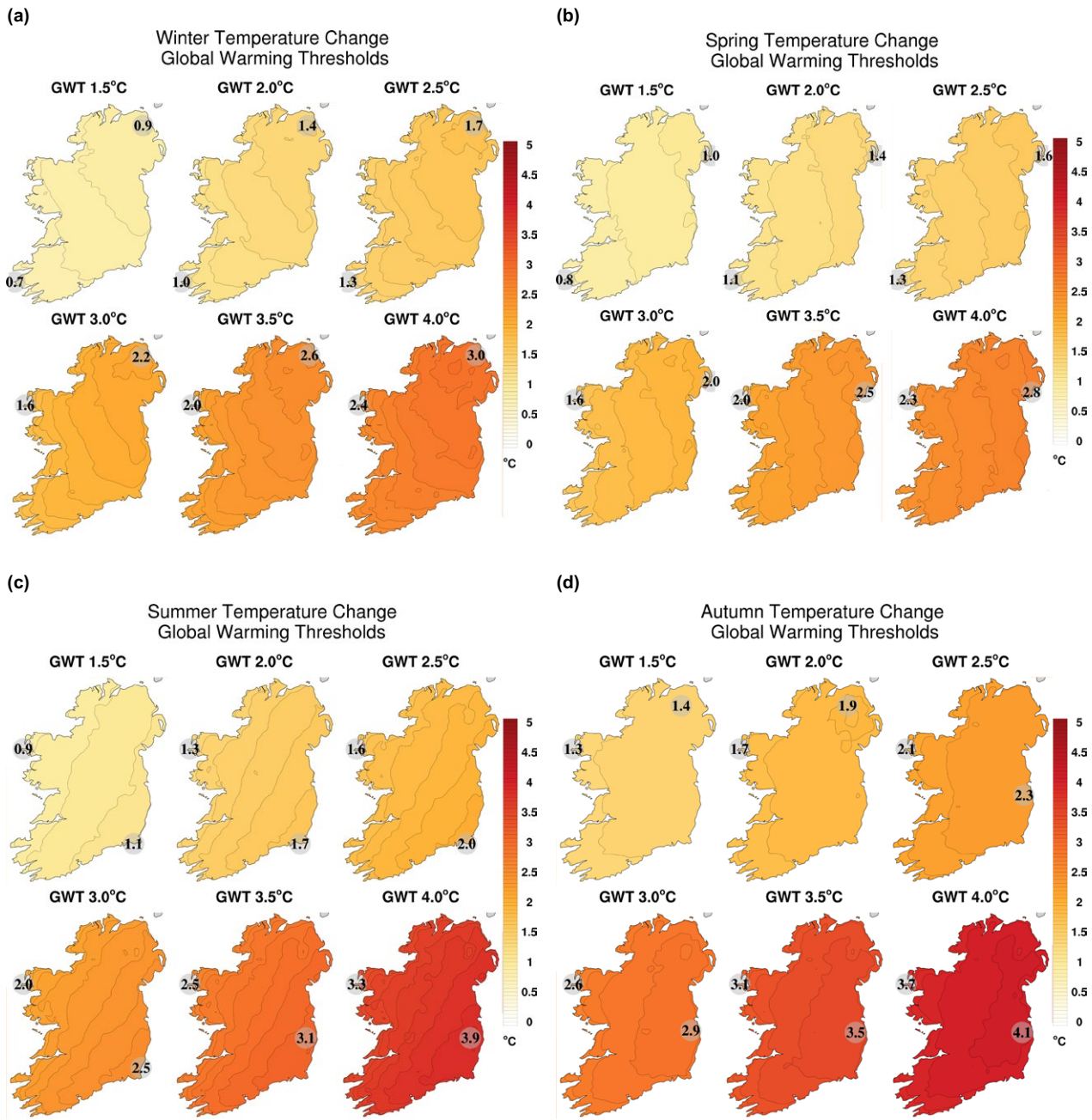

Figure 5.1. RCM 2 m temperature projections for Ireland for GWTs above the 1850–1900 mean: GWT = 1.5°C (58 ensemble members), GWT = 2.0°C (49 members), GWT = 2.5°C (40 members), GWT = 3.0°C (31 members), GWT = 3.5°C (22 members) and GWT = 4.0°C (13 members). The projections were produced using an ensemble of high-resolution (4 km) downscaled CMIP5-RCP and CMIP6-SSP GCMs. Hatchings being included would highlight areas of "uncertainty", "+" would highlight areas where $|\mu_{ensemble}| - \sigma_{ensemble} < 0$, "×" would highlight areas where the 20th and 80th percentile of ensemble projections have different signs and "∗" would highlight areas where both conditions occur. Note that for the annual and seasonal temperature projections, no such areas of uncertainty were identified over Ireland.

RCM–CMIP5-RCP projections of Nolan and Flanagan (2020). As such, the ensemble size is considerably larger (up to 58 members) and allows for a better quantification of uncertainty. This increased ensemble size allows for the IPCC AR6 "Approach C" (discussed in section 1.4.2) to be implemented, where robustness/certainty is based on both model agreement (≥80% agreement of ensemble members in the sign of projected change) and significance (in this case, the

"signal to noise ratio" test). Furthermore, the enhanced ensemble size allows for the assessment of a larger range of "likelihood" projections. Figure 5.3 presents various percentiles of the ensemble of projections of annual 2 m temperature for five GWT scenarios: the 10th (very likely), 33rd (likely), 50th (as likely as not), mean, 66th (unlikely) and 90th (very unlikely) projections. Similarly, the seasonal likelihood projections are presented in Figures 5.4–5.7.

(a)

(b)

(c)

(d)

Figure 5.2. RCM seasonal 2 m temperature GWT projections for Ireland above the 1850–1900 mean: GWT = 1.5°C (58 ensemble members), GWT = 2.0°C (49 members), GWT = 2.5°C (40 members), GWT = 3.0°C (31 members), GWT = 3.5°C (22 members) and GWT = 4.0°C (13 members). The projections were produced using an ensemble of high-resolution (4 km) downscaled CMIP5-RCP and CMIP6-SSP GCMs.
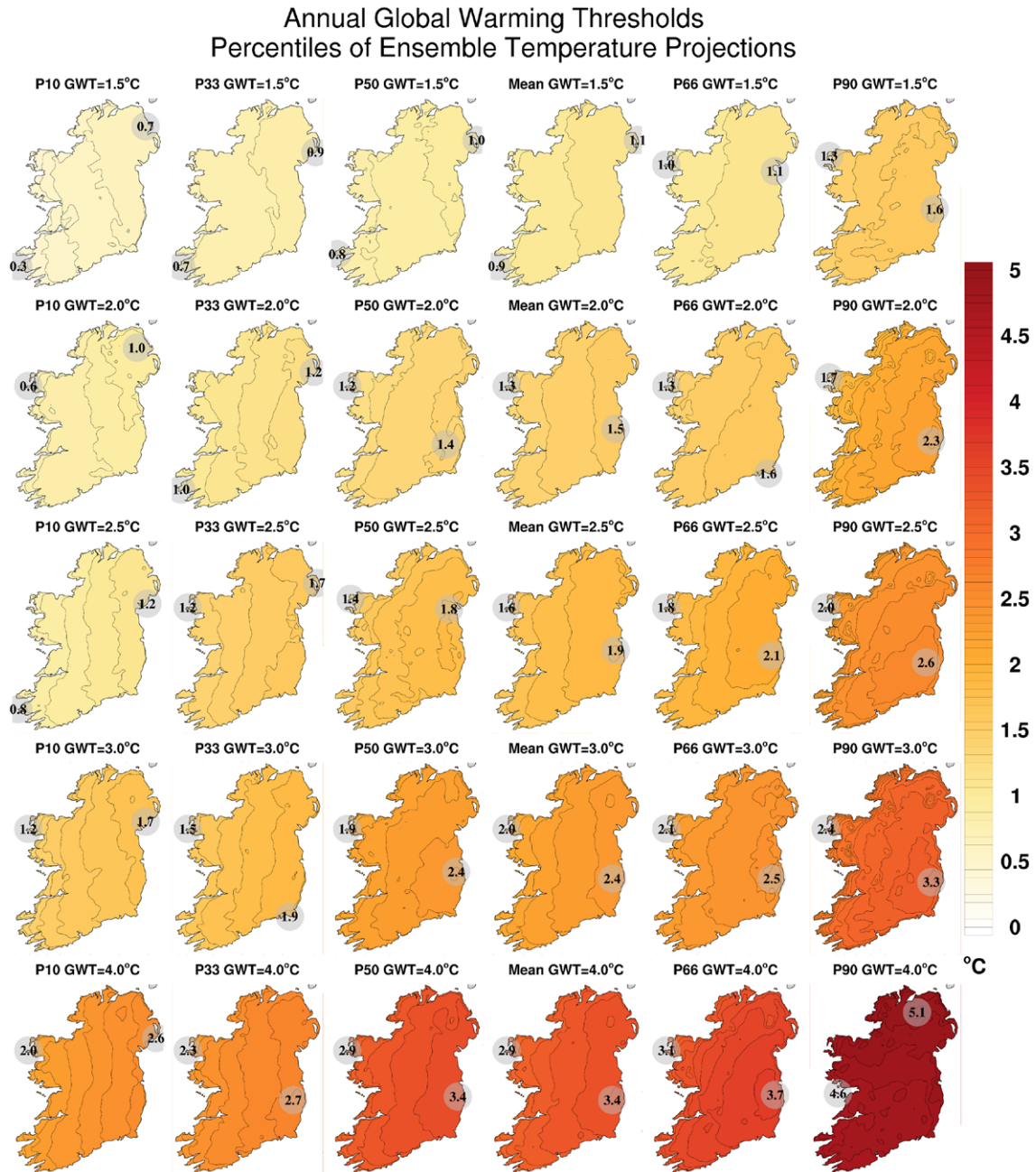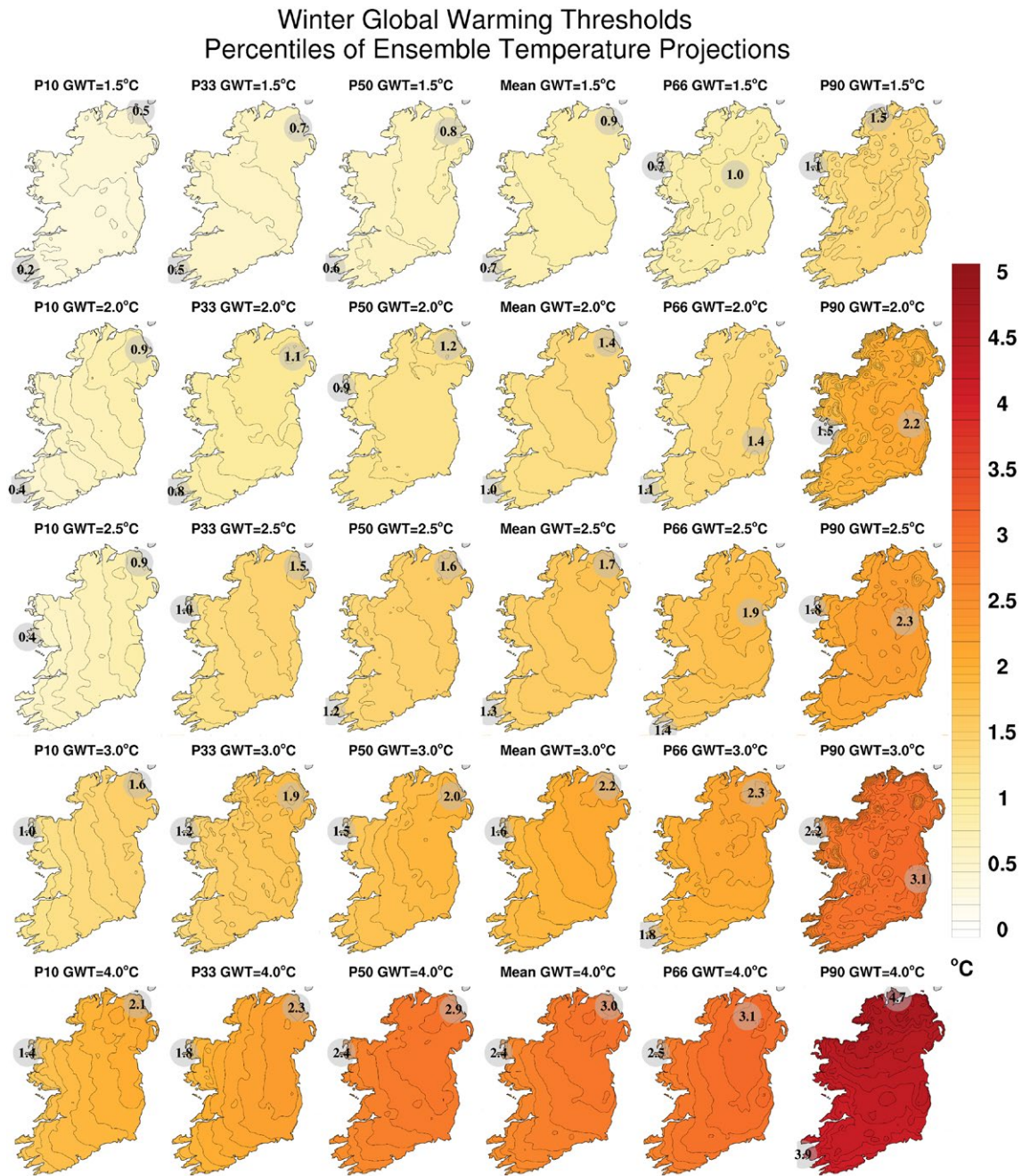
Figure 5.3. Percentiles of ensemble of RCM annual 2 m temperature GWT projections (°C) above the 1850–1900 mean: GWT = 1.5°C (58 ensemble members), GWT = 2.0°C (49 members), GWT = 2.5°C (40 members), GWT = 3.0°C (31 members) and GWT = 4.0°C (13 members). The projections were produced using an ensemble of high-resolution (4 km) downscaled CMIP5-RCP and CMIP6-SSP GCMs.

The preliminary GWT scenario projections for precipitation (%) presented in Figure 5.8 (annual), Figure 5.9 (seasonal) and Figures 5.10–5.14 (annual and seasonal likelihood projections) show substantially fewer areas of uncertainty (compared with the SSP-based projections of the current report), underpinning the importance of analysing large ensembles in the assessment of climate change.

Figure 5.4. Percentiles of ensemble of RCM winter 2 m temperature GWT projections (°C) above the 1850–1900 mean: GWT = 1.5°C (58 ensemble members), GWT = 2.0°C (49 members), GWT = 2.5°C (40 members), GWT = 3.0°C (31 members) and GWT = 4.0°C (13 members). The projections were produced using an ensemble of high-resolution (4 km) downscaled CMIP5-RCP and CMIP6-SSP GCMs.
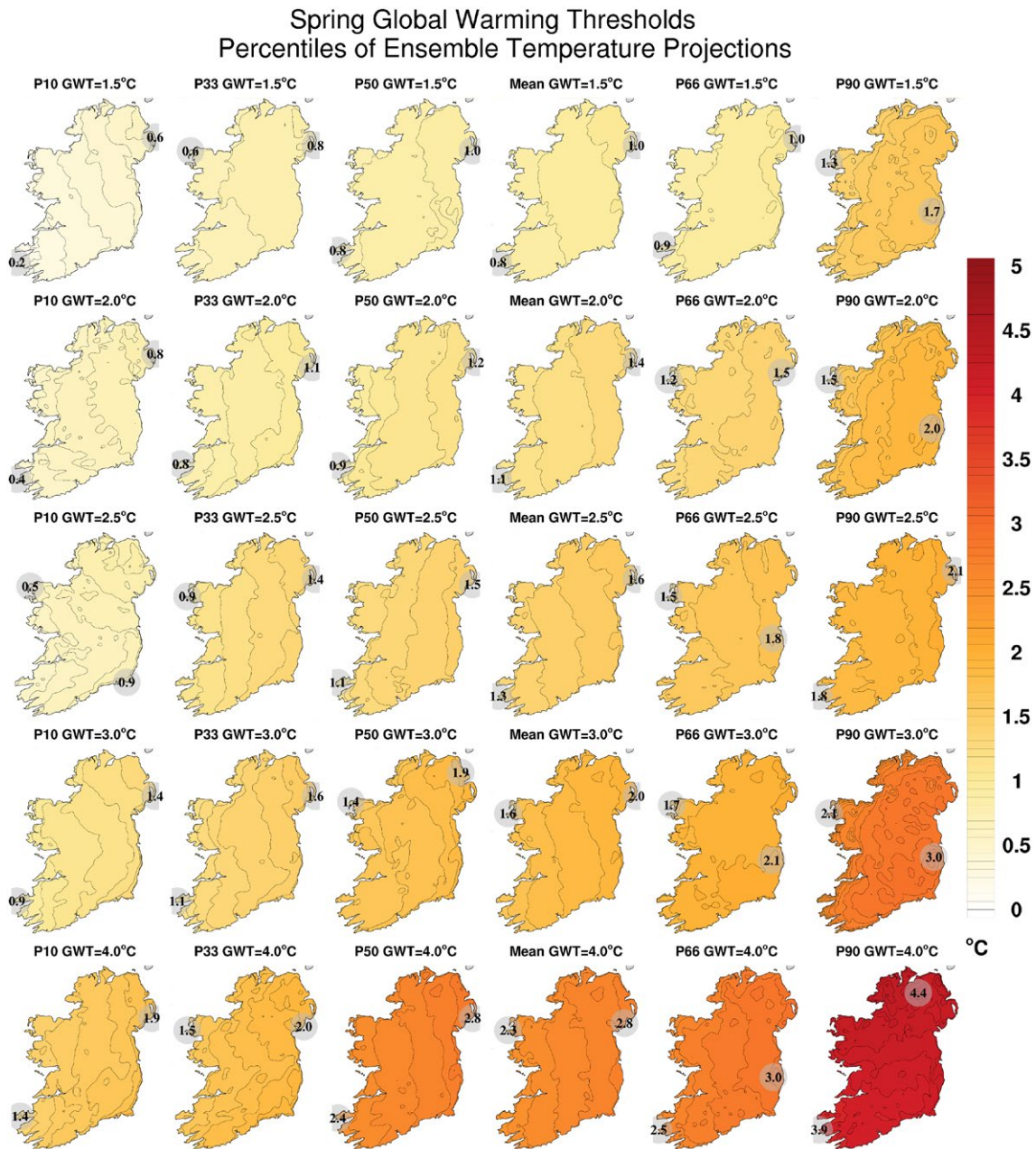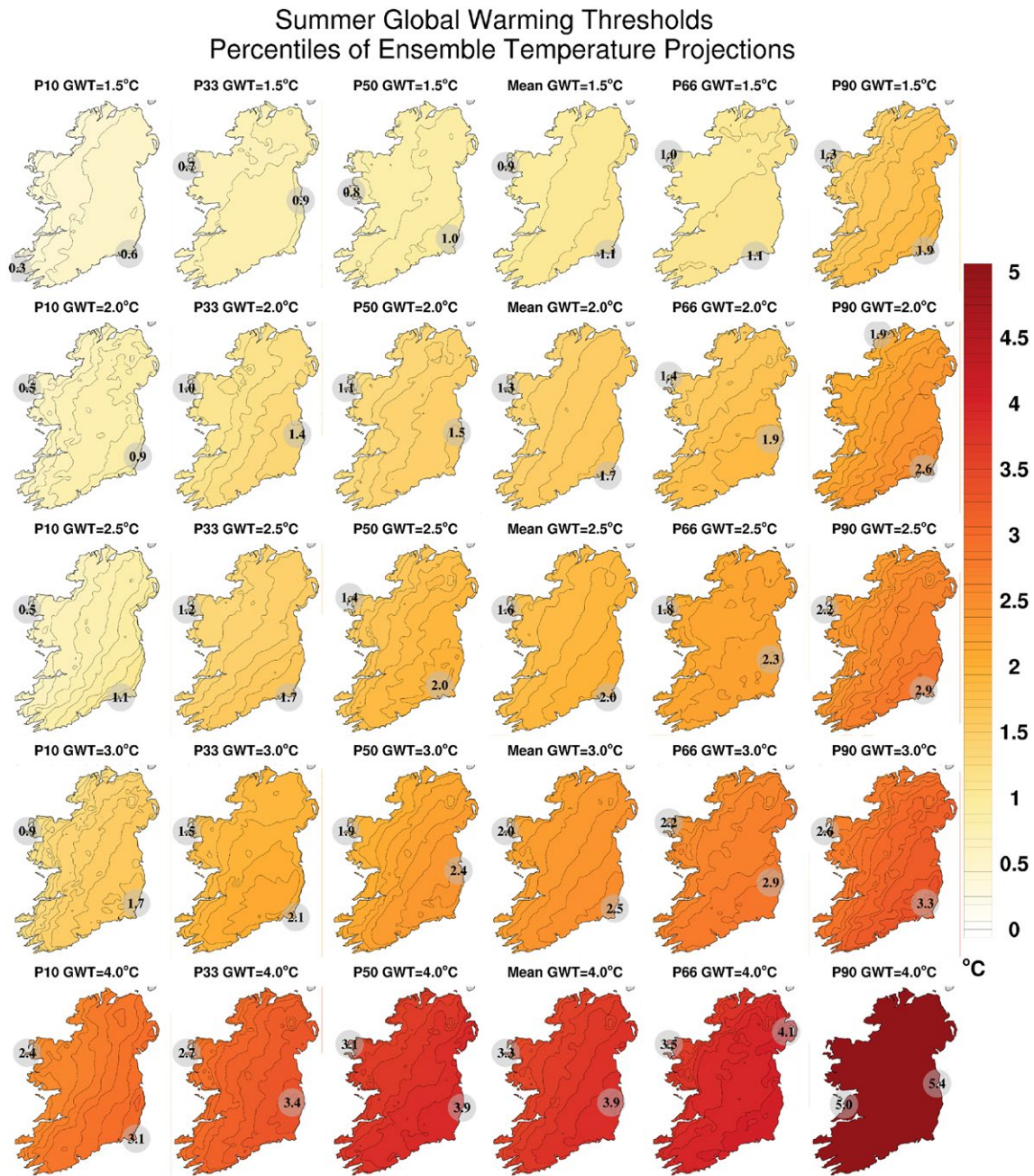
Figure 5.5. Percentiles of ensemble of RCM spring 2 m temperature GWT projections (°C) above the 1850–1900 mean: GWT = 1.5°C (58 ensemble members), GWT = 2.0°C (49 members), GWT = 2.5°C (40 members), GWT = 3.0°C (31 members) and GWT = 4.0°C (13 members). The projections were produced using an ensemble of high-resolution (4 km) downscaled CMIP5-RCP and CMIP6-SSP GCMs.
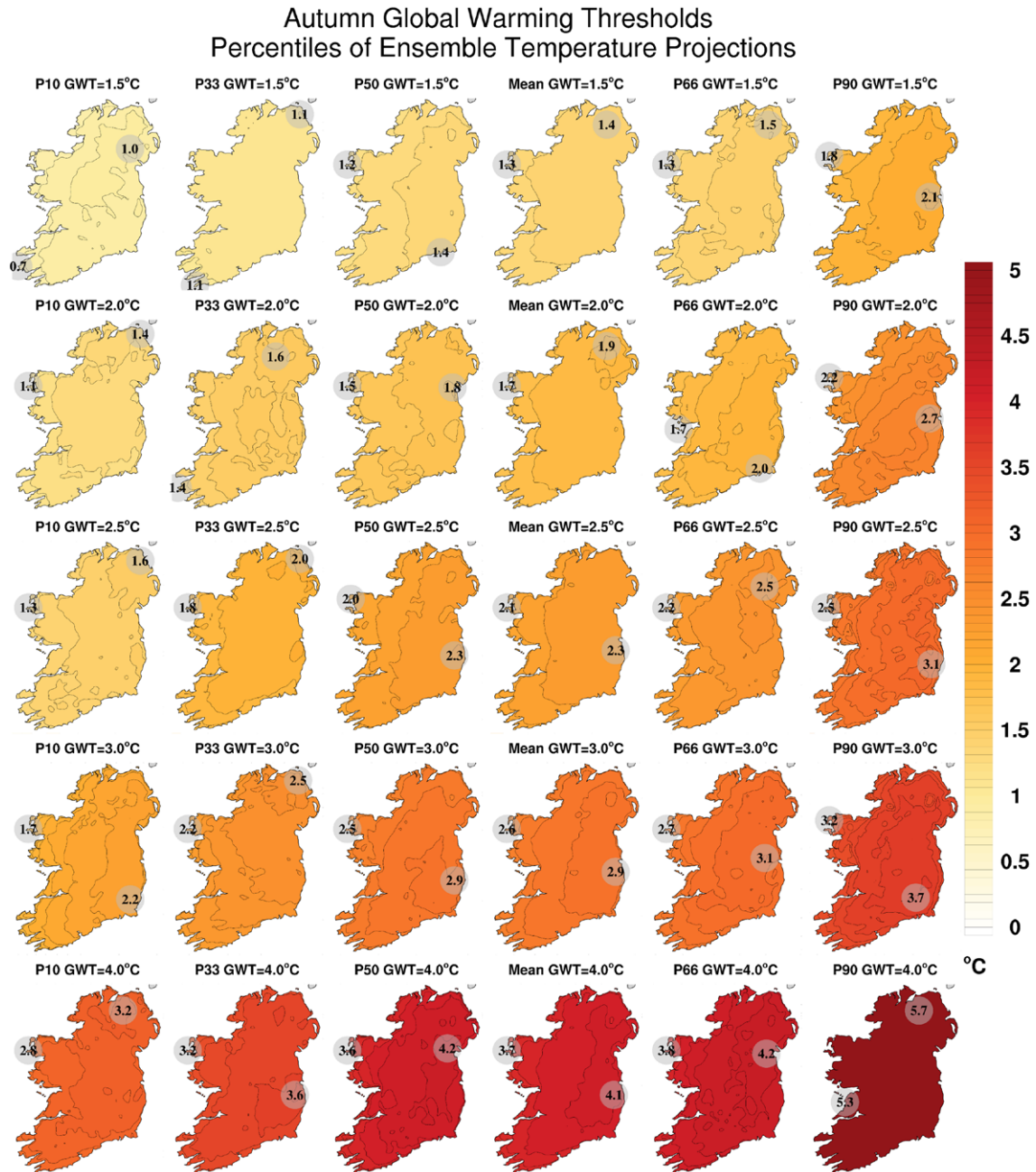
Figure 5.6. Percentiles of ensemble of RCM summer 2 m temperature GWT projections (°C) above the 1850–1900 mean: GWT = 1.5°C (58 ensemble members), GWT = 2.0°C (49 members), GWT = 2.5°C (40 members), GWT = 3.0°C (31 members) and GWT = 4.0°C (13 members). The projections were produced using an ensemble of high-resolution (4 km) downscaled CMIP5-RCP and CMIP6-SSP GCMs.

Figure 5.7. Percentiles of ensemble of RCM autumn 2 m temperature GWT projections (°C) above the 1850–1900 mean: GWT = 1.5°C (58 ensemble members), GWT = 2.0°C (49 members), GWT = 2.5°C (40 members), GWT = 3.0°C (31 members) and GWT = 4.0°C (13 members). The projections were produced using an ensemble of high-resolution (4 km) downscaled CMIP5-RCP and CMIP6-SSP GCMs.
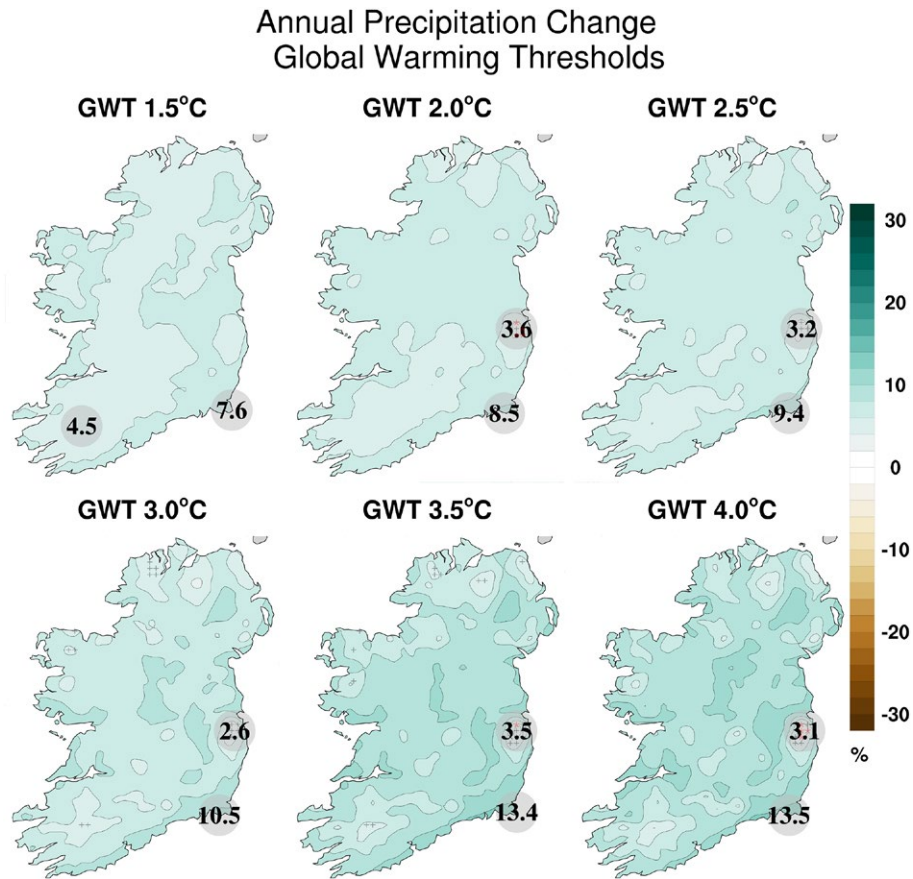
Figure 5.8. Annual RCM precipitation GWT projections (%) for Ireland above the 1850–1900 mean: GWT = 1.5°C (58 ensemble members), GWT = 2.0°C (49 members), GWT = 2.5°C (40 members), GWT = 3.0°C (31 members), GWT = 3.5°C (22 members) and GWT = 4.0°C (13 members). The projections were produced using an ensemble of high-resolution (4 km) downscaled CMIP5-RCP and CMIP6-SSP GCMs. Hatchings are included to highlight areas of "uncertainty", "+" highlights areas where $\left| \mu_{ensemble} \right| - \sigma_{ensemble} < 0$, "×" highlights areas where the 20th and 80th percentiles of ensemble projections have different signs and "∗" highlights areas where both conditions occur.

Figure 5.9. Seasonal RCM precipitation GWT projections (%) for Ireland above the 1850–1900 mean: GWT = 1.5°C (58 ensemble members), GWT = 2.0°C (49 members), GWT = 2.5°C (40 members), GWT = 3.0°C (31 members), GWT = 3.5°C (22 members) and GWT = 4.0°C (13 members). The projections were produced using an ensemble of high-resolution (4 km) downscaled CMIP5-RCP and CMIP6-SSP GCMs. Hatchings are included to highlight areas of "uncertainty", "+" highlights areas where $|\mu_{ensemble}| - \sigma_{ensemble} < 0$, "×" highlights areas where the 20th and 80th percentiles of ensemble projections have different signs and "∗" highlights areas where both conditions occur.

Figure 5.10. Percentiles of ensemble of RCM annual precipitation GWT projections (%) above the 1850–1900 mean: GWT = 1.5°C (58 ensemble members), GWT = 2.0°C (49 members), GWT = 2.5°C (40 members), GWT = 3.0°C (31 members) and GWT = 4.0°C (13 members). The projections were produced using an ensemble of high-resolution (4 km) downscaled CMIP5-RCP and CMIP6-SSP GCMs.

Figure 5.11. Percentiles of ensemble of RCM winter precipitation GWT projections (%) above the 1850–1900 mean: GWT = 1.5°C (58 ensemble members), GWT = 2.0°C (49 members), GWT = 2.5°C (40 members), GWT = 3.0°C (31 members) and GWT = 4.0°C (13 members). The projections were produced using an ensemble of high-resolution (4 km) downscaled CMIP5-RCP and CMIP6-SSP GCMs.
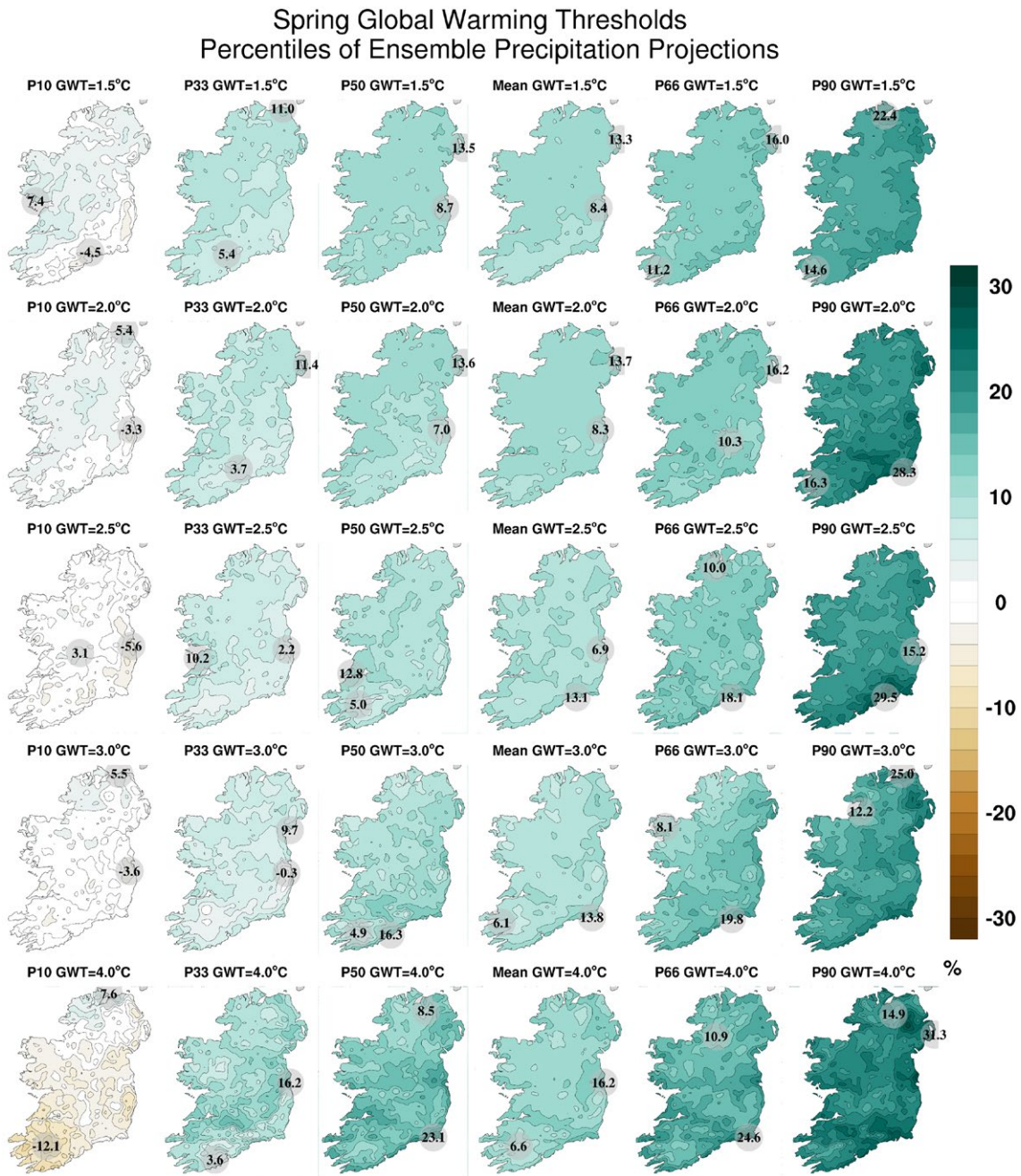
Figure 5.12. Percentiles of ensemble of RCM spring precipitation GWT projections (%) above the 1850–1900 mean: GWT = 1.5°C (58 ensemble members), GWT = 2.0°C (49 members), GWT = 2.5°C (40 members), GWT = 3.0°C (31 members) and GWT = 4.0°C (13 members). The projections were produced using an ensemble of high-resolution (4 km) downscaled CMIP5-RCP and CMIP6-SSP GCMs.

Figure 5.13. Percentiles of ensemble of RCM summer precipitation GWT projections (%) above the 1850–1900 mean: GWT = 1.5°C (58 ensemble members), GWT = 2.0°C (49 members), GWT = 2.5°C (40 members), GWT = 3.0°C (31 members) and GWT = 4.0°C (13 members). The projections were produced using an ensemble of high-resolution (4 km) downscaled CMIP5-RCP and CMIP6-SSP GCMs.
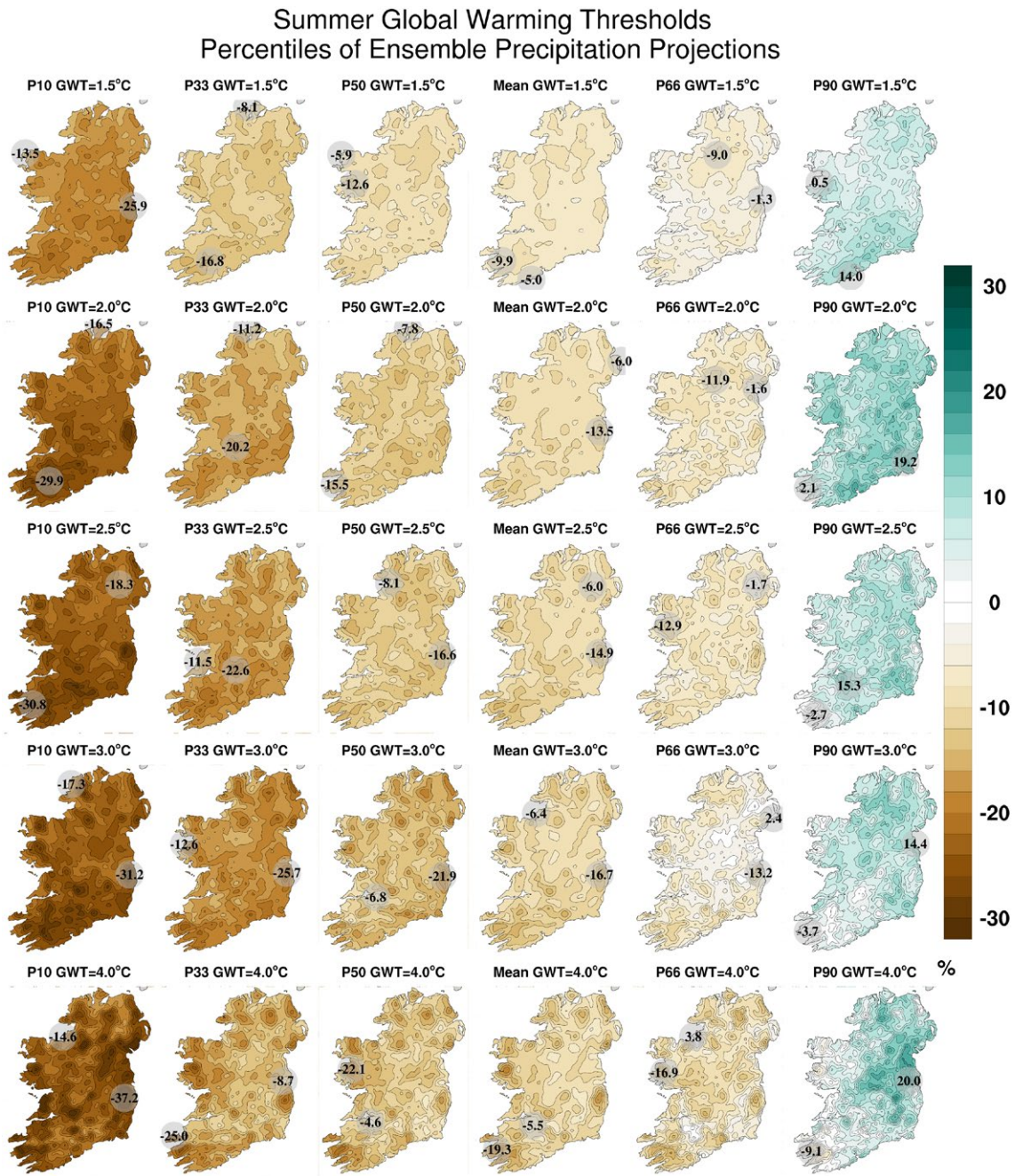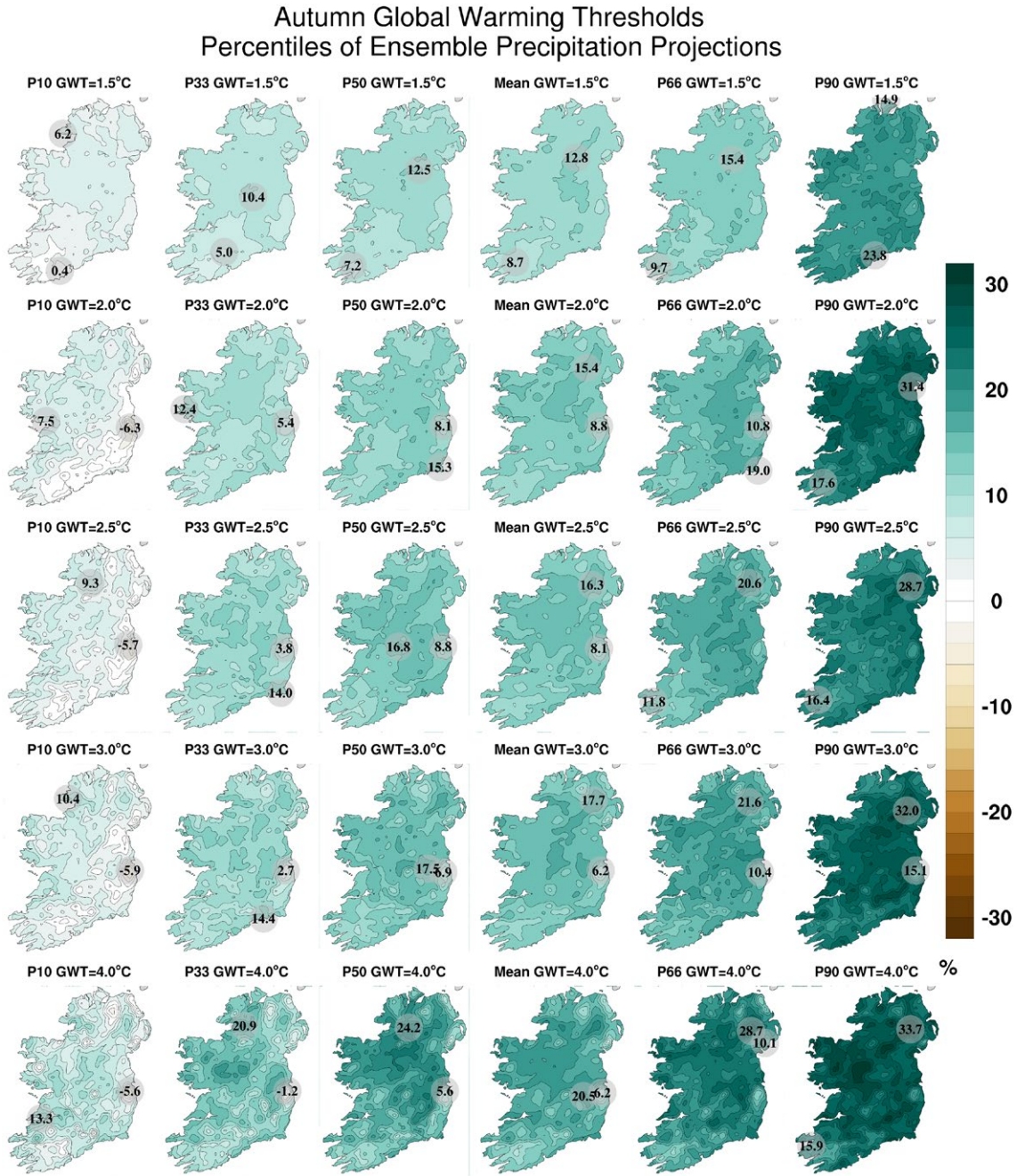
Figure 5.14. Percentiles of ensemble of RCM autumn precipitation GWT projections (%) above the 1850–1900 mean: GWT = 1.5°C (58 ensemble members), GWT = 2.0°C (49 members), GWT = 2.5°C (40 members), GWT = 3.0°C (31 members) and GWT = 4.0°C (13 members). The projections were produced using an ensemble of high-resolution (4 km) downscaled CMIP5–RCP and CMIP6–SSP GCMs.

6 Recommendations

While the RCM simulations of the current report have reduced, and better quantified, climate projection uncertainty, there still exists considerable uncertainty in the magnitude, and regional details, of precipitation-related projections for Ireland. Future work will focus on reducing this uncertainty by greatly increasing the ensemble size and employing more up-to-date RCMs (including fully coupled atmosphere–ocean–wave models), run at convection-resolving resolution (~1.5 km), to downscale additional CMIP6 ESMs (see Table 1.3). An increased ensemble of high-resolution RCMs will allow for more accurate national projections and quantification of uncertainty of precipitation and extreme events.

It is also important to stress that the projections, quantification of uncertainty and *likelihood* values presented in the current study are derived from the most up-to-date evidence available. Therefore, these results apply only to the specific sets of high-resolution models and experimental design of the current study. It is expected that future improvements in modelling will alter the projections, as uncertainty is expected to be gradually reduced.

Future work will assess the impact of climate change on North Atlantic storms. As extreme storm events are rare, this work will require analysing a very large ensemble, thus allowing a robust statistical analysis of extreme storm track projections. This work will be carried out once the downscaled CMIP6 EURO-CORDEX projection data become available.

The GWT scenario projections, presented in Chapter 5, will be extended to include additional variables such as wind speed, humidity and surface radiation.

The climate datasets will be shared with national research groups and continue to inform various climate impact studies such as those on renewable wind energy (Doddy *et al*., 2022), biodiversity (McGowan *et al*., 2021; Reyne *et al*., 2021, 2023), flooding (Morrissey *et al*., 2021), critical infrastructure (Hawchar *et al*., 2020; Saikia *et al*., 2023), pollution (Naughton *et al*., 2018; O'Driscoll *et al*., 2018) and agriculture (Abdalla *et al*., 2012, 2014). The archive of RCM data will be made available to the wider research community and general public through Climate Ireland (maps and visualisations) and ICHEC and Met Éireann (data hosting and sharing) platforms. The RCM data will be provided to the Met Éireann TRANSLATE project (O'Brien and Nolan, 2023; O'Brien *et al*., 2024) to be statistically downscaled and bias-corrected with the aim of providing standardised future climate projections for Ireland.

With regard to ongoing and future global climate modelling research, the principal investigator is working with Met Éireann on improving the EC-Earth ESM in the representation of the North Atlantic Ocean–Atmosphere Climate System. This research will provide more accurate projections of the North Atlantic and Irish climate and will contribute to CMIP7 (and the IPCC AR7 reports) by running an ensemble of high-resolution (~40 km) next-generation EC-Earth (version 4) simulations.

References

Abdalla, M., Rueangritsarakul, K., Jones, M., *et al.*, 2012. How effective is reduced tillage–cover crop management in reducing N$_2$O fluxes from arable crop soils? *Water, Air, and Soil Pollution* 223: 5155–5174.

Abdalla, M., Hastings, A., Helmy, M., *et al.*, 2014. Assessing the combined use of reduced tillage and cover crops for mitigating greenhouse gas emissions from arable ecosystem. *Geoderma* 223: 9–20.

Allen, R.G., Pereira, L.S., Raes, D., *et al.*, 1998. *Crop Evapotranspiration – Guidelines for Computing Crop Water Requirements – FAO Irrigation and Drainage Paper 56*. Food and Agricultural Organization of the United Nations, Rome. Available online: https://www.fao.org/4/X0490E/x0490e00.htm (accessed 22 May 2024).

Asher, E.E., Ashkenazy, Y., Havlin, S., *et al.*, 2021. Optimal COVID-19 infection spread under low temperature, dry air, and low UV radiation. *New Journal of Physics* 23: 033044.

Barreca, A.I. and Shimshack, J.P., 2012. Absolute humidity, temperature, and influenza mortality: 30 years of county-level evidence from the United States. *American Journal of Epidemiology* 176: S114–S122.

Bartók, B., Wild, M., Folini, D., *et al.*, 2017. Projected changes in surface solar radiation in CMIP5 global climate models and in EURO-CORDEX regional climate models for Europe. *Climate Dynamics* 49: 2665–2683.

Bieniek, P.A., Bhatt, U.S., Walsh, J.E., *et al.*, 2016. Dynamical downscaling of ERA-Interim temperature and precipitation for Alaska. *Journal of Applied Meteorology and Climatology* 55: 635–654.

Bigler, C. and Bugmann, H., 2018. Climate-induced shifts in leaf unfolding and frost risk of European trees and shrubs. *Scientific Reports* 8: 9865. https://doi.org/10.1038/s41598-018-27893-1.

Bock, L., Lauer, A., Schlund, M., *et al.*, 2020. Quantifying progress across different CMIP phases with the ESMValTool. *Journal of Geophysical Research: Atmospheres* 125: e2019JD032321.

Bootsma, A., Tremblay, G. and Filion, P., 1999. *Risk Analyses of Heat Units Available for Corn and Soybean Production in Quebec*. Agriculture and Agri-food Canada, Ottawa, Canada.

Bootsma, A., McKenney, D.W., Anderson, D., *et al.*, 2007. A re-evaluation of crop heat units in the Maritime Provinces of Canada. *Canadian Journal of Plant Science* 87: 281–287.

Byrne, M.P. and O'Gorman, P.A., 2018. Trends in continental temperature and humidity directly linked to ocean warming. *Proceedings of the National Academy of Sciences* 115: 4863–4868.

Camargo, S.J., 2013. Global and regional aspects of tropical cyclone activity in the CMIP5 models. *Journal of Climate* 26(24): 9880–9902.

Cámaro García, W.C.A. and Dwyer N., 2021. *Climate Status Report for Ireland 2020*. Environmental Protection Agency. Available online: https://www.epa.ie/publications/research/climate-change/research-386-the-status-of-irelands-climate-2020.php (accessed 21 July 2023).

Carleton, T., Cornetet, J., Huybers, P., *et al.*, 2021. Global evidence for ultraviolet radiation decreasing COVID-19 growth rates. *Proceedings of the National Academy of Sciences* 118: e2012370118.

Carlier, J., Doyle, M., Finn, J.A., *et al.*, 2021. A landscape classification map of Ireland and its potential use in national land use monitoring. *Journal of Environmental Management* 289: 112498.

Cavicchia, L. and von Storch, H., 2012. The simulation of medicanes in a high-resolution regional climate model. *Climate Dynamics* 39: 2273–2290. https://doi.org/10.1007/s00382-011-1220-0.

Coffel, E.D., Horton, R.M. and de Sherbinin, A., 2017. Temperature and humidity based projections of a rapid rise in global heat stress exposure during the 21st century. *Environmental Research Letters* 13: 014001.

Collins, J.F. and Cummins, T., 1996. *Agroclimatic Atlas of Ireland*. AGMET, Dublin.

Cucak, M., Sparks, A., Moral, R.D.A., *et al.*, 2019. Evaluation of the 'Irish rules': the potato late blight forecasting model and its operational use in the Republic of Ireland. *Agronomy* 9: 515.

Cullen, E., 2010. Lyme disease and climate change. *Irish Medical Journal* 103: 101–102.

Daloz, A., Camargo, S., Kossin, J., *et al*., 2015. Cluster analysis of downscaled and explicitly simulated North Atlantic tropical cyclone tracks. *Journal of Climate* 28: 1333–1361. https://doi.org/10.1175/JCLI-D-13-00646.1.

Daly, C., 2019. *Built & Archaeological Heritage: Climate Change Sectoral Adaptation Plan*. Department of Culture, Heritage and the Gaeltacht, Dublin.

Déqué, M., Rowell, D.P., Lüthi, D., *et al*., 2007. An intercomparison of regional climate simulations for Europe: assessing uncertainties in model projections. *Climatic Change* 81: 53–70.

Di Luca, A., Argueso, D., Evans, J., *et al*., 2016. Quantifying the overall added value of dynamical downscaling and the contribution from different spatial scales. *Journal of Geophysical Research: Atmospheres* 121: 1575–1590. https://doi.org/10.1002/2015JD024009.

Doddy Clarke, E., Sweeney, C., McDermott, F., *et al*., 2022. Climate change impacts on wind energy generation in Ireland. *Wind Energy* 25: 300–312.

Donat, M.G., Leckebusch, G.C., Wild, S., *et al*., 2010. Benefits and limitations of regional multi-model ensembles for storm loss estimations. *Climate Research* 44: 211–225.

Donzelli, G., Biggeri, A., Tobias, A., *et al*., 2022. Role of meteorological factors on SARS-CoV-2 infection incidence in Italy and Spain before the vaccination campaign. A multi-city time series study. *Environmental Research* 211: 113134.

Döscher, R., Acosta, M., Alessandri, A., *et al*., 2022. The EC-Earth3 Earth system model for the Coupled Model Intercomparison Project 6. *Geoscientific Model Development* 15: 2973–3020. https://doi.org/10.5194/gmd-15-2973-2022.

Dosio, A. and Fischer, E.M., 2018. Will half a degree make a difference? Robust projections of indices of mean and extreme climate in Europe under 1.5°C, 2°C, and 3°C global warming. *Geophysical Research Letters* 45: 935–944. https://doi.org/10.1002/2017GL076222.

Dowdy, A.J., Mills, G.A., Finkele, K., *et al*., 2010. Index sensitivity analysis applied to the Canadian forest fire weather index and the McArthur forest fire danger index. *Meteorological Applications* 17: 298–312.

Easterling, D.R., Meehl, G.A., Parmesan, C., *et al*., 2000. Climate extremes: observations, modeling, and impacts. *Science* 289: 2068–2074.

Ebi, K.L., Hallegatte, S., Kram, T., *et al*., 2014. A new scenario framework for climate change research: background, process, and future directions. *Climatic Change* 122: 363–372.

EC-Earth Consortium, 2019. EC-Earth-Consortium EC-Earth3 model output prepared for CMIP6 CMIP. Earth System Grid Federation. https://doi.org/10.22033/ESGF/CMIP6.181.

Eyring, V., Gillett, N.P., Achuta Rao, K.M., *et al*., 2021. Human influence on the climate system. In *Climate Change 2021: The Physical Science Basis*. Contribution of Working Group I to the Sixth Assessment Report of the Intergovernmental Panel on Climate Change. Cambridge University Press, Cambridge, UK, pp. 423–552. https://doi.org/10.1017/9781009157896.005.

Feser, F., 2006. Enhanced detectability of added value in limited-area model results separated into different spatial scales. *Monthly Weather Review* 134: 2180–2190. https://doi.org/10.1175/MWR3183.1.

Feser, F. and Barcikowska, M., 2012. The influence of spectral nudging on typhoon formation in regional climate models. *Environmental Research Letters* 7: 014024. https://doi.org/10.1088/1748-9326/7/1/014024.

Feser, F., Rockel, B., von Storch, H., *et al*., 2011. Regional climate models add value to global model data: a review and selected examples. *Bulletin of the American Meteorological Society* 92: 1181–1192. https://doi.org/10.1175/2011bams3061.1.

Flanagan, J. and Nolan, P., 2020. *Towards a Definitive Historical High-resolution Climate Dataset for Ireland – Promoting Climate Research in Ireland*. Environmental Protection Agency. Available online: https://www.epa.ie/publications/research/climate-change/research-350-towards-a-definitive-historical-high-resolution-climate-dataset-for-ireland--promoting-climate-research-in-ireland.php (accessed 8 December 2023).

Flanagan, J., Nolan, P., McGrath, R., *et al*., 2019. Towards a definitive historical high-resolution climate dataset for Ireland – promoting climate research in Ireland. *Advances in Science and Research* 15: 263–276.

Fraisse, J., Bellow, J. and Brown, C., 2010. Degree days: heating, cooling, and growing. Publication ABE381. University of Florida IFAS Extension, Gainesville, FL. Available online: http://edis.ifas.ufl.edu/ae428 (accessed 19 July 2023).

Frich P., Alexander L.V., Della-Marta P., *et al*., 2002. Observed coherent changes in climatic extremes during the second half of the twentieth century. *Climate Research* 19: 193–212. https://doi.org/10.3354/cr019193.

Fronzek, S., Carter, T.R. and Jylhä, K., 2012. Representing two centuries of past and future climate for assessing risks to biodiversity in Europe. *Global Ecology and Biogeography* 21: 19–35.

Gleeson, E., McGrath, R. and Treanor, M. (eds), 2013. *Ireland's Climate: The Road Ahead*. Met Éireann, Dublin.

Gutiérrez, J.M., Jones, R.G., Narisma, G.T., *et al*., 2021. Atlas. In *Climate Change 2021: The Physical Science Basis.* Contribution of Working Group I to the Sixth Assessment Report of the Intergovernmental Panel on Climate Change. Cambridge University Press, Cambridge, UK. Available online: http://interactive-atlas.ipcc.ch/ (accessed 7 November 2023).

Hawchar, L., Naughton, O., Nolan, P., *et al*., 2020. A GIS-based framework for high-level climate change risk assessment of critical infrastructure. *Climate Risk Management* 29: 100235.

Hersbach, H., Bell, B., Berrisford, P., *et al*., 2020. The ERA5 global reanalysis. *Quarterly Journal of the Royal Meteorological Society* 146: 1999–2049.

Hoegh-Guldberg, O., Jacob, D., Taylor, M., Bindi, M., Brown, S., Camilloni, I., Diedhiou, A., Djalante, R., Ebi, K.L., Engelbrecht, F., Guiot, J., Hijioka, Y., Mehrotra, S., Payne, A., Seneviratne, S.I., Thomas, A., Warren, R., Zhou, G., 2018. Impacts of 1.5ºC Global Warming on Natural and Human Systems. In *Global Warming of 1.5°C: IPCC Special Report on Impacts of Global Warming of 1.5°C above Pre-industrial Levels in Context of Strengthening Response to Climate Change, Sustainable Development, and Efforts to Eradicate Poverty*. Cambridge University Press, Cambridge, UK pp. 175–312, https://doi.org/10.1017/9781009157940.005.

Ianevski, A., Zusinaite, E., Shtaida, N., *et al*., 2019. Low temperature and low UV indexes correlated with peaks of influenza virus activity in northern Europe during 2010–2018. *Viruses* 11: 207.

IPCC (Intergovernmental Panel on Climate Change), 2013. *Climate Change 2013: The Physical Science Basis*. Contribution of Working Group I to the Fifth Assessment Report of the Intergovernmental Panel on Climate Change. Edited by Stocker, T.F., Qin, D., Plattner, G.-K., *et al*. Cambridge University Press, Cambridge, UK.

IPCC (Intergovernmental Panel on Climate Change), 2019. *IPCC Special Report on the Ocean and Cryosphere in a Changing Climate*. Edited by Pörtner, H.-O., Roberts, D.C., Masson-Delmotte, V., *et al*. Cambridge University Press, Cambridge, UK and New York, NY, USA. https://doi.org/10.1017/9781009157964.

IPCC (Intergovernmental Panel on Climate Change), 2021. *Climate Change 2021: The Physical Science Basis.* Contribution of Working Group I to the Sixth Assessment Report of the Intergovernmental Panel on Climate Change. Edited by Masson-Delmotte, V., Zhai, P., Pirani, A., *et al*. Cambridge University Press, Cambridge, UK.

IPCC (Intergovernmental Panel on Climate Change), 2023. *Climate Change 2023: Synthesis Report.* Contribution of Working Groups I, II and III to the Sixth Assessment Report of the Intergovernmental Panel on Climate Change. IPCC, Geneva, Switzerland. https://doi.org/10.59327/IPCC/AR6-9789291691647.

Jacob, D., Petersen, J., Eggert, B., *et al*., 2014. EURO-CORDEX: new high-resolution climate change projections for European impact research. *Regional Environmental Change* 14: 563–578.

Jerez, S., Tobin, I., Vautard, R., *et al*., 2015. The impact of climate change on photovoltaic power generation in Europe. *Nature Communications* 6: 1–8.

Johnson, D., Bessin, R. and Townsend, L., 1998. *Predicting Insect Development Using Degree Days*. College of Agriculture, Food and Environment, University of Kentucky, Lexington, KY.

Jones, C.D., Hickman, J.E., Rumbold, S.T., *et al*., 2021. The climate response to emissions reductions due to COVID19: initial results from CovidMIP. *Geophysical Research Letters*. https://doi.org/10.1029/2020GL091883.

Kalogirou, S.A., 2013. *Solar Energy Engineering: Processes and Systems*. Academic Press, Cambridge, MA.

Kanada, S., Nakano, M., Hayashi, S., *et al*., 2008. Reproducibility of maximum daily precipitation amount over Japan by a high-resolution non-hydrostatic model. *SOLA 4*: 105–108. https://doi.org/10.2151/sola.2008-027.

Kanamaru, H. and Kanamitsu, M., 2007. Fifty-seven-year California reanalysis downscaling at 10 km (CaRD10). Part II: comparison with North American regional reanalysis. *Journal of Climate* 20: 5572–5592. https://doi.org/10.1175/2007JCLI1522.1.

Kendon, E., Roberts, N., Senior, C., *et al*., 2012. Realism of rainfall in a very high-resolution regional climate model. *Journal of Climate* 25: 5791–5806. https://doi.org/10.1175/JCLI-D-11-00562.1.

Kendon, E., Roberts, N., Fowler, H., *et al*., 2014. Heavier summer downpours with climate change revealed by weather forecast resolution model. *Nature Climate Change* 4: 570–576. https://doi.org/10.1038/nclimate2258.

Kendon, M., MacCarthy, M. and Jevrejeva, S., 2015. *State of the UK Climate 2014*. Met Office Hadley Centre, Exeter, UK.

Kriegler, E., Edmonds, J., Hallegatte, S., *et al.*, 2014. A new scenario framework for climate change research: the concept of shared climate policy assumptions. *Climatic Change* 122: 401–414.

Lowe, J.A., Bernie, D., Bett, P.E., *et al.*, 2018. *UKCP18 Science Overview Report*. Met Office, Exeter, UK.

Lucas-Picher, P., Wulff-Nielsen, M., Christensen, J.H., *et al.*, 2012. Very high resolution regional climate model simulations over Greenland: identifying added value. *Journal of Geophysical Research: Atmospheres* 117. https://doi.org/10.1029/2011jd016267.

Mateus, C. and Coonan, B., 2022. *Distribution of Driving Rain in Ireland*. Met Éireann. Available online: http://hdl.handle.net/2262/101280 (accessed 7 November 2023).

Mavromatakis, F., Makrides, G., Georghiou, G., *et al.*, 2010. Modeling the photovoltaic potential of a site. *Renewable Energy* 35: 1387–1390.

McGowan, N.E., Roche, N., Aughney, T., *et al.*, 2021. Testing consistency of modelled predictions of the impact of climate change on bats. *Climate Change Ecology* 2: 100011.

McGrath, R. and Lynch, P. (eds), 2008. *Ireland in a Warmer World: Scientific Predictions of the Irish Climate in the Twenty-first Century*. Community Climate Change Consortium for Ireland (C4I). Available online: https://maths.ucd.ie/~plynch/Publications/Ireland_in_a_Warmer_World.pdf (accessed 11 April 2024).

McGrath, R. and Nolan, P., 2024. Use of proxy observations to evaluate the accuracy of precipitation spatial gridding. *International Journal of Climatology*. https://doi.org/10.1002/joc.8579

McGrath, R., Nishimura, E., Nolan, P., *et al.*, 2005. *Climate Change: Regional Climate Model Predictions for Ireland*. Environmental Protection Agency, Johnstown Castle, Ireland.

McMaster, G.S. and Wilhelm, W., 1997. Growing degree-days: one equation, two interpretations. *Agricultural and Forest Meteorology* 87: 291–300.

Met Éireann, 2023. Met Éireann publishes Ireland's new climate averages for 1991-2020. Available online: https://www.met.ie/met-eireann-publishes-irelands-new-climate-averages-for-1991-2020 (accessed 6 November 2023).

Met Office, 2022. *UK Climate Projections: Headline Findings, August 2022*. Available online: https://www.metoffice.gov.uk/binaries/content/assets/metofficegovuk/pdf/research/ukcp/ukcp18_headline_findings_v4_aug22.pdf (accessed 7 November 2023).

Miller, P., Lanier, W. and Brandt, S., 2001. *Using Growing Degree Days to Predict Plant Stages*. Montana State University, Bozeman, MT.

Morrissey, P., Nolan, P., McCormack, T., *et al.*, 2021. Impacts of climate change on groundwater flooding and ecohydrology in lowland karst. *Hydrology and Earth System Sciences* 25: 1923–1941.

Moss, R.H., Edmonds, J.A., Hibbard, K.A., *et al.*, 2010. The next generation of scenarios for climate change research and assessment. *Nature* 463: 747–756.

Murphy, J.M., Sexton, D.M.H., Jenkins, G.J., *et al.*, 2009. *UK Climate Projections Science Report: Climate Change Projections.* Met Office Hadley Centre, Exeter, UK.

Naughton, O., Donnelly, A., Nolan, P., *et al.*, 2018. A land use regression model for explaining spatial variation in air pollution levels using a wind sector based approach. *Science of the Total Environment* 630: 1324–1334.

Nicastro, F., Sironi, G., Antonello, E., *et al.*, 2021. Solar UV-B/A radiation is highly effective in inactivating SARS-CoV-2. *Scientific Reports* 11: 14805. https://doi.org/10.1038/s41598-021-94417-9.

Nolan, P., 2015. *Ensemble of Regional Climate Model Projections for Ireland*. Environmental Protection Agency, Johnstown Castle, Ireland.

Nolan, P. and Flanagan, J., 2020. *High-Resolution Climate Projections for Ireland – A Multi-model Ensemble Approach*. Environmental Protection Agency. Available online: http://epa.ie/pubs/reports/research/climate/researchreport339/ (accessed 8 December 2023).

Nolan, P. and McKinstry, A., 2020. *EC-Earth Global Climate Simulations: Ireland's Contributions to CMIP6*. Environmental Protection Agency. Available online: https://www.epa.ie/publications/research/climate-change/research-310-ec-earth-global-climate-simulations-irelands-contributions-to-cmip6.php (accessed 19 July 2023).

Nolan, P., Lynch, P., McGrath, R., *et al.*, 2012. Simulating climate change and its effects on the wind energy resource of Ireland. *Wind Energy* 15: 593–608.

Nolan, P., Lynch, P. and Sweeney, C., 2014. Simulating the future wind energy resource of Ireland using the COSMO-CLM model. *Wind Energy* 17: 19–37.

Nolan, P., O'Sullivan, J. and McGrath, R., 2017. Impacts of climate change on mid-twenty-first-century rainfall in Ireland: a high-resolution regional climate model ensemble approach. *International Journal of Climatology* 37: 4347–4363.

Noone, C., McClean, D., Gallagher, D., *et al*., 2023. *Ireland's Climate Change Assessment. Volume 1: Climate Science – Ireland in a Changing World*. Environmental Protection Agency, Johnstown Castle, Ireland.

Noti, J.D., Blachere, F.M., McMillen, C.M., *et al*., 2013. High humidity leads to loss of infectious influenza virus from simulated coughs. *PloS One* 8: e5745.

Nottmeyer, L., Armstrong, B., Lowe, R., *et al*., 2023. The association of COVID-19 incidence with temperature, humidity, and UV radiation: a global multi-city analysis. *Science of The Total Environment* 854: 158636.

O'Brien, E. and Nolan, P., 2023. TRANSLATE: standardized climate projections for Ireland. *Frontiers in Climate* 5: 1166828. Available online: https://www.frontiersin.org/articles/10.3389/fclim.2023.1166828/full (accessed 21 July 2023).

O'Brien, E., Ryan, Nolan, P., *et al*., 2024. *TRANSLATE Research Report*. Met Éireann, Dublin.

O'Driscoll, C., Ledesma, J.L., Coll, J., *et al*., 2018. Minimal climate change impacts on natural organic matter forecasted for a potable water supply in Ireland. *Science of the Total Environment* 630: 869–877.

O'Neill, B.C., Kriegler, E., Riahi, K., *et al*., 2014. A new scenario framework for climate change research: the concept of shared socioeconomic pathways. *Climatic Change* 122: 387–400.

O'Neill, B.C., Tebaldi, C., van Vuuren, D.P., Eyring, V., *et al*., 2016. The scenario model intercomparison project (ScenarioMIP) for CMIP6. *Geoscientific Model Development* 9: 3461–3482.

OMAFRA (Ontario Ministry of Agriculture, Food and Rural Affairs), 2017. *Agronomy Guide for Field Crops: Publication 811*. OMAFRA, Guelph, Canada.

O'Sullivan, J., Sweeney, C., Nolan, P., *et al*., 2016. A high-resolution, multi-model analysis of Irish temperatures for the mid-21st century. *International Journal of Climatology* 36: 1256–1267.

Palmer, T. E., McSweeney, C. F., Booth, B.B.B., *et al*., 2023. Performance-based sub-selection of CMIP6 models for impact assessments in Europe. *Earth System Dynami*cs 14: 457–483. https://doi.org/10.5194/esd-14-457-2023.

Powers, J.G., Klemp, J.B., Skamarock, W.C., *et al*., 2017. The weather research and forecasting (wrf) model: overview, system efforts, and future directions. *Bulletin of the American Meteorological Society* 98: 1717–1737.

Prein, A.F., Gobiet, A., Suklitsch, M., *et al*., 2013. Added value of convection permitting seasonal simulations. *Climate Dynamics* 41: 2655–2677.

Project Team ECA&D (Project Team European Climate Assessment & Dataset), 2013. *European Climate Assessment & Dataset (ECA&D): Algorithm Theoretical Basis Document (ATBD), Version 10.7*. Available online: https://www.ecad.eu/documents/atbd.pdf (accessed 21 May 2024).

Rana, A. Nikulin, G., Kjellström, E., *et al*., 2020. Contrasting regional and global climate simulations over South Asia. *Climate Dynamics* 54: 2883–2901. https://doi.org/10.1007/s00382-020-05146-0

Rauscher, S.A., Coppola, E., Piani, C., *et al*., 2010. Resolution effects on regional climate model simulations of seasonal precipitation over Europe. *Climate Dynamics* 35: 685–711. https://doi.org/10.1007/s00382-009-0607-7.

Reyne, M., McGowan, N.E., Flanagan, J., *et al*., 2021. Will predicted positive effects of climate change be enough to reverse declines of the regionally endangered natterjack toad in Ireland? *Ecology and Evolution* 11: 5049–5064.

Reyne, M.I., Dicks, K., Flanagan, J., *et al*., 2023. Landscape genetics identifies barriers to natterjack toad metapopulation dispersal. *Conservation Genetics* 24: 375–390.

Riahi, K., van Vuuren, D.P., Kriegler, E., *et al*., 2017. The shared socioeconomic pathways and their energy, land use, and greenhouse gas emissions implications: an overview. *Global Environmental Change* 42: 153–168.

Robinson, S.I., McLaughlin, Ó.B., Marteinsdóttir, B., *et al*., 2018. Soil temperature effects on the structure and diversity of plant and invertebrate communities in a natural warming experiment. *Journal of Animal Ecology* 87: 634–646.

Rockel, B., Will, A. and Hense, A., 2008. Special issue regional climate modelling with COSMO-CLM (CCLM). *Meteorologische Zeitschrift* 17: 347–348.

Romero Starke, K., Mauer, R., Karskens, E., *et al*., 2021. The effect of ambient environmental conditions on COVID-19 mortality: a systematic review. *International Journal of Environmental Research and Public Health* 18: 6665.

Ruosteenoja, K., 2021. *Applicability of CMIP6 Models for Building Climate Projections for Northern Europe*. Available online: https://helda.helsinki.fi/handle/10138/334477 (accessed 11 April 2023).

Sabri, N.S.A., Zakaria, Z., Mohamad, S.E., *et al.*, 2018. Importance of soil temperature for the growth of temperate crops under a tropical climate and functional role of soil microbial diversity. *Microbes and Environments* 33: 144–150.

Sagripanti, J.L. and Lytle, C.D., 2007. Inactivation of influenza virus by solar radiation. *Photochemistry and Photobiology* 83: 1278–1282.

Saikia, S.D., Ryan, P., Nuyts, S., *et al.*, 2023. *Impacts of Projected Future Changes in Precipitation on the Wwtp Influent Volumes Connected by Combined Sewer Collection Systems*. Available online: https://www.researchgate.net/publication/371068642_Impacts_of_Projected_Future_Changes_in_Precipitation_on_the_Wwtp_Influent_Volumes_Connected_by_Combined_Sewer_Collection_Systems (accessed 11 April 2024).

Semmler, T., McGrath, R., Steele-Dunne, S., *et al.*, 2010. Influence of climate change on heating and cooling energy demand in Ireland. *International Journal of Climatology* 30: 1502–1511.

Shaman, J., Pitzer, V.E., Viboud, C., *et al.*, 2010. Absolute humidity and the seasonal onset of influenza in the continental United States. *PLOS Biology* 8: e1000316.

Shaman, J., Goldstein, E. and Lipsitch, M., 2011. Absolute humidity and pandemic versus epidemic influenza. *American Journal of Epidemiology* 173:127–135. https://doi.org/10.1093/aje/kwq347.

Shkol'nik, I.M., Meleshko, V.P., Efimov, S.V., *et al.*, 2012. Changes in climate extremes on the territory of Siberia by the middle of the 21st century: an ensemble forecast based on the MGO regional climate model. *Russian Meteorology and Hydrology* 37: 71–84. https://doi.org/10.3103/S106837391202001X.

Skamarock, W.C., Klemp, J.B., Dudhia, J., *et al.*, 2008. *A Description of the Advanced Research WRF Version 3*. TN-475_STR. National Center for Atmospheric Research, Boulder, CO, USA. Available online: https://opensky.ucar.edu/islandora/object/technotes%3A500/datastream/PDF/download/citation.pdf (accessed 18 May 2024).

Smith, B., Wårlind, D., Arneth, A., *et al.*, 2014. Implications of incorporating N cycling and N limitations on primary production in an individual-based dynamic vegetation model. *Biogeosciences* 11: 2027–2054.

Smith, L.P., 1976. *The Agricultural Climate of England and Wales: Ministry of Agriculture, Fisheries and Food Technical Bulletin 35*. Her Majesty's Stationery Office, London.

Spinoni, J., Vogt, J. and Barbosa, P., 2015. European degree-day climatologies and trends for the period 1951–2011. *International Journal of Climatology* 35: 25–36.

Steele-Dunne, S., Lynch, P., McGrath, R., *et al.*, 2008. The impacts of climate change on hydrology in Ireland. *Journal of Hydrology* 356: 28–45.

Süss, J., Klaus, C., Gerstengarbe, F.-W., *et al.*, 2008. What makes ticks tick? Climate change, ticks, and tick-borne diseases. *Journal of Travel Medicine* 15: 39–45.

Tamerius, J.D., Shaman, J., Alonso, W.J., *et al.*, 2013. Environmental predictors of seasonal influenza epidemics across temperate and tropical climates. *PLoS Pathogens* 9(3): e1003194.

Taylor, K.E., Stouffer, R.J. and Meehl, G.A., 2012. An overview of CMIP5 and the experiment design. *Bulletin of the American Meteorological Society* 93: 485–498.

Tiedtke, M., 1989. A comprehensive mass flux scheme for cumulus parameterization in large-scale models. *Monthly Weather Review* 117: 1779–1799.

Tonui, J.K. and Tripanagnostopoulos, Y., 2008. Performance improvement of PV/T solar collectors with natural air flow operation. *Solar Energy* 82: 1–12.

Troen, I. and Petersen, E.L., 1989. *European Wind Atlas*. Risø National Laboratory for the Commission of the European Communities, Roskilde, Denmark.

Ulazia, A., Sáenz, J., Ibarra-Berastegi, G., *et al.*, 2019. Global estimations of wind energy potential considering seasonal air density changes. *Energy* 187: 115938.

UN (United Nations), 2015. Adoption of the Paris Agreement. Conference of the Parties, 12 December 2015, FCCC/CP/2015/L.9/Rev/1.

van der Linden, P. and Mitchell, J.F.B., 2009. *ENSEMBLES: Climate Change and Its Impacts: Summary of Research and Results from the ENSEMBLES Project*. Met Office Hadley Centre, Exeter, UK.

van Vuuren, D.P., Edmonds, J., Kainuma, M., *et al.*, 2011. The representative concentration pathways: an overview. *Climatic Change* 109: 5.

van Vuuren, D.P., Kriegler, E., O'Neill, B.C., *et al.*, 2014. A new scenario framework for climate change research: scenario matrix architecture. *Climatic Change* 122: 373–386.

Walsh, S., 2010. *Distribution of Driving Rain in Ireland*. Met Éireann, Dublin. Available online: http://edepositireland.ie/handle/2262/70489 (accessed 21 July 2023).

Walsh, S., 2016. *Long-Term Rainfall Averages for Ireland, 1981–2010.* Met Éireann, Dublin. Climatological Note No. 15. Available online: http://hdl.handle.net/2262/76135 (accessed 20 May 2024).

Walsh, S., 2017. *Long-Term Temperature Averages for Ireland, 1981–2010.* Met Éireann, Dublin. Climatological Note No. 16. Available online: http://hdl.handle.net/2262/79901 (accessed 20 May 2024).

Wang, S., McGrath, R., Semmler, T., *et al*., 2006. The impact of the climate change on discharge of Suir River Catchment (Ireland) under different climate scenarios. *Natural Hazards and Earth System Sciences* 6: 387–395.

Waring, R.H. and Running, S.W., 2007. Spatial scaling methods for landscape and regional ecosystem analysis. In *Forest Ecosystems*. Third edition*.* Academic Press, San Diego, CA.

Werner C., Nolan P. and Naughton, O., 2019. *High-resolution Gridded Datasets of Hydro-climate Indices for Ireland*. Environmental Protection Agency, Johnstown Castle, Ireland.

Williams, C.M., Henry, H.A. and Sinclair, B.J., 2015. Cold truths: how winter drives responses of terrestrial organisms to climate change. *Biological Reviews* 90: 214–235.

Winterfeldt, J., Geyer, B. and Weisse, R., 2011. Using Quikscat in the added value assessment of dynamically downscaled wind speed. *International Journal of Climatology* 31: 1028–1039. https://doi.org/10.1002/joc.2105.

WMO, 2017. *WMO Guidelines on Generating a Defined Set of National Climate Monitoring Products*. World Meteorological Organization, Geneva, Switzerland.

Zängl, G., Reinert, D., Rípodas, P., *et al*., 2015. The ICON (ICOsahedral Non-hydrostatic) modelling framework of DWD and MPI-M: description of the nonhydrostatic dynamical core. *Quarterly Journal of the Royal Meteorological Society* 141: 563–579.

Zappa, G., Shaffrey, L.C., Hodges, K.I., *et al*., 2013. A multimodel assessment of future projections of North Atlantic and European extratropical cyclones in the CMIP5 climate models. *Journal of Climate* 26: 5846–5862.

Zhao, M., Held, I.M., Lin, S.J., *et al*., 2009. Simulations of global hurricane climatology, interannual variability, and response to global warming using a 50-km resolution GCM. *Journal of Climate* 22: 6653–6678.

Zotarelli, L., Dukes, M.D., Romero, C.C., *et al*., 2010. *Step by Step Calculation of the Penman–Monteith Evapotranspiration (FAO-56 Method)*. Institute of Food and Agricultural Sciences, University of Florida, Gainesville, FL. Available online: https://www.agraria.unirc.it/documentazione/materiale_didattico/1462_2016_412_24509.pdf (accessed 19 July 2023).

Abbreviations

AOGCM	Atmospheric–ocean general circulation model
AR	Assessment report
CDD	Cooling degree day
CHU	Crop heat unit
CLM	Climate Limited-area Modelling
CMIP	Coupled Model Intercomparison Project
CORDEX	Coordinated Regional Climate Downscaling Experiment
COSMO	Consortium for Small-scale Modeling
ECMWF	European Centre for Medium-Range Weather Forecasts
EPA	Environmental Protection Agency
ERA5	Fifth-generation ECMWF atmospheric reanalysis of the global climate
ERA-Interim	ECMWF global atmospheric reanalysis
ESM	Earth system model
GDD	Growing degree day
GWT	Global warming threshold
HDD	Heating degree day
ICHEC	Irish Centre for High-End Computing
IPCC	Intergovernmental Panel on Climate Change
MAE	Mean absolute error
PISCES	Pelagic Interactions Scheme for Carbon and Ecosystem Studies
PV	Photovoltaic
RCM	Regional climate model
RCP	Representative concentration pathway
ScenarioMIP	Scenario Model Intercomparison Project
SDII	Simple Daily Intensity Index
SSP	Shared socioeconomic pathway
SWR	Shortwave radiation
TED	Total energy demand
UKCP	United Kingdom Climate Projections
UV	Ultraviolet
WMO	World Meteorological Organization
WRF	Weather Research and Forecasting

An Ghníomhaireacht Um Chaomhnú Comhshaoil

Tá an GCC freagrach as an gcomhshaol a chosaint agus a fheabhsú, mar shócmhainn luachmhar do mhuintir na hÉireann. Táimid tiomanta do dhaoine agus don chomhshaol a chosaint ar thionchar díobhálach na radaíochta agus an truaillithe.

Is féidir obair na Gníomhaireachta a roinnt ina trí phríomhréimse:

Rialáil: Rialáil agus córais chomhlíonta comhshaoil éifeachtacha a chur i bhfeidhm, chun dea-thorthaí comhshaoil a bhaint amach agus díriú orthu siúd nach mbíonn ag cloí leo.

Eolas: Sonraí, eolas agus measúnú ardchaighdeáin, sprioctdhírithe agus tráthúil a chur ar fáil i leith an chomhshaoil chun bonn eolais a chur faoin gcinnteoireacht.

Abhcóideacht: Ag obair le daoine eile ar son timpeallachta glaine, táirgiúla agus dea-chosanta agus ar son cleachtas inbhuanaithe i dtaobh an chomhshaoil.

I measc ár gcuid freagrachtaí tá:

Ceadúnú

> Gníomhaíochtaí tionscail, dramhaíola agus stórála peitril ar scála mór;
> Sceitheadh fuíolluisce uirbigh;
> Úsáid shrianta agus scaoileadh rialaithe Orgánach Géinmhodhnaithe;
> Foinsí radaíochta ianúcháin;
> Astaíochtaí gás ceaptha teasa ó thionscal agus ón eitlíocht trí Scéim an AE um Thrádáil Astaíochtaí.

Forfheidhmiú Náisiúnta i leith Cúrsaí Comhshaoil

> Iniúchadh agus cigireacht ar shaoráidí a bhfuil ceadúnas acu ón GCC;
> Cur i bhfeidhm an dea-chleachtais a stiúradh i ngníomhaíochtaí agus i saoráidí rialáilte;
> Maoirseacht a dhéanamh ar fhreagrachtaí an údaráis áitiúil as cosaint an chomhshaoil;
> Caighdeán an uisce óil phoiblí a rialáil agus údaruithe um sceitheadh fuíolluisce uirbigh a fhorfheidhmiú
> Caighdeán an uisce óil phoiblí agus phríobháidigh a mheasúnú agus tuairisciú air;
> Comhordú a dhéanamh ar líonra d'eagraíochtaí seirbhíse poiblí chun tacú le gníomhú i gcoinne coireachta comhshaoil;
> An dlí a chur orthu siúd a bhriseann dlí an chomhshaoil agus a dhéanann dochar don chomhshaol.

Bainistíocht Dramhaíola agus Ceimiceáin sa Chomhshaol

> Rialacháin dramhaíola a chur i bhfeidhm agus a fhorfheidhmiú lena n-áirítear saincheisteanna forfheidhmithe náisiúnta;
> Staitisticí dramhaíola náisiúnta a ullmhú agus a fhoilsiú chomh maith leis an bPlean Náisiúnta um Bainistíocht Dramhaíola Guaisí;
> An Clár Náisiúnta um Chosc Dramhaíola a fhorbairt agus a chur i bhfeidhm;
> Reachtaíocht ar rialú ceimiceán sa timpeallacht a chur i bhfeidhm agus tuairisciú ar an reachtaíocht sin.

Bainistíocht Uisce

> Plé le struchtúir náisiúnta agus réigiúnacha rialachais agus oibriúcháin chun an Chreat-treoir Uisce a chur i bhfeidhm;
> Monatóireacht, measúnú agus tuairisciú a dhéanamh ar chaighdeán aibhneacha, lochanna, uiscí idirchreasa agus cósta, uiscí snámha agus screamhuisce chomh maith le tomhas ar leibhéil uisce agus sreabhadh abhann.

Eolaíocht Aeráide & Athrú Aeráide

> Fardail agus réamh-mheastacháin a fhoilsiú um astaíochtaí gás ceaptha teasa na hÉireann;
> Rúnaíocht a chur ar fáil don Chomhairle Chomhairleach ar Athrú Aeráide agus tacaíocht a thabhairt don Idirphlé Náisiúnta ar Ghníomhú ar son na hAeráide;

> Tacú le gníomhaíochtaí forbartha Náisiúnta, AE agus NA um Eolaíocht agus Beartas Aeráide.

Monatóireacht & Measúnú ar an gComhshaol

> Córais náisiúnta um monatóireacht an chomhshaoil a cheapadh agus a chur i bhfeidhm: teicneolaíocht, bainistíocht sonraí, anailís agus réamhaisnéisiú;
> Tuairiscí ar Staid Thimpeallacht na hÉireann agus ar Tháscairí a chur ar fáil;
> Monatóireacht a dhéanamh ar chaighdeán an aeir agus Treoir an AE i leith Aeir Ghlain don Eoraip a chur i bhfeidhm chomh maith leis an gCoinbhinsiún ar Aerthruailliú Fadraoin Trasteorann, agus an Treoir i leith na Teorann Náisiúnta Astaíochtaí;
> Maoirseacht a dhéanamh ar chur i bhfeidhm na Treorach i leith Torainn Timpeallachta;
> Measúnú a dhéanamh ar thionchar pleananna agus clár beartaithe ar chomhshaol na hÉireann.

Taighde agus Forbairt Comhshaoil

> Comhordú a dhéanamh ar ghníomhaíochtaí taighde comhshaoil agus iad a mhaoiniú chun brú a aithint, bonn eolais a chur faoin mbeartas agus réitigh a chur ar fáil;
> Comhoibriú le gníomhaíocht náisiúnta agus AE um thaighde comhshaoil.

Cosaint Raideolaíoch

> Monatóireacht a dhéanamh ar leibhéil radaíochta agus nochtadh an phobail do radaíocht ianúcháin agus do réimsí leictreamaighnéadacha a mheas;
> Cabhrú le pleananna náisiúnta a fhorbairt le haghaidh éigeandálaí ag eascairt as taismí núicléacha;
> Monatóireacht a dhéanamh ar fhorbairtí thar lear a bhaineann le saoráidí núicléacha agus leis an tsábháilteacht raideolaíochta;
> Sainseirbhísí um chosaint ar an radaíocht a sholáthar, nó maoirsiú a dhéanamh ar sholáthar na seirbhísí sin.

Treoir, Ardú Feasachta agus Faisnéis Inrochtana

> Tuairisciú, comhairle agus treoir neamhspleách, fianaise-bhunaithe a chur ar fáil don Rialtas, don tionscal agus don phobal ar ábhair maidir le cosaint comhshaoil agus raideolaíoch;
> An nasc idir sláinte agus folláine, an geilleagar agus timpeallacht ghlan a chur chun cinn;
> Feasacht comhshaoil a chur chun cinn lena n-áirítear tacú le hiompraíocht um éifeachtúlacht acmhainní agus aistriú aeráide;
> Tástáil radóin a chur chun cinn i dtithe agus in ionaid oibre agus feabhsúchán a mholadh áit is gá.

Comhpháirtíocht agus Líonrú

> Oibriú le gníomhaireachtaí idirnáisiúnta agus náisiúnta, údaráis réigiúnacha agus áitiúla, eagraíochtaí neamhrialtais, comhlachtaí ionadaíocha agus ranna rialtais chun cosaint chomhshaoil agus raideolaíoch a chur ar fáil, chomh maith le taighde, comhordú agus cinnteoireacht bunaithe ar an eolaíocht.

Bainistíocht agus struchtúr na Gníomhaireachta um Chaomhnú Comhshaoil

Tá an GCC á bainistiú ag Bord lánaimseartha, ar a bhfuil Ard-Stiúrthóir agus cúigear Stiúrthóir. Déantar an obair ar fud cúig cinn d'Oifigí:

1. An Oifig um Inbhunaitheacht i leith Cúrsaí Comhshaoil
2. An Oifig Forfheidhmithe i leith Cúrsaí Comhshaoil
3. An Oifig um Fhianaise agus Measúnú
4. An Oifig um Chosaint ar Radaíocht agus Monatóireacht Comhshaoil
5. An Oifig Cumarsáide agus Seirbhísí Corparáideacha

Tugann coistí comhairleacha cabhair don Ghníomhaireacht agus tagann siad le chéile go rialta le plé a dhéanamh ar ábhair imní agus le comhairle a chur ar an mBord.